

Cell culture models of Chorea Acanthocytosis and their evaluation

D I S S E R T A T I O N

zur Erlangung des akademischen Grades

**Doctor rerum naturalium
(Dr. rer. nat.)**

vorgelegt

**der Fakultät Mathematik und Naturwissenschaften
der Technischen Universität Dresden**

von

Dipl.-Chem. Hannes Glaß

geboren am 09.05.1986 in Dresden

Verteidigt am 17.04.2018

Die Dissertation wurde in der Zeit von 07/2012 bis 10/2017 an der Klinik und Poliklinik für Neurologie der Medizinischen Fakultät Carl Gustav Carus der TU Dresden angefertigt.

Gutachter:

Prof. Dr. rer. nat. Elly Margaret Tanaka

Prof. Dr. med. Dr. rer. medic. Andreas Hermann

Table of Contents

List of abbreviations	7
Introduction	10
1. Neurodegenerative diseases	10
1.1. <i>Chorea-acanthocytosis – a clinical overview</i>	10
1.2. <i>Chorea-Acanthocytosis – genetic considerations</i>	12
2. Disease modelling	14
2.1. <i>Human disease models</i>	15
2.2. <i>Induced pluripotent stem cells</i>	16
2.3. <i>Multipotent neuronal progenitor cells</i>	18
3. Objectives of this thesis	19
Materials & Methods	21
1. Cell culture procedures	40
1.1. <i>Coating</i>	40
1.2. <i>Matrigel</i>	40
1.3. <i>PLO/laminin</i>	40
1.4. <i>Gelatin coating</i>	41
1.5. <i>Mouse embryonic fibroblast isolation</i>	41
1.6. <i>Generation of feeder cells</i>	41
1.7. <i>Human fibroblast culture</i>	42
1.8. <i>Reprogramming</i>	42
1.9. <i>iPSC culture</i>	43
1.10. <i>Culture of small molecule neuronal precursor cells (smNPC)</i>	45
1.11. <i>MSN differentiation</i>	45
1.12. <i>mDAN differentiation</i>	46
2. Nucleic acid biochemistry	47
2.1. <i>mRNA isolation</i>	47
2.2. <i>cDNA generation</i>	47
2.3. <i>Polymerase chain reaction (PCR)</i>	47
2.4. <i>Agarose gel electrophoresis</i>	48
3. Cell survival analysis	49
3.1. <i>PrestoBlue cell viability assay</i>	49
3.2. <i>Cytotoxicity detection kit</i>	50
3.3. <i>DNA damage analysis</i>	51
4. Metabolic characterization	51
5. Protein biochemistry	53
5.1. <i>Alkaline phosphatase staining</i>	53
5.2. <i>Preparation of immunocytochemistry samples</i>	53

5.3.	<i>Isolation of globular and filamentous actin</i>	55
5.4.	<i>Whole cell protein Isolation</i>	55
5.5.	<i>Cytosolic protein isolation</i>	56
5.6.	<i>Protein concentration measurement</i>	56
5.7.	<i>Western blot</i>	56
6.	<i>Live cell imaging</i>	58
7.	<i>Statistics</i>	60

Results..... 61

1.	<i>Generation of induced pluripotent stem cells</i>	61
1.1.	<i>Silencing of exogenous transcription factors</i>	62
1.2.	<i>Karyotyping of iPSC clones</i>	64
1.3.	<i>Evaluation of pluripotency</i>	64
1.4.	<i>Alkaline phosphatase staining</i>	65
1.5.	<i>Staining of pluripotency markers</i>	66
1.6.	<i>Three germ layer formation</i>	67
1.7.	<i>Confirmation of ChAc phenotype by CHOREIN western blot</i>	69
2.	<i>Characterization of differentiation potential</i>	71
2.1.	<i>Differentiation efficiency</i>	71
2.2.	<i>Characterization by qPCR</i>	76
2.3.	<i>Ratio of polymerized and unpolymerized cytoskeleton proteins</i>	80
2.4.	<i>Cell survival upon stress induction</i>	81
2.5.	<i>DNA damage in mature neurons</i>	85
2.6.	<i>Characterization of metabolism</i>	87
3.	<i>Live cell imaging</i>	90
3.1.	<i>Mitochondrial dynamics</i>	90
3.1.1.	<i>Morphological analysis</i>	91
3.1.1.1.	<i>Undirected neurons (96 well plate format)</i>	91
3.1.1.2.	<i>Microfluidic chambers</i>	94
3.1.2.	<i>Trafficking analysis</i>	97
3.1.2.1.	<i>96 well</i>	98
3.1.2.2.	<i>Microfluidic chambers</i>	102
3.1.3.	<i>JC-1</i>	107
3.1.3.1.	<i>96 well</i>	108
3.1.3.2.	<i>Microfluidic chambers</i>	108
3.2.	<i>Lysosomal dynamics</i>	109
3.2.1.	<i>Morphological analysis</i>	109
3.2.1.1.	<i>96 well</i>	109
3.2.1.2.	<i>Microfluidic chambers</i>	112
3.2.2.	<i>Trafficking</i>	115
3.2.2.1.	<i>96 well</i>	115

3.2.2.2.	Microfluidic chambers	119
4.	Comparison with Huntington's disease	124
4.1.	<i>DNA damage</i>	124
4.2.	<i>Characterization of metabolism</i>	125
4.3.	<i>Live cell imaging</i>	126
4.3.1.	<i>Mitochondria</i>	126
4.3.1.1.	Morphological analysis	126
4.3.1.2.	Trafficking	127
4.3.1.3.	JC-1	128
4.3.2.	<i>Lysosomes</i>	129
4.3.2.1.	Morphological analysis	129
4.3.2.2.	Trafficking	130
	Discussion	134
1.	Characterization of ChAc lines	134
1.1.	<i>ChAc stem cell lines show no impaired differentiation potential</i>	134
1.2.	<i>Neurons from MSN differentiation have an altered G/F actin ratio</i>	136
1.3.	<i>Mature neurons from ChAc lines are susceptible to UPR, proteotoxicity and DNA damage.</i> ..	137
1.4.	<i>ChAc neurons are not susceptible to DNA damage</i>	138
1.5.	<i>Energy dynamics in ChAc and Huntington lines feature a shift to glycolysis</i>	138
2.	Live cell imaging of ChAc lines	139
2.1.	<i>Video analysis is reproducible and sensitive</i>	139
2.2.	<i>ChAc lines have altered mitochondria shape and trafficking</i>	141
2.3.	<i>Treatments are not selective on ChAc lines mitochondria</i>	144
2.4.	<i>Mitochondrial potential is altered in ChAc lines</i>	144
2.5.	<i>ChAc lysosomes feature normal morphology but altered trafficking</i>	145
2.6.	<i>Lysosomes of MSN cultures respond poorly to treatments</i>	148
3.	MSN and mDAN differentiation highlight different aspects of the disease	149
	References	151
	List of figures	166
	List of tables	169
	Acknowledgments	170
	Appendix	171

List of abbreviations

2-DG	2-Deoxyglucose
AA	Ascorbic acid
AP	Alkaline phosphatase
BDNF	Brain derived neurotrophic factor
ChAc	Chorea Acanthocytosis
CHAT	Choline acetyl transferase
CTIP2	B-Cell CLL/Lymphoma 11B
DARPP-32	Dopamine- and cAMP-regulated neuronal phosphoprotein
dbcAMP	N ⁶ ,2'-O-Dibutyryl adenosine 3',5'-cyclic monophosphate
DLX2	Distal-less 2
DMEM	Dulbeccos modified Eagle's medium
DMSO	Dimethylsulfoxide
DNA	Deoxyribonucleic acid
DTT	Dithiothreitol
EB	Embryoid body
EDTA	Ethylenediaminetetraacetic acid
ESC	Embryonic stem cell
FCCP	Carbonyl cyanide-p-trifluoromethoxyphenylhydrazone
FCS	Fetal calf serum
Fgf2/8	Fibroblast growth factor 2/8
FLK-1	Fetal liver kinase 1
GABA	γ-Aminobutyric acid
GAD67	Glutamate decarboxylase 67kDa
GALC	Galactosylceramidase
GAPDH	Glyceraldehyde 3-phosphate dehydrogenase
GDNF	Glia derived neurotrophic factor
GFP	Green fluorescent protein
HMBS	Hydroxymethylbilane synthase
Htt	Huntington's disease
ICC	Immuno cyto chemistry
iPSC	Induced pluripotent stem cell

IWP2	N-(6-Methyl-2-benzothiazolyl)-2-[(3,4,6,7-tetrahydro-4-oxo-3-phenylthieno[3,2-d]pyrimidin-2-yl)thio]-acetamide
KNIME	Konstanz information miner
KROX20	Early growth response protein 2
LB medium	Lysogeny broth medium
LDH	Lactate dehydrogenase
LHX3	LIM/homeobox protein 3
LHX6	LIM/homeobox protein 6
LHX8	LIM/homeobox protein 8
MAP2	Microtubule associated protein 2
mDAN	Midbrain dopaminergic neuron
MEF	Mouse embryonic fibroblast
MFC	Micro fluidic chamber
MMC	Mitomycin C
MSN	Medium spiny neuron
NEAA	Non-essential amino acids
NKX2.1	NK2 homeobox 1
NPC	Neuronal progenitor cell
NSC	Neural stem cell
OCT4A	Octamer binding protein 4A
PAX6	Paired box protein 6
PBS	Phosphate buffered saline
PCR	Polymerase chain reaction
PFA	Paraformaldehyde
PLO	Poly-L-Ornithine
PP2	4-Amino-3-(4-chlorophenyl)-1-(t-butyl)-1H-pyrazolo[3,4-d]pyrimidine, 4-Amino-5-(4-chlorophenyl)-7-(t-butyl)pyrazolo[3,4-d]pyrimidine
PS	Penicillin/Streptomycin
PSG	Penicillin/Streptomycin/Glutamate
RNA	Ribonucleic acid
SDS	Sodium dodecyl sulfate
SMA	Smooth muscle actin
SMI-32	Neurofilament Heavy

SOX2	(Sex determining region Y)-Box2
SPSS	Statistical Package for the Social Sciences
SSEA-3/4	Stage specific embryonic antigen 3/4
TH	Thyrosine hydroxylase
NTRK1/2/3	Tropomyosin receptor kinase A/B/C
VPS13A	Vacuolar protein sorting-associated protein 13A
w/c	Whole cell

Introduction

1. Neurodegenerative diseases

Neurodegenerative diseases pose a major challenge on a personal level as well as for the society as a whole. They have a significant impact on the quality of life of affected patients as well as their relatives. The main feature of these maladies is the progressive loss of neurons. The specific region where the neuronal loss occurs first and foremost dictates the main symptoms of the specific diseases. For example, loss of dopaminergic neurons in the substantia nigra causes Parkinson's disease, loss of neurons of the basal ganglia are the underlying cause of Huntington's disease and degeneration of the second motor neuron is causative to some forms of amyotrophic lateral sclerosis (ALS) (Sveinbjornsdottir, 2016; Walker, 2007; Zarei, et al., 2015). Although these findings suggest a region specific pathological mechanism that is caused by individual mutations, almost all patients feature severe alteration of brain regions that were not primarily affected by the disease. Pathological hallmarks of Parkinson's disease have not only been identified in the substantia nigra but also in the basal forebrain and the neocortex (Davie, 2008). MRI evaluation of Huntington patients revealed consistent cortical and subcortical atrophy during early course of the disease (Dogan, et al., 2013). In ALS patients, it has been shown that the cingulate cortex is affected as well (Sudharshan, et al., 2011). Specific mechanisms for the degenerative processes remain elusive for a lot of cases. A common denominator of neurodegenerative diseases is DNA damage, which can be found in the genomic as well as the mitochondrial DNA and is also part of normal aging (Maynard, et al., 2015). However, whether these alterations are symptoms or the cause of the neurodegeneration is still subject of scientific debate (Coppede and Migliore, 2015; Madabhushi, et al., 2014). Often the disease is not initiated by a familial mono genetic cause but a combination of so called genetic risk factors that, together with environmental influence, result in the neurodegeneration. Therefore, it seems that the underlying molecular pathway of the pathology of these maladies can only be attributed to the dysregulation of a complex system. Using modern approaches of genetic epidemiology these factors can be identified (Khoury, et al., 1993). Investigation of the subpopulations of patients that have a verified monogenetic cause can however help to dissect the mechanisms and may give insight into their sporadic forms as well.

1.1. Chorea-acanthocytosis – a clinical overview

A distinct group of neurodegenerative diseases are the neuroacanthocytosis syndromes. This group is comprised of McLeod syndrome, Huntington's disease-like 2, Pantothenate kinase-associated neurodegeneration and Chorea-acanthocytosis (ChAc) (Walker, et al.,

2011). They all share a combination of a movement disorder, severe neurological alterations and misshapen erythrocytes called acanthocytes (See Figure 1).

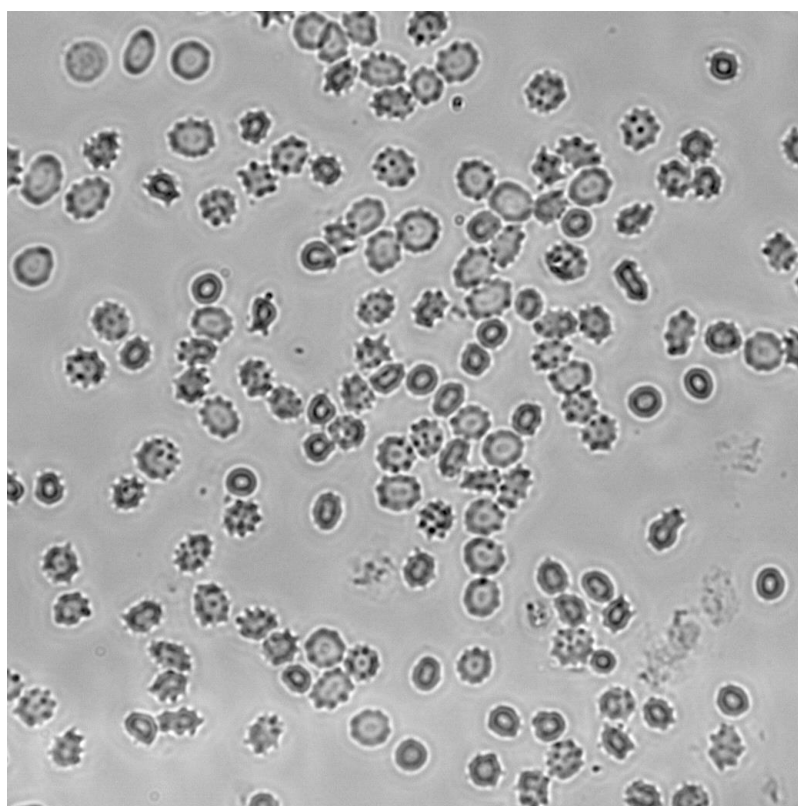


Figure 1: Acanthocytes are a common feature of the neuroacanthocytosis syndromes (Source: Dept. Neurology, UKD).

ChAc is very rare disease and its prevalence and incidence are unknown. Some references indicate that 300 to 500 people are affected world-wide, while others estimate up to 1000 patients (Danek and Walker, 2005; Walker, et al., 2011). Notably, there are some geographically isolated clusters in Japan and the French-Canadian population that are probably related to a founder effect (Dobson-Stone, et al., 2005; Ueno, et al., 1982). The mean onset age of the disease is about 30 years and life expectancy is reduced with disease progression of 15 to 20 years (Velayos Baeza A, 2014; Walker, et al., 2011). Clinical features are involuntary choreatiform movements with occasional upper body spasms, orofacial hyperkinesia, dystonia and a gait similar to that of Huntington's disease patients (Walker, et al., 2011). Very typical are head drops that develop during disease progression (Schneider, et al., 2010). Patients are also often diagnosed with epilepsy and Parkinsonism (Rampoldi, et al., 2002). The most prominent features of the disease are the involuntary movements of face, pharynx, larynx, mouth and tongue, resulting in difficulties with vocalization, swallowing and severe self-mutilation. Diagnostic imaging systems show an initial atrophy of the basal ganglia (See Figure 2). Even though in most post mortem

studies no evidence was found that ChAc is a proteinopathy, there was one case reported where the patient's brain featured inclusion bodies positive for expanded polyglutamine repeats, ubiquitin and torsin A (Walker, et al., 2002).

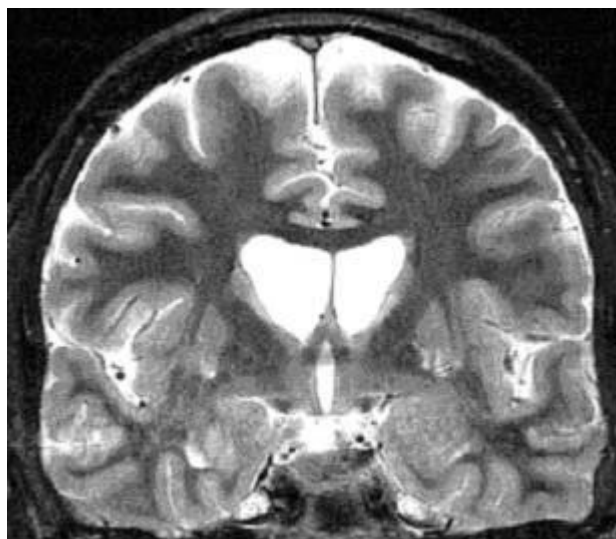


Figure 2: Image of the brain of a patient suffering from Chorea-Acanthocytosis taken with magnetic resonance tomography. Increased size of the lateral ventricles indicates a loss of neurons in the neighboring head of caudate nuclei and the putamen. Image taken from (Danek, 2005)

In later stages, loss of neurons can be observed in the substantia nigra, which is associated with Parkinsonism and patients can develop a poly-neuropathy, which is often not clinically relevant (Velayos Baeza A, 2014). Diagnosis is mainly established by using optimized protocols for acanthocyte detection if a patient is suffering from unexplained movement disorders, hyperkinesia, dystonia or very prominent orofacial dyskinesia (Storch, et al., 2005). Western blot analysis of CHOREIN protein was successfully established for diagnosis (Dobson-Stone, et al., 2004). Current treatment approaches are mainly targeted towards the neuropsychiatric effects to increase the quality of life of patients as well as non-pharmaceutical assisting devices like feeding tubes, to prevent weight loss as a result of the dysarthria, or computer-assisted speech systems to counter muteness (Walker, et al., 2011). Local application of botulinum toxin can be used to treat the dystonic components of the movement disorder (Velayos Baeza A, 2014). These treatment approaches are, however, purely symptomatic. Even though some approaches rely on the current experience in treatment of Huntington patients, no prospective treatment studies could have been conducted due to the low number of ChAc patients.

1.2. Chorea-Acanthocytosis – genetic considerations

ChAc is an autosomal recessive inherited disease caused by mutations in the *VPS13A* gene. This gene spans 240kb and contains 74 exons. Its cytogenetic location is 9q21.2

and encodes two different isoforms of the protein CHOREIN. Transcript variant A contains exon 1-68 and 70-73 resulting in a 3174 amino-acid protein, while variant B is encoded by exon 1-69 and yields a 3095 amino-acid protein (Velayos Baeza A, 2014). A study in 2005 identified 75 different mutations, which are distributed over the gene, in 58 patients. Mutation in different paralogs of the *VPS13A* gene cause different diseases. Alterations in *VPS13B* are causative for Cohen's disease (Kolehmainen, et al., 2003). *VPS13C* is associated with juvenile type-2 Parkinson's disease (Lesage, et al., 2016). Geographical isolated populations with distinct genetic alterations that are currently known are the Japanese Ehime deletion, a deletion of 260bp in exon 60 and 61, and the French-Canadian subpopulation with a deletion of exon 70-73. *VPS13A* encodes the 360kDa protein CHOREIN. Even though its function is not yet completely understood it is suggest being involved in vacuolar sorting. The yeast analogue *VPS13* is important for membrane morphogenesis during sporulation. Phosphatidylinositol phosphate levels that are pivotal for successful membrane closure are regulated by interaction of *VPS13* with phospholipase D (Park and Neiman, 2012). This interaction was recently described in *Homo sapiens* (Park, et al., 2015). In 2012, Foller et al. described a link between CHOREIN and the acanthocyte phenotype of ChAc patients' erythrocytes, which is mediated by the phosphoinositide 3 kinase – RAC1 – PAK1 pathway, leading to alterations in the cytoskeleton (Foller, et al., 2012). A disturbance in the ratio of globular (G) and filamentous (F) actin, which was significantly shifted towards G-Actin in ChAc patients, was observed in primary erythrocytes as well as the K562 erythroleukemic cell line. Changes in the membrane of ChAc patients erythrocytes were attributed to hyper active LYN-kinase (De Franceschi, et al., 2011). These features of ChAc have so far not been investigated in neurons. The first publication, that linked ChAc to neurons, analyzed subcellular localization of CHOREIN in dopaminergic neurons and found a co-localization with synaptotagmin I in dense-core vesicles (Hayashi, et al., 2012). Furthermore it was shown that CHOREIN interacts with β -adducin, β -actin as well as tubulin and HDAC6 (Sasaki, et al., 2016; Shiokawa, et al., 2013). In *Dictyostelium* and HeLa cells, defects in autophagy were attributed to CHOREIN mutations, indicating a possible role in vacuolar sorting as postulated earlier (Munoz-Braceras, et al., 2015). Similar defects in autophagy were recently described in erythroid precursors of ChAc patients that impair erythroid maturation (Lupo, et al., 2016). Park et al. described recently the important function of the yeast orthologue *VPS13* for mitochondrial functional (Park, et al., 2016). Even though some aspects of the molecular interaction have been discovered, the main mechanisms, especially in the primarily affected neurons of the basal ganglia, remain elusive. Until now ChAc related research focused mainly on clinical studies and the features of the blood

phenotypes. However, state of the art techniques of disease modelling allow the investigation of the disease relevant neurons.

2. Disease modelling

Modelling of diseases has become a very important field in recent years (See Figure 3).

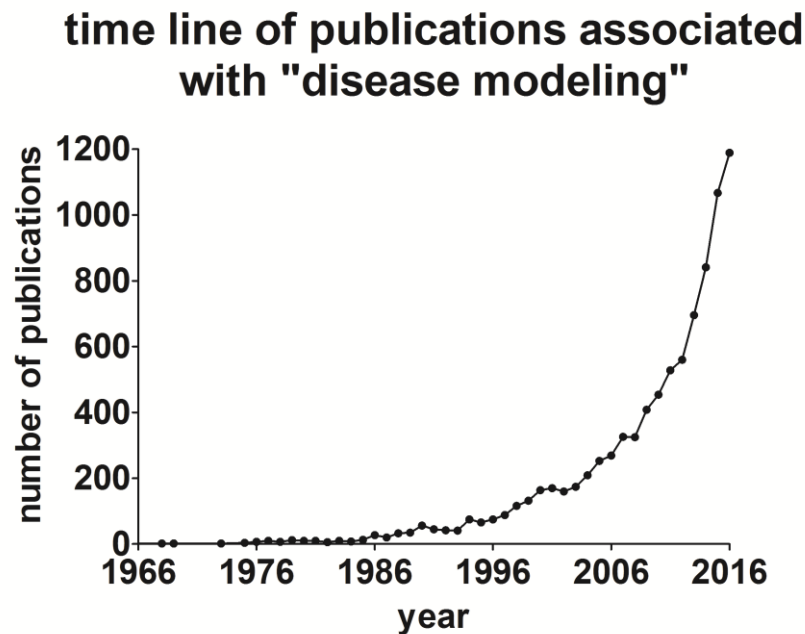


Figure 3: Time line of publications associated with the term "disease modelling". New techniques like sophisticated animal and new cell culture models lead to an increase in publications. Source: PubMed

The basic understanding of protein kinetics and how proteins interact physiologically at a cellular level is not enough to characterize the more complex pathophysiological interaction. Systemic implications on the whole organism as well as individual symptoms cannot be predicted. Therefore different models have been developed throughout the years. Non-human animal models, like mice and rats, are widely used to investigate diseases. Using genetic engineering to incorporate defined mutations in a known and stable genetic background, enables the researcher to investigate the phenotypes and mechanisms associated with that specific mutation. Influences of the genetic background can be minimized with this approach. Furthermore, with the induction of specific lesions by using drugs or mechanical interference, neurological disease events can be recapitulated without the need of introduction of mutations. These models give researchers the opportunity to observe the whole organism, including behavioral and physical changes on a macroscopic level as well as investigation at a cellular level and the implication on a specific organ. The limitations of these models are the evolutionary and genetic difference to humans. Some of the induced phenotypes do not recapitulate the disease progression

in human. Furthermore, some behavioral changes might be differentially reflected in animal models. Another issue is the reproducibility of the evidence found in an animal model in human models. Therefore, the knowledge obtained always has to be carefully validated in human systems. For the modelling of neurodegenerative diseases one of the main effectors, the age, can only be poorly mimicked in animal models due to their significantly shorter life cycles and different senescence. Anatomical differences pose another issue when modelling a human disease in animals. For example, the direct monosynaptic connection of the pyramidal tract with the lower motor neurons is very pronounced in primates, while not present in rodents (Shapovalov, 1974).

2.1. Human disease models

Although the clinical examination of disease progression in patients and post mortem analysis led to invaluable achievements in understanding and development of effective treatments, the early stages and the molecular pathways involved in degenerative diseases cannot be unraveled by these study designs. For an in depth model there are two major approaches, the culture of primary tissue obtained from biopsies and the culture of immortalized cell lines. Primary cells can be directly obtained from a patient and therefore already feature the genotype that led to the phenotype of the patient. The amount of cells that can be obtained from a patient, however, is very limited and is far exceeded by the needs of modern scientific standards. Another problem that arises in the modelling of neurodegenerative diseases is that the affected tissue itself cannot be easily accessed. During the process of neurectomy the neuronal axon is severely damaged, causing the neuron to die and thus rendering it impossible to be successfully cultured. Furthermore, it has to be considered that different mutations can affect tissues differentially and a genotype that affects the brain might not be impairing for fibroblasts or keratinocytes. Post mortem biopsies are severely damaged from undersupply of oxygen and nutrients, rendering the tissue unsuitable for cell culture. Aberrations of morphology could be attributed to the necrosis itself and might not represent the pathological conditions that caused the disease. The usage of immortalized cell lines like human embryonic kidney (HEK), fibroblast lines, embryonic stem cell lines (ESC) or cancer cell lines like the HeLa cell line can be very useful to investigate molecular mechanisms (Masters, 2002). These cell lines can be easily manipulated and investigated with a large spectrum of analytical tools. A lot of these cell lines however, contain severe genomic alterations that accumulated over their long term culture and exhibit aberrant transcriptome homeostasis that can hardly be considered as physiological (Landry, et al., 2013). Since some of these lines come from a malign background themselves, like the cancer stem

cells, it has to be very carefully evaluated how these background interacts with the disease phenotype of the introduced mutation. Another limitation of these cell models is the lack of functional readouts for disease specific cell types. This implication is very crucial for neurodegenerative diseases since the characterization of synaptic properties like neurotransmitter uptake or the propagation of an action potential is pivotal but unobtainable by some of these models. A third approach that has the advantage of high amount of obtainable tissue and accessibility to genetic engineering while maintaining the flexibility to generate various different cell types is the use of embryonic and fetal stem cells. ESC are pluripotent and therefore can be propagated by self-renewal or yield cells of each of the three germ layers, namely ectoderm, mesoderm and endoderm, by applying specific differentiation protocols (Takahashi and Yamanaka, 2006) Fetal stem cell also exhibit a strong self-renewal but their differentiation capacity is limited to the germ layer they have been derived from. Because both stem cells types are obtained by sacrificing *in vitro* fertilized oocytes and the modification of human embryonic tissue is highly restricted, the usage of these cell lines is under morale debate (Lako, et al., 2010). Therefore this approach cannot be applied broadly.

2.2. Induced pluripotent stem cells

In 2006, the discovery of so called induced pluripotent stem cells (iPSCs) by Shinya Yamanaka using mouse cells and the subsequent application of the very same protocol in human cells in 2007, gave researchers an invaluable novel tool for a human cell culture based model (Takahashi and Yamanaka, 2006; Yu, et al., 2007). Since these cells can be obtained by the introduction of exogenous transcription factors from almost any somatic cell, it is possible to generate a disease and patient specific iPSC line that has the same genetic background and disease causing mutations as the donor (See Figure 4). Furthermore these cells can be, like embryonic stem cells, propagated to vast amounts and differentiated into all three germ layers and therefore can give rise to mature functioning cells like, hepatocytes, osteoblasts, and neurons. These cells don't require the sacrifice of an individual and therefore minimize the morale problems. Because of their great contribution to the scientific field, Shinya Yamanaka and John Gurdon received the Nobel Prize for medicine in 2012 (Gurdon, 1962). The standard procedure in generating iPSCs starts with obtaining tissue from an individual. Commonly used samples are skin biopsies from the thigh, yielding fibroblasts that can be isolated and cultured as cell lines as well as from hair follicle from which keratinocytes can be obtained. Both fibroblasts and keratinocytes can be easily purified and expanded by means of reproducible, inexpensive and simple protocols (Aasen, et al., 2008).

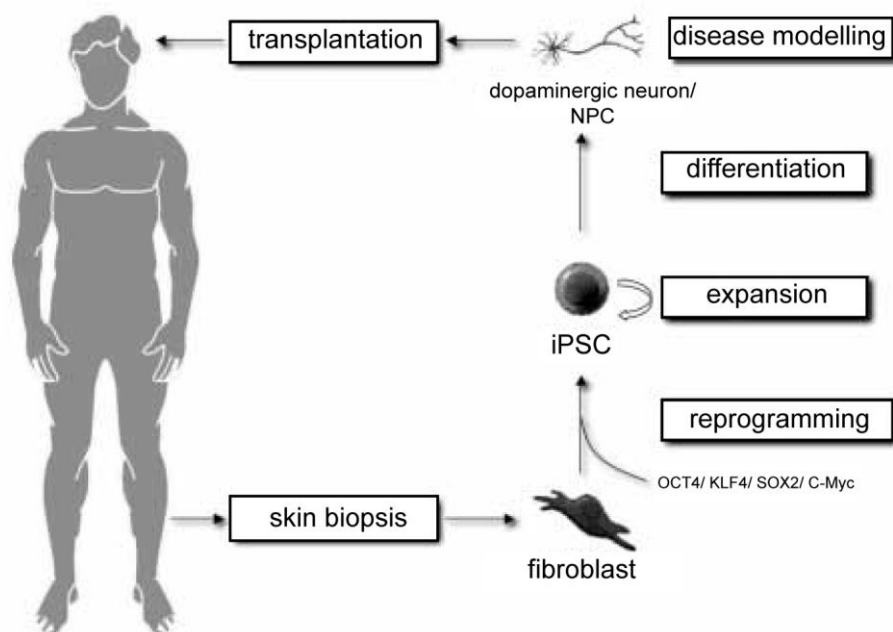


Figure 4: Schematic of application iPSC technology in translational research. Modified from (A. Storch, 2010)

The reversion of a somatic cell into an embryonic stem cell like stage is achieved by overexpression of a specific set of transcriptions factors. The first established set, the so called Yamanaka set, is comprised of *OCT4*, *SOX2*, *KLF4* and *MYCC* (Takahashi and Yamanaka, 2006). *OCT4*, *SOX2* and *KLF4* form an active complex that acts as a master regulator of stemness and pluripotency promoting transcription factors (Wei, et al., 2009). *MYCC* is enhancing their efficiency by facilitation epigenetic remodeling (Wernig, et al., 2008). A second set was successfully established as well. The so called Thomson set relies on the overexpression of *OCT4*, *SOX2*, *NANOG* and *LIN28A* (Yu, et al., 2007). The role of *OCT4* and *SOX2* as the major active components remains the same, while *LIN28A* is introduced as a modulator of *OCT4* post-transcriptional regulation (Qiu, et al., 2010). *NANOG*, a downstream target of the *OCT4*, induces a self-maintaining circuit and provides rapid and stable transformation into an ESC-like state (Kim, et al., 2008). The original publication used a monocistronic retrovirus based system for the introduction of these transgenes. The advantage of their system was the efficient infection and flexibility in the use of various transcription factors and different ratios for establishing a working protocol (Takahashi and Yamanaka, 2006). The disadvantages are related to high throughput generation of iPSC lines for disease modelling. Because of the need of production of several viruses, there is always an uncertain ratio of the transcriptions factors in the infected cells and possibly introduction of genetic mutations due to the

genomic integration of the virus itself. Once the desired transcription factors and their ratio had been identified new systems like the polycistronic lentivirus based system were established (Papapetrou, et al., 2009; Warlich, et al., 2011). These vectors come intrinsically with a working set of transcription factors at a functioning ratio and reporter expression for easy visual detection of genuinely infected cells. In order to circumvent poor reproducibility of iPSC line quality due to unpredictable phenotypes caused by random genomic integration of the virus, non-integrative system like transfection of plasmids, mRNA and use of the transcription factors as proteins itself were established (Warren, et al., 2010; Zhou, et al., 2009). These systems, however, suffer from even lower efficiency compared to the already low efficiency of iPSC clones obtained from viral approaches (Aasen, et al., 2008). State of the art reprogramming utilizes non integrative Sendai virus, an RNA virus, for efficient transfection and overexpression of transgenes without altering the host genome (Fusaki, et al., 2009).

Ever since iPSC technology was used for disease modelling a debate about good practice and quality standards arose. For the first time in 2008, Maherali and Hochedlinger collected comprehensive guidelines on iPSC line quality controls to establish a higher quality of the iPSC disease modelling field itself (Maherali and Hochedlinger, 2008). These guidelines cover the investigation of residual expression of the introduced transgenes, the inspection of the karyotype of the fully reprogrammed iPSC line and the proof of genuine pluripotency, including the assessment of embryonic markers as well as the characterization of three germ layer differentiation capacity. It is highlighted that the differentiation capacity should not only be estimated by *in vitro* assays but for human cell lines by means of a teratoma formation assay and for other species by *in vivo* studies involving germline transmission, chimera generation or the tetraploid complementation assay. Showing the capability to generate organs or even a complete organism is the most stringent functional test for a bona fide pluripotent stem cell.

iPSCs are capable to generate different kinds of somatic cells by applying specific differentiation protocols. These cells will be generated and used in this study to proliferate and derive patient specific neurons that can be analyzed under various treatment conditions. Stable iPSC cell lines can be shared with other labs. This is a great opportunity for scientists to contribute their expertise to the field that would be restricted by the limited amount of primary cultures.

2.3. Multipotent neuronal progenitor cells

Most applications, however, require only a very narrow range of cell types. In case one particular germ layer or highly selective cell is required, it is usually better to reduce the

potency of the cell line by generating precursor or progenitor cell lines. This process is usually initiated by withdrawal of stemness promoting conditions like growth factors and addition of supplements that promote differentiation into certain germ layer. At a certain point additional supplements are added that stabilize the cell culture in this committed stem cell stage. In 2013, Reinhardt et al. published a protocol that generated neuronal precursor cells out of iPSC. Since the process involved the application of small molecules, these cells were named small molecule neural precursor cell (smNPC) (Reinhardt, et al., 2013). These cells are already committed to a neuroectodermal mid-/hind-brain fate. The biggest advantages of these cells are that further differentiation into mature neurons takes less time, since previous induction of ectodermal lineage is not required, and the resulting cell culture is more homogeneous with few contaminating cells from other germ layers. These smNPC are currently used to model diseases, which involve mid- and hind-brain neurons, like Parkinson's disease or ALS. Neurons from more anterior regions of the brain cannot be readily obtained from these precursor cells. Modelling of diseases that affect the anterior cortex, like frontotemporal lobar degeneration, or the basal ganglia, like Huntington's disease or ChAc, still require differentiation protocols that start from the pluripotent state. There is currently a hypothesis under debate that all neural differentiation protocols go through a transient anterior stage (Pankratz, et al., 2007). Sustaining these cells in this stage could allow a common anterior progenitor cell line that can give rise to cortical neurons. A different approach is a partial reprogramming. In order to avoid the problems of embryonic stem cell culture it is possible to use transcription factors that promote a direct conversion into NPCs (Han, et al., 2012; Ring, et al., 2012). Transdifferentiation of a given somatic cell into a neuron has been published as well (Caiazzo, et al., 2011). In this study smNPCs were used along the iPSC line to investigate the influence of ChAc differently regionalized neurons. While analysis of iPSC derived MSN of basal ganglia focuses on the somatic cause of the chorea, dopaminergic neurons derived from smNPCs give insight into the pathological changes that lead to Parkinsonism of ChAc patients.

3. Objectives of this thesis

The first aim of this thesis is to generate an iPSC based cell culture model of ChAc. Therefore, two differentiation protocols that yield medium spiny neurons and midbrain dopaminergic neurons should be established. Phenotypical screening for differences in differentiation capacity, survivability and energy homeostasis will be conducted. Furthermore, a robust and sensitive workflow for live cell imaging of mitochondria and lysosomes has to be established.

The second aim is to compare the two differentiation protocols in order to elucidate which is superior in disease modeling of ChAc.

The third aim is to investigate whether the ChAc phenotypes and their respective treatments, which were previously described in patient red blood cells, are present in neurons.

Materials & Methods

Table 1: Cell lines and organism used during this thesis

Cell lines used	Obtained from
CF-1 MEF and Feeder	mice obtained from Charles River, cell lines isolated
smNPCs for mDAN differentiation	cell lines were kindly provided by the group of Jared Sternecker
iPSC for MSN differentiation	iPSC lines were generated during the project

Table 2: Instruments

Instrument	Company
Absorbance Plate reader - Sunrise	Tecan group Ltd., Männedorf, Switzerland
Analytical Balance - CP225D-0CE	Satorius AG, Göttingen, Germany
Balance – SBA 52	Scaltec Instruments GmbH, Heiligenstadt, Germany
Cell culture Microscope - Axiovert	Carl Zeiss, Jena, Germany
Centrifuge – Centrifuge 5403	Eppendorf, Hamburg, Germany
Centrifuge – Heraeus Biofuge Primo	Thermo Fisher Scientific, Massachusetts, USA
Centrifuge - MiniSpinPlus	Eppendorf, Hamburg, Germany
Fluorescence Microscope - AFLX6000 TIRF	Leica Camera, Wetzlar, Germany
Fluorescence Microscope - DMIRE2	Leica Camera, Wetzlar, Germany
Fluorescence Microscope - Observer.Z1	Carl Zeiss, Jena, Germany

Instrument	Company
Fluorescence Plate reader - Genios	Tecan group Ltd., Männedorf, Switzerland
Gel documentation – Dunkelhaube D4	Biostep GmbH, Burkhardtsdorf, Germany
Gel electrophoresis – E865	Consort, Turnhout, Belgium
Gel electrophoresis PSU – EPS 600	Pfizer, New York, USA
Hemocytometer – Neubauer improved	Paul Marienfeld GmbH Co. KG, Lauda-Königshofen, Germany
Hybridization oven – HB-1000	UVP, Upland, Canada
Imager - LAS3000	Fujifilm, Tokyo, Japan
Incubator – Heracell 150i	Thermo Fisher Scientific, Massachusetts, USA
Laminar Flow hood – Clean Wizard V 100	Kojair Tech Oy, Vilppula, Finland
Laminar Flow hood – Herasafe	Thermo Fisher Scientific, Massachusetts, USA
Multichannel multistep pipette - Transferpette -8	Brand GmbH & Co. KG, Wertheim, Germany
pH meter – inoLab ph 720	Wtw GmbH, Weilheim, Germany
Photometer - Biophotometer	Eppendorf, Hamburg, Germany
Real time PCR cycler - MX3000P	Agilent, Santa Clara, USA
Shaker – incubating orbital shaker 3500i	VWR International, Radnor Township, USA
Shaker – RotaMax 150	Heidolph, Schwabach, Germany
Stereo preparation microscope – Stemi DV4SteREO CL 1500 ECO	Carl Zeiss, Jena, Germany

Instrument	Company
Thermomixer – Thermomixer Comfort	Eppendorf, Hamburg, Germany
Transilluminator – BioView UST 30M-8R	Biostep GmbH, Burkhardtsdorf, Germany
Laboratory water bath	Memmert GmbH & Co. KG, Schwabach, Germany
Water purification system - GenePure	Thermo Fisher Scientific, Massachusetts, USA
Western Bloter - iBlot	Thermo Fisher Scientific, Massachusetts, USA

Table 3: Primary antibodies used for ICC

Antibody	Host	Dilution	Manufacturer (catalog number)
α -Fetoprotein	mouse	1:500	Abcam® , Cambridge, United Kingdom (ab3980)
β -Catenin	mouse	1:1000	BD Bioscience, Bedford, USA (#9562)
ChAT	rabbit	1:1500	Merck Millipore, Billerica, USA (AB143)
Ctip2	rabbit	1:1000	Abcam® , Cambridge, United Kingdom (ab18465)
Cytochrome C	mouse	1:500	BD Bioscience, Bedford, USA (556432)
Darpp32 (H-62)	rabbit	1:200	Santa Cruz Biotechnology Inc., Santa Cruz, USA (sc11365)
Fibronectin	rabbit	1:500	Sigma Aldrich, St. Louis, USA (F7387)
Flk-1	rabbit	1:500	Santa Cruz Biotechnology Inc., Santa Cruz, USA (sc504)
GABA	rabbit	1:1000	Sigma Aldrich, St. Louis, USA (A2052)

Antibody	Host	Dilution	Manufacturer (catalog number)
GalC	mouse	1:500	Merck Millipore, Billerica, USA (MAB342)
Gata4	goat	1:1000	R&D Systems, Minneapolis, USA (AF2606)
Gata6	rabbit	1:500	Abcam® , Cambridge, United Kingdom (ab39123)
Lin28A	mouse	1:2000	Cell Signaling Technologies, Inc., Massachusetts, USA (#5930)
Map2	chicken	1:500	Abcam® , Cambridge, United Kingdom (ab5392)
Map2	mouse	1:500	BD Bioscience, Bedford, USA (556320)
Nanog	rabbit	1:500	Cell Signaling Technologies, Inc., Massachusetts, USA (#35580)
Nestin	rabbit	1:500	Merck Millipore, Billerica, USA (ABD69)
Oct4	rabbit	1:500	Abcam® , Cambridge, United Kingdom (ab19857)
Olig2	rabbit	1:500	Merck Millipore, Billerica, USA (AB9610)
Pecam-1	mouse	1:100	BD Bioscience, Bedford, USA (555444)
S100β	rabbit	1:2000	Swant Inc., Marly, Switzerland (37A)
α-SMA	mouse	1:100	Dako North America, Inc., Carpinteria, USA (M0851)
SMI32	chicken	1:10000	Covance, New Jersey, USA (PCK-592P)
Sox2	mouse	1:500	R&D Systems, Minneapolis, USA (MAB2018)
SSEA3	rat	1:500	Abcam® , Cambridge, United Kingdom (ab16286)

Antibody	Host	Dilution	Manufacturer (catalog number)
SSEA4	mouse	1:500	Abcam® , Cambridge, United Kingdom (ab16287)
TH	rabbit	1:500	Pel Freez Biologicals, Arkansas, USA (P60101)
Tra 1_60	mouse	1:500	Abcam® , Cambridge, United Kingdom (ab16288)
Tuj1	mouse	1:2000	Covance, Princeton, USA (MMS-435P)
Tuj1	chicken	1:500	Merck Millipore, Billerica, USA (AB9354)
Vimentin	mouse	1:1000	Sigma Aldrich, St. Louis, USA (V2258)

Table 4: Primary antibodies used for western blot

Antibody	Host	Dilution	Manufacturer (catalog number)
Acetyl. Tubulin	mouse	1:5000	Sigma Aldrich, St. Louis, USA (T7451)
Actin	rabbit	1:500	Cell Signaling Technologies, Inc., Massachusetts, USA (#4967)
CHOREIN	rabbit	1:500	Sigma Aldrich, St. Louis, USA (HPA021662)
GAPDH	mouse	1:100000	Merck Millipore, Billerica, USA (MAB374)
α -Tubulin	mouse	1:5000	Abcam® , Cambridge, United Kingdom (ab7291)

Table 5: Secondary antibodies

Antibody	Host	Dilution	Manufacturer (catalog number)
α -ms/rb/ch Alexa Fluor 488 IgG	donkey	1:500	Thermo Fisher Scientific, Massachusetts, USA (A21202/A21206/A11039)

Antibody	Host	Dilution	Manufacturer (catalog number)
α -ms/rb/ch Alexa Fluor 594 IgG	donkey	1:500	Thermo Fisher Scientific, Massachusetts, USA (A21203/A21207/ab9652)
α -ms/rb Alexa Fluor 647 IgG	donkey	1:500	Thermo Fisher Scientific, Massachusetts, USA (A31571/A3157)
α -ms RhodaminRed IgM	donkey	1:200	Jackson ImmunoResearch Laboratories Inc., Pennsylvania, USA (715-295-020)
α -ch Alexa Fluor 647 IgY	donkey	1:500	Jackson ImmunoResearch Laboratories Inc., Pennsylvania, USA (703-605-155)
α -ms hrp conjugated IgG	donkey	1:5000	Jackson ImmunoResearch Laboratories Inc., Pennsylvania, USA (715-035-150)
α -rb hrp conjugated IgG	donkey	1:5000	Jackson ImmunoResearch Laboratories Inc., Pennsylvania, USA (711-035-152)

Table 6: Fluorescent reporters

Name	Dilution	Manufacturer (catalog number)
Phalloidin conjugated to Rhodamin Red	1:100	Thermo Fisher Scientific, Massachusetts, USA (R415)
DNase conjugated to Alexa Fluor 488	1:500	Thermo Fisher Scientific, Massachusetts, USA (D12371)
LysoTracker Red	1:20000	Thermo Fisher Scientific, Massachusetts, USA (L7528)
MitoTracker DeepRed	1:20000	Thermo Fisher Scientific, Massachusetts, USA (M22426)

Name	Dilution	Manufacturer
JC-1	1:1000	Thermo Fisher Scientific, Massachusetts, USA (M34152)
Hoechst33342	1:1333	Thermo Fisher Scientific, Massachusetts, USA (H3570)

Table 7: Software

Type	Software	Company
Image acquisition	Zen 2011	Carl Zeiss AG, Oberkochen, Germany
Data mining and organization	KNIME 3.1.1	KNIME.COM AG, Zurich, Switzerland
Image and video evaluation	FIJI 1.48a	Open source GPLv2
Western blot evaluation	TotalLab Quant	TotalLab Limited, Newcastle, UK
Statistics	SPSS 23	IBM, New York, USA
Statistics	GraphPad Prism 7	GraphPad Software Inc., La Jolla, USA
Image processing	Photoshop CS6	Adobe Systems, San Jose, USA

Table 8: Chemicals

Chemical	Manufacturer
2-Deoxy-Glucose	Sigma Aldrich, St. Louis, USA
Accutase	Sigma Aldrich, St. Louis, USA

Chemical	Manufacturer
Agarose	Biozym Biotech Trading GmbH, Oldendorf, Germany
Ampicilin	Carl Roth GmbH & Co. KG, Karlsruhe, Germany
Ascorbic Acid	Sigma Aldrich, St. Louis, USA
B27-Supplement w/o Vitamin A	Thermo Fisher Scientific, Massachusetts, USA
BDNF	Promega, Madison, USA
b-Mercaptoethanol	Thermo Fisher Scientific, Massachusetts, USA
CHIR 99021	Cayman chemical company, Ann Arbor, USA
Collagenase Type IV	Thermo Fisher Scientific, Massachusetts, USA
dbcAMP	Sigma Aldrich, St. Louis, USA
DMEM	Thermo Fisher Scientific, Massachusetts, USA
DMEM F12	Thermo Fisher Scientific, Massachusetts, USA
DMSO	Sigma Aldrich, St. Louis, USA
DNA Marker	Thermo Fisher Scientific, Massachusetts, USA
Dorsomorphin	Tocris Bioscience, Bristol, UK
Dry milk powder	Carl Roth GmbH & Co. KG, Karlsruhe, Germany
DTT	Carl Roth GmbH & Co. KG, Karlsruhe, Germany
EDTA	Carl Roth GmbH & Co. KG, Karlsruhe, Germany
Ethanol	VWR International GmbH, Dresden, Germany
Etoposide	Sigma Aldrich, St. Louis, USA
Fetal bovine serum	Sigma Aldrich, St. Louis, USA

Chemical	Manufacturer
Fetal calf serum	Merck Group, Darmstadt, Germany
FCCP	Tocris Bioscience, Bristol, UK
FGF2	Sigma Aldrich, St. Louis, USA
FGF8	R&D Systems, Minneapolis, USA
Fluoromount	SouthernBiotech, Birmingham, USA
Fugene	Promega, Madison, USA
Gelatine	Sigma Aldrich, St. Louis, USA
Glucose	Sigma Aldrich, St. Louis, USA
Glutamax	Thermo Fisher Scientific, Massachusetts, USA
Glycerol	MP biomedicals, Santa Ana, USA
Glycine	Carl Roth GmbH & Co. KG, Karlsruhe, Germany
GNDF	Sigma Aldrich, St. Louis, USA
Heparin	Sigma Aldrich, St. Louis, USA
IWP2	Sigma Aldrich, St. Louis, USA
Kanamycin	Carl Roth GmbH & Co. KG, Karlsruhe, Germany
KO DMEM	Thermo Fisher Scientific, Massachusetts, USA
KO Serum	Thermo Fisher Scientific, Massachusetts, USA
Laminin	Roche Holding AG, Basel, Switzerland
LB Medium	Thermo Fisher Scientific, Massachusetts, USA
L-Canavanine	Sigma Aldrich, St. Louis, USA

Chemical	Manufacturer
Loading Buffer	anamed Elektrophorese GmbH, Groß-Bieberau, Germany
Matrigel	BD Bioscience, Bedford, USA (556320)
Methanol	VWR International GmbH, Dresden, Germany
MG132	Sigma Aldrich, St. Louis, USA
Mikrozyd	Schülke&Mayr, Norderstedt, Germany
Mitomycin C	Tocris Bioscience, Bristol, UK
N2-Supplement	Thermo Fisher Scientific, Massachusetts, USA
NaCl	Merck Group, Darmstadt, Germany
Sodium deoxycholate	Sigma Aldrich, St. Louis, USA
Sodium orthovanadate	Sigma Aldrich, St. Louis, USA
NEAA	Thermo Fisher Scientific, Massachusetts, USA
Neurobasal	Thermo Fisher Scientific, Massachusetts, USA
Oligomycin	Tocris Bioscience, Bristol, UK
PBS	Thermo Fisher Scientific, Massachusetts, USA
PD0325901	Sigma Aldrich, St. Louis, USA
PFA	Electron Microscopy Sciences, Hatfield, USA
Phalloidin	Tocris Bioscience, Bristol, UK
Phosphatase Inhibitor Cocktail	Thermo Fisher Scientific, Massachusetts, USA
Poly-L-ornithine	Sigma Aldrich, St. Louis, USA
PP2	Tocris Bioscience, Bristol, UK

Chemical	Manufacturer
Protamin Sulfat	Sigma Aldrich, St. Louis, USA
Protease Inhibitor Cocktail	Thermo Fisher Scientific, Massachusetts, USA
Penicillin and streptomycin	Thermo Fisher Scientific, Massachusetts, USA
Penicillin, streptomycin and glutamine	Thermo Fisher Scientific, Massachusetts, USA
Pure water	Thermo Fisher Scientific, Massachusetts, USA
Purmorphamin	Cayman chemical company, Ann Arbor, USA
Pyruvate	Thermo Fisher Scientific, Massachusetts, USA
RedSafe	Thermo Fisher Scientific, Massachusetts, USA
Restriction enzymes	New England Biolabs Inc., Ipswich, USA
ROCK Inhibitor Y-27632	Abcam, Cambridge, United Kingdom
Rotenone	Sigma Aldrich, St. Louis, USA
SB431542	Tocris Bioscience, Bristol, UK
SDS	Carl Roth GmbH & Co. KG, Karlsruhe, Germany
Sucrose	Carl Roth GmbH & Co. KG, Karlsruhe, Germany
TGF- β 3	Peprtech, Rocky Hill, USA
Tris-HCL	Carl Roth GmbH & Co. KG, Karlsruhe, Germany
TritonX-100	Thermo Fisher Scientific, Massachusetts, USA
Trypsin	Thermo Fisher Scientific, Massachusetts, USA
Tunicamycin	Enzo life science, East Farmingdale, USA
Tween 20	Serva Elektrophoresis GmbH, Heidelberg, Germany

Chemical	Manufacturer
Uridine	Sigma Aldrich, St. Louis, USA
Western blot marker	Thermo Fisher Scientific, Massachusetts, USA

Table 9: Consumables

Material	Company
96 well clear bottom white PS	Thermo Fisher Scientific, Massachusetts, USA
96well CELLSTAR flat bottomed dishes	Greiner Bio-One GmbH, Kremsmünster, Austria
Bottle-top vacuum filters	Corning Inc., Corning, USA
Cell culture Dishes	Thermo Fisher Scientific, Massachusetts, USA
4-,6-,12-,24-,96-well	Sarstedt AG & Co., Nümbrecht, Germany
	TPP Techno Plastic Products AG, Trasadingen, Switzerland
Cell scraper	TPP Techno Plastic Products AG, Trasadingen, Switzerland
Centrifuge tubes	Greiner Bio-One GmbH, Kremsmünster, Austria
Dissecting set	Manufactures D'Outils Dumont SA, Montignez, Switzerland
Microfluidic chambers	Xona Microfluidics LLC, Temecula, USA
Millex HV low binding PVDV membrane filters 0.45 µm	Merck Millipore, Billerica, USA
NuPAGE Protein gels	Thermo Fisher Scientific, Massachusetts, USA

Material	Company
Pipette tips	Biosphere Corporation, Dnipropetrovsk, Ukraine
Pipettes	Gilson Inc., Middleton, USA Eppendorf, Hamburg, Germany VWR International, Radnor Township, USA
SafeSeal reaction tubes	Sarstedt AG & Co., Nümbrecht, Germany
Serological pipette 5, 10, 25 and 50ml	Thermo Fisher Scientific, Massachusetts, USA

Table 10: Assays and kits

Assay	Company
Alkaline Phosphatase Staining kit II	Stemgent Inc., Cambridge, USA
QuantiTect Reverse Transcription kit	Qiagen, Hilden, Netherlands
Cytotoxicity detection kit	Roche Holding AG, Basel, Switzerland
Nuclear Extract kit	Active Motif, Carlsbad, USA
QuantiTect SYBR Green PCR kit	Qiagen, Hilden, Netherlands
NulceoBond Xtra Maxi kit	Macherey-Nagel GmbH & Co. KG, Düren, Germany
Roti Nanoquant	Carl Roth GmbH & Co. KG, Karlsruhe, Germany
RNEasy Plus Mini kit	Qiagen, Hilden, Netherlands
Seahorse XF Assay	Agilent Technologies, Santa Clara, USA

Assay	Company
Presto Blue Cell viability reagent	Thermo Fisher Scientific, Massachusetts, USA
NuPAGE Running Buffer	Thermo Fisher Scientific, Massachusetts, USA
Amersham ECL Prime Western Blotting Detection Reagent	GE Healthcare, Chicago, USA
SuperSignal West Maximum Sensitivity	Thermo Fisher Scientific, Massachusetts, USA

Table 11: Primers designed

Primer	Forward sequence	Reverse sequence	Product size (bp)
18S	CGTAGTTCGACCATA AACGATGCC	GTGGTGCCCTTCCGT CAATTCC	152
ACTB	TCAAGATCATTGCTCC TCCTGAG	ACATCTGCTGGAAGGT GGACA	87
ADD2	TGCAGAGTCCCTCTTT CAGG	ATGAAGTCCGCGATCT GTCG	109
ASCL1	GTCTCCCGGGGATTTT GTAT	TCTCCATCTTGGCAGA GCTT	199
BLCAP	CGGCCGGCTCGACTA GAAGACTAA	CCCTCCGCTTTCTTCA ACCCTCAC	216
CFL1	CTCGTCTTCTGCGGCT CTCGG	CTTGCGCTTCTTCACC TCCTCTGG	147
CFLAR	AGGAGCAGGGACAAG TTACA	TCCTGAAGTTATTTGA AGGATCCT	100

Primer	Forward sequence	Reverse sequence	Product size (bp)
CHAT	ACCTACCTGATGAGCA ACCG	TTGTAGCAGGCACCAT ACCC	133
cMYC	AGCAGCGACTCTGAG GAGGAACA	GGACCAGTGGGCTGT GAGGAG	145
CTIP2	CGATGCCAGAATAGAT GCCG	GCTCCTCTATCTCCAG ACCC	146
CTTN	ACCCAGGTGTCCTCTG CCTACC	GCCTGTCCTCCTGCTC TTTCTCC	118
DARPP32	CTTCGGGAGCTGGGT TATCC	CCACAGGTTGTCTTTT GCCC	137
DLX2	AAGAGCAGCTATGACC TGGG	GGACTIONCTTTGGCTT CCCC	145
EMX2	CTACCCTCCTCGCACT CG	GGCTAGTGTCGTTCCC TTGG	127
FOXG1	CCCTCCCATTCTGTA CGTTT	CTGGCGGCTCTTAGA GAT	204
GAD67	GGCACGACTGTTTATG GAGC	GAGTTTATGGCGGTG CTTCC	135
GSX2	CCGCCACCACCTACAA CG	CCGTCCTCATCCTCTT GCC	102
HMBS	TGCCAGAGAAGAGTG TGGTGGGA	TTCCGAAGCCGGGTG TTGAGG	118
HPRT	CCTCCTCCTCTGCTCC GCCA	GGTTCATCATCACTAA TCACGACGCCAG	113
IL13RA2	TTTACTGGTATGAGGG CTTGG	AGGCTTGTTCTCTGAT GATCC	152

Primer	Forward sequence	Reverse sequence	Product size (bp)
Klf4	TCCTCCCGGCTTCCAT CCCC	TGTGGGTGGCGGTCC TTTTCC	182
Krox20	CCCTTTGACCAGATGA ACGG	TTTCTAGGTGCAGAGA CGGG	122
LHX3	GCGATGCTGCTGGAA ACG	GCTGCACTTGAGACAC TTGC	180
LHX6	CAACAACCTCATCTGG CACG	CGAATCGGCTGAAGTA GTCC	128
LHX8	GATTAGTGTGGAAGGT GCCC	GTGCATCTGGGTTGTT GTCC	140
LIN28A	GCAGCTTCTTCTCCGA ACCAACCC	GGCGCAGCCACCTGC AAAC	139
MAP2	CTCTCCCAAGACCTTC CTCC	TTCCCTGCTCTGCGAA TTGG	142
NANOG	AGCAATGGTGTGACG CAGAAGGC	TGGAAGGTTCCCAGTC GGGTTCA	99
NEUROD 1	CCGTCCGCCGAGTTT G	GCGGTGCCTGAGAAG ATTG	101
NKAIN2	CAGATTGTCCTCGCAC TGG	TGATAGCCATAAGAGT CAAAGCC	113
NKX2.1	AACCCAGACCCGCGC TT	GGGCCATGTTCTTGCT CAC	115
NNAT	CCAGCGGATCTCGGC AAACCC	CCTGCGCTCCCCAA CACCT	203
NTRK1	TCTCTCCTTCAACGCT CTGG	CACAAGAACAGTGCA GAGGG	101

Primer	Forward sequence	Reverse sequence	Product size (bp)
NTRK2	TCTGAACTGATCCTGG TGGG	CTTGCTGCTTTCATTC AGGC	126
NTRK3	CGCCAGTATCAACATC ACGG	TGTAGAGCTCCATGTC CACG	104
OCT4A	CTTCGCAAGCCCTCAT TTCACCA	GTCCGAGGATCAACC CAGCCC	154
PAX6	AGCACCAGTGTCTACC AACC	CGCTGTAGGTGTTTGT GAGG	109
PCDHB2	CTTTCTAAGGCGGTCG CTCC	CAGGACTTGCCTTTGT TTCGG	188
PFN1	GTGGAACGCCTACATC GACAACC	TGCCAACCAGGACAC CCACC	152
PLXNA2	AGTCCCATCAGCAGTA CACC	TTGACCTCCCGTAGAA CTCG	171
REX1	GTGCTTCGCGGTAACA GGGGT	GCGGTGAGTGGGGTG GGTTT	145
RPL39L	GATTTGCGTCCTAGAG TGGG	GGCCAGGAATCGCTT AATGG	178
RRS1	AAGCCTCAGCTGGAT GTGACTAGGG	CCTCCCTTTCTCTTGC CCTTCTGG	110
SMOC1	CATCAGTGGCTCTTCT GTGC	GACCCGTCATCTTTCC TTCC	102
SOX2	CAGCCCATGCACCGC TACGA	TCGGACTTGACCACC GAACCC	158
SPON1	AATTCGACAACAGAGT GATGAGG	TAAGCCTACGTTCCAG TCGG	104

Primer	Forward sequence	Reverse sequence	Product size (bp)
SST	AGTTTGACCAGCCACT CTCC	TTGGCCAGTTCCTGCT TCC	192
TH	AGCTCCTGAGCTTGTC CTTG	TGTCCACGCTGTACTG GTTC	234
TUBB3	GGCCTCTTCTCACAAG TACG	CCACTCTGACCAAAGA TGAAA	129
VPS13A	TGGAGAGAAGCACGA AAACTC	TGGGCATCCTTACATC CATGA	109
Viral SOX2- E2A- CMYC	ATGAGCCAGCACTACC AGAG	GGTGAAGCTAACGTTG AGGG	165
Viral OCT4- P2A-KLF4	GCATAGCAACTCTTCC GGA	GTTCTCCCGCCATCT GTT	194

Table 12: Media compositions

Medium	Composition
293T media	89% DMEM
	10% FCS
	1% PS
Ectoderm differentiation media	48.6% DMEM/F12
	48.6% Neurobasal
	0.5% N2-Supplement
	1% B27 Supplement (w/o VitaminA)
	1% PSG
	0.1% β -Mercaptoethanol
	0.2% BSA Fraction V 7.5%

Medium	Composition	
Endo- /Mesoderm differentiation media	76.9%	DMEM (high glucose)
	20%	FCS Gold
	1%	PSG
	1%	NEAA
	0.1%	β -Mercaptoethanol
	1%	α -Thioglycerol
Human Fibroblast media	87.6%	DMEM
	10%	FCS
	0.4%	Uridin
	1%	Sodium pyruvate
	1%	PS
iPSC proliferation media	77.8%	KO-DMEM
	20%	KO-Serum
	1%	NEAA
	1%	PSG
	0.2%	β -Mercaptoethanol
MEF feeder media	77.8%	KO-DMEM
	20%	KO-Serum
	1%	NEAA
	1%	PSG
	0.2%	β -Mercaptoethanol
MEF feeder media	87.9%	KO-DMEM
	10%	FCS Gold
	1%	NEAA
	1%	PSG
	0.1%	β -Mercaptoethano
MEF Isolation/Proliferation media	85.9%	DMEM (low glucose)
	12%	FCS
	1%	NEAA
	1%	PSG
	0.1%	β -Mercaptoethanol
N2 media	98%	DMEM/F12
	1%	N2-Supplement
	1%	PSG

Medium	Composition
N2B27 media	48.75% DMEM/F12
	48.75% Neurobasal
	0.5% N2-Supplement
	1% B27-Supplement (w/o Vitamin A)
	1% PSG

1. Cell culture procedures

1.1. Coating

One of the most crucial aspects of successful cell line passaging is the adhesion of living cells in the new cell culture dishes. Different cell types require different coatings in order to maximize the yield.

1.2. Matrigel

Matrigel coating was needed for proliferation conditions of smNPCs and during the induction phase of mDAN differentiations. Matrigel was thawed and prediluted with KO-DMEM at a ratio of 1:5. This predilution was aliquoted and stored at -20°C. Once needed it was further diluted at 1:20 to yield a working solution with a final dilution of 1:100. Application of 0.1ml/cm² resulted in a loading of approximately 9ug/cm². Although different lots had different protein concentrations it has to be noted that this was not accounted for and the dilution steps were never adjusted. The coated plates were stored one to seven days at 4°C before usage.

1.3. PLO/laminin

PLO/laminin coating was used during maturation of mDAN and the adherent steps of MSN differentiation. It was applied for direct coating of cell culture dishes as well as coating of glass cover slip. These coverslips were treated with 65% HNO₃ overnight, washed three times with ddH₂O, one time with abs. ethanol, air dried and sterilized for 4h at 180°C before coating. The first step was conducted by incubating a 15% PLO solution at 0.1ml/cm² overnight at 37°C. The dishes were then washed twice with PBS and one time with ddH₂O before letting them air dry. For the second step 50ug/ml laminin solution was prepared in PBS and 0.1ml/cm² were applied per dish and incubated overnight at 37°C. The solution was then aspirated and the wells were incubated with a 1:1 mixture of Neurobasal and DMEM/F12. Dishes coated this way were used right away or stored for up to one month at -20°C.

1.4. Gelatin coating

Gelatin coated dishes were used for iPSC culture. Bovine gelatin was solved in warm ddH₂O with a final concentration of 0.1%. It was then sterile filtered using a 0.22µM bottle top filter and stored in a 4°C fridge. For coating 0.1ml/cm² gelatin solution was added in cell culture dishes. These dishes were then incubated for at least 30min at 37°C before MEF Feeder were thawed and seeded on them.

1.5. Mouse embryonic fibroblast isolation

Fibroblasts of mouse embryos were used as co-culture of iPSC during proliferation. In this study, fibroblasts of CF-1 were used. Breeding and keeping of animals was carried out by a technical assistant at the experimental facility of the MTZ. Pregnant mice were sacrificed at embryonic day 12. Carbon dioxide was used to euthanize the mice before they were killed by cervical dislocation. The abdomen of the mouse was than sprayed with Mikrozid and opened with a scissor. Both uterus horns were investigated for embryos and dissected. The horns were put in 70% ethanol for 30 seconds and then transferred into a PBS filled petri dish under a clean bench. The embryos were exposed by opening the amniotic sac and removing the placenta. The head and red organs were removed to decrease the potential contaminations from undesired cells. The remaining body was minced and the tissue collected and centrifuged at 200g for 5min at RT. The supernatant was discarded and the pellet was resuspended in 1.5 times volume of trypsin solution. The solution was incubated for 5min at 37°C. Then the same volume of DNase I solution was added and incubation continued for 10 min. Cells were centrifuged at 200g for 5min at RT. Supernatant was discarded and the pellet resuspended with MEF isolation media. Cells were triturated with a 1000µl pipette and then filtered with a 100µm cell strainer. T150 flasks, which where pre-coated with gelatin for 30min, were used for attachment and proliferation of the isolated fibroblasts. The cell amount gained from 2-3 embryos was seeded into one flask. Media was changed after one day to clear the culture of dead and non-adhered cells. Cells were passaged once they reached confluency and splitted in a ratio of 1:3.

1.6. Generation of feeder cells

Fibroblasts proliferate very fast and have to be inactivated. Cells were treated with the DNA cross linker mitomycin C to be used as feeder cells when they reached a passage number of three. Fibroblast cultures that reached confluency were washed three times with PBS and then incubated with MEF media containing 10µg/ml MMC for 2h at 37°C. Cells were then washed three times with PBS and treated with trypsin until they detached. The reaction was stopped by adding the same volume MEF media to the flasks. Cell

suspension was collected, centrifuged at 200g for 5min and resuspended with DMEM. Cells were then counted and solved in MEF freezing media before they were aliquoted in batches of one or two million cells. MEF feeder cells obtained were stored in the -80°C and were used as co-culture layer for proliferation of iPSCs.

1.7. Human fibroblast culture

Fibroblast lines were obtained from patients clinically diagnosed with ChAc and sex/age-matched controls. The established lines were cultured in fibroblast media in T25 flasks and passaged once a week when confluency was reached. Splitting was done by washing the cells twice with warm PBS followed by incubation with 0.25% Trypsin/EDTA solution for 2min. The enzymatic reaction was stopped using serum-containing fibroblast media. The cell suspension was then collected and centrifuged 4 min at 200g. The cell pellet was resuspended in fibroblast media and either plated on new T25 flasks for expansion, prepared for cryopreservation or counted and used in reprogramming experiments. For long term storage cells were resuspended in freezing media containing 70% fibroblast media, 20% FCS and 10% DMSO, and aliquoted in cryo tubes. These tubes were then placed in freezing containers in a -80°C freezer overnight and then transferred to the liquid nitrogen storage.

1.8. Reprogramming

Prior to reprogramming, HEK 293T cells were thawed and cultivated on 10cm dishes using 293T media. Upon reaching confluency cells were washed twice with PBS and treated with 1ml 0.05% Trypsin/EDTA solution for 2 min at 37°C. The enzymatic reaction was stopped by adding 5 ml of the FBS containing 293T media and then the cell suspension was collected and centrifuged for 5min at 200g. The supernatant was aspirated and the pellet resuspended with 293T media. To keep the cells in proliferation the suspension was splitted at a ratio of 1:10. For the generation of virus supernatant, cells were counted using a Neugebauer counting chamber, and $5 \cdot 10^6$ cells were plated on one 10cm dish. One day after seeding the medium was changed to transfection medium containing 85% DMEM (high glucose) and 15% FCS without antibiotics. Two 2ml reaction tubes were prepared. In the first tube a total of 15µg plasmid DNAs and 45µl of polyethyleneimine (PEI) were mixed and incubated for 15min. The plasmid DNAs consisted of 3.19µg polycistronic *OCT4/KLF4/SOX2/MYCC* (OKSM) lentiviral vector, 7.66µg pMDLg/pRRE (expressing HIV-1 and gag/pol), 3.19µg pRSV-Rev and 0.96µg pMD2.G (vesicular stomatitis virus glycoprotein VSV-G). In the second tube DMEM (high glucose) was added. The added volume was 1ml minus the volume of the plasmids/PEI mix. After the incubation time the plasmid/PEI solution was added to the DMEM and

mixed thoroughly and incubated for 30min at RT. The final solution was pipetted to the 293T cells. To minimize the toxic effect of transfection agents the medium of the 293T cells was replaced with human fibroblast media 8h after transfection. The next day the virus containing supernatant of the 293T cells was collected and filtered using a 0.45µm PVDF. The virus solution was used right away or frozen in a -80°C freezer for short term storage. One day prior to infection, human fibroblasts were trypsinized, counted and seeded at specific cell density. In three wells of a 6 well plate 50000 cell/well were seeded and in two wells, 25000 fibroblasts were seeded. For infection all wells were treated at least two times with supernatant containing virus particles and one well of the 25000 and one well of the 50000 seeded cells was infected a third time. This procedure was chosen to have a broad range of virus particle to fibroblast ratio. The lowest ratio was therefore achieved in the two treatments/50000 cells condition and the highest ratio in the three treatments/25000 cells combination. This procedure ensured that within this range the optimal virus particle to cell ratio was present and iPSC were reproducibly obtained. On the day of the first infection, for each fibroblast line two 10cm dishes were coated with gelatin and 10⁶ MEF Feeders were freshly thawed and plated on these dishes. The next day the infected fibroblast were washed twice with PBS (Ca-/Mg-) and treated with 0.05% Trypsin/EDTA solution for 2 min. The reaction was stopped using fibroblast media and the suspensions from all wells were pooled and centrifuged for 4 min at 200g. The infected cells were then counted and seeded at a density of 25000 and 50000 cells per 10cm dish in fresh fibroblast medium containing 5ng/ml FGF2 and 1mM valporic acid. On the next day, half of the medium was replaced with iPSC proliferation medium supplemented with 5ng/ml FGF2 and 1mM valporic acid. From this time point on medium was changed daily to fresh iPSC proliferation medium containing 5ng/ml FGF2 and 1mM valporic acid. The valporic acid was omitted once first colonies emerged. After two weeks, the media was aspirated and the cells were treated with collagensase IV for 5 min. The collagenase was discarded and fresh iPSC medium was applied. The colonies were morphologically selected, picked into 12well and cultivated until good looking colonies were visible. This was continued until stable and morphologically bona fide lines emerged. Once a stable line was generated, iPSC were propagated on 6 well plates and characterized via alkaline phosphatase-staining, silencing analysis by PCR, pluripotency staining as well as three germ layer formation by immunocytochemistry and karyotyping.

1.9. iPSC culture

After successful reprogramming and characterization of iPSC the stable lines were propagated and repeatedly subjected to cryopreservation and thawing. Normal expansion

procedure included daily media change with iPSC medium supplemented with 5ng/ml FGF2 and passaging using either a picking or a cleaning approach. Once the cells were in culture for one week, the MEF feeder started to detach and the media was changed to a mixture of conditioned iPSC medium and fresh iPSC medium. The day prior to passaging, MEF feeders were seeded at a density of 250000 cells per 6 well. Two hours before the start of the passaging procedure, the medium of these feeders was changed to iPSC medium supplemented with FGF2 and the Rhok inhibitor Y-27632. Cleaning was used when the lines had only a minor contamination with differentiated or morphological aberrant colonies. These were mechanically detached and discarded using a stereo microscope and pipette tips that were located under a clean bench. The remaining bona fide iPSC colonies were treated for 5min at 37°C with 1mg/ml collagenase IV solution. The enzyme containing medium was then aspirated and the cells were treated with iPSC medium without growth factors. Then the colonies were detached using cell scrapers, pooled, centrifuged at 100g for 1min and plated at a ratio of 1:4 on freshly prepared 6 wells containing MMC treated MEF feeders. The picking technique was used when there were only few bona fide iPSC colonies present in the well. Supernatant was aspirated and 1mg/ml Collagenase IV added and incubated for 5min at 37°C. Enzyme solution was then aspirated and iPSC media w/o growth factors was applied to the cells. Using the stereo microscope single colonies were detached as a whole and transferred to the 6 well containing MEF feeder using a 10µl pipette. Wells were rested for at least 20h to ensure proper attachment. Media was changed the next day to iPSC media supplemented with FGF2 and Y-27632.

For cryopreservation, cells were grown until large, undifferentiated colonies emerged. Wells were then subjected to the cleaning method of passaging. After centrifugation the cell pellet was resuspended with iPSC freezing media: 40% KO-DMEM, 50% KO-Serum, 10% DMSO and 10µl Y-27632. One well of iPSC was resuspended in 2ml freezing media and divided in two cryo tubes. These tubes were then placed in freezing containers and transferred to a -80°C freezer. One day after this, cryo tubes were transferred to liquid nitrogen tank for long term storage.

One day before thawing of iPSC lines, MMC treated MEF feeder were seeded on 6 well plates at a density of 250000 cells per well. 2h before thawing the medium of the feeder was replaced by iPSC medium supplemented with FGF2 and Y-27632. Cryo tubes were taken from liquid nitrogen storage and warmed in the water bath until there was only a small fraction of ice left. Cell solution was then mixed with 2ml of cold iPSC media to dilute the DMSO and centrifuged at 100g for 1 min. Supernatant was discarded and cells were

resuspended in prewarmed feeder conditioned iPSC media and then plated on one 6 well. For two days after thawing media was replaced daily with iPSC media supplemented with FGF2 and Y-27632. From day three on Y-27632 was omitted and cells were normally cultured.

1.10. Culture of small molecule neuronal precursor cells (smNPC)

SmNPCs were kindly provided by Jared Sternecker and received at early passage numbers. The cells were grown on matrigel coated plates, which were prepared one day prior to thawing or passaging. N2B27 media was supplemented with 3 μ M CHIR99021, 150 μ M ascorbic acid (AA) and 0.5 μ M purmorphamine (PMA) and changed every other day during proliferation phase. Cells were initially seeded at a density of 150000 cell/cm². Confluency was reached roughly one week past seeding. For passaging or initiation of differentiation, cells were washed twice with warm PBS and treated 10min at 37°C with accutase. The enzymatic reaction was stopped by adding double the volume of warm DMEM/F12. The cell suspension was collected and centrifuged at 250g for 5 minutes. The supernatant was then discarded and the cells were resuspended in 1ml warm N2B27 media supplemented with growth factors. The suspension was diluted 1:100 and counted using a Neugebauer counting chamber.

1.11. MSN differentiation

Medium spiny neurons were obtained by applying a multistep protocol starting from iPSCs. The iPSCs were cultured in 6 wells under normal proliferation conditions until the colonies reached a considerable size and had a low level of spontaneous differentiation. Partly differentiated or morphological aberrant colonies were scraped off under the stereo microscope. These bad colonies were discarded with the supernatant and 2mg/ml collagenase IV solution was applied for 1h. After this incubation the colonies were detached as a whole by gentle pipetting. Colonies were collected and allowed to settle by gravity for 5 min. Collagenase containing supernatant was discarded and the cells resuspended in 10ml iPSC media supplemented with 5 μ M Y-27632, 1 μ M IWP2, 1 μ M dorsomorphin and 10 μ M SB-431542 and transferred to 3cm non adherent petri dishes. This first step led to the formation of embryoid bodies (EBs). Media was replaced every other day (See Figure 5). From day 6 to day 10 dorsomorphin and SB-431542 were omitted from the media but 0.2 μ M PMA was added. On day 12, the EBs were plated on two matrigel coated 6well plates. Media was thereafter changed to patterning/maturation condition consisting of N2B27 media supplemented with 20ng/ml BDNF, 10ng/ml GDNF and 0.5 μ M dbcAMP. After one week cells were passaged by washing twice with PBS and incubating with accutase for 10min. The reaction was stopped with 1.5 fold volume of

DMEM/F12 and cells were collected and centrifuged at 250g for 5 min. Cells were resuspended in maturation media and plated on freshly prepared matrigel plates. This expansion step accumulated progenitor cells and generate a homogenous culture. After another week of expansion, cells were passaged a second time using the same strategy as before. Prior to seeding the cells were counted and plated at the following densities: 800000 cells/6well, 200000 cells/4 well, 50000 cells/96 well and 300000 cells/MFC. Developing neurons were left in maturation media for at least 2 weeks before experiments were conducted.

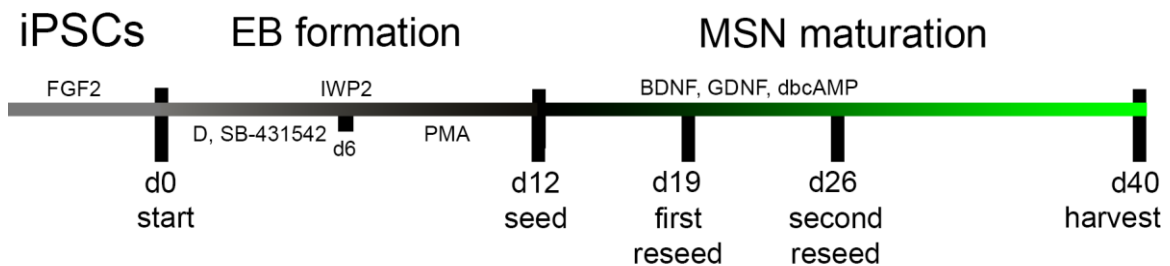


Figure 5: MSN differentiation scheme

1.12. mDAN differentiation

Midbrain dopaminergic neurons were differentiated using a multistep protocol. Initially 400000 smNPCs per line were seeded in a well of a 6 well plate and media was changed every other day. For the first 2 days cells were cultivated under normal proliferation conditions using N2B27 supplemented with 3 μ M CHIR99021, 150 μ M AA and 0.5 μ M PMA. On day 2 media was changed to induction conditions which used N2B27 supplemented with 200 μ M AA, 10ng/ml FGF8 and 1 μ M PMA. On day 10 cells were split and reseeded into their final format. For ICC, cells were placed in 4 well plates with coated cover slips at a density of 200000 cells/well. For survival analysis and live cell imaging of total network, cells were seeded on 96 well plates at a density of 50000 cells/well. For further RNA and protein isolations, cells were seeded in 6 wells at a density of 800000 cells/well (See Figure 6). For compartmentalized analysis of live cell imaging, MFC were used and 300000 cells were injected per macro channel. Maturation media consisted of N2B27 supplemented with 20ng/ml BDNF, 10ng/ml GDNF, 1ng/ml TGF β 3, 0.5mM dbcAMP and 200 μ M AA. After the reseed the media was changed every other day. Cells were cultured under maturation conditions until they were treated or harvested for further analysis.

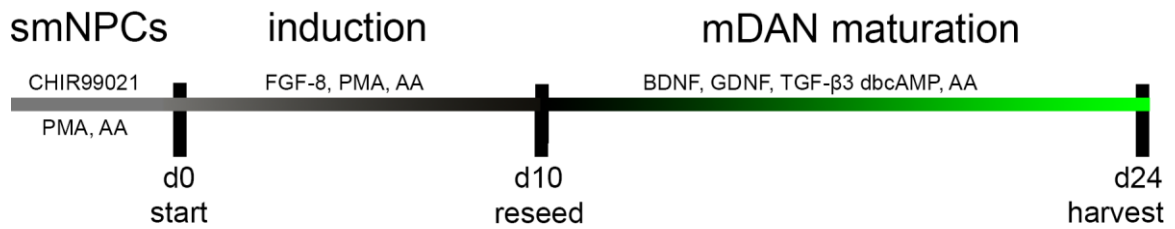


Figure 6: mDAN differentiation scheme

2. Nucleic acid biochemistry

2.1. mRNA isolation

mRNA isolation was achieved by using a kit. All procedures were done according to the manufacturer's recommendations. In the final step DNase and RNase free PCR grade water was used to elute RNA. RNA was measured using an eppendorf photometer and calculating RNA concentration using the 260nm readout and assessing the quality using the 260nm/280nm and 260nm/230nm ratio. Isolated RNA was stored in -80°C freezer before cDNA was generated.

2.2. cDNA generation

cDNA was generated using a Reverse Transcriptase Kit and conducted according to manufacturer's instructions. cDNA was generated using 1000ng of RNA as assessed with the Eppendorf photometer. In case total RNA amount was lower than 1000ng, as much RNA as possible was used. Samples with a total RNA amount of less than 200ng were not used. Generated cDNA was stored in -20°C freezer before PCR analysis.

2.3. Polymerase chain reaction (PCR)

Polymerase chain reaction was conducted using the commercially available kit Brilliant II SYBR Green QRT PCR. PCR setup and primer design was done in compliance to the MIQE guidelines (Bustin, et al., 2009). The kit contained a premixed reaction solution with the necessary dNTPs, H₂O, MgCl₂ and the reference dye ROX. Master mixes were prepared as follow:

X+1x12.5µl	Sybr mix
X+1x1µl	cDNA
X+1x7.5µl	dH ₂ O

X: number of reactions

21µl of the mix was then pipetted into a white 96 well PCR plate. 4µl of a 10µM primer mix was pipetted into the wells to yield a final reaction volume of 25µl. The plates were centrifuged for 1min at 200g and then transferred into the preconditioned MX Pro 3000 PCR devices. For quality control, no-template-controls (NTC), positive and negative controls were used. The software was configured as follows:

Table 13: Setup of PCR experiments

Segment	Temperature	Time	Function
Segment one - activation	1 Cycle		
	95°C	15 min	activation of polymerase
Segment two - amplification	40 Cycles		
	94°C	15 sec	melting of DNA
	57°C	30 sec	annealing of primers
	72°C	30 sec	elongation of DNA fragment fluorescent measurement for amplification plot
Segment three - dissociation	1 Cycle		
	94°C	60 sec	melting of DNA
	55°C	30 sec	annealing of all products
	ramp to 95°C with at least 0.5°C difference per step		fluorescent measurement for dissociation plot
	95°C	30 sec	melting of DNA

After the PCR was conducted, fluorescent thresholds were calculated using the adaptive baseline approach of the MxPro software. For further quality control amplification and dissociation plots were interrogated and PCR products were analyzed using agarose gel electrophoresis to determine fragment size. qPCR results were evaluated using the $\Delta\Delta C_t$ method.

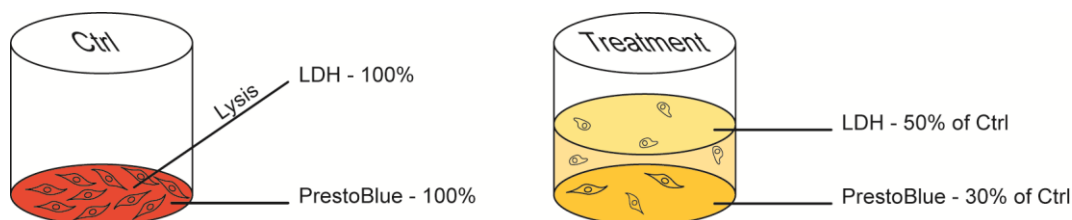
2.4. Agarose gel electrophoresis

Fragment size of the product of a newly established primer combination was investigated as a part of quality control after qPCR experiments. This was achieved by agarose gel electrophoresis. A 2% agarose gel was cast using TAE buffer containing 40mM Tris,

20mM acetic acid, and 1mM EDTA and a 1:20000 dilution of the nucleic acid stain RedSafe. PCR reactions were mixed with 5µl loading buffer and 8µl of the mixture were pipetted into each well of the cast agarose gel. Electrophoresis was conducted with 140V and 80mA for 1h before a picture was taken at the gel documentation using the transilluminator and saved as tiff.

3. Cell survival analysis

Cell survival experiments were done on mature neurons of MSN and mDAN differentiated cultures. Stressors were applied one week after the last reseed. Cells were incubated with stressors and mock controls over the course of 6 days. The stressors used were tunicamycin, an inhibitor of N-linked glycosylation that cause ER related unfolded protein response (UPR) or L-canavanine, an arginine analogue that is incorporated during protein biosynthesis by the cell and causes protein misfolding (Chan and Egan, 2005; Mytilineou, et al., 2004). Supernatants were collected and pooled for lactate dehydrogenase (LDH) release assay on day 3 and day 6. PrestoBlue assay was conducted on day 6. Cell composition was calculated for day 6. To achieve this, the following model was used. The initial assumption is that on day 6 a certain amount of cells is dead and released its LDH in the supernatant while another fraction is still metabolic active. Since PrestoBlue and the LDH positive control, where all attached cells are lysed, are done in the same well, normalization was set to 100%.



$$\text{cell composition at point of measurement: } \frac{30\%}{30\%+50\%} = 37,5\% \text{ living}$$

Figure 7: Scheme for the assessment of cell composition at time point of measurement

3.1. PrestoBlue cell viability assay

PrestoBlue assay was carried out according to manufacturer's recommendations. The working solution was prepared by diluting the stock solution with phenol red free N2B27 at a ratio of 1:10. The cells were incubated 4h with 55µl of the working solution in the 37°C incubator. The same volume was incubated under cell free conditions and used as a

negative control. 50µl of the incubated supernatant were analyzed with a Tecan Sunrise absorbance plate reader using the following settings:

Measurement wavelength:	570nm
Reference wavelength:	600nm
Shake duration (inside low):	2sec
Shake settle time:	2sec
Number of kinetic cycles:	3

Reference corrected OD values were normalized to mock control conditions.

3.2. Cytotoxicity detection kit:

The cytotoxicity detection kit was based on the lactate dehydrogenase (LDH) assay. LDH is released by a cell upon its death into the supernatant and can be measured subsequently. The amount of LDH is direct proportional to the amount of cell death (Burd and Usategui-Gomez, 1973). The assay used contains a tetrazolium salt that is turned over to its formazan form when exposed to electron donors like NADH. NADH is produced by LDH that is released by the dead cells and sodium lactate, which is provided by the assay. The amount of formazan can be assessed by absorption measurements in a plate reader. One of the limiting factors of this assay is that the half-life of free LDH in supernatant is only nine hours. Since the whole treatment was conducted over six days, the LDH released in the very beginning has already been degraded on day 6. In order to overcome this problem supernatant was pooled on day 3 and day 6. Keeping the decay of LDH in mind, it is, however, possible to estimate whether the cell death occurred earlier or later in the treatment. To eradicate minute differences in the ratio between stem cells and motor neurons in patient lines vs. wild type lines, as well as the different absolute cell amounts in between experiments, mock controls were carried out for each line and experiment.

Cytotoxicity detection kit was used according to manufacturer's instructions. Working solution was prepared freshly by diluting the catalyst with the dye solution at a ratio of 1:46. 50µl of the pooled supernatant was mixed with 50µl of the working solution. Working solution mixed with phenol red free N2B27 was used as a negative control. Mock treated control wells were incubated with 0.5% triton X-100 for 30 min and the lysate was mixed with working solution and served as positive control. The reaction volume was then incubated for 25min at RT. Then the plate was centrifuged 5min at 200g to eliminate

bubbles. Samples were measured in the Tecan Sunrise absorbance plate reader using the following settings:

Measurement wavelength:	492nm
Reference wavelength:	620nm
Shake duration (inside low):	2s
Shake settle time:	2s
Number of kinetic cycles:	3

Reference corrected OD values were normalized to triton X-100 lysed controls.

3.3. DNA damage analysis

DNA damage was assessed by staining of γ H2A.X. This method investigates the phosphorylation of serine 139 of the histone H2A.X. This modification is initiated by the cell very quickly after detection of DNA double strand breaks (DSB) and is a marker for DNA damage (Kinner, et al., 2008). Treatment with 10 μ M Etoposide for 1h was done as positive control, since Etoposide is known as an inducer of DSB in cells (Long, et al., 1985). To identify and quantify the DSB, Apotome microscopy was conducted using a 63x oil objective. Analysis of the spots was done in Fiji using a semi-automated macro.

4. Metabolic characterization

Analysis of mitochondrial activity was carried out using the Seahorse XFe96 analyzer. This device is capable of measuring changes in the pH value and the oxygen concentration simultaneously in real time. The layout of the probe and the well plate is designed to create a cavity with a small volume of approximately 2 μ l. Cells that are captured in this region cause a shift in pH and oxygen, which can be measured. The utility plate of the measurement stack provides four ports that can be used to inject substances that modulate the metabolic activity of the investigated cells. The default assay medium is a pH of 7.4 unbuffered, glucose-free solution. The cells are measured in five sets of three measurements. After an initial calibration the substances in the ports are injected one by one. Before each individual measurement the plates are mixed and the cells are allowed to settle. The setup up of the whole experiment is depicted in Table 14.

Table 14: Experimental setup of Seahorse XFe96 device

Section	Substance	Measurement
Calibration	-	3 cycles: 3 min shaking
Baseline activity		1 min resting 5min measurement
Port A	10mM glucose	3 cycles: 3min shaking
Glycolytic increase	1mM pyruvate	1min resting 5min measurement
Port B	1µM oligomycin A	3 cycles: 3min shaking
Coupling efficiency		1min resting 5min measurement
Glycolytic Reserve		5min measurement
Port C	0.7µM FCCP	3 cycles: 3min shaking
Spare respiratory capacity		1min resting 5min measurement
Port D	50mM 2-DG	3 cycles: 3min shaking
non-respiratory oxygen consumption	1.5µM rotenone	1min resting 5min measurement
non-glycolytic extracellular acidification	2.5µM antimycin A	5min measurement

The first port was used to inject glucose and pyruvate to start the glycolysis and oxidative phosphorylation. The increase in the extracellular acidification rate (ECAR) compared to the basal level is the glycolytic increase. The second injection was used to add oligomycin A, an inhibitor of complex V. This causes a drop in oxygen consumption due to the inability of the mitochondrion to convert the proton gradient into chemical energy. The only remaining oxygen consumption results from the activity of endogenous uncoupling protein like UCP1 (Nicholls, et al., 1978). Therefore coupling efficiency can be calculated. Furthermore the cell has to rely solely on glycolysis to meet its energy demand. This increase in extracellular acidification rate is reflecting the glycolytic reserve. The third port harbors FCCP, an uncoupling agent that diminishes the proton gradient and thereby increases the oxygen consumption. This happens because the mitochondrion tries to

reestablish the proton gradient and a major component of this machinery is the oxygen dependent complex IV of the electron transport chain. The spare respiratory capacity can be obtained from this data. The last port is used to inhibit glycolysis with 2-deoxy-D-glucose (2-DG), a competitive inhibitor of the phosphoglucosomerase, and to inhibit the oxidative phosphorylation by inhibition of complex I with rotenone and complex III with antimycin A. The remaining oxygen consumption and extracellular acidification is contributed by non-respiratory and non-glycolytic processes.

5. Protein biochemistry

5.1. Alkaline phosphatase staining

Staining of alkaline phosphatase (AP) was conducted according to manufacturer's instruction.

5.2. Preparation of immunocytochemistry samples

All cells were washed two times with warm PBS and then fixed with 4% warm PFA pH 7.4 solution for 12min. After fixation cells were washed three times with PBS. If the desired antigen was a surface protein no permeabilization step was conducted. Otherwise a treatment of 0.2% triton X-100 in PBS was used to permeabilize the cells. Blocking solution was made by using PBS and adding the following ingredients:

1%	bovine serum albumin
5%	donkey serum
0.3M	glycine
0.025%	triton X-100

Fixated cells were incubated with blocking solution for one hour. Primary antibody combinations were used according to Table 15 and solved in blocking solution. Incubation was done overnight at 4°C.

Table 15: Primary antibody combinations used for ICC grouped by their application

Pluripotency					
ms Sox2	488	rb Nanog	594	-	
rb Oct4	488	ms Lin28A	594	-	
ms SSEA4	488	-		rat SSEA3	647
-		ms Tra 1_60	594	-	

Three germ layer formation: ectoderm

rb Nestin	488	ms Tuj1	594	-
ms MAP2	488	rb S100 β	594	-
rb Olig2	488	ms Vimentin	594	-
ms Galc	488	-	-	-

Three germ layer formation: endoderm

ms α -Fetoprotein	488	gt Gata4	594	-
rb Gata6	488	ms β -Catenin	594	-

Three germ layer formation: mesoderm

ms Pecam-1	488	rb Flk-1	594	-
ms SMA	488	rb Fibronectin	594	-

mDAN differentiation

ms Sox2	488	rb Nestin	594	ch Tuj1	647
rb TH	488	ms MAP2	594	-	
ms Galc	488	rb S100 β	594	-	
ms CytochromeC	488	ch MAP2	594	-	

MSN differentiation

ms Sox2	488	rb Nestin	594	ch Tuj1	647
rb Darpp32	488	ms MAP2	594	-	
ms Galc	488	rb S100 β	594	-	
ms MAP2	488	rb GABA	594	-	
rb Chat	488	ms MAP2	594	-	
ms Cytochrome C	488	ch MAP2	594	-	

The samples were washed three times for 5-10min. Secondary antibodies were solved in blocking solution and incubated for one hour. Antibody solution was then aspirated and the samples washed three times with PBS. Cell nucleus staining was achieved by application of a solution containing 0.75 μ l Hoechst33342/ml PBS was prepared and applied to the cells for 5 min. Samples were washed again three times and then mounted

on object slides using fluoromount as mounting media. Samples were stored overnight at 4°C and for further preservation, coverslips were enclosed with nail polish to prevent movement. Samples were stored in 4°C fridges for microscope analysis.

5.3. Isolation of globular and filamentous actin

In order to assess the ratio of globular (G) and filamentous (F) actin a protocol from Papakonstanti was modified (Papakonstanti and Stournaras, 2007). Two 6 wells of matured neurons were first washed with ice cold phosphatase inhibitor. The solution was then discarded and the cells incubated 5min with 200µl cold G-actin extraction buffer. The soluble fraction was then collected and stored at -80°C. 200µl of cold RIPA buffer was put in the well. Then the cells were scraped off, collected in a 1.5ml reaction tube and incubated on ice for 15min. To separate the insoluble fraction the tube was centrifuged +10000g for 2min at 4°C and the supernatant was transferred into a new tube while the pellet was discarded. The F-actin containing fraction that was obtained was stored at -80°C before analyzed with western blot. Importantly, this protocol does not use any internal protein control or prior protein quantification but the ratio of G vs F actin is assessed solely by applying the same volume of G and F actin containing lysates.

RIPA Buffer:

1% TritonX-100
50mM Tris-HCl
0.15M NaCl
1% Sodiumdeoxycholate
0.1% SDS
1mM EDTA
1mM DTT
pH 7.4
1% Protease Inhibitor Cocktail

Extraction Buffer:

0.3% Triton X-100
5mM Tris-HCl
300mM Sucrose
2µM Phalloidin
2mM EGTA
pH 7.4
1% Protease Inhibitor Cocktail

5.4. Whole cell protein Isolation

Whole cell protein was isolated from one 6 well of matured neurons. Remaining media in the wells was first discarded and then the wells were washed with ice cold phosphatase inhibitor. Cells were then scraped off, collected in 1.5ml reaction tubes and centrifuged for 4min at 250g. The inhibitor solution was then aspirated and the pellet resuspended in 60µl cold RIPA buffer. Lysis buffer was incubated for 15min on ice. The samples were then

centrifuged for 2min at +10000g to precipitate the insoluble fraction. Supernatant was collected and stored in a -80°C freezer.

5.5. Cytosolic protein isolation

Cytosolic protein extraction was done to increase the yield of CHOREIN in the sample and solely conducted for CHOREIN western blot experiments. The nuclear extraction kit of Active motif was used and protocol was stopped at the step of separation of cytosolic and nuclear fraction. Until this point the protocol was followed according to the manufacturer's recommendations.

5.6. Protein concentration measurement

Protein concentration was assessed using a modified Bradford assay in conjunction with an absorbance plate reader. The used assay was modified from the commercial available kit Rothi Nanoquant. For each experiment, a complete standard curve consisting of premade solutions containing 0, 5, 10, 25, 50 and 75ng/μl BSA was measured and the content of the samples was calculated using a linear regression method. First the working solution was prepared by diluting the concentrate stock 1:5 with RNase/DNase free water. 40μl of the standard solutions were mixed with 160μl working solution in a well of a 96 well plate. 1μl of each sample were mixed with 39μl RNase/DNase free water and 160ul working solution. The complete plate was then analyzed using the following measurement parameters:

Measurement wavelength:	450nm
Reference wavelength:	590nm
Shake duration (inside low):	2sec
Shake settle time:	2sec
Number of kinetic cycles:	3

Data was exported to Excel and the 450nm/590nm ratio was plotted over the concentration and a linear regression was calculated for the standard curve. Protein content of the unknown samples was calculated using the standard curve parameters and a dilution coefficient of 40.

5.7. Western blot

Protein samples were thawed up on ice. For each lane 3μl of NuPage loading buffer were added to 18μg protein and filled up with ddH₂O to yield a final volume of 12μl. All samples were heated to 95°C for 5min before cooling down on ice and centrifugation. Pre-cast gels

were prepared and set up in the gel electrophoresis container. The box was then filled with the running buffer according to the gel type used. Markers for the determination of the electrophoresis process included SeaBlue and Magic marker. A volume of 10µl containing 15µg of protein was loaded into the wells of the prepared gel. Voltage, ampere and time course were selected individually for the corresponding application (See Table 16).

Table 16: Settings for SDS PAGE electrophoresis for different applications

Application	Voltage	Ampere	time
CHOREIN western blot	90V for the first cm then: 140V	60mA	2h
Cytoskeleton analysis	140V	60mA	1-1,5h

Successful electrophoresis was determined by the separation of bands within the reference marker lanes. Then the protein containing gels were transferred to nitrocellulose membranes using the iBlot dry blotting system. The gels were first incubated in transfer buffer solution for 9min. The blotting stack was assembled according to the manual. Blotting conditions were optimized for the corresponding application. Blotting of CHOREIN was done using program 3 (20V) for 12min and analysis of cytoskeleton proteins used the same program for 9min. After the blotting process was finished, the membrane was cropped for application of desired antibodies and blocked for 1 hour using 5% milk powder solved in PBS with 0.05% Tween-20 (PBS-T). Primary antibodies were solved in a PBS-T containing 1% milk powder. The membrane was incubated in the primary antibody solution overnight at 4°C and then washed three times with PBS-T. Secondary antibodies were solved in PBS-T containing 1% milk powder and applied to the membrane for 1h at RT. Membranes were washed afterwards four times with PBS-T. Membranes were developed using Amersham ECL kit according to the manufacturer's instructions and developed using the LAS3000 imaging system with settings according to Table 17.

Table 17: Settings for Western Blot development

	Mode	Sensitivity	Exposure	Aperture	Light
Overview	Precision	Standard	1/100 sec	2.8	White Epi
ECL development	Increment	Standard/ High	10sec	0.8	Off

Representative pictures were converted to tiff and analyzed using the TotalLab Quant software. The pictures with the highest dynamic range and no overexposed pixels were chosen for evaluation.

6. Live cell imaging

Live cell imaging was conducted on mature neurons obtained from both differentiation protocols in either 96well plates or MFC. These cells were treated 2 days prior to imaging with 10mM glycolate and 10mM D-lactate, 10 μ M phalloidin, 0.1% DMSO or 10 μ M PP2. Either the combination of MitoTracker Deepred with LysoTracker Red or the mitochondrial potential marker JC-1 was imaged. The utilized concentration can be seen in Table 18.

Table 18: Tracker and concentrations used for live cell imaging

Tracker	Final concentration
MitoTracker Deepred	50nM
LysoTracker Red	50nM
JC-1	200nM

All videos were taken with a 100x 1.4 objective. The time interval between two images was fixed to 0.3 seconds and was controlled by a hardware sequencer. Each video was imaged for 2minutes resulting in a set of 400 images. Gain was set to 300 and the exposure times to 115ms. These settings were not changed between videos. Brightness of the obtained images was regulated by adjustment of the laser power.

The dye JC-1 was used to visualize the mitochondrial potential. This dye has a free form that exhibits green fluorescence (Smiley, et al., 1991). In the presence of a proton gradient induced potential, the dye forms J-aggregates that have a shift in fluorescence towards red. When a mitochondrion is excited by 488nm, the ratio of the resulting green and red fluorescence is an indicator for its membrane potential. Intensity in the channels of the JC-1 images was assessed by a semi-automated macro. Analysis of morphological features of lysosomes and mitochondria was achieved using a semi-automated macro on single images. Trafficking analysis is carried out with the whole video using the TrackMate plugin provided with the Fiji suite. KNIME was used for data mining the resulting files.

The filter criteria and settings for TrackMate were as follows:

Detector:	DoG detector
Estimated radius:	0.8
Quality:	100
Tracker:	Linear motion LAP tracker
Kalman radius:	1.25
Initial distance:	2
Max linking distance:	2
Gap Closing:	2
Track duration:	3

There was no further filter added in the subsequent analysis. In the first step of the work flow of the data analysis, all individual tracks of every video of each individual line within one experiment were pooled. A histogram with 100 segments ranging from 0 to 100 μ m with an equidistant binning allowed brief investigation of the distribution of the tracks. In the next step the probability of an object moving further than a particular displacement was calculated. Then the complementary cumulative distribution function of this probability was plotted. The resulting graph resembled an exponential decay (See Figure 8).

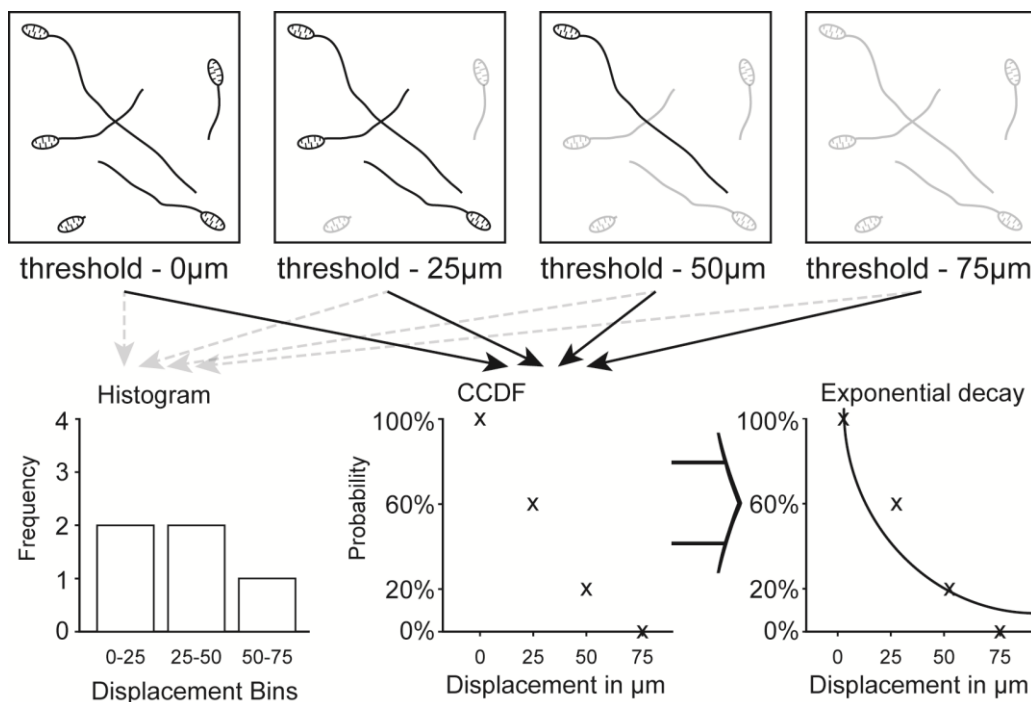


Figure 8: Scheme of processing work of tracking analysis. CCDF = complementary cumulative distribution function.

Regression analysis was used to obtain parameters of a two phase exponential decay with the following equation: $Y = N_{first}e^{-k_{first}X} + N_{second}e^{-k_{second}X}$. The first decay, which occurs at short distances, describes the distribution of stationary tracks while the second decay can be interpreted as the influence of the actual moving tracks on the data. In the next step the crossing point of the first derivatives of both functions was calculated using following equation:

$$X_{cross} = \frac{\ln\left(\frac{k_{first}N_{first}}{k_{second}N_{second}}\right)}{k_{second} - k_{first}}$$

This distance represents the point where the fraction of moving tracks starts to have bigger influence on the overall data than the stationary fraction. In the last step, all tracks that moved less than this distance were considered stationary and all tracks the displaced further were considered as moving.

7. Statistics

All statistics shown in this work were calculated using GraphPad Prism. When experiments with one independent variable and only two groups were analyzed, a t-test was conducted. When the variances were different in between the two groups, Welch's correction was applied. Experimental setups with one independent variable but more than two groups were analyzed using a one-way ANOVA. Multiple comparisons were corrected using Tukey's procedure. In case the experiment was comprised of two independent variables, a two-way ANOVA was calculated. Tukey's procedure was used for the correction of multiple comparisons. Furthermore for each statistical analysis the effect size ω^2 was calculated.

Results

1. Generation of induced pluripotent stem cells

Patient and control fibroblast lines were expanded and prepared for the reprogramming procedure. Successful infection was confirmed by analyzing the expression of the dtTomato reporter (see Figure 9). The yielded iPSC were then morphologically selected and clonally picked. The first experiments were aimed to identify bona fide clones for characterization.

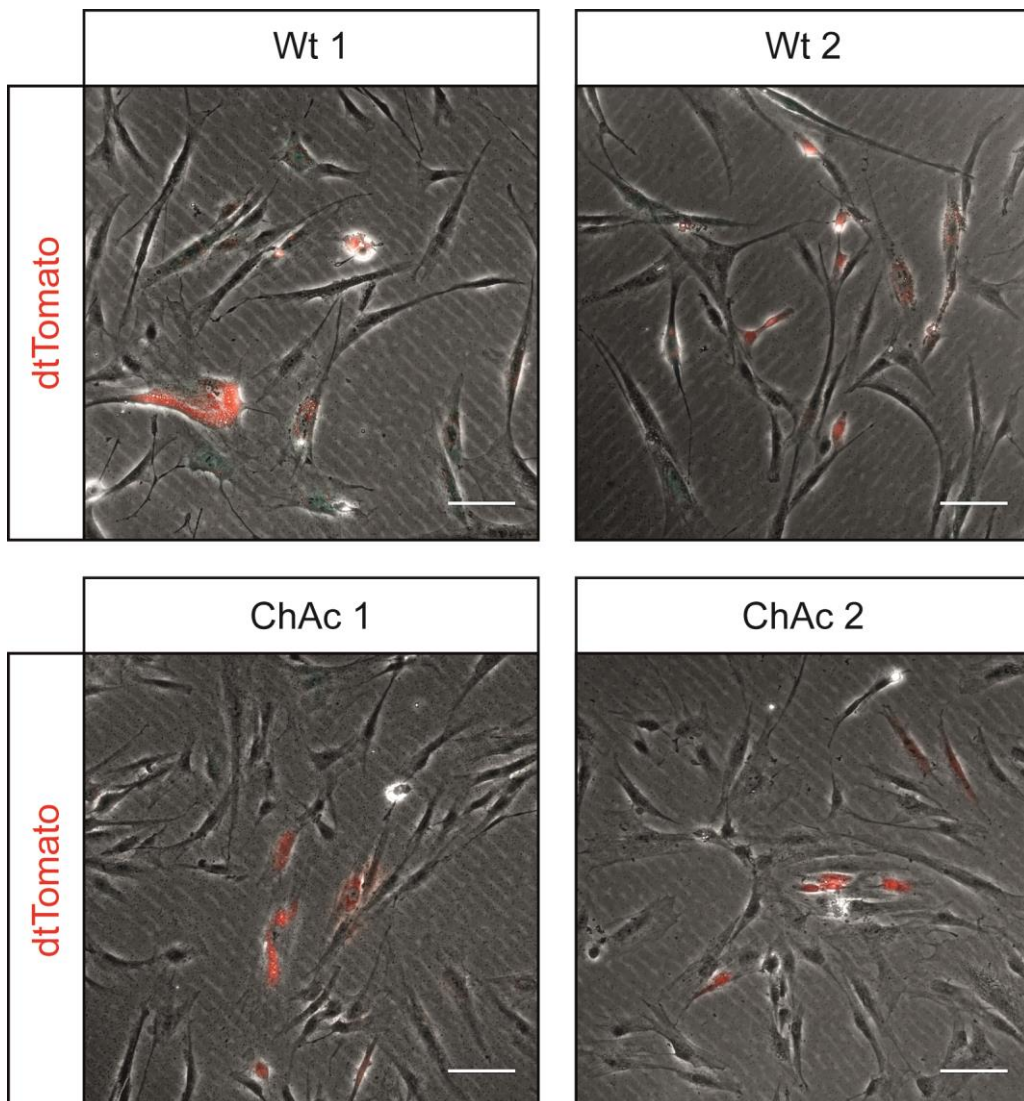


Figure 9: Successful infection: Representative pictures of freshly infected human fibroblast lines from wild type controls or ChAc lines. DtTomato expression is a sign of successful infection and virus integration. Not all cells were infected. Scale bar = 50µm.

1.1. Silencing of exogenous transcription factors

All clones that had a stable and good looking morphology were checked for the silencing of the exogenous transcription factors. Silencing is important for differentiation capacity, reproducibility and reliability of the further obtained results. Silencing is also mandatory for good practice of iPSC culture as published by Maherali and Hochedlinger (Maherali and Hochedlinger, 2008). Silencing was investigated by qPCR. The expression of lentiviral mRNA was calculated relative to GAPDH and relative to the total expression of the transcription factor, including viral and endogenous expression. Thereby the contribution of the residual expression of the integrated virus was estimated. A clone was considered as silenced, when the expression relative to GAPDH was below 0.2% and the mean residual contribution relative to the total expression of the transgene was less than 5%. In total 14 clones were analyzed at low passage numbers (\leq P10). One clone had to be cultivated significantly longer than the others before yielding a stable morphology. 10 clones displayed bona fide silencing of transgenes, while four clones maintained substantial expression above the threshold. One of the clones however did meet the necessary requirement when analyzed again at higher passage number (see Table 19).

Table 19: Silencing of generated iPSC lines

Cell line	Passage	Silencing relative to GAPDH	Mean residual contribution (transgenes above 5%)	Continued
ChAc 1.1	P5	0.27%	17.6% (<i>OCT4</i> , <i>KLF4</i> , <i>cMYC</i>)	-
ChAc 1.1	P16	0.03%	16.45% (<i>OCT4</i> , <i>KLF4</i> , <i>cMYC</i>)	-
ChAc 1.1	P39	0.04%	23.12% (<i>OCT4</i> , <i>KLF4</i> , <i>cMYC</i>)	Yes
ChAc 1.2	P7	0.04%	1.9%	Yes
ChAc 1.3	P7	0.05%	2.4% (<i>KLF4</i>)	Yes
ChAc 1.4	P5	0.01%	0.6%	Yes
ChAc 1.5	P5	<0.01%	0.5%	Yes
ChAc 2.1	P21	0.05%	1.4%	Yes
ChAc 2.2	P10	0.79%	25.6% (<i>OCT4</i> , <i>KLF4</i> , <i>cMYC</i>)	No
wt 1.1	P6	<0.01%	2.01% (<i>KLF4</i>)	No
wt 1.2	P10	<0.01%	0.2%	Yes
wt 1.3	P7	0.05%	3.2% (<i>KLF4</i>)	Yes

Cell line	Passage	Silencing relative to GAPDH	Mean residual contribution (transgenes above 5%)	Continued
wt 2.1	P5	0.12%	3.5% (<i>KLF4</i>)	-
wt 2.1	P11	0.04%	2.4% (<i>KLF4</i>)	Yes
wt 2.2	P5	<0.01%	0.1%	Yes
wt 2.2	P11	<0.01%	0.1%	Yes
wt 2.3	P11	0.01%	0.8%	Yes
wt 4.1	P6	0.06%	3.4% (<i>KLF4</i>)	No
wt 4.2	P5	0.02%	2.7% (<i>KLF4</i>)	Yes

The silencing was successfully demonstrated for at least two clones from the lines ChAc 1, wt 1 and wt 2. The reprogramming procedure of ChAc 2 and wt 4 did yield two morphologically stable clones per line. When further investigated, however, only one clone from each line was considered silenced. Furthermore, silencing improved in a clone that was investigated two times at P5 and P11 (wt 2.1), while another clone maintained its silencing during the same time (wt 2.2). All silenced clones were further characterized. Hierarchical clustering was performed on the data gathered from the silencing and characterization PCR of reprogrammed clones (See Figure 10). Three clusters, which were separated by a large distance, were identified. The grey box marks the cluster that was identified as the freshly infected fibroblast lines, which had a high expression of exogenous transcription factors and no activation of endogenous transcription factors or genes downstream of these factors. The red box highlights a cluster that was entirely comprised of partially reprogrammed cell lines, which harbored some residual exogenous expression as well partial activation of the endogenous transcription factors. Only ChAc lines were found in this group. The green box identifies the last and biggest cluster, populated only by silenced and bona fide reprogrammed iPSC. The distance between these cell lines was very small, showing that they all reached a similar level of quality in regards to the PCR markers tested. Even though there were two subpopulations observed within this group, they were not enriched in either wild type or ChAc cell lines and their overall distance was very low.

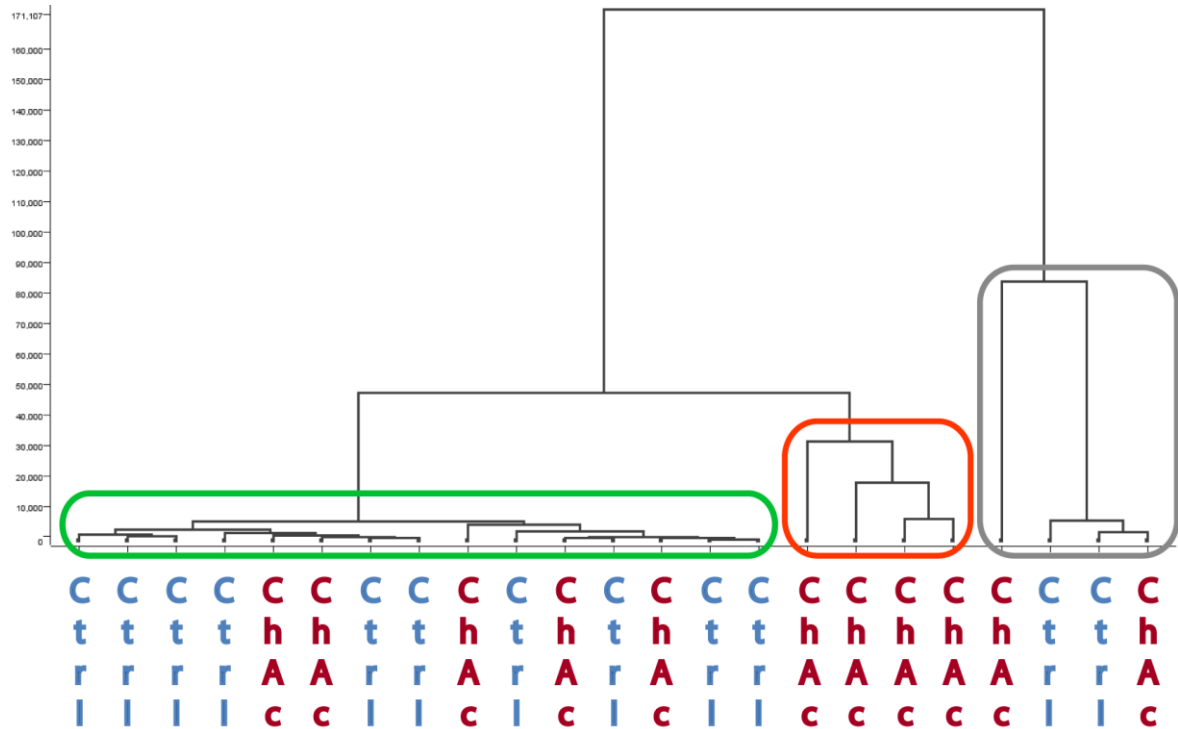


Figure 10: Hierarchical clustering of iPSC after silencing/characterization PCR. The grey box shows the cluster defined by freshly infected fibroblasts. The red box is comprised of partially reprogrammed and unsilenced iPSC. The green box depicts the cluster of bona fide reprogrammed, hence silenced iPSC lines. No additional subpopulations of wild type or ChAc lines were observed within this cluster.

1.2. Karyotyping of iPSC clones

The karyotype of all iPSC clones has to be analyzed. Since the reprogramming process affects chromatin state and DNA-methylation, genomic alterations like deletions, multiplications, loss of heterozygosity (LOH) or gene duplications can occur and impair the quality of the clone. The iPSC samples were sent to conduct single nucleotide polymorphism karyotyping. The clones wt 1.2, wt 1.3, wt 2.1, wt 2.3, ChAc 1.1 and ChAc 1.2 were investigated. All clones showed minor deletions or multiplications most frequent on chromosome 20 and 12. Minor alterations spanning only few kb were detected in almost all clones distributed evenly across all chromosomes. Most of the LOHs detected were regions that overlapped with the used reference map of the database of genomic variants. These overlaps are prone for these events. Wt 1.2 showed severe chromosomal aberrations of about 12000 kB. Notably multiple gains of chromosome 1 and major losses of chromosomes 8 and 22 were detected. Wt 1.2 was omitted from further experiments.

1.3. Evaluation of pluripotency

After the silencing and the correct karyotype were confirmed, the pluripotent properties of the generated lines were assessed.

1.4. Alkaline phosphatase staining

Alkaline phosphatase (AP) is an enzyme, which has an elevated expression in iPSC compared to dermal fibroblast. The AP assay gives a quick and robust readout for the early stages of reprogramming since it is one of the earliest markers of iPSC conversion. Representative examples of AP positive iPSC from each line are shown in Figure 11. The MEF feeder, on which the iPSC cells were grown, acted as a negative control since these cells genuinely do not express AP. All of the clones investigated were AP positive and thus none was excluded.

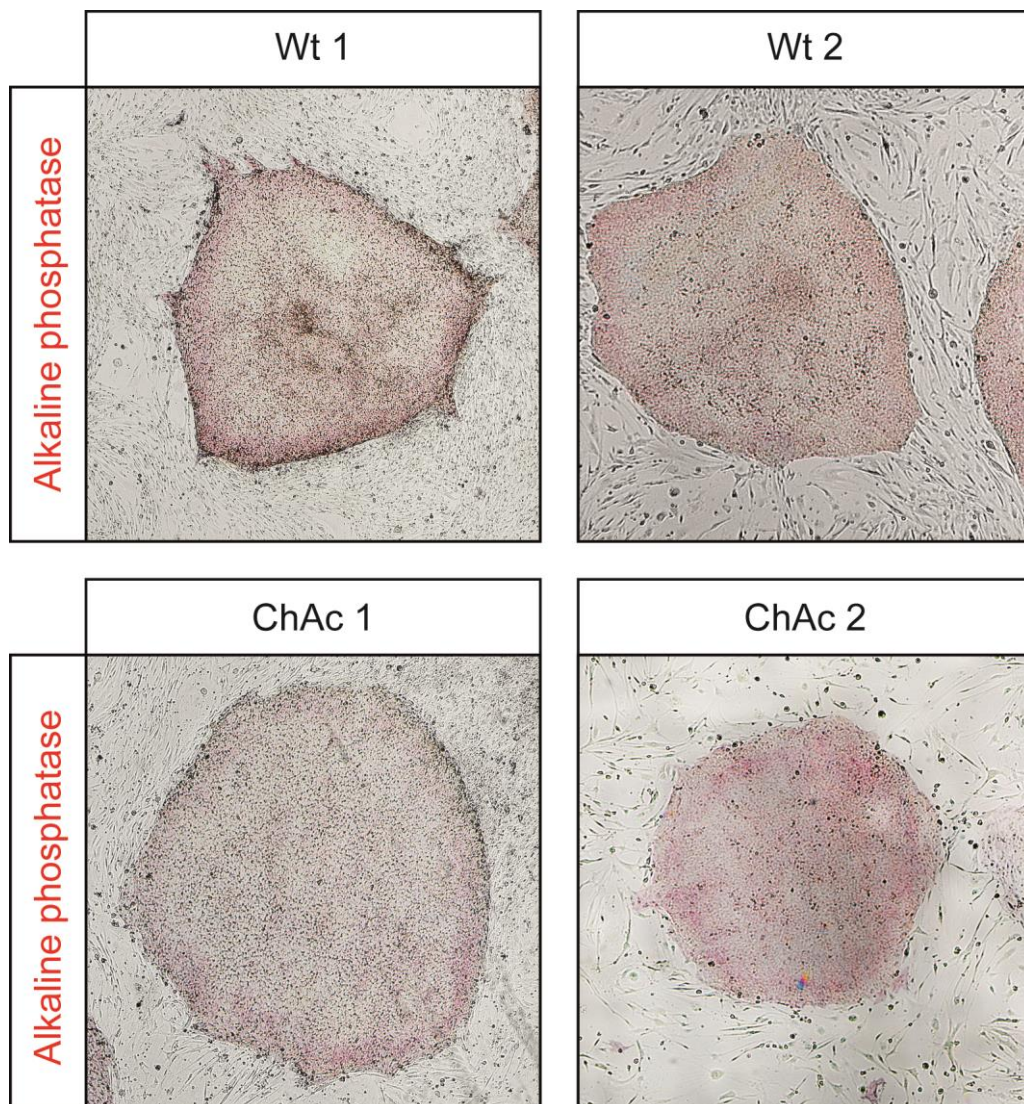
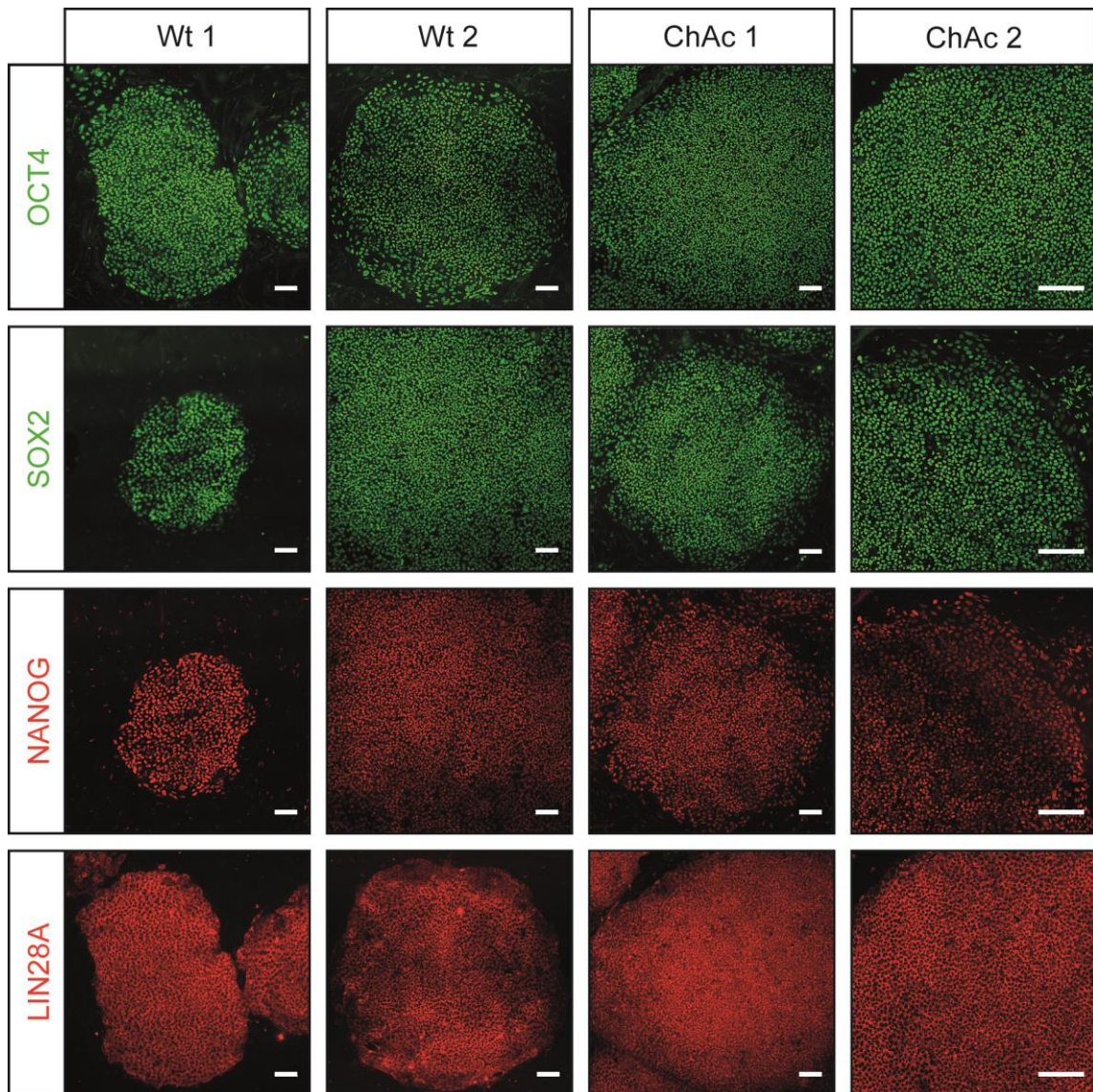


Figure 11: Alkaline phosphatase staining. Colonies stained in red, displaying a round and regular shape, represent morphological bona fide iPSC clones. MEF feeder cells surrounding these colonies have no expression of alkaline phosphatase and act as intrinsic negative control.

1.5. Staining of pluripotency markers

In order to further validate a genuine pluripotent behavior the next step was to stain for stringent markers of pluripotent stem cell *in vitro*. Markers included the transcription factors OCT4 and SOX2 that have been transduced as well. Since the silencing of these factors has been proved previously, their proper endogenous expression and localization has to be addressed as well. Other markers investigated were the transcription factor Nanog, which acts downstream of the OCT4 driven pluripotency complex and LIN28A a translational activator of OCT4 translation. The cell surface markers SSEA3 and Tra1-60 are important markers of pluripotent stem cells and their presence serves as a good indicator for successful reprogramming. All of the clones investigated showed proper morphology and were positive for the major markers of a genuine pluripotent ESC-like stage (see Figure 12).



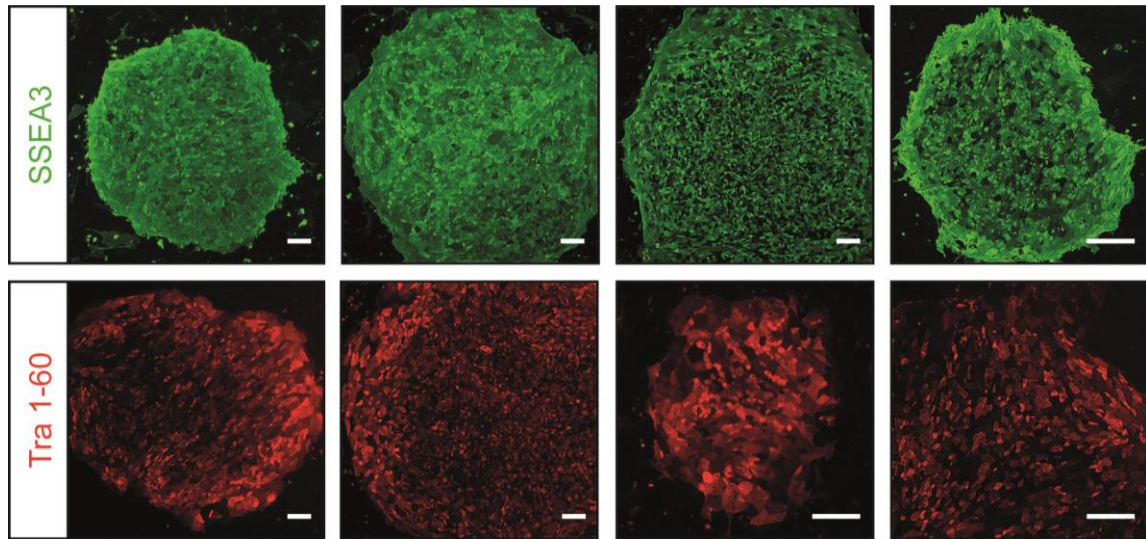


Figure 12: Pluripotency staining. OCT4 and SOX2 staining show endogenous expression, since their silencing was confirmed by PCR experiments before. Nanog and LIN28A are markers that are important for stemcell maintance are activated during reprogramming. SSEA3 and Tra 1-60 are embryonic stem cell specific cell surface markers that are considered hallmarks of *in vitro* cultures of pluripotent stem cells. Scale bar = 200 μ m

1.6. Three germ layer formation

The three germ layer formation is a very stringent assay which shows that one batch of pluripotent stem cells can give rise to cells from all three different germ layers including ectoderm, mesoderm and endoderm. For ectoderm the markers NESTIN, TUJ1, MAP2, GALC, and S100 β /GFAP were chosen. They provide a broad view over the neuro-ectoderm and label neural stem cells, neurons, astrocytes and oligodendrocytes (See Figure 13).

Demonstration of capability to differentiate into endoderm was achieved by labeling the markers AFP and GATA4. All silenced lines showed bona fide expression of the investigated markers (See Figure 14A). Successful mesoderm differentiation was observed by staining of FLK-1, PECAM-1 and α -SMA, important markers of mesodermal lineage (See Figure 14B).

All lines were capable of giving rise to cells contributing to each germ layer, thus further proving the pluripotent nature of the cell lines generated on a functional level.

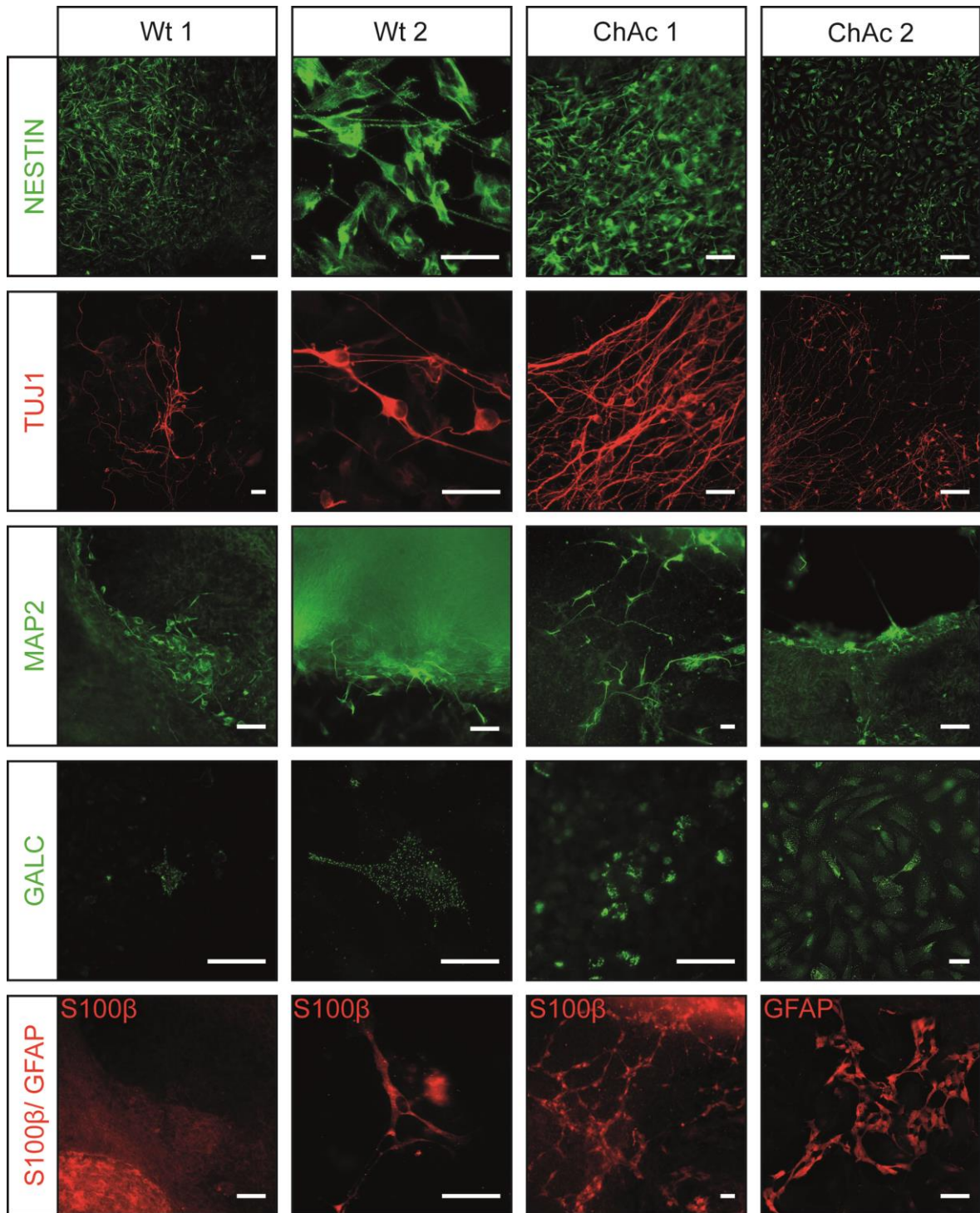


Figure 13: Three germ layer formation I. Representative pictures of neuro-ectodermal marker staining of three germ layer formation. All lines gave rise to NPCs, neurons, oligodendrocytes and astrocytes. Scale bar = 50µm.

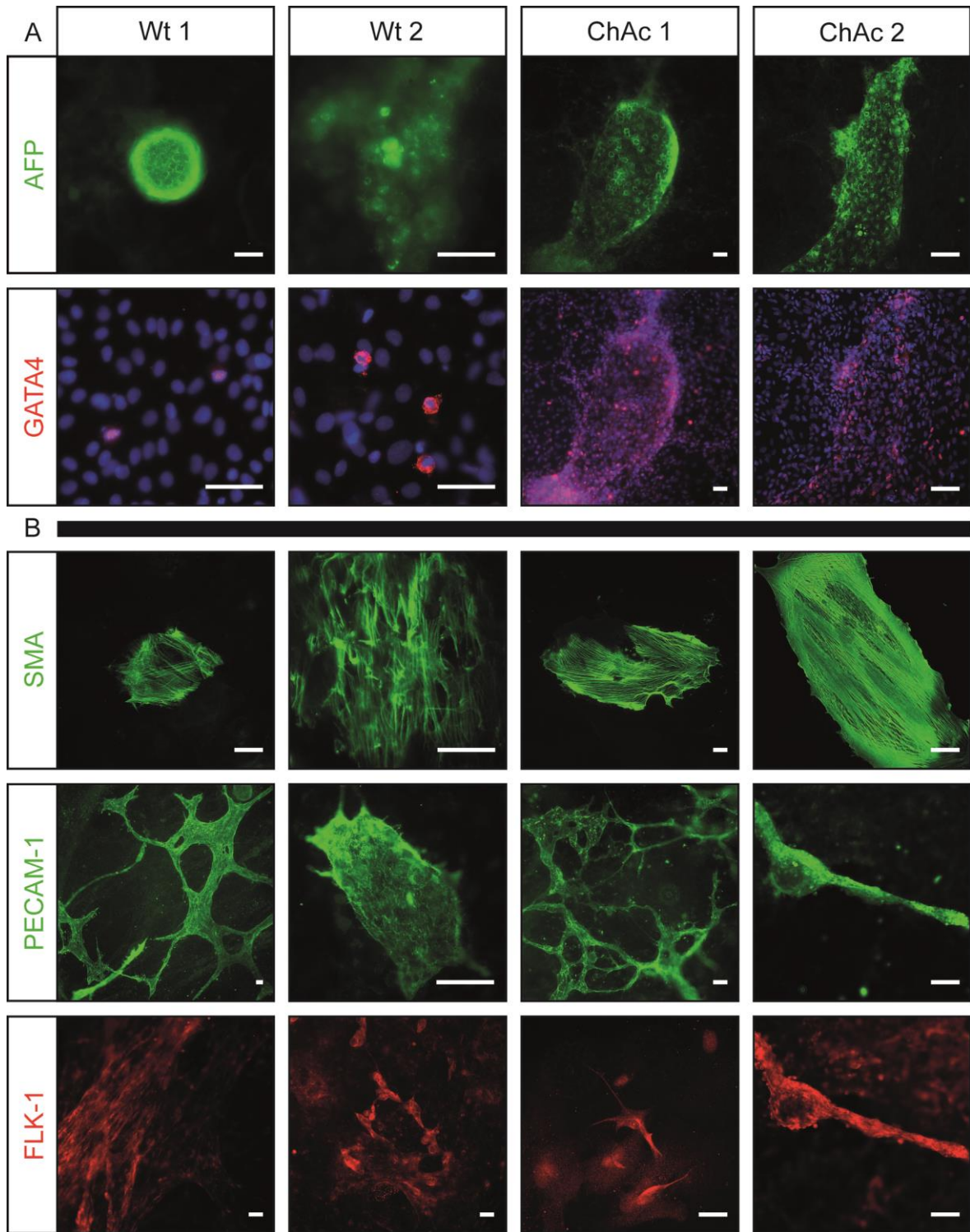


Figure 14: Three germ layer formation II. Representative pictures of A) endodermal differentiation and B) mesodermal differentiation. All lines were positive for the investigated markers, indicating steady pluripotent capability to give rise to these two germ layers. Scale bar = 50 μ m.

1.7. Confirmation of ChAc phenotype by CHOREIN western blot

The last step of characterization of the generated iPSC lines was the confirmation of the disease specific phenotype. This was investigated by western blot analysis of CHOREIN

protein. Absence of CHOREIN is a clear diagnostic indication of ChAc. To verify this, the already thoroughly characterized lines, obtained from another lab, were used as either positive or negative controls. Therefore antibody specific patterns were obtained for CHOREIN positive and negative cell lines (see Figure 15) (Walker, 2015).

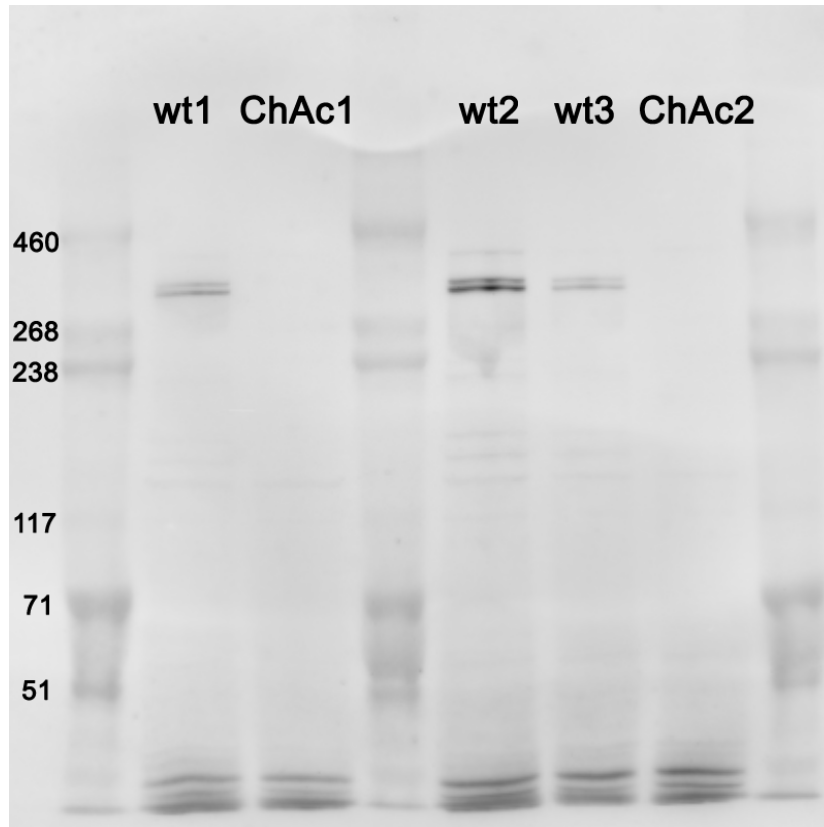


Figure 15: CHOREIN western blot of generated lines. Wild type CHOREIN has a size of 360 kDA. wt 1 and wt 2 show expression of CHOREIN while in ChAc 1 CHOREIN is absent. ChAc1 was used a negative control and wt 3 was used as a positive control. Both lines were reprogrammed, characterized and contributed from the group of Jared Sternecker, of the MPI Münster.

All control lines were positive for CHOREIN and all generated ChAc lines featured its absence.

In summary, all lines obtained were bona fide pluripotent iPSCs and the patient specific lines retained the ChAc phenotype on the CHOREIN protein level. The following lines were used for the disease modeling experiments using MSN differentiation protocol: wt 1.2, wt 1.3, wt 2.1, wt 2.2, wt 2.3, ChAc 1.1, ChAc 1.3, ChAc 1.4 and ChAc 2.1. For mDAN differentiation, smNPC lines were contributed from the group of Jared Sternecker: wild type: 393.1, 393.2, T12.2 and T12.9; ChAc: D1.17, D2.9 and D2.14. The lines T12.9 and D2.9 were obtained as iPSC lines as well and used for the MSN experiments accordingly.

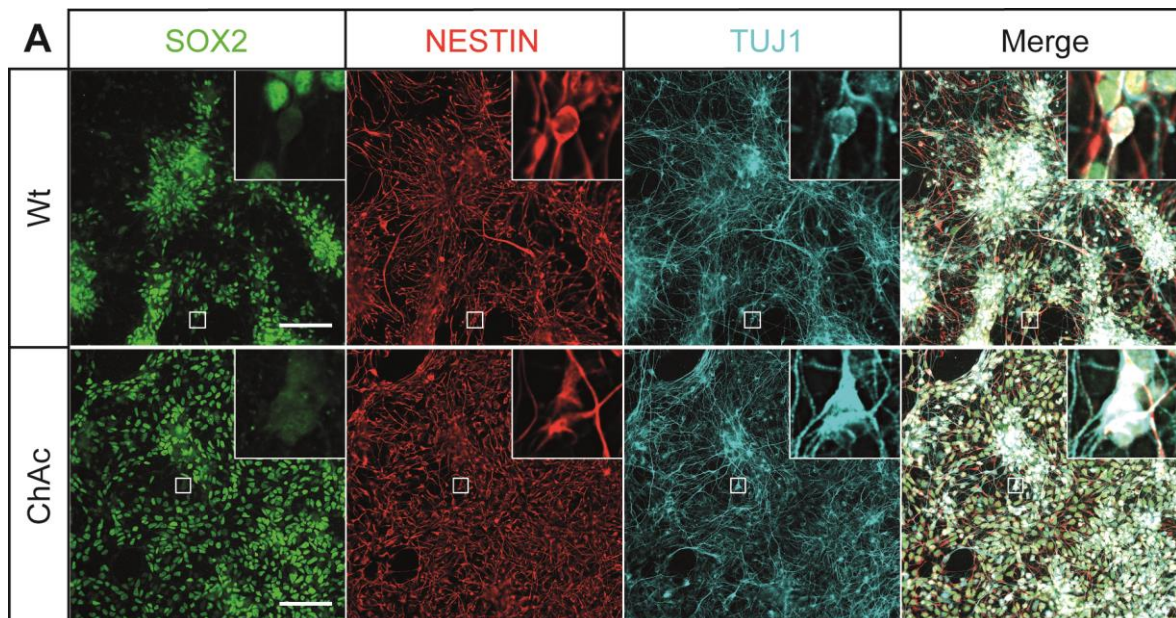
2. Characterization of differentiation potential

All experiments that were conducted to model the disease used mature neurons for which two differentiation protocols were established. The first started from iPSC stage and yielded a mixed striatal culture containing MSN as well cholinergic interneurons. This protocol recapitulates the developmental processes of neurons that are primarily affected by ChAc. The second protocol started from the more committed stage of NPCs and allowed rapid generation of dopaminergic neurons. The first task, however, was to compare the differentiation capacity of wild type and ChAc cell lines. Interpretation of experiments that characterizes the disease is highly influenced by the quality of differentiation protocols.

2.1. Differentiation efficiency

Differentiation efficiency was assessed by ICC. The markers SOX2 and NESTIN were used to identify undifferentiated stem cell state, TUJ1 as an early marker showed neuronal cell fate, MAP2 was stained to detect mature neurons and GABA, CHAT, CTIP2 and DARPP32 were used to identify the subtype of neurons.

There was no significant difference observed in the expression of markers SOX2, MAP2 and the sub-classification of these neurons after the striatal differentiation protocol was successfully performed. A large amount of cells were negative for SOX2, TUJ1 or MAP2 and showed no typical neuronal morphology (See Figure 16, Figure 18 & Figure 17).



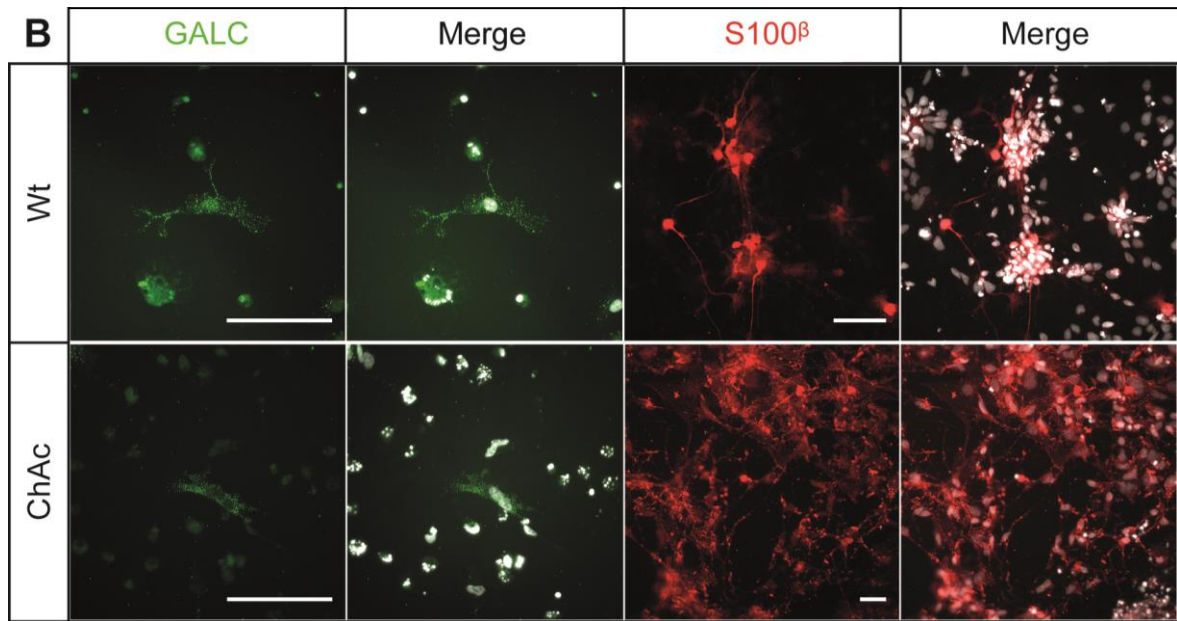


Figure 16: MSN protocol characterization I. A) Staining of SOX2 and NESTIN reveal the fraction of NPCs. Wild type and ChAc cell lines can both give rise to healthy neuronal cultures. Box: TUJ1-positive immature neurons are SOX2 negative. B) Wild type lines and ChAc lines are both able to give rise to GALC-positive oligodendrocytes as well S100 β -positive astrocytes. Scale bar = 100 μ m

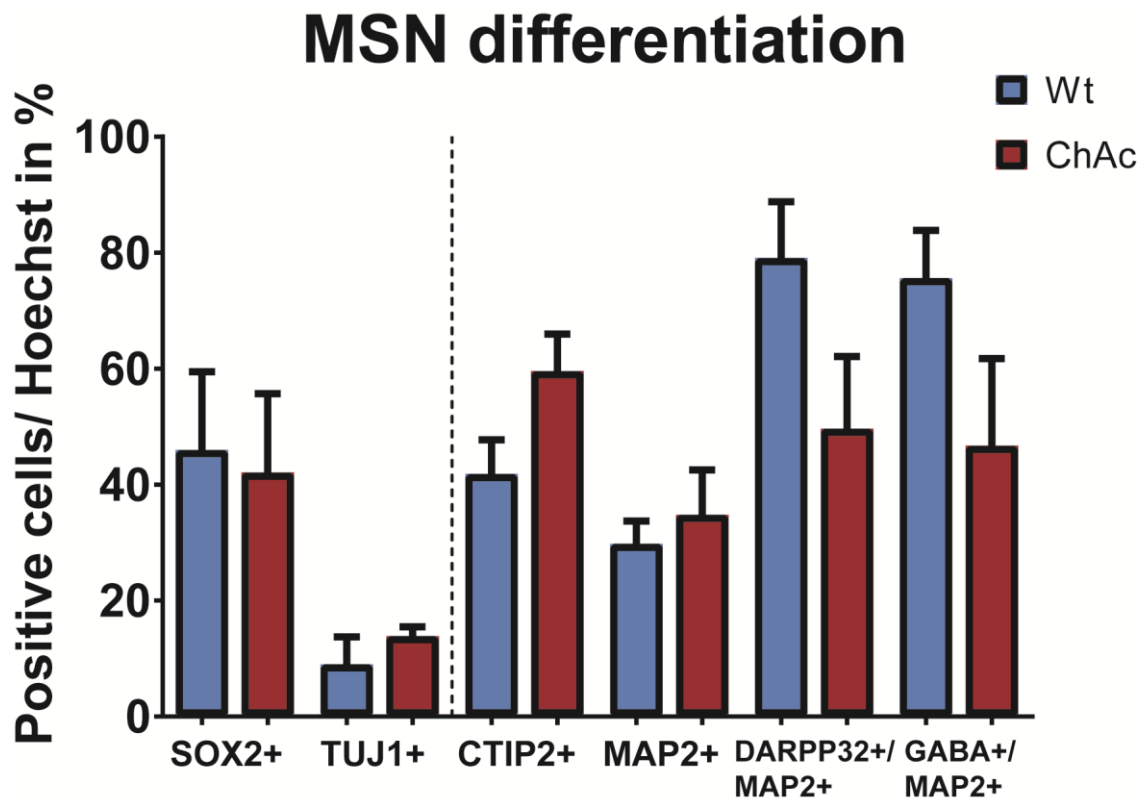


Figure 17: Quantification of MSN differentiation capacity. There were no differences detected between wild type and ChAc lines. Markers left of the dashed line represent NPCs and immature cells and to the right are markers for mature neurons. Bars represent mean + SEM, n \geq 4

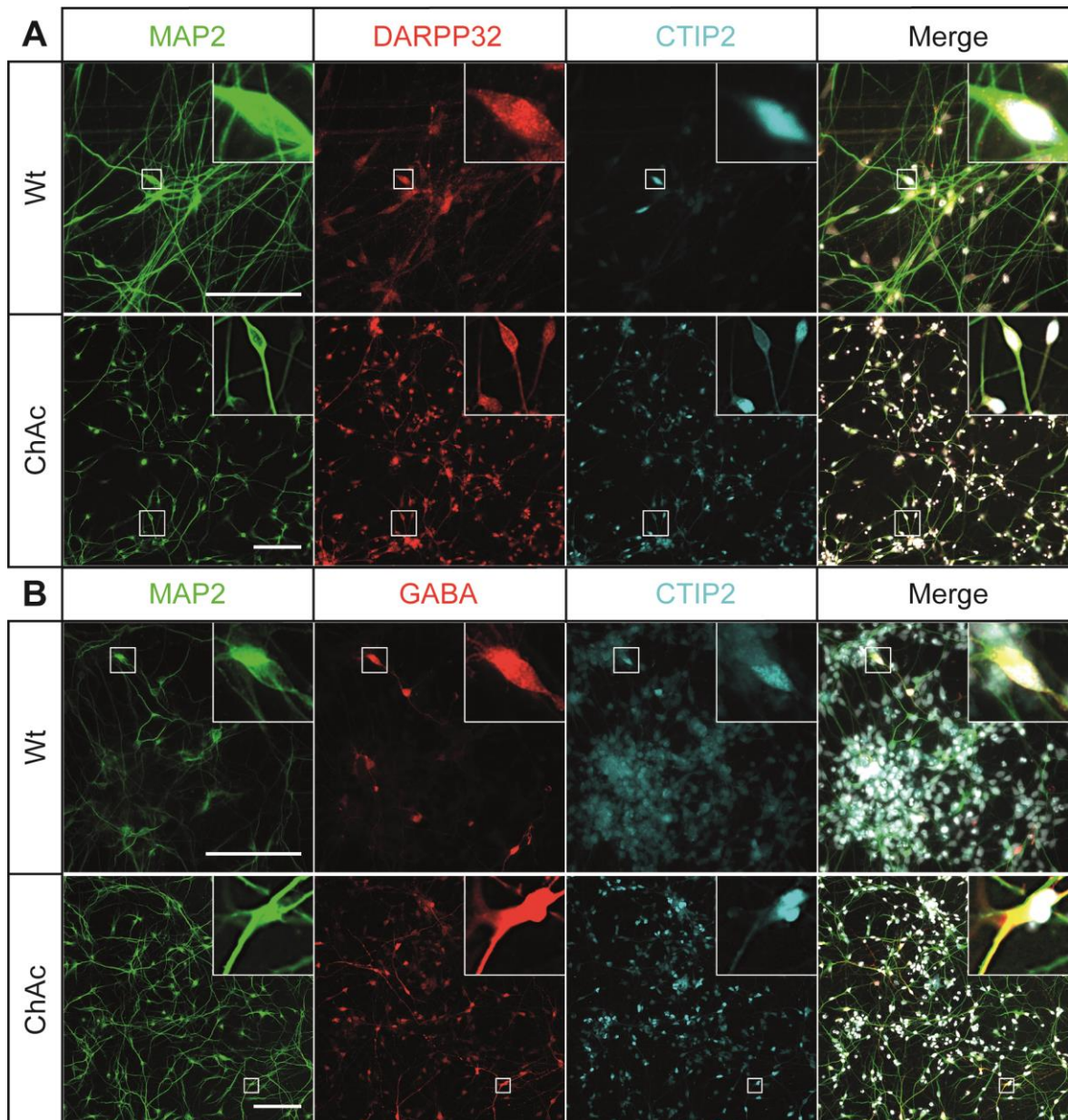


Figure 18: MSN protocol characterization II. A) Both wild type and ChAc lines are capable of differentiating into MAP2/DARPP32/CTIP2 triple positive mature medium spiny neurons. B) Furthermore these cells are able to give rise to MAP2/GABA/CTIP2 triple positive neurons. Scale bar = 100 μ m

The differentiation following the mDAN protocol successfully yielded mature dopaminergic neurons as shown by co-labelling of MAP2 and TH. Some cells retained their NPC characteristics as shown by staining of SOX2 and NESTIN. The cells were able to give rise to GALC and GFAP-positive oligodendrocytes and astrocytes, respectively. The yield was, however, not quantified because only very few positive cells were observed. This further indicates the neuronal character of the used progenitor cell lines. Overall, there

was no difference observed in differentiation capacity when comparing wild type and ChAc cell lines (See Figure 19 & Figure 21).

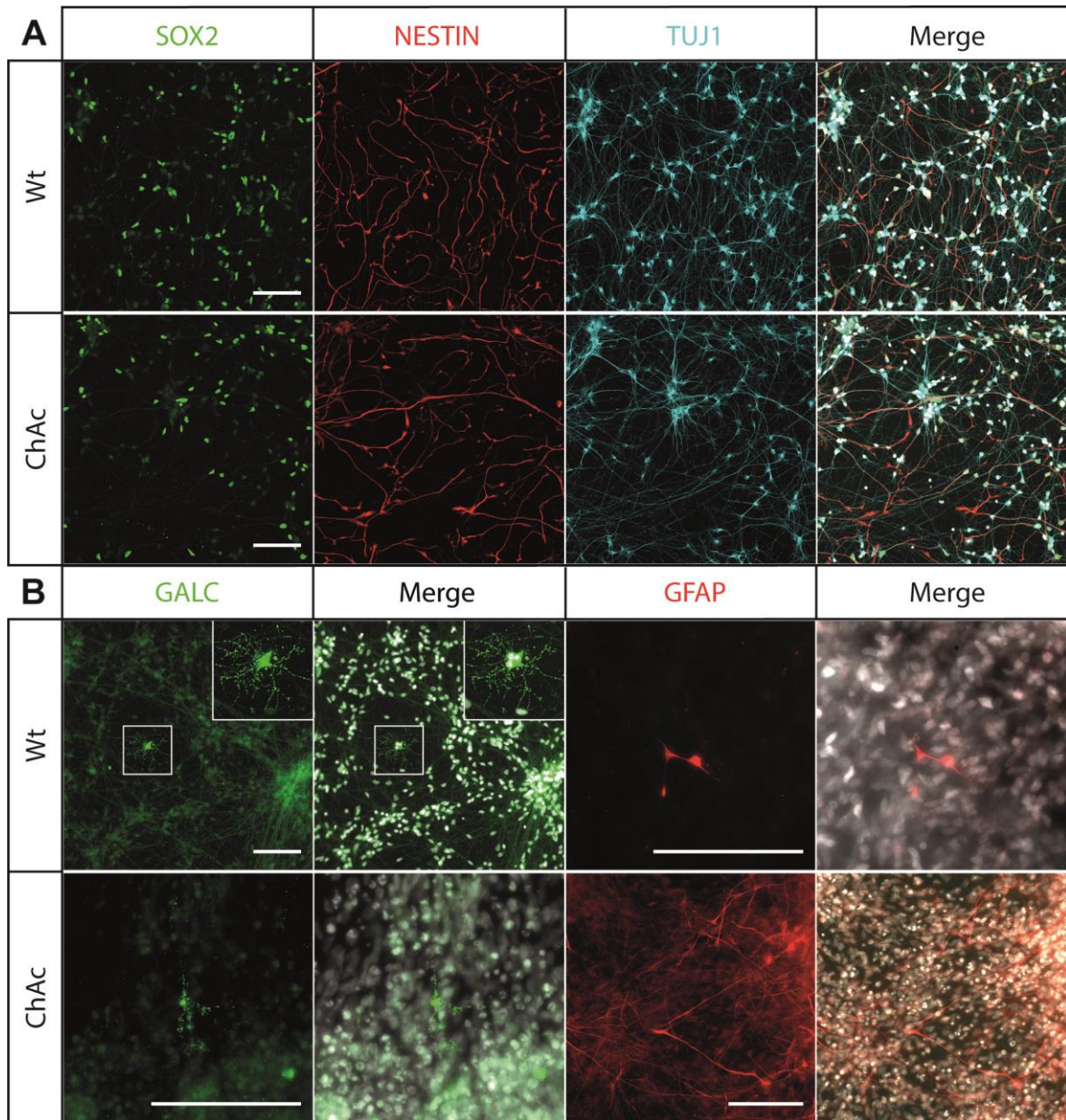


Figure 19: mDAN protocol characterization I. Staining of SOX2 and NESTIN label NPCs and immature neurons. Wild type and ChAc lines give rise to homogenous healthy neuronal cultures and yield both GALC-positive oligodendrocytes as well as GFAP-positive astrocytes. Scale bar 100µm

Some of the TH-negative neurons are of hindbrain origin and a by-product of the mDAN differentiation as shown with the motor neuron marker SMI32. When perinuclear co-localization was investigated, only few neurons were positive, even though the culture appears to contain more motor neurons (See Figure 20 & Figure 21).

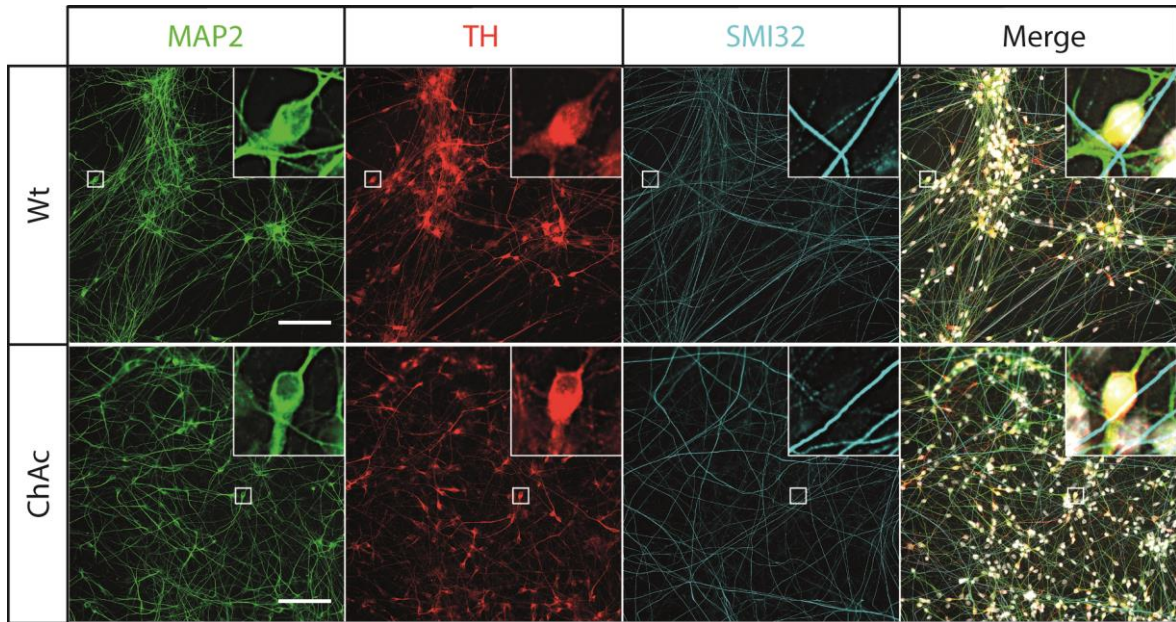


Figure 20: mDAN protocol characterization II. Wild type and ChAc cells both give rise to MAP2 and TH double positive neurons. SMI32 positive motor neurons are an undesired by-product of mDAN differentiation due to the posterior nature of the NPCs used. Box: MAP2 and TH double positive neurons are negative for the motor neuron marker SMI32. Scale bar = 100 μ m

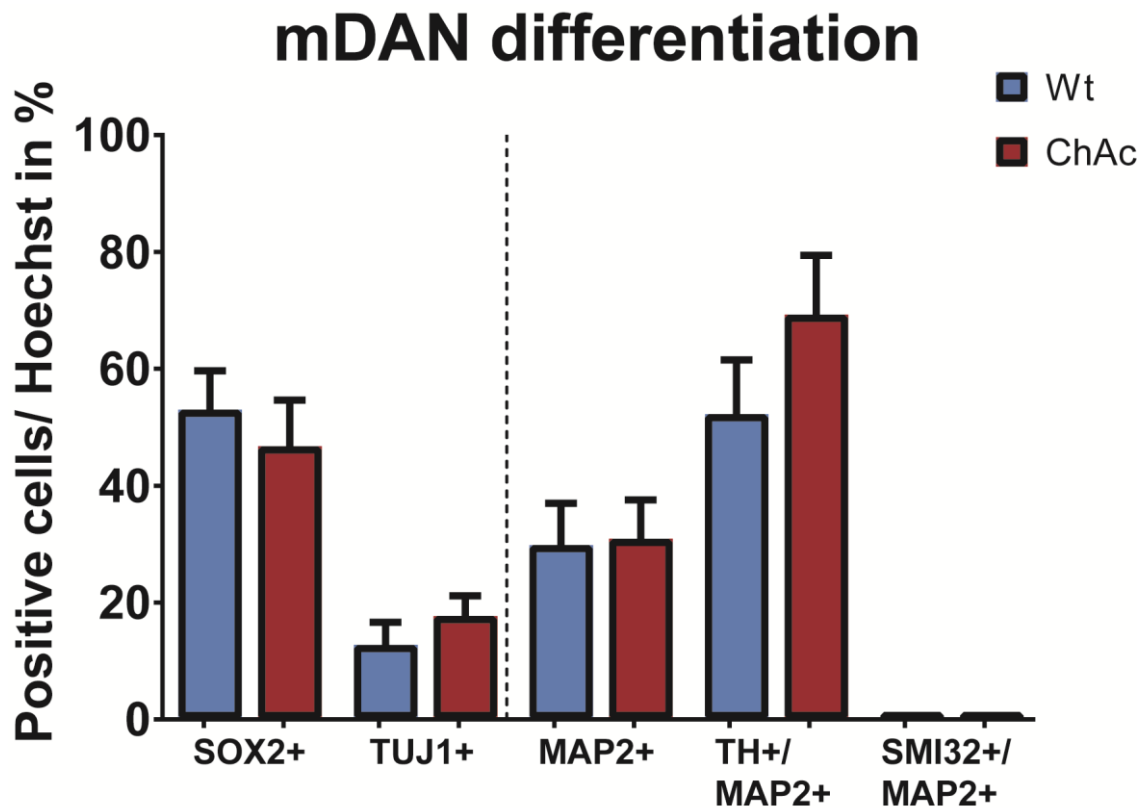


Figure 21: Quantification mDAN differentiation capacity. There were no differences detected between wild type and ChAc lines. Markers left of the dashed line represent NPC and immature cells, to the right are markers for mature neurons. Bars represent mean + SEM, n \geq 5

Taken together, there was no difference observed in the SMI32 and MAP2 double positive cells, but ChAc lines gave rise to more MAP2+ TH+ double positive cells.

2.2. Characterization by qPCR

To further investigate differences in the differentiation behavior, qPCR was conducted with a total of 20 genes (See Table 20).

Table 20: Genes investigated to characterize MSN differentiation

Gene name	Marker for
KLF4	Proliferation - pluripotent stem cells
LIN28	Proliferation - pluripotent stem cells
NANOG	Proliferation - pluripotent stem cells
OCT4	Proliferation - pluripotent stem cells
REX1	Proliferation - pluripotent stem cells
SOX2	Proliferation - pluripotent & neural stem cells
EMX2	Patterning - cortical transcription factor
PAX6	Patterning - cortical transcription factor
FOXP1	Patterning - rostral transcription factor
LHX6	Patterning - ventral transcription factor - medial ganglionic eminence
LHX8	Patterning - ventral transcription factor - medial ganglionic eminence
NKX2.1	Patterning - ventral transcription factor - medial ganglionic eminence
ASCL1	Patterning - ventral transcription factor - lateral ganglionic eminence
DLX2	Patterning - ventral transcription factor - lateral ganglionic eminence
GSX2	Patterning - ventral transcription factor - lateral ganglionic eminence
KROX20	Patterning - caudal transcription factor
MAP2	Maturation - pan neuronal
GAD67	Maturation - MSN
CTIP2	Maturation - MSN
DARPP32	Maturation - MSN
CHAT	Maturation - Cholinergic interneurons

These genes were chosen because they reflect the entire differentiation process covering iPSC transcription factors, neuronal patterning factors and markers for mature neurons. Hierarchical clustering of the qPCR data was calculated and probed for clusters. The originating iPSC lines clustered close together and were distant from the differentiated mature neurons. Within the neuronal fraction there was no obvious clustering observed (See Figure 22).

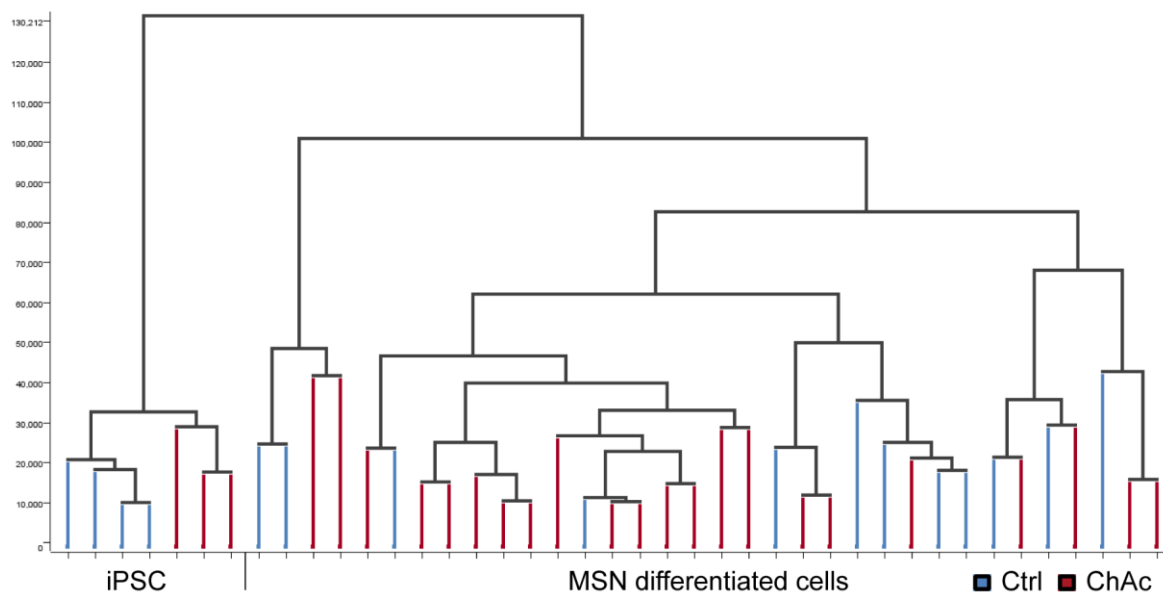


Figure 22: Hierarchical clustering of PCR data for the characterization of MSN differentiation. Blue indicates wild type lines and red are ChAc lines. The left most cluster represents the proliferation stage of iPSC lines. Overall, no obvious clustering of wild type or ChAc lines was observed. Some clusters are formed from individual experiments indicating that the inter-experimental variances are bigger than intra-experimental.

The target genes that were selected for the characterization of the mDAN protocol were based on a microarray analysis conducted with one ChAc cell line in a collaborating lab. The 13 most prominent hits were selected for in depth PCR expression analysis. Furthermore, some genes were added in the analysis because they were previously linked to ChAc in other modelling systems, they were putatively linked to play a role in ChAc as suggested in the literature or they are important in other diseases that share similar clinical symptoms like Huntington (See Table 21).

Table 21: Genes investigated to characterize mDAN differentiation

Gene name	Investigated because
<i>VPS13A</i> - vacuolar protein sorting 13 homolog A	Linked to Chorea Acanthocytosis
<i>TH</i> - tyrosine hydroxylase	Differentiation capacity
<i>TUBB3</i> - tubulin beta 3 class III	Differentiation capacity
<i>ACT1</i> - actin	Actin Phenotype in erythrocytes
<i>CFL1</i> - cofilin 1	Actin Phenotype in erythrocytes
<i>CTTN</i> - cortactin	Actin Phenotype in erythrocytes
<i>PFN1</i> - profilin 1	Actin Phenotype in erythrocytes
<i>BLCAP</i> - bladder cancer associated protein	Prominent hit in microarray analysis
<i>CFLAR</i> - CASP8 and FADD like apoptosis regulator	Prominent hit in microarray analysis
<i>IL13RA2</i> - interleukin 13 receptor subunit alpha 2	Prominent hit in microarray analysis
<i>LHX3</i> - LIM/homeo box 3	Prominent hit in microarray analysis
<i>NEUROD1</i> – neuronal differentiation 1	Prominent hit in microarray analysis
<i>NKAIN2</i> - Na/K transporting ATPase interacting 1	Prominent hit in microarray analysis
<i>NNAT</i> - neuronatin	Prominent hit in microarray analysis
<i>PCDH</i> - protocadherin	Prominent hit in microarray analysis
<i>PLXNA2</i> - plexin A2	Prominent hit in microarray analysis
<i>RPL39L</i> - ribosomal protein L39 like	Prominent hit in microarray analysis
<i>SMOC1</i> - SPARC related modular calcium binding 1	Prominent hit in microarray analysis
<i>SPON1</i> - spondin 1	Prominent hit in microarray analysis
<i>SST</i> - somatostatin	Prominent hit in microarray analysis
<i>ADD2</i> - adducin 2	Linked to Huntington
<i>RRS1</i> - ribosome biogenesis regulator homolog 1	Linked to Huntington
<i>TRK1</i> - tropomyosin receptor kinase A	Linked to Huntington
<i>TRK2</i> - tropomyosin receptor kinase B	Linked to Huntington
<i>TRK3</i> - tropomyosin receptor kinase C	Linked to Huntington

When hierarchical clustering was performed, one of the genes, NNAT, was highly overexpressed in ChAc lines. When NNAT expression was omitted from the hierarchical cluster analysis, there was no clustering between wild type and ChAc lines. However, when NNAT expression was considered there were two clusters observed. The first cluster was comprised of wild type lines and the second cluster contained all the ChAc lines and notably one wild type line.

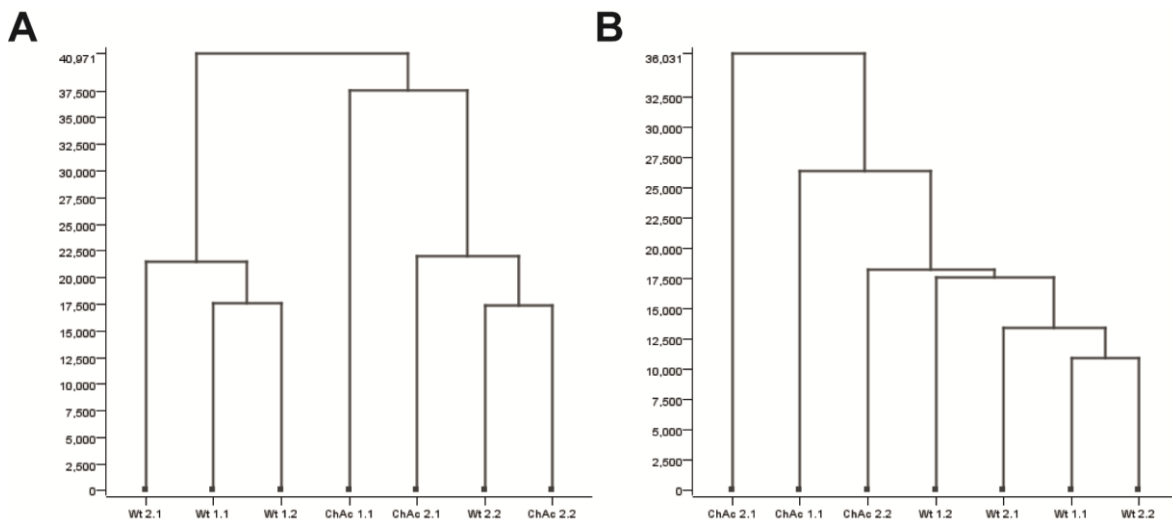


Figure 23: Hierarchical clustering of the PCR data of mDAN differentiation. A) Analysis conducted with the result of NNAT expression shows a clear clustering of wild type and ChAc lines, with the exception of wt 2.2. B) Exclusion of the NNAT expression shows that no specific cluster can be observed.

In summary, all lines were able to give rise to mature neurons following MSN as well as mDAN differentiation protocol. ICC and qPCR analysis of matured cultures revealed that there was no difference between wild type and ChAc. When mDAN cultures were investigated an increased amount of MAP2/ TH double positive cells was detected. Hierarchical clustering of qPCR results of 25 investigated genes revealed a separate clustering of ChAc lines and wild type lines with the notable exception of Wt 2.2. When the expression of NNAT was omitted, there was no clustering observed (See Table 22).

Table 22: Characterization of the applied differentiation protocols

	MSN differentiation	mDAN differentiation
ICC	ChAc and wild type lines are capable of differentiating into mature MSN there was no difference in the differentiation capacity observed	ChAc and wild type lines are capable of differentiating into mature mDAN

	MSN differentiation	mDAN differentiation
PCR	<p>cluster of mature differentiated cultures is distant of iPSC cluster</p> <p>no cluster within mature MSN cultures is observed</p>	<p>clustering of ChAc and wild type lines is observed when expression of <i>NNAT</i> is considered</p> <p>no clustering is observed when expression of <i>NNAT</i> is omitted</p>

2.3. Ratio of polymerized and unpolymerized cytoskeleton proteins

One of the well-known impairments in ChAc disease is the alteration of the ratio between G and F actin in erythrocytes. To evaluate whether this is also aberrant in neurons, the ratio was analyzed by western blot. As microtubules play an important role in transport and are an essential part of the cytoskeleton, the ratio of polymerized and unpolymerized tubulin was investigated as well. Modifications of tubulins are important for their function. Acetylation of tubulin is important for protein interaction of microtubules (Howes, et al., 2014).

In mature MSN cultures the G/F actin ratio was significantly increased, while in mature mDAN there was no difference observed (See Figure 24). Differences in the distribution of tubulin were neither detected in mDAN nor MSN cultures. In the western blot, there was also no difference detected in the amount of acetylated tubulin relative to total α -Tubulin.

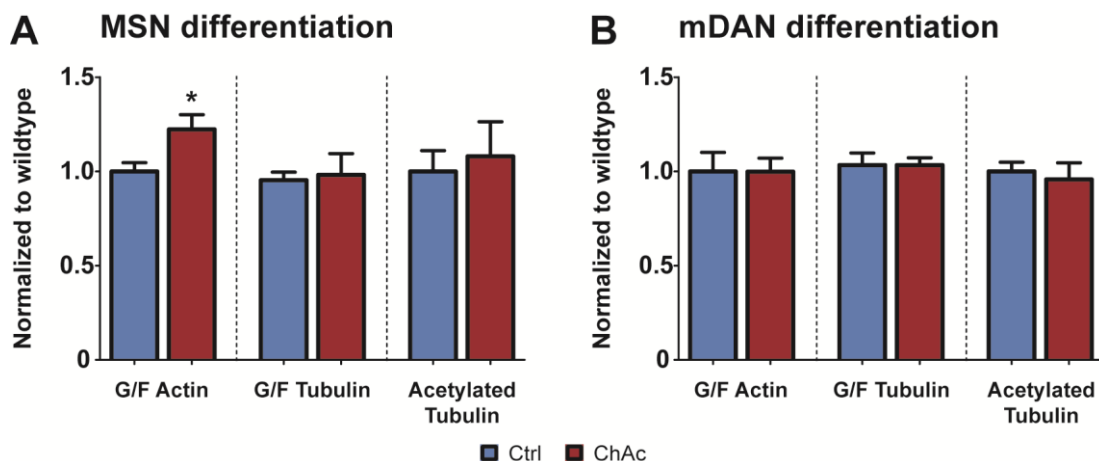


Figure 24: Evaluation of western blots of cytoskeleton proteins and acetylated tubulin ratio of both differentiation protocols. A) There was a significant increase observed in the G/F actin ration when ChAc lines were compared to wild type. B) No differences in the investigated cytoskeleton components were observed in mDAN differentiation. Bars represent mean +SEM. $n \geq 12$, */**/** represent $p=0.05/0.01/0.001$

2.4. Cell survival upon stress induction

Since there were no obvious differences in neuronal differentiation and cell survival by *VPS13A* mutations, the vulnerability for different stressors in ChAc neurons was investigated. Because one of the first putative roles of CHOREIN was vesicle sorting and several indications suggested that it might be important in autophagy and lysosomal pathway, cell survival under proteasomal stress was evaluated. Proteotoxic stress was induced using L-canavanine, an arginine analogue that causes misfolding of protein and thereby challenges the protein biosynthesis as well as recycling. Tunicamycin, an inhibitor of N-linked glycosylation, causes cell cycle arrest as well as endoplasmic reticulum-related unfolded protein response. Matured neurons were treated for six days with three different concentrations of the two toxins. Cell viability was then assessed using the resazurin-based PrestoBlue and lactate dehydrogenase (LDH) release assay.

When MSN differentiated neurons were treated with L-canavanine, there was no significant interaction and no significant influence of the genotype. The treatment however showed a significant influence ($p < 0.0001$, $F(3, 87) = 148.5$, $\omega^2 = 0.839$, two-way ANOVA) (See Figure 25 A). When treated with tunicamycin, there was a significant interaction between the treatment and the genotype ($p = 0.0269$, $F(1, 49) = 3.331$, $\omega^2 = 0.111$). The influence of the treatment was significant ($p < 0.0001$, $F(3, 49) = 39.82$, $\omega^2 = 0.610$) and the influence of the genotype was significant as well ($p < 0.0001$, $F(3, 49) = 21.26$, $\omega^2 = 0.065$) (See Figure 25 D).

LDH is released into the supernatant upon disruption of cell membrane and is therefore a direct marker of cell death. L-canavanine addition yielded no interaction between treatment and genotype and no influence of the treatment. The genotype was significantly influencing the LDH release ($p = 0.0038$, $F(1, 80) = 8.914$, $\omega^2 = 0.106$) (See Figure 25 B). Tunicamycin resulted in a significant influence of the genotype ($p = 0.0065$, $F(1, 80) = 7.81$, $\omega^2 = 0.098$) (See Figure 25 E).

The cell composition on the day of investigation gives insight into the kinetics of the poison by highlighting the ratio between dead and living cells. L-canavanine treatment yielded a significant effect of the genotype ($p = 0.0009$, $F(1, 80) = 11.85$, $\omega^2 = 0.093$) as well as the treatment ($p < 0.0001$, $F(3, 80) = 13.3$, $\omega^2 = 0.31$) (See Figure 25 C). Treatment with tunicamycin resulted in a significant treatment effect ($p = 0.02$, $F(3, 80) = 3.466$; $\omega^2 = 0.179$) but not of the genotype nor the interaction (See Figure 25 F). Taken together, these results indicate that mature MSN derived from ChAc cell lines are less metabolic active after 6 days of tunicamycin treatment and that the majority of the cell death occurred in both ChAc and wild type lines earlier during the treatment. L-canavanine did not affect

ChAc cell lines' metabolic activity differently. However, the cell death in ChAc cell lines seems to peak at a different time point than in wild type lines.

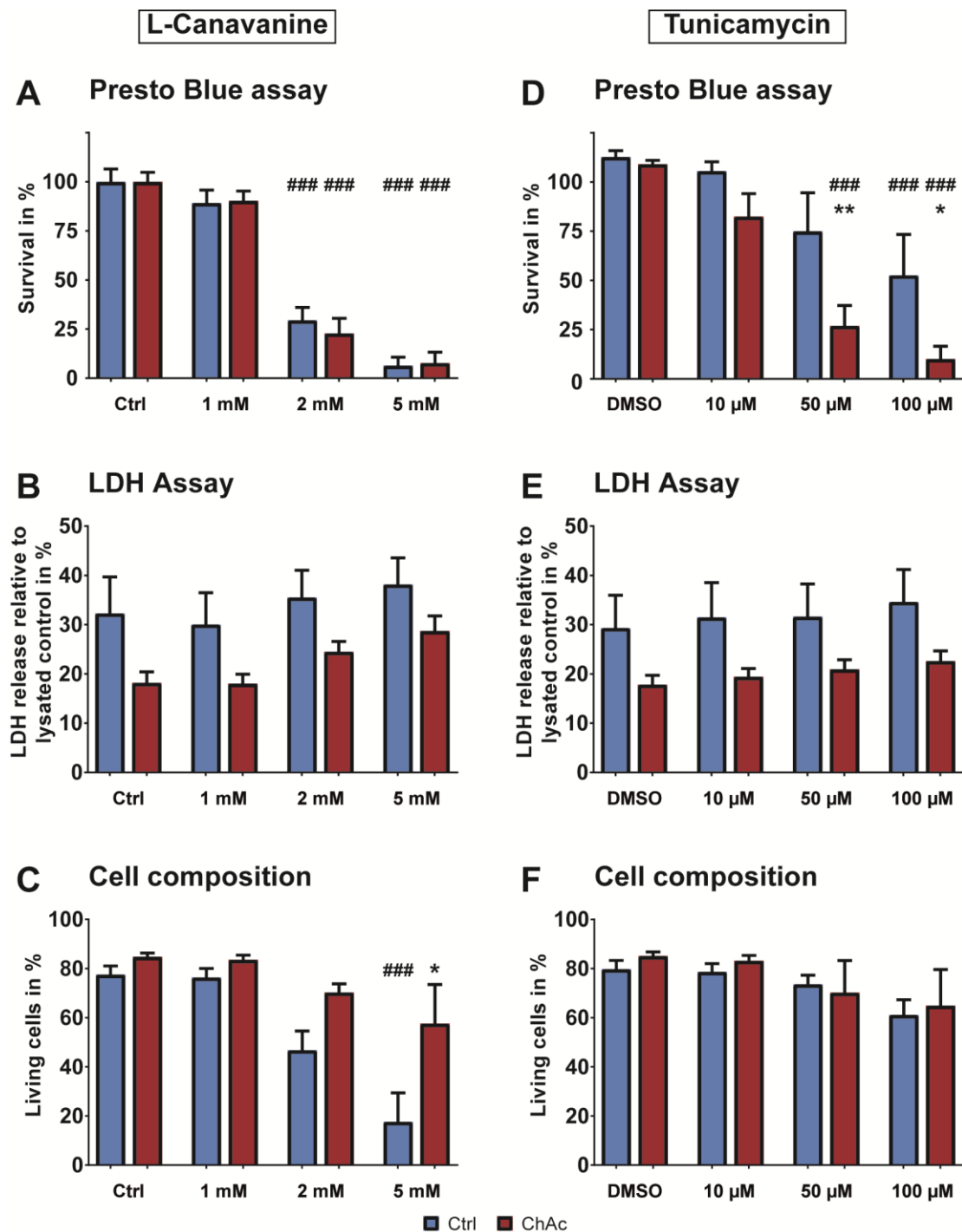


Figure 25: Survival of mature MSN cultures. A-C) Treatment with L-canavanine resulted in reduced metabolic activity and increased LDH release. Cell composition indicated an early cell death in ChAc lines. D-F) Treatment with tunicamycin showed a decreased metabolic activity and increased LDH release. Analysis of cell composition revealed no differential temporal response to the poison. Bars represent mean + SEM. $n \geq 9$. * indicate significant differences within a treatment. # indicate significant differences to control condition. */**/**; #/###/#### represent $p=0.05/0.01/0.001$

Mature mDAN cultures were treated the same way. Application of L-canavanine over the course of the experiment showed a significant interaction between treatment conditions and genotype ($p=0.0476$, $F(3, 52)=2.826$, $\omega^2=0.033$) as well as significant influence of both genotype ($p=0.0007$, $F(1, 52)=13.07$, $\omega^2=0.04$) and treatment ($p<0.0001$, $F(3, 52)=92.13$, $\omega^2=0.796$) (See Figure 26 A). For tunicamycin, no significant interaction between genotype and treatment were observed. Both genotype ($p=0.0134$, $F(1, 52)=6.556$, $\omega^2=0.019$) and treatment ($p<0.0001$, $F(3, 52)=113$, $\omega^2=0.844$) influence were significant however (See Figure 26 D).

LDH release was measured for the treatments as well. L-canavanine addition yielded no interaction between treatment and genotype. The genotype was significantly influencing the LDH release ($p<0.0001$, $F(1, 68)=22.06$, $\omega^2=0.171$) as well as the treatment ($p<0.0001$, $F(3, 68)=13.6$, $\omega^2=0.324$) (See Figure 26 B). Tunicamycin resulted in no observable interaction between treatment and genotype. The genotype however was significant ($p=0.003$, $F(1, 68)=14.46$, $\omega^2=0.132$) as well as the treatment ($p<0.0001$, $F(3, 68)=10.63$, $\omega^2=0.297$) (See Figure 26 E).

The cell composition on the day of investigation was probed for mDAN differentiation as well. L-canavanine treatment yielded a significant interaction ($p<0.0001$, $F(3, 68)=20$, $\omega^2=0.142$). The genotype was rated significant ($p<0.0001$, $F(1, 64)=53.45$, $\omega^2=0.123$) as well as the treatment ($p<0.0001$, $F(3, 64)=88.54$, $\omega^2=0.605$) (See Figure 26 C). Treatment with tunicamycin resulted in a significant interaction ($p=0.0082$, $F(1, 64)=4.27$, $\omega^2=0.08$), genotype ($p<0.0001$, $F(1, 64)=22.01$, $\omega^2=0.116$) and treatment ($p<0.0001$, $F(1, 64)=32.98$, $\omega^2=0.513$) (See Figure 26 F). Midbrain dopaminergic neurons showed an increased susceptibility to both drugs, including a differential temporal pattern.

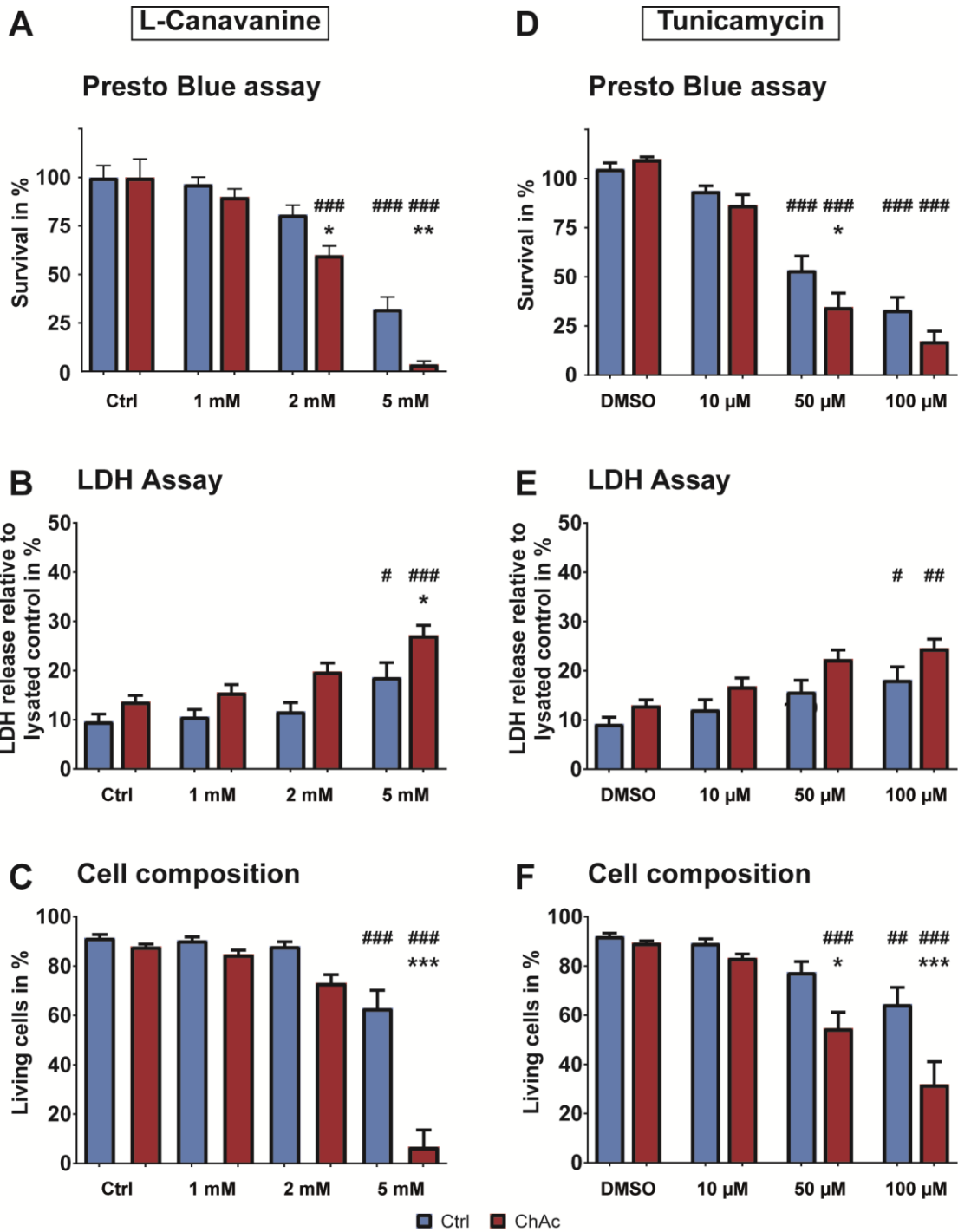


Figure 26: Survival of mature mDAN cultures. A-C) Treatment with L-canavanine resulted in reduced metabolic activity and increased LDH release. Cell composition indicated an acute late-phase cell death in ChAc lines. D-F) Treatment with tunicamycin showed a decreased metabolic activity and increased LDH release. Analysis of cell composition revealed a later cell death. Bars represent mean + SEM. $n \geq 8$. * indicate significant differences within a treatment. # indicate significant differences to control condition. */**/***; ###/###/### represent $p=0.05/0.01/0.001$

2.5. DNA damage in mature neurons

To identify whether increased DNA damage or susceptibility to it is present in ChAc patient derived mature neurons, DSB were analyzed under control conditions and after treatment with the DNA damage inducer etoposide. Phosphorylation of histone H2A.X at serine 139 is a well-established marker for DSB in cells and can be investigated using conventional ICC protocols. When subjected to MSN differentiation, ChAc neurons showed significantly less DSB than wild type under control conditions. When treated with etoposide however there was significant interaction between the influence of the treatment and the genotype ($p=0.048$, $F(1, 867)=3.937$, $\omega^2=0.004$, two-way ANOVA). There was no influence of the genotype observed, but the treatment had a significant influence ($p<0.0001$, $F(1, 867)=230.211$, $\omega^2=0.210$) (See Figure 27 A).

The size of the spots was investigated as well. There was a significant interaction between the genotype and etoposide treatment observed ($p=0.0062$, $F(1, 2413)=7.517$, $\omega^2=0.004$). The genotype ($p=0.0132$, $F(1, 2413)=6.153$, $\omega^2=0.003$) and the treatment was significant as well ($p=0.0411$, $F(1, 2413)=4.178$, $\omega^2=0.002$) (See Figure 27 B).

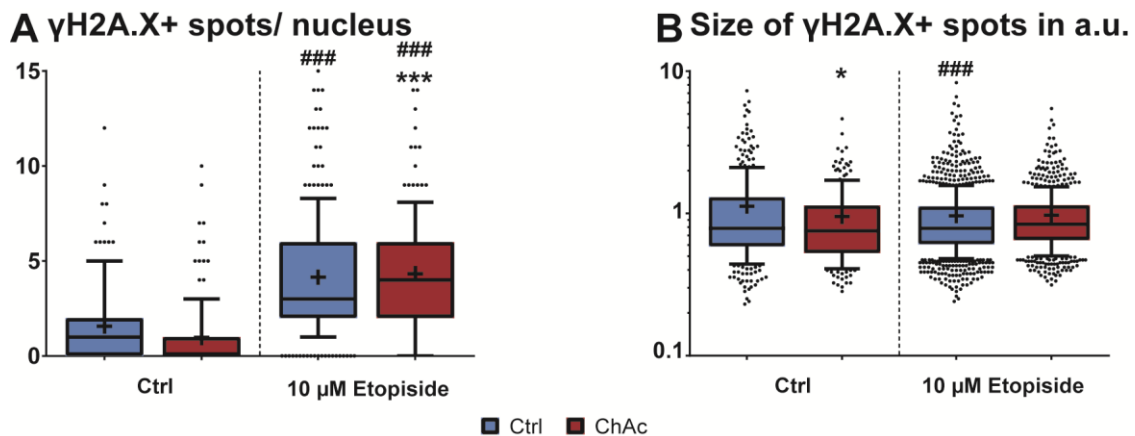


Figure 27: DNA damage in MSN differentiation. A) Analysis of $\gamma\text{H2A.X}$ showed increased DSB upon acute treatment for 1h with 10 μM etoposide that resulted in increase of $\gamma\text{H2A.X}$ spots per nucleus in ChAc lines. B) Analysis of the size of $\gamma\text{H2A.X}$ spots showed a decrease in size under control as well as treatment conditions. Boxes represent 25-75 percentiles, line represents median, whiskers represent 10-90%, + represents mean. n = at least 168 nuclei from 8 independent experiments. * indicate significant differences within a treatment. # indicate significant differences to control condition. */**/***; #/###/#### represent $p=0.05/0.01/0.001$, respectively.

Neurons that were differentiated according to mDAN protocol were subjected to etoposide treatment as well. There was a significant interaction observed between genotype and treatment ($p<0.0001$, $F(1, 2626)=22.32$, $\omega^2=0.007$). The influence of the treatment ($p<0.0001$, $F(1, 2626)=465.1$, $\omega^2=0.149$) and of the genotype ($p=0.035$; $F(1, 2626)=8.525$, $\omega^2=0.003$) were both significant (See Figure 28 A). The size of the $\gamma\text{H2A.X}$ spots showed

that there is no interaction and no influence of genotype. The treatment however had a significant influence ($p < 0.0001$, $F(1, 7784) = 33.78$, $\omega^2 = 0.004$) (See Figure 28 B).

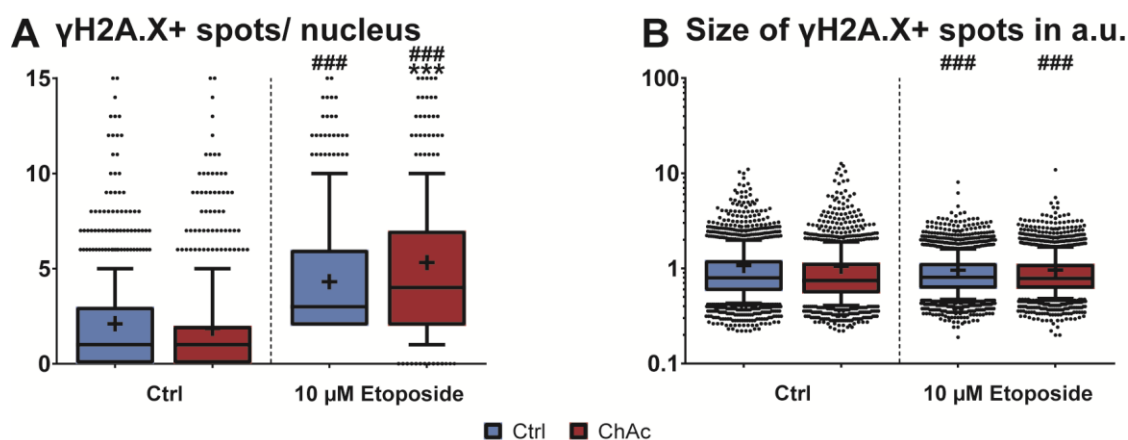


Figure 28: DNA damage in mDAN differentiation. A) Analysis of γ H2A.X showed increased DSB upon acute treatment for 1h with 10 μ M etoposide that resulted in increase of γ H2A.X spots per nucleus in ChAc lines. B) Size of γ H2A.X spots is unaffected by genotype and treatment. Boxes represent 25-75 percentiles, line represents median, whiskers represent 10-90%, + represents mean. n = at least 433 nuclei from 8 independent experiments. * indicate significant differences within a treatment. # indicate significant differences to control condition. */**/***; #/#/#/#/#/# represent $p = 0.05/0.01/0.001$, respectively.

The experiments showed that in both differentiation protocols ChAc patient derived neurons gain more DNA damage than healthy controls when treated with etoposide.

In summary, no increased cell death or DNA damage under control conditions was detected. However, both protocols showed an increased vulnerability to disruptions to proteostasis as well as DNA damage induction by etoposide. A major difference between mDAN and MSN differentiated neurons was the differential reaction to the stressors used. While mixed striatal cultures showed an increased vulnerability to tunicamycin, midbrain dopaminergic neurons were more susceptible to L-canavanine poisoning. Analysis of the cell composition highlighted a difference in the time point of cell death (See Table 23).

Table 23: Summary of stressing experiments

L-canavanine	MSN differentiation	mDAN differentiation
PrestoBlue	1mM had no effect on wild type and ChAc	1mM had no effect on wild type and ChAc
	2mM and 5mM decreased cell survival, however, wild type and ChAc were similar	2mM and 5mM decreased cell survival and ChAc was more severely affected

L-canavanine	MSN differentiation	mDAN differentiation
LDH	ChAc lines had an reduced LDH release	ChAc lines had an increased LDH release
composition	ChAc lines showed a more pronounced early cell death	ChAc lines showed a more pronounced acute late cell death
tunicamycin	MSN differentiation	mDAN differentiation
PrestoBlue	10µM had no effect on wild type and ChAc 50µM and 100µM decreased cell survival and ChAc was more severely affected	10µM had no effect on wild type and ChAc 50µM and 100µM decreased cell survival and ChAc was more severely affected
LDH	ChAc lines had an reduced LDH release	ChAc lines had an increased LDH release
composition	wild type and ChAc behaved similar	ChAc lines showed an more pronounced acute late cell death
γH2A.X	MSN differentiation	mDAN differentiation
Count of spots	strong effect of etoposide treatment no effect of the genotype	strong effect of etoposide treatment weak effect of the genotype
Size of the spots	weak effect of the genotype	no effect of the genotype

2.6. Characterization of metabolism

Glycolysis and oxidative phosphorylation are important pathways for the cell to meet energy requirements of various processes. It is known that these metabolic pathways are tightly regulated and dependent on each other. To elucidate whether their balance is shifted, complex multi-step analysis of mature neurons was conducted. The seahorse

device allows simultaneous measurement of changes in pH and oxygen concentration and provides the possibility to inject multiple substances to investigate their influence. Alterations in oxygen consumption and extracellular acidification rate can be used to characterize the energy metabolism of the cells and for an in depth analysis of metabolic parameters, since the interactions of the injected substances with different complexes of the electron transport chain are known. For characterization of metabolism the increase in glycolysis, the glycolytic reserve, the non-glycolytic acidification rate, the coupling efficiency, the spare respiratory capacity and the non-respiratory oxygen consumption were calculated.

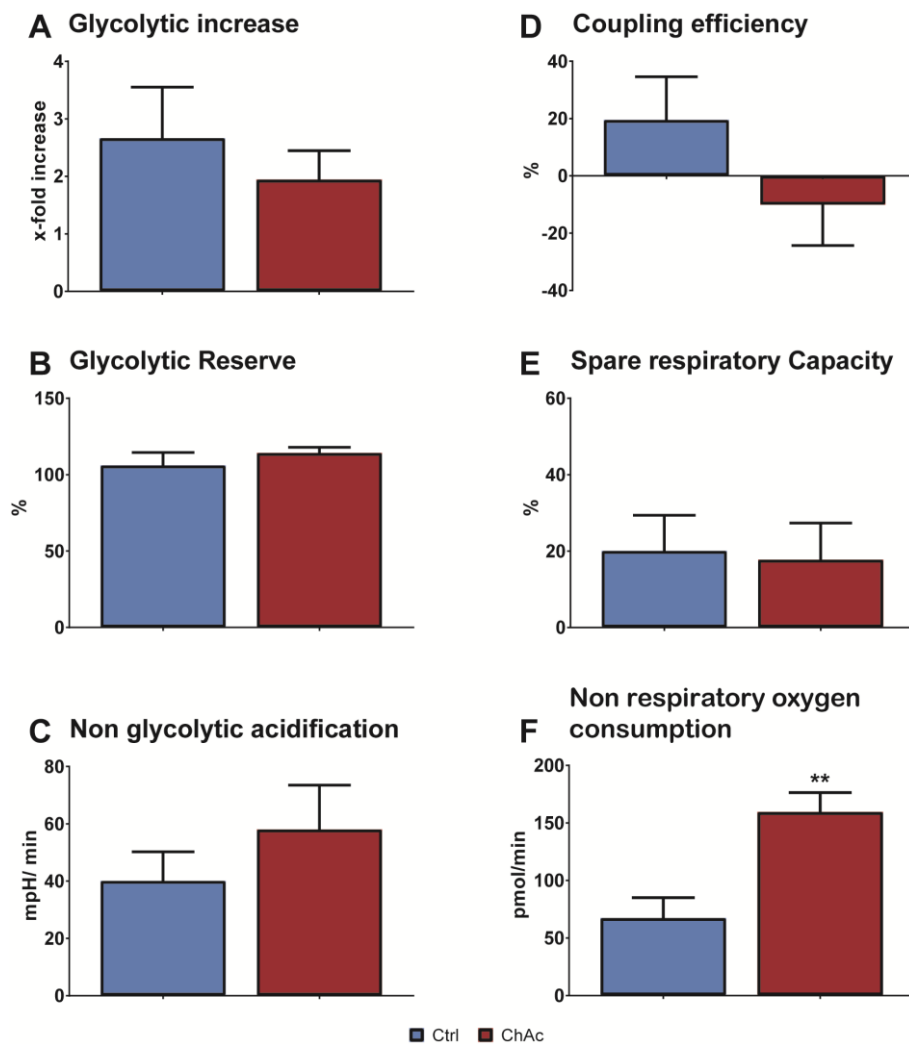


Figure 29: Metabolic characterization of mature neurons after MSN differentiation. A-C) No differences were observed during the characterization of glycolysis. D-F) Mature MSN neurons have a low coupling efficiency and comparable low spare respiratory capacity. The non-respiratory oxygen consumption was significantly increased in ChAc lines. Bars represent mean + SEM. $n \geq 4$. * indicate significant differences. **/*** represent $p=0.05/0.01/0.001$, respectively.

When mature MSN were investigated, there was no difference observed in glycolytic increase, glycolytic reserve, non-glycolytic acidification rate, the spare respiratory capacity and coupling efficiency of mitochondria. There was, however, a significant increase in non-respiratory oxygen consumption (See Figure 29 A-F).

Following the mDAN differentiation protocol there was no difference observed in glycolytic increase, glycolytic reserve and non-glycolytic acidification rate. Characteristics of oxidative phosphorylation were altered. Coupling efficiency and spare respiratory capacity were higher in patient derived neurons than in wild type controls. The non-respiratory oxygen consumption was decreased in mDAN derived from ChAc compared to wild type (See Figure 30 A-F).

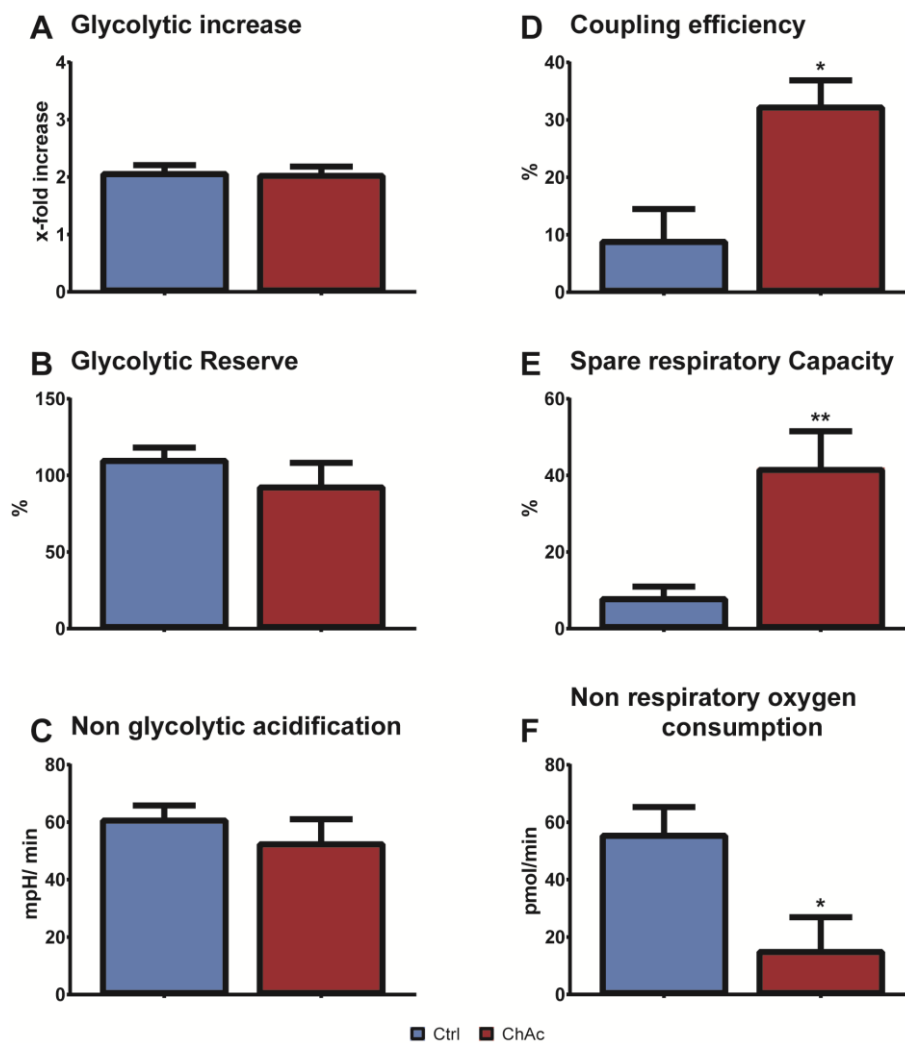


Figure 30: Metabolic characterization of mature neurons after mDAN differentiation. A-C) No differences were observed during the characterization of glycolysis. D-F) Mature mDAN from ChAc lines have significantly higher coupling efficiency as well as higher spare respiratory capacity. The non-respiratory oxygen consumption was significantly decreased in ChAc lines. Bars represent mean + SEM. $n \geq 5$. * indicate significant differences. */**/** represent $p=0.05/0.01/0.001$, respectively.

In summary in neither differentiation protocol there was a disturbance in glycolytic parameters observed. Analysis of mitochondrial characteristics revealed differential results between MSN and mDAN derived neurons. While mixed striatal cultures harbored a reduction in coupling efficiency, mDAN differentiations exhibited an increase. Furthermore, the spare respiratory capacity was unaltered in MSN differentiations but increased in mDAN cultures. The non-respiratory oxygen consumption was lowered in both protocols, suggesting a putative pan neuronal phenotype.

Table 24: Summary of the results of the metabolic analysis

	MSN differentiation	mDAN differentiation
Glycolytic parameters	No alterations in glycolytic parameters	no alterations in glycolytic parameters
Mitochondrial parameters	low coupling efficiency ChAc lines showed a reduced non-respiratory oxygen consumption	ChAc lines showed an increased coupling efficiency, spare respiratory capacity and non-respiratory oxygen consumption

3. Live cell imaging

In neurons the energy demand along a neurite is not constant. There are local energy sinks that require a larger supply with ATP. Therefore it is crucial that there is a proper distribution of mitochondria. This distribution is achieved by axonal transport along the microtubule. Furthermore dynamics of fusion, fission and recycling of damaged mitochondria have to be maintained over a long distance. Live cell trafficking analysis of mitochondria was used to investigate the morphology and functions of mitochondria.

The trafficking of lysosomes was investigated to elucidate whether the autophagic recycling and endosomal signaling pathways are disturbed. Likewise, the morphology and trafficking parameters of lysosomal compartments were analyzed.

3.1. Mitochondrial dynamics

To investigate if the shape and transport of mitochondria is impaired in patient neurons, live cell imaging of mitochondrial marker MitoTracker DeepRed was utilized. Videos were taken for 2 min and consisted of 400 frames resulting in a frame time interval of 0.3

seconds. For the morphological analysis of mitochondria, the first frame of each video was analyzed. Trafficking parameters were obtained from the whole video.

3.1.1. Morphological analysis

The investigated morphological parameters included the amount of organelles per arbitrary neurite length, the shape and the size.

3.1.1.1. Undirected neurons (96 well plate format)

Mature neurons that were differentiated according to MSN protocol were analyzed and the amount of mitochondria per arbitrary neurite length was evaluated. Counting of organelles, assessment of their morphological features as well as measurement of network size was done using semi-automated macros in FIJI to avoid bias. The shape of the mitochondria was described using the estimated aspect ratio. The object recognition tries to fit ellipses to the mitochondria and then the aspect ratio can be calculated by dividing the major radius with the minor. Round objects will therefore have a ratio close to one. When a mitochondrion in a neurite is estimated as a rod like object, the area it occupies in an image is linearly correlated to its volume and therefore its biomass. Since the biomass of a mitochondrion is a crucial readout for its capability to generate ATP, the size of a mitochondrion can be used to estimate this ability (Agnello, et al., 2008). Size of mitochondria was measured in pixel and compared using two-way ANOVA.

There were significantly less mitochondria in neurons from ChAc patients than in wild type. In an attempt to rescue this phenotype, three different substances were investigated. Conditions included untreated control, DMSO mock, the Lyn kinase inhibitor PP2, which was used in previous studies to treat the abnormally shaped membranes of erythrocytes and a mixture of glycolate and D-lactate (GADL), that was shown to activate and rescue the mitochondria of Parkinson's disease patients cells (De Franceschi, et al., 2011; Toyoda, et al., 2014). The phenotype of the disease was investigated by comparing wild type and ChAc lines under control conditions using a t-test, when needed with Welch's correction, and estimating the effect size using Cohen's d. Results of the treatment conditions were analyzed using two-way ANOVA with the genotype (wild type and ChAc) and different treatment conditions as the independent variables.

The number of mitochondria was significantly reduced in ChAc lines and the effect was large ($p < 0.0001$, $t(40.89) = 4.556$, $d = 1.12$). For GADL treatment, the genotype had a significant influence ($p = 0.0003$, $F(1, 85) = 14.26$, $\omega^2 = 0.15$). There was, however, no effect of the treatment observed and no interaction between genotype and treatment. The

evaluation of the treatment with PP2 and the DMSO vehicle control showed no effects of genotype, treatment and interaction between genotype and treatment (See Figure 31 A).

Mixed striatal cultures had normally shaped mitochondria and there was no differential behavior when GADL or PP2 were applied. Statistical analysis did not reveal any interactions between treatment conditions and genotype (See Figure 31 B).

There was a very large effect observed on the size of ChAc mitochondria, resulting in a smaller size ($p < 0.0001$, $t(36.29) = 6.54$, $d = 1.47$). MSN differentiated mature neurons from ChAc patients showed a decreased size of the mitochondria. The genotype itself was considered significant ($p = 0.0003$, $F(1, 82) = 14.55$, $\omega^2 = 0.152$) but there was no influence of the treatment. An interaction between GADL treatment and the genotype was observed ($p = 0.0345$, $F(1, 82) = 4.621$, $\omega^2 = 0.055$). The treatment with PP2 revealed an influence of the genotype ($p = 0.0082$, $F(1, 84) = 7.329$, $\omega^2 = 0.089$) but no significant effect of the treatment and no interactions between PP2 treatment and genotype (See Figure 31 D).

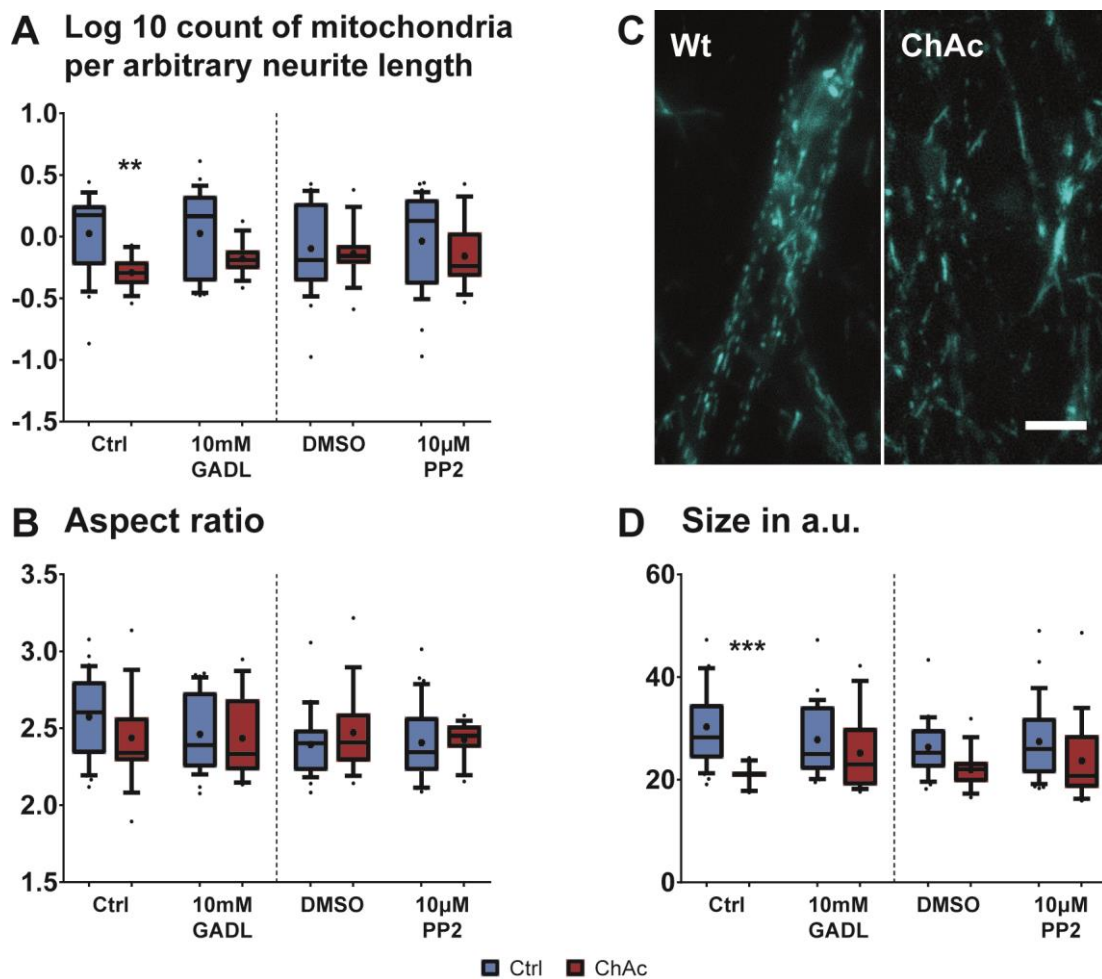


Figure 31: Morphological analysis of mitochondria of MSN differentiation. A) The number of mitochondria per neurite length is reduced in ChAc lines. B) The aspect ratio of mitochondria was not different. C) Representative picture of wild type and ChAc neuronal net with the latter showing a

decreased count. D) The size of the observed mitochondria is reduced in neurons from ChAc patients. Boxes represent 25-75 percentiles, line represents median, whiskers represent 10-90%, + represents mean. n = at least 26 images from 4 independent experiments. * indicate significant differences within a treatment. # indicate significant differences to control condition. */**/***; ###/#### represent $p=0.05/0.01/0.001$, respectively. Scale bar = 10 μ m

Neurons yielded by mDAN differentiation showed a small but significant reduction of mitochondria per neurite length ($p=0.0003$, $t(320.2)=3.668$, $d=0.40$). GADL, Phalloidin and PP2 were applied to cells and their effect was investigated. There was a significant influence of the genotype ($p=0.0031$, $F(1, 442)=8.833$, $\omega^2=0.021$) as well as an influence of the GADL treatment ($p<0.0001$, $F(1, 442)=15.45$, $\omega^2=0.035$). Interaction between treatment and genotype was not observed. Upon application of phalloidin, the influence of the genotype remained ($p=0.004$, $F(1, 392)=8.4$, $\omega^2=0.023$). The treatment, however, had no effect and there was no interaction between the genotype and the treatment. Investigation of PP2 showed the effect of the genotype ($p=0.0332$, $F(1, 271)=4.582$, $\omega^2=0.020$) but treatment had no effect and there was no significant interaction (See Figure 32 A).

Analysis of the aspect ratio of mitochondria in dopaminergic cultures revealed a medium effect resulting in shortened mitochondria ($p<0.0001$, $t(294.3)=5.538$, $d=0.60$). Aspect ratio was reduced under control conditions. The influence of the genotype was considered significant ($p=0.0123$, $F(1, 449)=6.315$, $\omega^2=0.015$) as well as the influence of the treatment with GADL ($p<0.0001$, $F(1, 449)=32.59$, $\omega^2=0.068$). ChAc patient's cell reacted differently to GADL treatment as statistics revealed an interaction between genotype and treatment ($p=0.0101$, $F(1, 449)=6.669$, $\omega^2=0.015$). During phalloidin treatment, the influence of the genotype was also observed ($p=0.001$, $F(1, 400)=50.8$, $\omega^2=0.113$), but not of the treatment itself. Moreover, interaction between treatment and genotype was rated significant ($p=0.0110$, $F(1, 400)=6.533$, $\omega^2=0.016$) (See Figure 32 B).

When the size of mDAN mitochondria was measured, they showed a reduced size. This effect was rated small ($p=0.0042$, $t(310)=2.883$, $d=0.33$). Treatment with GADL showed that the influence of the genotype ($p<0.0001$, $F(1, 409)=45.33$, $\omega^2=0.086$) and of the GADL treatment ($p<0.0001$, $F(1, 409)=60.9$, $\omega^2=0.115$) were significant. There was an interaction between the treatment and genotype ($p<0.0001$, $F(1, 409)=20.9$, $\omega^2=0.041$) that was significant as well. Phalloidin application on midbrain dopaminergic neurons revealed a significant influence of the genotype ($p<0.0001$, $F(1, 377)=20.42$, $\omega^2=0.051$) and the treatment ($p=0.0001$, $F(1, 377)=14.55$, $\omega^2=0.038$). However, no interaction between the treatment and the genotype was found. When treated with PP2, no influence of genotype, treatment or interactions were observed (See Figure 32 D).

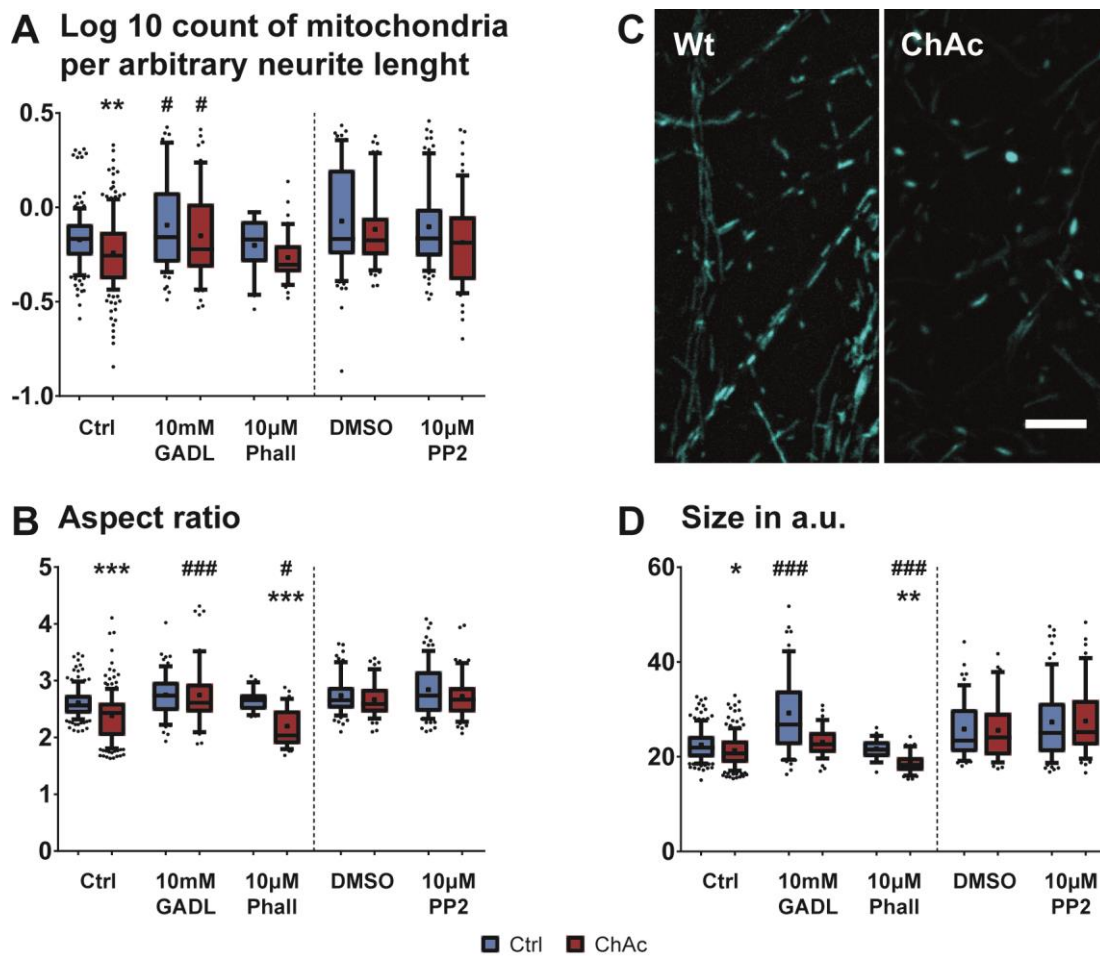


Figure 32: Morphological analysis of mitochondria of mDAN differentiation. A) The number of mitochondria per neurite length is reduced in ChAc lines under control conditions. GADL treatment increased the count in wild type and ChAc lines. B) The aspect ratio of investigated mitochondria was reduced for ChAc lines under control conditions but was rescued with GADL treatment. C) Representative picture of wild type and ChAc neuronal, with the latter showing a decreased count and aspect ratio. D) The size of the observed mitochondria is different under control conditions. GADL treatment increases the size. Phalloidin treatment reduces the size. Boxes represent 25-75 percentiles, line represents median, whiskers represent 10-90%, + represents mean. n = at least 26 images from 5 independent experiments. * indicate significant differences within a treatment. # indicates significant differences to control condition. */**/***, #/###/#### represent p=0.05/0.01/0.001, respectively. Scale bar = 10µm

3.1.1.2. Microfluidic chambers

Microfluidic chambers (MFCs) were used to differentiate whether observed defects were present in both proximal and distal neurite positions. Furthermore, in later analyses the direction of a moving track can be evaluated and the estimated parameters of motility, speed and the like can be further differentiate into an anterograde and retrograde fraction.

When the identity of the neurons that grew through the channels of an MFC was investigated, only a minority of the neurons was TH positive. Most of the neurons that were observed were motor neurons (See Figure 33).

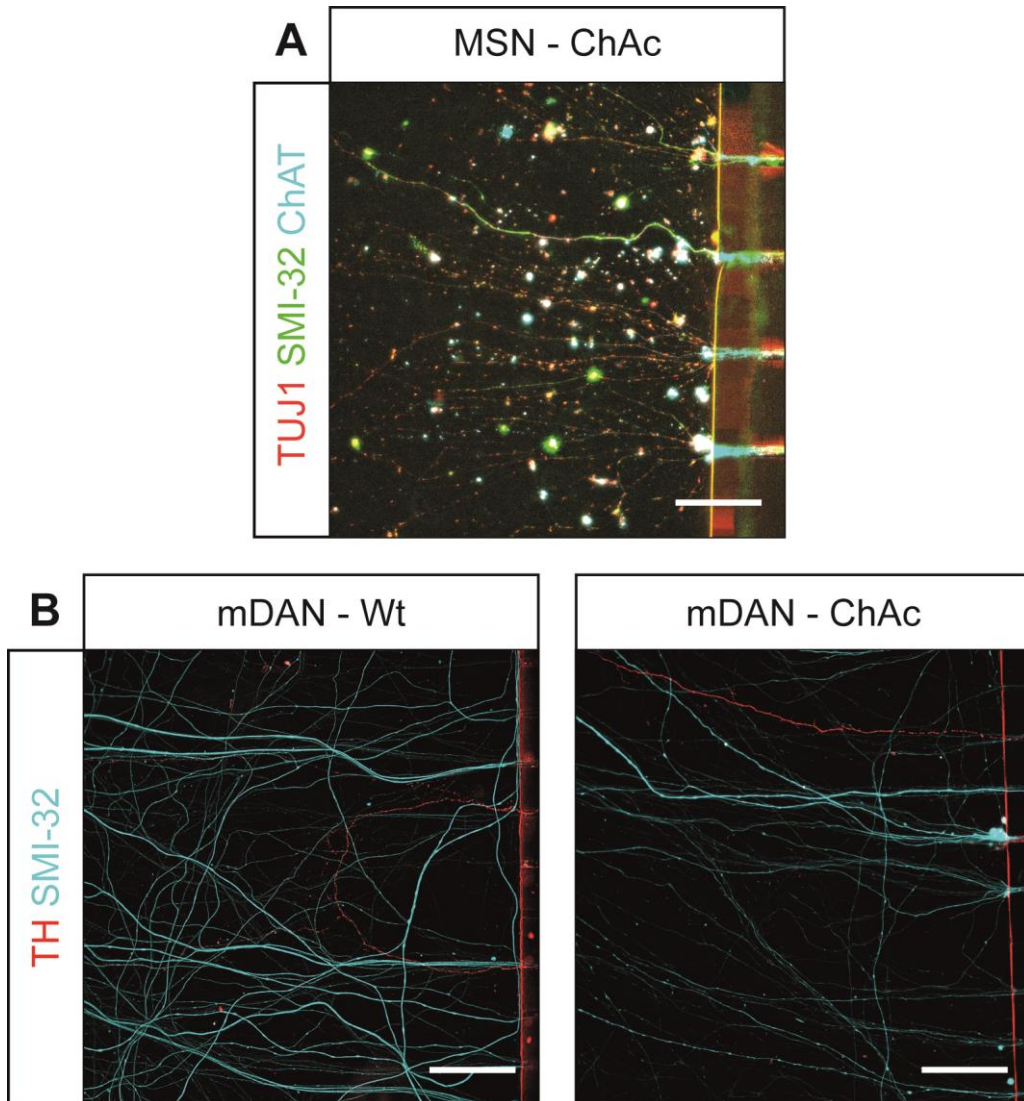


Figure 33: Characterization of the channel-exits of MFC. A) MSN are growing inefficiently through the channels. Only cholinergic interneurons were detected. TUJ1 is a pan neuronal marker. SMI-32 labels a neurofilament. CHAT is a marker for cholinergic interneurons. B) Few dopaminergic neurons grow through the channels. TH is a marker for dopaminergic neurons. SMI-32 labels motor neurons in the mDAN protocol. Scale bar = 100 μm

As a first parameter, the amount of mitochondria per arbitrary neurite length was investigated. The parameters for the two-way ANOVA were the genotype and the positions (distal vs. proximal). Striatal cultures of patient cell lines showed a reduced amount of mitochondria (See Figure 34 A). Influence of the genotype was considered significant ($p=0.0067$, $F(1, 122)=7.602$, $\omega^2=0.064$), however, the influences of the position and interaction, however, were not significant. The shape of the mitochondria was

investigated using the aspect ratio of both radii of the fitted ellipses. Neurons derived by MSN differentiation showed no alteration in the aspect ratio and there was no influence of the genotype, position and no interaction (See Figure 34 B).

When the amount of mitochondria in MFCs of mDAN cultures was investigated, there was no significant influence of the genotype, position or interaction observed (See Figure 34 C). Analysis of the aspect ratio revealed a significant influence of the genotype ($p=0.0002$, $F(1, 445)=14.17$, $\omega^2=0.033$), but no influence of the position. Furthermore, no interaction between position and genotype was observed (See Figure 34 D).

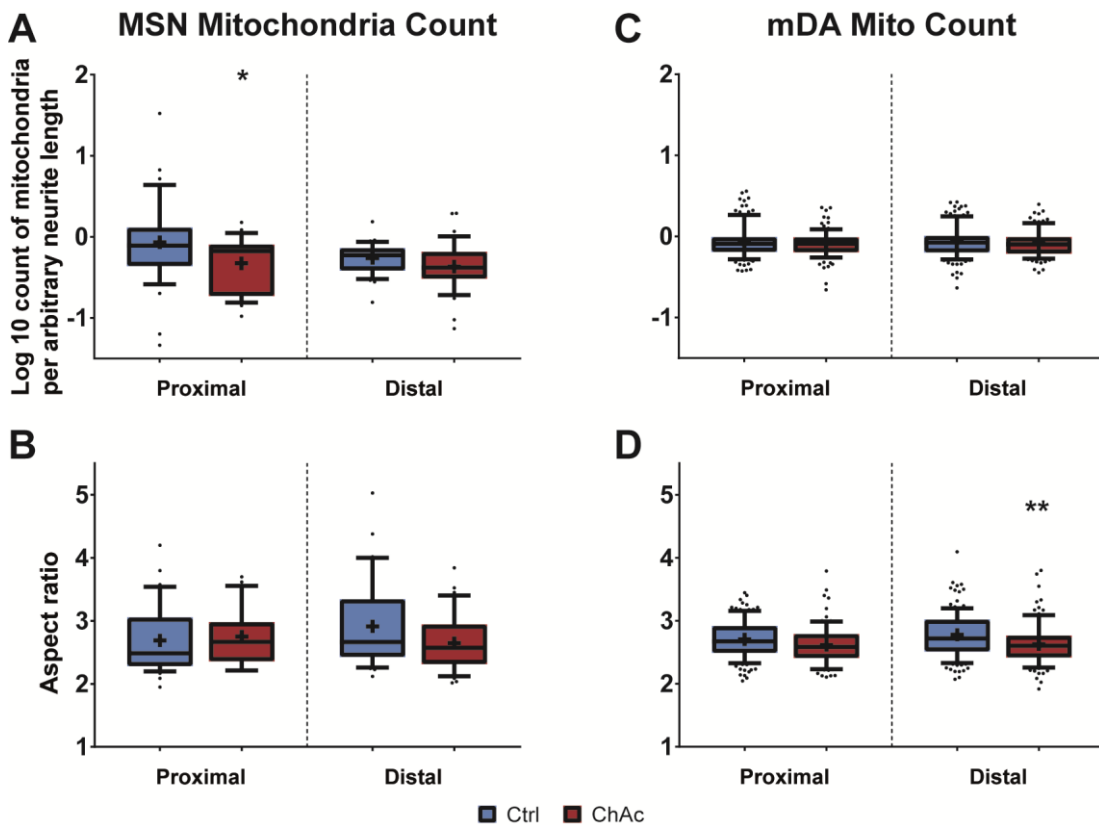


Figure 34: Morphological analysis of MFC cultures. A) MSN differentiated cultures showed a reduction in number of mitochondria per neurite length that was most pronounced in the proximal region of patient lines. B) MSN differentiated cultures had no difference in aspect ratio. $n(A/B)$ = at least 26 images from 6 independent experiments. C) mDAN differentiated cultures showed no reduction in the count of mitochondria per neurite length. D) Mitochondria of mDAN differentiated neurons had a reduced aspect ratio that was most pronounced in distal position. $n(C/D)$ = at least 94 images from 18 independent experiments. Boxes represent 25-75 percentiles, line represents median, whiskers represent 10-90%, + represents mean. * indicate significant differences within a treatment. **/***, represent $p=0.05/0.01/0.001$, respectively.

In summary, ChAc lines have less mitochondria in undirected 96-wells in both differentiation protocols. These mitochondria were smaller and mDAN cultures even

showed a shortening, while the aspect ratio in MSN differentiations was not different. When MFC were investigated, the reduction in the amount was only observed in mixed striatal but not midbrain dopaminergic cultures. The change in the aspect ratio was reproduced in the distal parts of the channels. GADL treatment had no effect on the phenotypes in MSN cultures but increased the count, aspect ratio and size in mDAN cultures. The treatment, however, was not specific for ChAc lines but also in wild type lines. PP2 treatment had no effect (See Table 25).

Table 25: Summary of morphological features of mitochondria in ChAc

	MSN differentiation	mDAN differentiation
96 well	ChAc lines had fewer mitochondria	ChAc lines had fewer mitochondria
	There was no difference in the aspect ratio	ChAc lines had shorter mitochondria
	ChAc lines had smaller mitochondria	GADL treatment increased count, aspect ratio and size
	GADL and PP2 treatment had no effect	
MFC	ChAc lines had fewer mitochondria in proximal position	No difference in the count
	no difference in distal parts	ChAc lines had shorter mitochondria
	no difference in the aspect ratio	

3.1.2. Trafficking analysis

Using the tracking algorithms from the FIJI suite all objects in each frame of one video were first detected and then the nearest spots between each picture of a stack were linked. The linear motion tracker minimizes linking costs and favors linear movement. The translocation of the spots in between pictures is interpreted as movement and parameters like speed, distance travelled and angle of movement were calculated. In the end, databases with characteristics for individual tracks were generated. These databases were processed as explained in the Materials and Methods section.

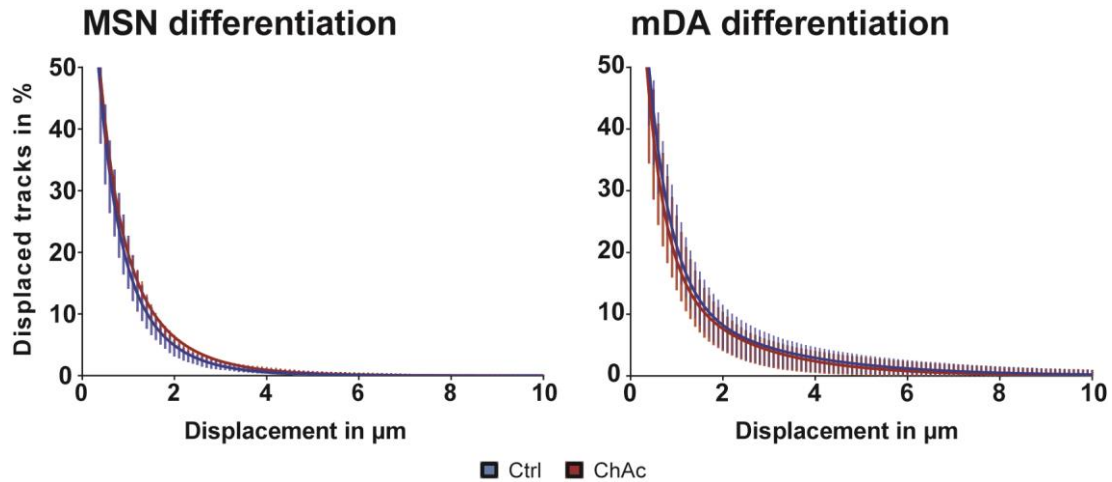


Figure 35: Examples of plots obtained from trafficking analysis of mitochondria. Stripes indicate the standard deviation of the amount of displaced tracks of the original data set. Lines indicate the fitted curves of the calculated two-phase decay model regression.

3.1.2.1. 96 well

The motility of mitochondria in cell culture was described by two parameters. The first is the estimation of the amount of moving mitochondria and the second describes the motility of this moving fraction. The fraction of moving objects was estimated using two-way ANOVA as described in the Materials and Methods section.

Neither the amount of moving mitochondria, nor the mean speed of the motile fraction was different under control conditions. When the addition of GADL was compared to control condition, the moving fraction of mitochondria of mixed striatal cultures harbored no influence from the genotype. The influence of the treatment, however, was significant ($p < 0.0001$, $F(1, 18) = 53.93$, $\omega^2 = 0.748$). There was no interaction between genotype and treatment. The motility was not significantly influenced by the genotype, treatment or any interaction. In the comparison of DMSO mock control with PP2, there was no significant influence of the genotype or the treatment observed. There was, however, a significant interaction between genotype and treatment ($p = 0.0015$, $F(1, 16) = 14.63$, $\omega^2 = 0.476$) that influenced the amount of the moving fraction. The motility of the mitochondria was not influenced by either genotype, treatment nor interaction when the cells were investigated under these conditions (See Figure 36 A & B).

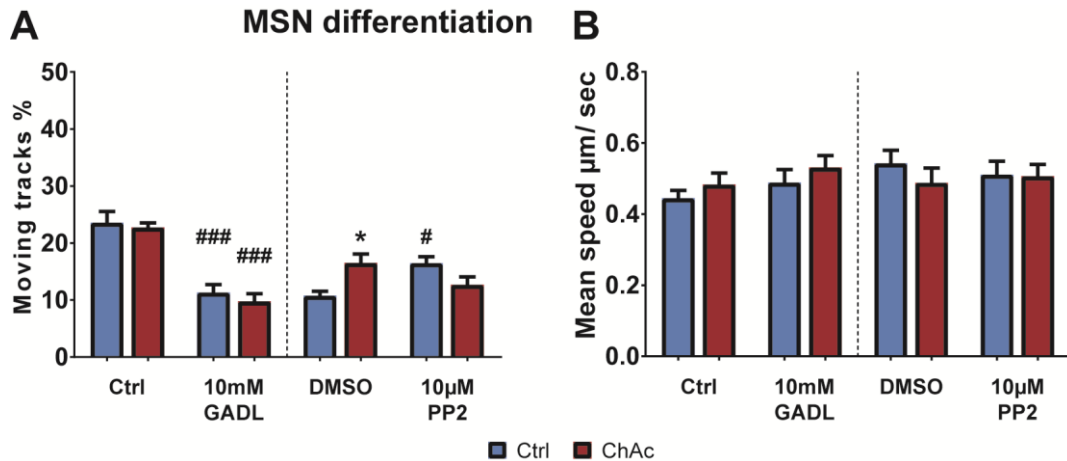


Figure 36: Trafficking analysis of mitochondria of MSN differentiated cultures. A) MSN differentiated cultures showed no difference between wild type and ChAc lines. GADL treatment reduced the moving fraction. B) There was no difference observed in the mean speed of moving mitochondria. Bars represent mean + SEM. $n \geq 4$. * indicate significant differences within a treatment. # indicate significant differences to control condition. */**/***; #/###/#### represent $p=0.05/0.01/0.001$, respectively.

The fraction of moving mitochondria of mid brain dopaminergic neurons from ChAc lines was moderately increased in ChAc lines ($p=0.0017$, $t(56)=3.3$, $d=0.88$). The mean speed under control conditions, however, was largely reduced ($p<0.0001$, $t(56)=4.504$, $d=1.19$). GADL treatment of mDAN cultures showed significant influence of the genotype ($p=0.008$, $F(1, 81)=7.399$, $\omega^2=0.055$), the treatment ($p<0.001$, $F(1, 81)=62.2$, $\omega^2=0.414$), but no interaction in regards to the moving fraction. The motility was also influenced by genotype ($p=0.007$, $F(1, 81)=7.667$, $\omega^2=0.069$) treatment ($p=0.0017$, $F(1, 81)=10.51$, $\omega^2=0.108$) and the interaction of both ($p=0.0137$, $F(1, 81)=6.346$, $\omega^2=0.069$). The treatment with the actin stabilizer phalloidin showed no significant influence of genotype, treatment or any interaction. The motility, however, was influenced by the genotype ($p<0.0001$, $F(1, 65)=32.62$, $\omega^2=0.326$), but not the treatment. A significant interaction was observed as well ($p=0.0497$, $F(1, 65)=4$, $\omega^2=0.048$). When PP2 was added a significant influence of the genotype ($p=0.0102$, $F(1, 59)=7.042$, $\omega^2=0.099$), significant influence of the treatment ($p=0.0039$, $F(1, 59)=9.031$, $\omega^2=0.123$) and the interaction ($p=0.0254$, $F(1, 59)=5.259$, $\omega^2=0.077$) on the amount of moving mitochondria was observed. The motility of the mitochondria was not influenced by the addition of PP2 when compared to DMSO control condition (Figure 37 A & B).

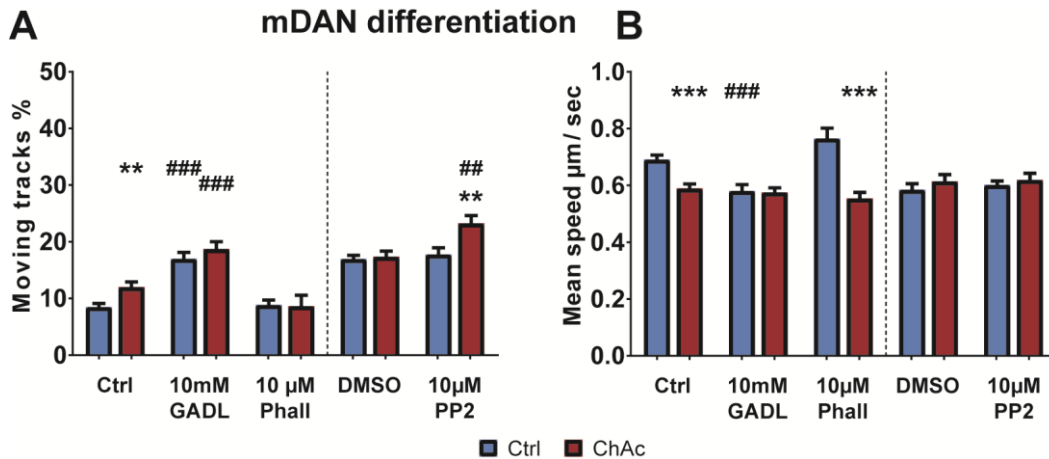


Figure 37: Trafficking analysis of mitochondria of mDAN differentiated cultures. A) mDAN differentiated ChAc cultures showed an increased moving fraction. GADL treatment further increased the moving fraction. PP2 treatment selectively increased the moving fraction of mitochondria of ChAc lines. B) Wild type lines had an increased average movement speed under control conditions that dropped to ChAc levels after GADL treatment. Bars represent mean + SEM. $n \geq 5$ * indicate significant differences within a treatment. # indicate significant differences to control condition. */**/***; #/#/#/#/# represent $p=0.05/0.01/0.001$, respectively.

Another characteristic of organelle trafficking in cells is that it is not random but rather direct movement. For example, mitochondria travel directly to parts of the cell that exhibit an increased energy demand (Safiulina and Kaasik, 2013). To estimate whether there was a difference in the directedness of the movement, the total displacement of a track was divided by the total track length. An object that moved from its start A to its end B in direct manner will have a directedness close to 1, while an object just moving around its stationary position will have a directedness close to 0. To quantify this parameter, the amount of tracks that moved with directedness above 0.75 was compared between wild type and ChAc patients under different treatment conditions.

The fraction of directly moving mitochondria was not different in mixed striatal cultures when wild type and ChAc lines were compared under control conditions. The analysis of the directedness of mitochondrial movement during treatment, showed that there was no significant effect of the genotype, treatment of GADL, and no interaction. Treatment of the lines with PP2 had no effect on directedness compared to DMSO mock control (See Figure 38 A).

There was no difference in the amount of directly moving mitochondria under control conditions between wild type and ChAc lines in mDAN differentiation protocol. When the cell lines were treated with GADL, there was no influence of the genotype. However, a significant effect of the treatment ($p < 0.0001$, $F(1, 432) = 52.64$, $\omega^2 = 0.11$) was observed.

The influence of the interaction between genotype and treatment, however, was not significant. Treatment with phalloidin revealed a significant influence of the genotype ($p=0.0003$, $F(1, 348)=13.43$ $\omega^2=0.034$). The influence of the treatment was not considered significant. Furthermore, a significant interaction ($p=0.0004$, $F(1, 348)=12.92$, $\omega^2=0.035$) was observed. When PP2 was applied, genotype, treatment and interaction were all considered not significant (See Figure 38 B).

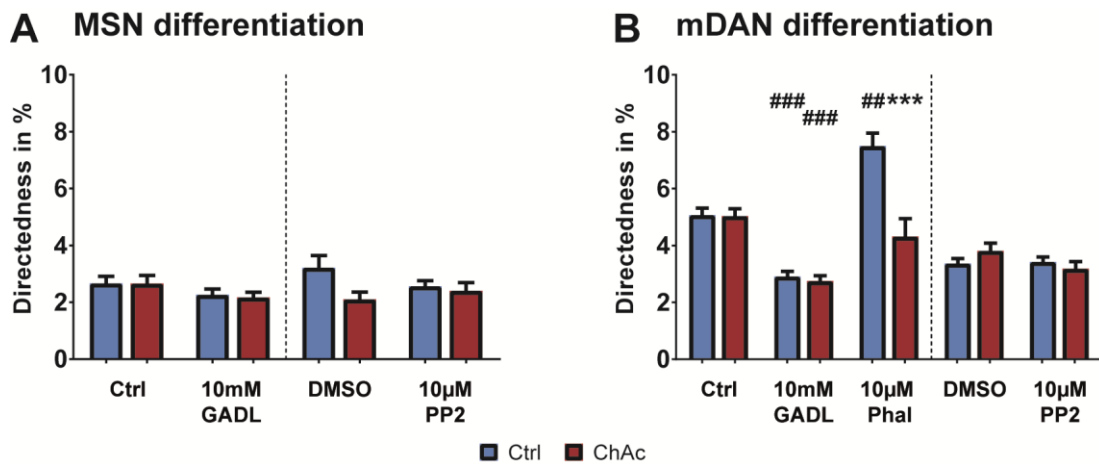


Figure 38: Analysis of direct movement in both differentiations protocols. A) MSN differentiation had no observable difference in the fraction of direct movement. $n \geq 4$. B) Fraction of direct movement was influenced by the treatment but not the genotype in mDAN differentiation. Application of phalloidin caused differential response in wild type and ChAc lines. $n \geq 5$. Bars represent mean + SEM. * indicate significant differences within a treatment. # indicate significant differences to control condition. **/***, ###/#### represent $p=0.05/0.01/0.001$, respectively.

Since the mean speed of all moving tracks corresponds to overall fitness of the cell and is governed by global effects, the analysis of sub fractions might be useful to determine the status of individual mitochondria themselves, and local events like energy demanding hot spots. Therefore the speed of the 10% fasted tracks was investigated.

MSN protocol derived neurons showed no significant difference under control conditions, GADL or PP2 treatment as well as no dependency on the genotype. There was no interaction between the treatment and the genotype (See Figure 39 A).

There was a medium sized effect on the maximum speed observed, when mitochondria of wild type and ChAc lines were compared under control conditions ($p=0.0405$, $t(56)=2.097$, $d=0.56$). However, no response to GADL or PP2 was evident. The treatment with 10µM phalloidin, however, showed a significant influence of the genotype ($p=0.0004$, $F(1, 65)=13.98$, $\omega^2=0.175$) as well as an interaction ($p=0.0488$, $F(1, 65)=4.031$, $\omega^2=0.059$) (See Figure 39 B).

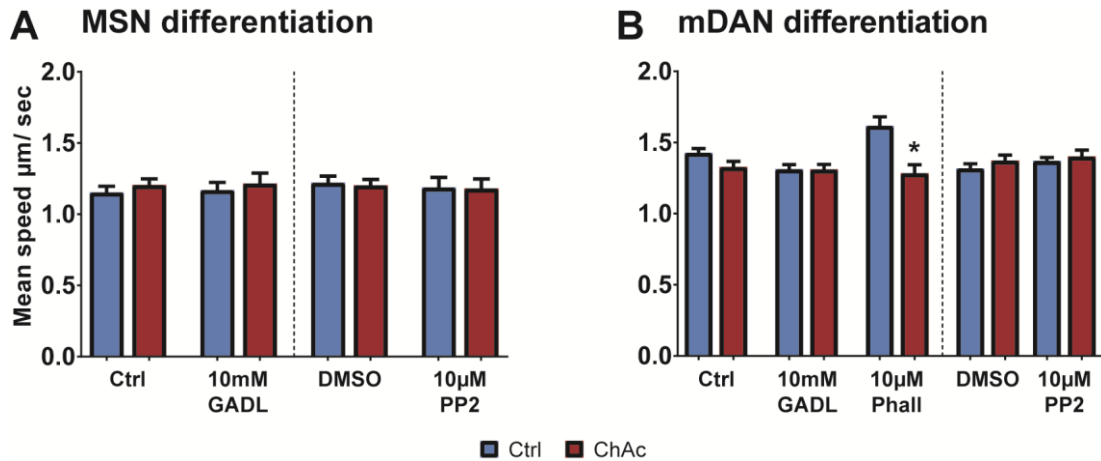


Figure 39: Speed of the top decile of the fastest mitochondria of both differentiation protocols. A) There was no difference observed in MSN differentiated neurons. $n \geq 4$. B) mDAN differentiated neurons showed no difference in the max speed that was accounted to influence of the genotype. Differential response to phalloidin treatment was observed. $n \geq 5$. Bars represent mean + SEM. * indicate significant differences within a treatment. * represents $p=0.05$, respectively.

3.1.2.2. Microfluidic chambers

Trafficking analysis in MFCs allows differentiation between anterograde and retrograde transport and its dependency on proximal or distal position in a neurite.

The moving fraction of mitochondria of mature neurons, which were yielded by the MSN differentiation protocol, was not influenced by the proximal/distal position or the genotype. There was no interaction observed (See Figure 40 A). The motility of the mitochondria was not influenced by genotype or position as well. The trend of a possible interaction between genotype and position was not rated significant (See Figure 40 B).

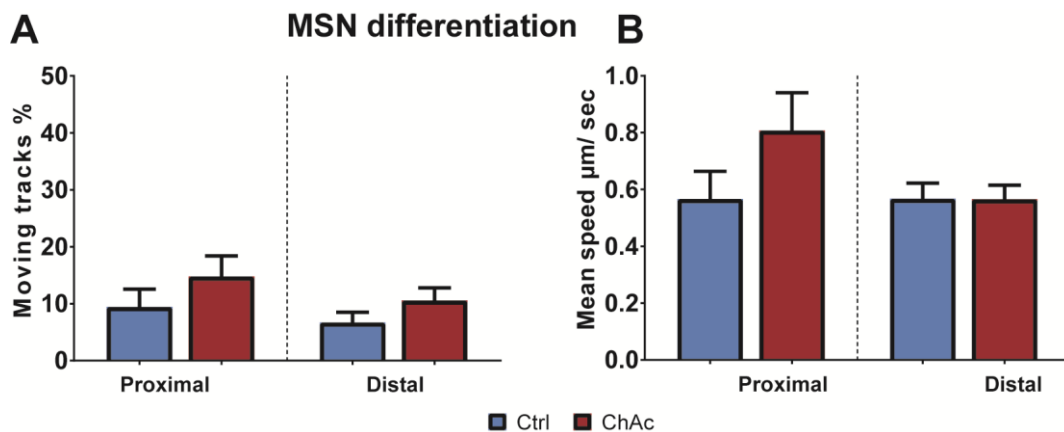


Figure 40: Trafficking analysis of mitochondria of MSN differentiated MFC cultures. A) MSN differentiated cultures showed no differences but a trend of increased movement was observed B) The genotype as well as the position had no significant influence on the MSN differentiation cultures. A trend of increased mean speed of mitochondria of ChAc lines in proximal parts was observed. Bars represent mean + SEM. $n \geq 6$.

Analysis of mature neurons derived from mDAN differentiation showed that the genotype and the position had no influence on the amount of moving organelles. The interaction between both was not significant (See Figure 41 A). When the motility of the moving fraction was evaluated, a significant influence of the genotype ($p < 0.0001$, $F(1, 85) = 20.2$, $\omega^2 = 1.62$), the position ($p = 0.0001$, $F(1, 85) = 16.23$, $\omega^2 = 0.132$) and an interaction ($p = 0.0054$, $F(1, 75) = 8.135$, $\omega^2 = 0.070$) was discovered (See Figure 41 B).

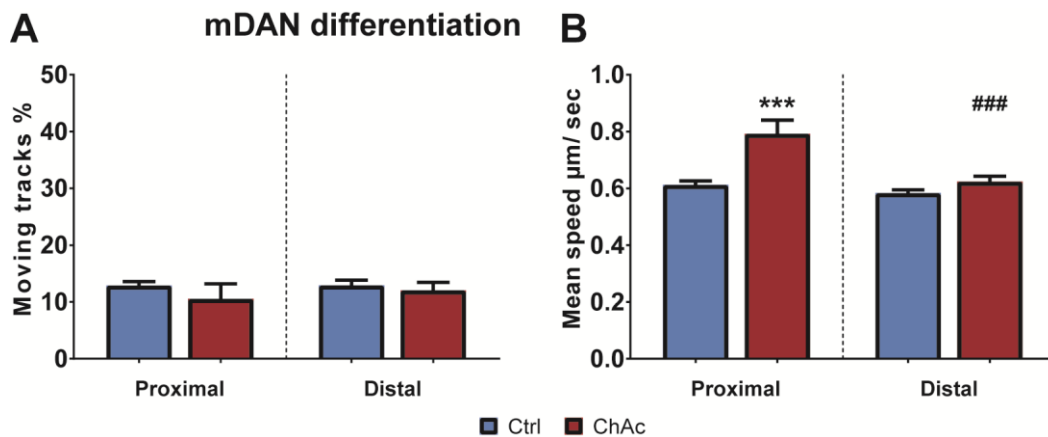


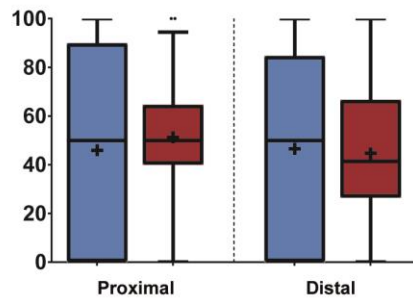
Figure 41: Trafficking analysis of mitochondria of mDAN differentiated MFC cultures. A) mDAN differentiated cultures showed no differences in the moving fraction. B) mDAN differentiated cultures showed an increased speed in ChAc lines that was more pronounced in proximal position. Bars represent mean + SEM. $n \geq 18$. * indicate significant differences within a treatment. # indicate significant differences to control condition. ***, ### represent $p = 0.001$, respectively.

In order to further characterize trafficking of mitochondria, the fraction of anterograde movement was analyzed and the average speed of the anterograde and retrograde fraction was investigated. Only tracks with a directedness above 0.75 were included in the analysis to make sure that the investigated mitochondria were moving in the according direction and not just randomly drifting due to focus or stage shift or minute pseudo stationary movement.

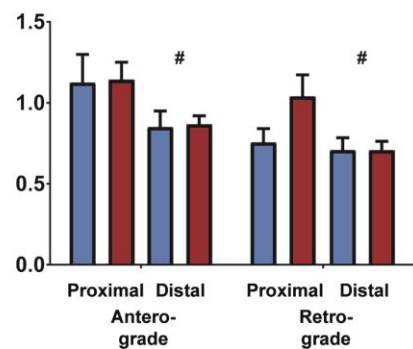
When the iPSCs were differentiated according to MSN differentiation protocol, the fraction of anterograde transport of mitochondria was not influenced by the genotype or the position. Furthermore, there was no interaction between the two (See Figure 42 A). Upon investigating the speed of the anterograde fraction of moving mitochondria, a significant influence by position ($p = 0.0104$; $F(1, 69) = 6.949$; $\omega^2 = 0.103$) but not of genotype or interaction between the two was observed. The speed of retrograde transport of mitochondria was not influenced of genotype, position or interaction (See Figure 42 B).

MSN differentiation

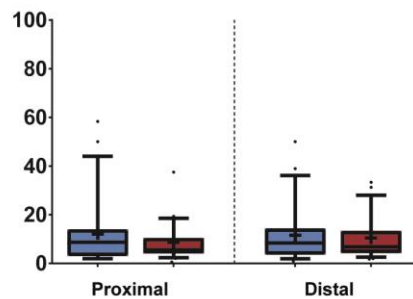
A Anterior moving tracks in %



B Mean speed in $\mu\text{m}/\text{sec}$

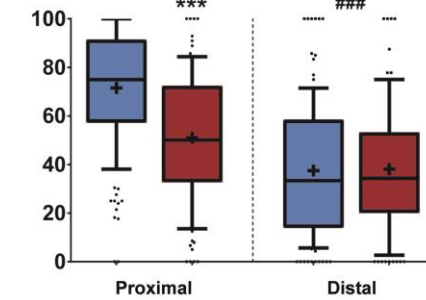


C Direct movement in %

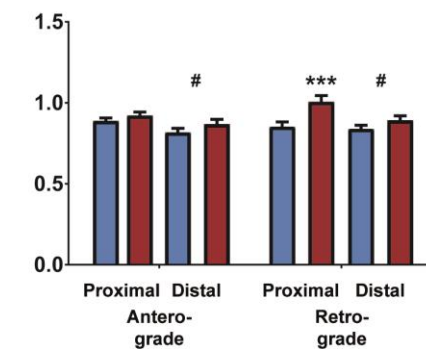


mDAN differentiation

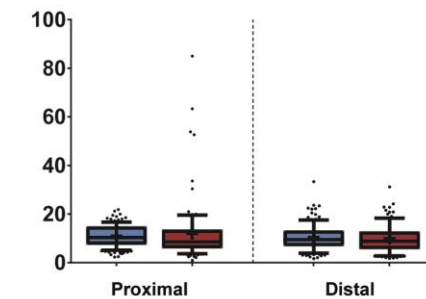
D Anterior moving tracks in %



E Mean speed in $\mu\text{m}/\text{sec}$



F Direct movement in %



■ Ctrl ■ ChAc

Figure 42: Detailed characterization of mitochondria trafficking in MFC. A) No difference in the anterograde fraction of moving mitochondria in MSN differentiation detected. B) Genotype had no influence on the mean speed of anterograde moving mitochondria but position had. There was a trend observed for retrograde movement in the proximal position indicating the increased mean speed for ChAc lines. C) No difference in direct movement was detected in MSN differentiations. $n(\text{A-C}) \geq 6$ D) There was a difference in anterograde moving fraction detected between proximal and distal position in mDAN differentiations. Decrease in anterograde movement in proximal parts was observed in ChAc lines. E) No influence of the position was observed in wild type lines in regards to retrograde transport. ChAc lines showed an increased mean speed in proximal positions that reduced to wild type level in distal parts. F) No difference in direct movement was detected in mDAN differentiations. $n(\text{D-F}) \geq 18$. Bars represent mean + SEM. Boxes represent 25-75 percentiles, line represents median, whiskers represent 10-90%, + represents mean. * indicate significant differences within a treatment. # indicate significant differences to control condition. */**/***; #/###/#### represent $p=0.05/0.01/0.001$, respectively

Neurons derived from mDAN differentiation showed significant influence of the genotype ($p < 0.0001$, $F(1, 436) = 16.33$, $\omega^2 = 0.031$) and the position ($p < 0.0001$, $F(1, 436) = 89.39$, $\omega^2 = 0.161$). Furthermore, the interaction between both was significant ($p < 0.0001$, $F(1, 436) = 18.45$, $\omega^2 = 0.035$) (See Figure 42D). The speed of the anterograde fraction was not significantly influenced by the genotype, but by the position ($p = 0.0059$, $F(1, 411) = 7.66$, $\omega^2 = 0.02$). There was no interaction observed (See Figure 42 E). The speed of the retrograde fraction was significantly influenced by the genotype ($p = 0.0003$, $F(1, 401) = 13.24$, $\omega^2 = 0.034$), the position ($p = 0.0297$, $F(1, 401) = 4.76$, $\omega^2 = 0.014$) but not the interaction (See Figure 42 E).

The directedness of the trafficking in regards to the position in the investigated neurite can also give crucial information. In both differentiation protocols there was no influence of the genotype and no influence of the position when the directedness of movement of mitochondria was investigated (See Figure 42 C & F).

The mean speed of the mitochondria above the ninth decile was investigated for MFC cultures as well. There was no significant influence of position, genotype or interaction observed in mixed striatal cultures when cultured in MFC (See Figure 43 A). Mature cultures yielded from mDAN differentiation protocol showed a significant influence of the genotype ($p = 0.0137$, $F(1, 85) = 6.335$, $\omega^2 = 0.075$). The influence of the position and the interaction was not considered significant (See Figure 43 B).

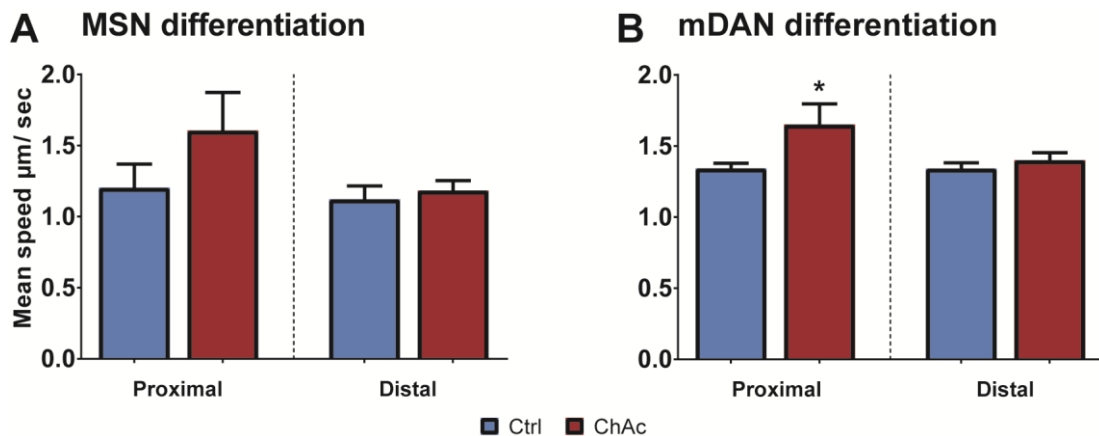


Figure 43: Mean speed of the top decile fastest mitochondria in MFC of both differentiation protocols. A) MSN differentiated neurons indicate no difference in the top speed. A trend was observed in the proximal position. $n \geq 6$. B) mDAN differentiation revealed an increased average speed of fast moving mitochondria in proximal position that dropped to wild type levels in distal parts. $n \geq 18$. Bars represent mean + SEM. * indicate significant differences within a treatment. * represent $p = 0.05$.

In summary, when undirected 96-wells were investigated MSN derived cultures showed no difference in the amount of moving mitochondria or their mean speed. mDAN cultures

harbored a reduction in the moving fraction, but an increase in the mean speed. Directedness and the top speed was unaffected by the ChAc genotype. Investigation of MFC revealed no difference in the moving fraction in mixed striatal as well as midbrain dopaminergic cultures. The mean speed of ChAc patients' mitochondria was elevated in proximal positions for both differentiation protocols. Furthermore midbrain dopaminergic cultures showed an increase in the retrograde transport of mitochondria at the proximal site. Treatment with GADL reduced the moving fraction in MSN but increased it in mDAN cultures. The mean speed was unaffected in both differentiation protocols. PP2 had exhibited a differential result in MSN cultures, where the moving fraction was increased for wild type but decreased for ChAc lines. mDAN differentiations showed a selective increase in the moving fraction for ChAc lines when treated with PP2. The mean speed was unaffected in both differentiation protocols (See Table 26).

Table 26: Summary of analysis of the dynamic parameters of mitochondria

96-well	MSN differentiation	mDAN differentiation
Movement	no difference between wild type and ChAc	ChAc lines have increased movement under control condition
Mean speed	no difference between wild type and ChAc	ChAc lines had a reduced mean speed
Directedness	no differences between wild type and ChAc	no differences between wild type and ChAc
Max speed	no differences between wild type and ChAc	no differences between wild type and ChAc
MFC	MSN differentiation	mDAN differentiation
Movement	no differences between wild type and ChAc no difference between proximal and distal no differences between wild type and ChAc in the anterograde fraction	no differences between wild type and ChAc no difference between proximal and distal ChAc lines had an increase in retrograde transport in proximal parts
Mean speed	no differences between wild type and ChAc no difference between proximal and distal	ChAc lines had an increased speed in proximal position No difference between wild type and ChAc in distal part

MFC	MSN differentiation	mDAN differentiation
Mean speed	anterograde and retrograde moving mitochondria in proximal parts are faster than the ones in distal parts	anterograde and retrograde moving mitochondria in proximal parts are faster than the ones in distal parts ChAc lines had an increased speed of retrograde moving mitochondria
Directedness	no differences between wild type and ChAc no difference between proximal and distal no differences between wild type and ChAc	no differences between wild type and ChAc no difference between proximal and distal ChAc lines had an increased speed in proximal position
Max Speed	no difference between proximal and distal	No difference between wild type and ChAc in distal part
Treatments	MSN differentiation	mDAN differentiation
Moving	GADL treatment decreased the moving fraction ChAc lines reacted differently to PP2 treatment	GADL treatment increases the moving fraction Only ChAc lines reacted to PP2 treatment by increase in moving fraction
Mean speed	no response to any treatment	ChAc lines responded to no treatment
Directedness	no response to any treatment	GADL reduced the direct moving fraction
Max speed	no response to any treatment	no response to any treatment

3.1.3. JC-1

The JC-1 dye is used to characterize the mitochondria on a functional level. JC-1 is sensitive to the intermembrane potential of mitochondria. In high potential mitochondria the dye dimerizes and emits light at around 590nm while in depolarized mitochondria the dye has a monomeric form and emits at 529nm. To assess the polarization of a mitochondrion, the emission of both channels was measured and the ratio between red and green channels calculated. A high ratio indicates a strong polarization.

3.1.3.1. 96 well

The JC-1 ratio of mitochondria in mixed striatal cultures was increased by a huge amount in ChAc lines compared to wild type, when investigated under control conditions. Upon treatment with GADL, the genotype had a significant influence ($p < 0.0001$, $F(1, 105) = 63.11$, $\omega^2 = 0.367$), but there was no influence of the treatment. The interaction between the treatment and genotype was significant as well ($p = 0.0187$, $F(1, 105) = 5.704$, $\omega^2 = 0.038$). The treatment with PP2 resulted in an influence of the genotype ($p < 0.0001$, $F(1, 87) = 86.43$, $\omega^2 = 0.49$) but no influence of the treatment or interaction was observed (See Figure 44 A).

ChAc patients' neurons derived from mDAN protocol had a large reduction of JC-1 ratio ($p < 0.0001$, $t(63.98) = 4.289$, $d = 0.92$). Treatment with GADL results in no influence of the genotype but a significant influence of the treatment ($p < 0.0001$, $F(1, 123) = 17.71$, $\omega^2 = 0.118$) and a significant interaction ($p = 0.0002$, $F(1, 123) = 15.21$, $\omega^2 = 0.102$). When treated with PP2, there was no influence of the genotype, treatment or interaction observed (See Figure 44 B).

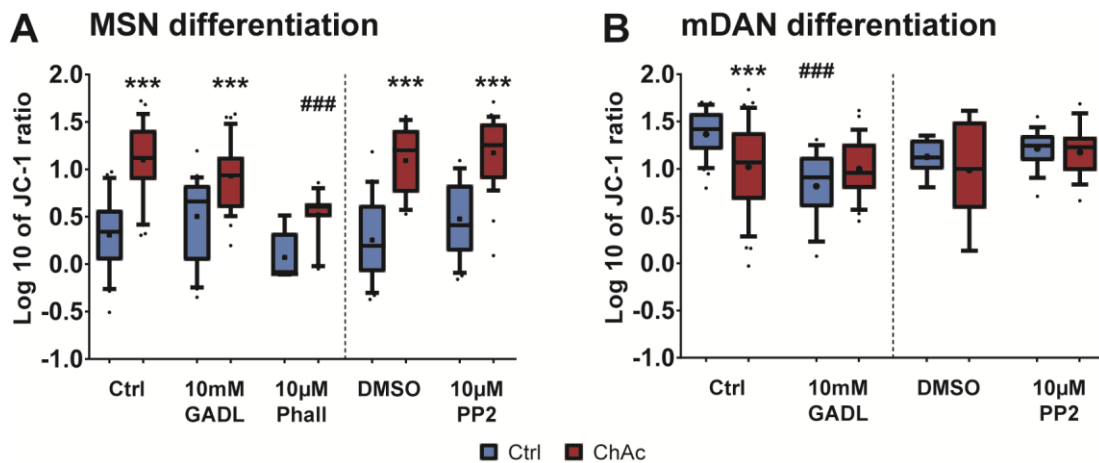


Figure 44: Analysis of membrane potential marker JC-1. A) MSN differentiated neurons showed a significantly increased ratio of JC-1 in ChAc lines. GADL treatment lowered the ratio in ChAc but not wild type lines. n at least 6 images from 5 independent experiments. B) mDAN differentiated neurons harbored a decreased mitochondrial potential. Treatment with GADL reduced wild type lines to ChAc levels but had no influence on ChAc lines. n = at least 8 images from 6 independent experiments. Boxes represent 25-75 percentiles, line represents median, whiskers represent 10-90%, + represents mean. * indicate significant differences within a treatment. # indicate significant differences to control condition. ***, ### represent $p = 0.001$, respectively.

3.1.3.2. Microfluidic chambers

Polarization of mitochondria was measured in MFC as well and analyzed dependent on a proximal and distal position in the neurite under control conditions. When cells were

differentiated according the mDAN protocol, there was a significant influence of the genotype ($p < 0.0001$, $F(1, 2917) = 233$, $\omega^2 = 0.064$) as well as the position ($p < 0.0001$, $F(1, 2917) = 306.9$, $\omega^2 = 0.084$). Furthermore there was a significant interaction between position and genotype ($p < 0.0001$, $F(1, 2917) = 219.9$, $\omega^2 = 0.060$) (See Figure 45).

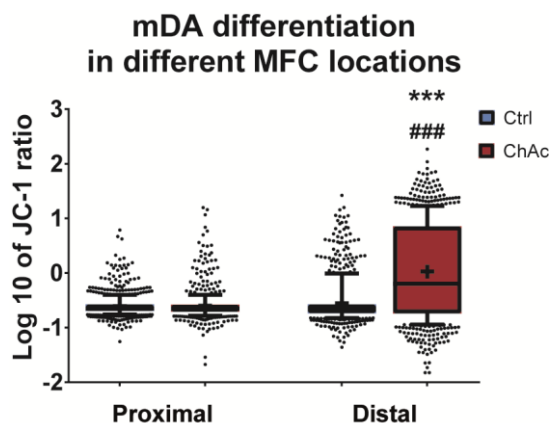


Figure 45: Analysis of membrane potential marker JC-1 in MFC with mDAN differentiated neurons. While potential of wild type was the same when proximal and distal positions were compared, ChAc lines had a significantly increased ratio in the distal position. Boxes represent 25-75 percentiles, line represents median, whiskers represent 10-90%, + represents mean. $n =$ at least 604 mitochondria from two independent experiments. * indicate significant differences within a treatment. # indicate significant differences to control condition. ***, ### represent $p = 0.001$, respectively.

3.2. Lysosomal dynamics

Lysosomes are organelles that are important for several vital processes in a cell including autophagy and the endocytic pathway. They contain various hydrolytic enzymes and have an acidic lumen. This acidity is utilized by the pH sensitive LysoTracker to visualize lysosomes in living cells which allows their observation in life-cell microscopy. To characterize the lysosomal compartment read-outs like the morphological and trafficking analyses similar to the mitochondrial study were conducted.

3.2.1. Morphological analysis

3.2.1.1. 96 well

The number of lysosomes per arbitrary neurite length was analyzed for mixed striatal cultures. Within the control condition there was a large effect that resulted in significantly fewer lysosomes ($p = 0.003$, $t(39.95) = 3.156$, $d = 0.83$). There was no difference observed in control, GADL-treated and PP2-treated conditions. No influence of the genotype or interaction between the treatments and genotype was discovered (See Figure 46 A).

Since the shape of a lysosome is almost spherical, the aspect ratio is expected to be close to 1. However, depending on the cargo that is digested the shape can diver a lot.

Lysosomes of mixed striatal cultures showed no differences between ChAc patients and healthy controls across control conditions as well as treatment with GADL or PP2 (Figure 46 B).

Under Control conditions the size of the lysosomes was significantly reduced. The effect was moderate ($p=0.0238$, $t(36.87)=2.359$, $d=0.61$). When control conditions were compared with GADL treatment, no influence of the genotype, treatment or any interaction was observed. When the neurons were treated with PP2 and compared to DMSO mock control, however, the genotype showed significant influence ($p=0.0278$, $F(1, 81)=5.016$, $\omega^2=0.065$) as well as the treatment ($p=0.0317$, $F(1, 81)=4.779$, $\omega^2=0.063$). No interaction was observed in this set (See Figure 46 D).

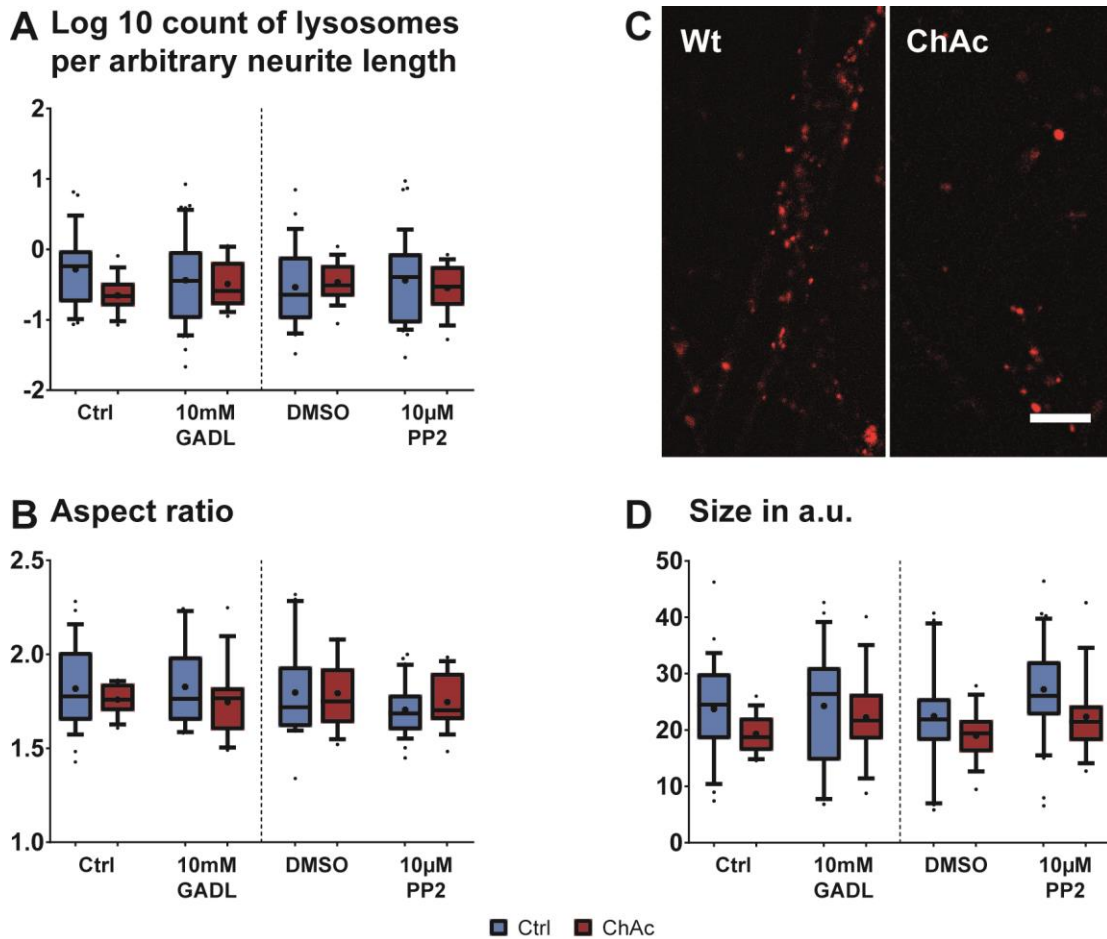


Figure 46: Morphological analysis of lysosomes of MSN differentiation. A) MSN differentiation showed no significant differences in the number of lysosomes per neurite length. B) The aspect ratio of was not altered in MSN differentiated neurons. C) Representative picture of wild type and ChAc neuronal network showing similar morphological features. B) The size of the observed lysosomes is not different. Boxes represent 25-75 percentiles, line represents median, whiskers represent 10-90%, + represents mean. n = at least 13 images from 4 independent experiments. Scale bar = 10μm

There was a small but significant effect on the amount of lysosomes in dopaminergic neurons observed, resulting in an increase of their amount ($p=0.0175$, $t(281)=2.39$, $d=0.28$). The treatment of mDAN cultures with GADL unraveled no influence of genotype or the treatment, but a significant interaction was observed ($p=0.0311$, $F(1, 395)=4.682$, $\omega^2=0.014$). When treated with phalloidin, there was no influence of genotype, treatment or interaction observed. When the PP2 treatment was compared to mock control, there was no influence of genotype, treatment or interaction observed as well (See Figure 47 A).

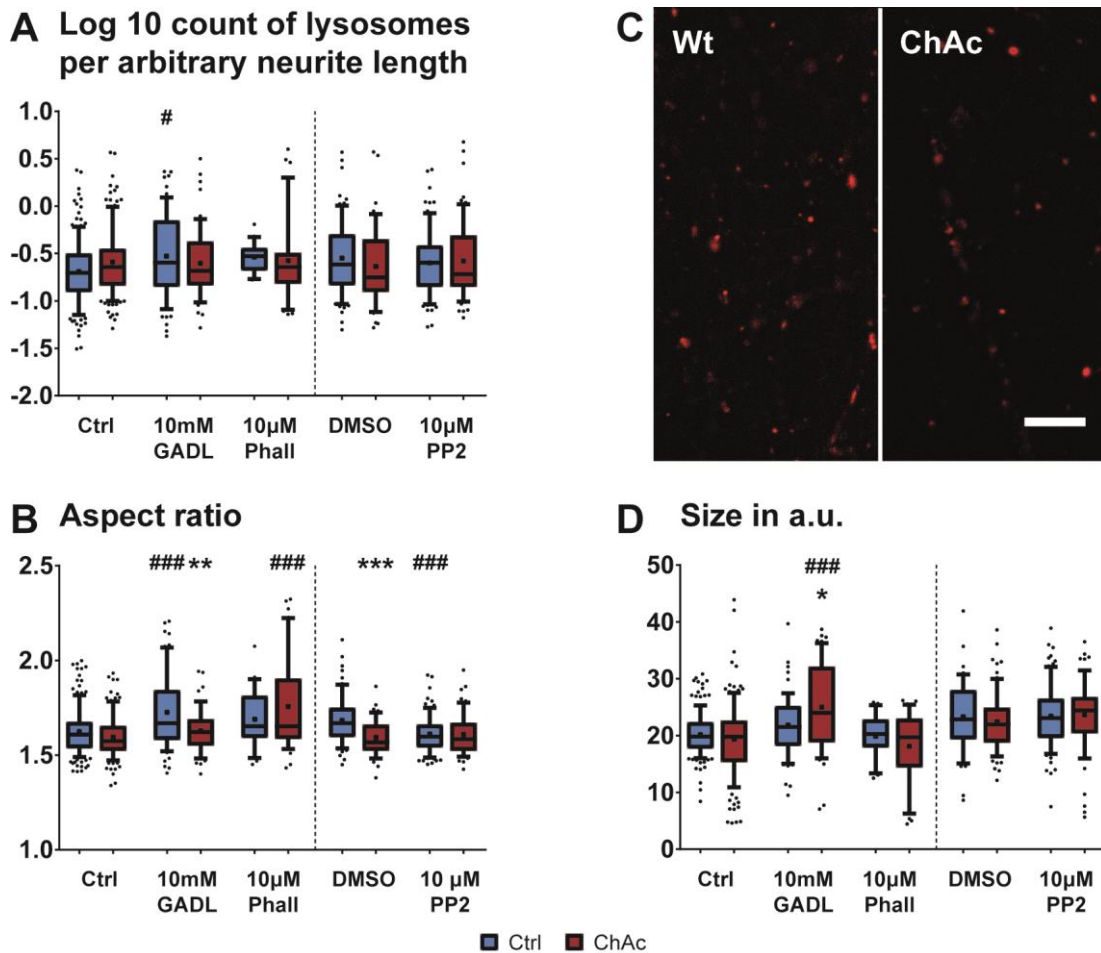


Figure 47: Morphological analysis of lysosomes of mDAN differentiation. A) mDAN differentiation showed no significant difference in the number of lysosomes per neurite length. B) The aspect ratio was not altered in mDAN differentiated neurons under control conditions but in GADL, phalloidin and PP2 treatments. C) Representative picture of wild type and ChAc neuronal net showing similar morphological features under control conditions. D) The the observed lysosomes is not different under control conditions. GADL treatment increased size of lysosomes. Boxes represent 25-75 percentiles, line represents median, whiskers represent 10-90%, + represents mean. $n =$ at least 22 images from 5 independent experiments. * indicate significant differences within a treatment. # indicate significant differences to control condition. */**/***/; ####/### represent $p=0.05/0.01/0.001$, respectively. Scale bar = 10µm

Even though there was no difference observed under control conditions, investigated neurons derived from mDAN differentiations showed significant influence of genotype ($p < 0.0001$, $F(1, 364) = 15.75$, $\omega^2 = 0.041$), influence of treatment ($p < 0.0001$, $F(1, 364) = 18.35$, $\omega^2 = 0.048$) and an interaction ($p = 0.0281$, $F(1, 364) = 4.862$, $\omega^2 = 0.015$) when treated with GADL compared to control. When phalloidin was used, the genotype showed no influence. The treatment, however, was significantly influencing the aspect ratio ($p < 0.0001$, $F(1, 312) = 27.8$, $\omega^2 = 0.083$). A significant interaction between genotype and treatment was observed as well ($p = 0.0295$, $F(1, 312) = 4.784$, $\omega^2 = 0.017$). Addition of PP2 revealed a significant effect of the genotype ($p = 0.0012$, $F(1, 247) = 10.69$, $\omega^2 = 0.043$) and a significant interaction between the genotype and the treatment ($p = 0.0025$, $F(1, 247) = 9.358$, $\omega^2 = 0.038$). The influence of the treatment was not considered significant (See Figure 47 B).

The size of lysosomes of mature neurons generated by mDAN protocol was not different under control conditions but influenced by treatment with GADL ($p < 0.0001$, $F(1, 375) = 30.99$, $\omega^2 = 0.076$) and an interaction between the treatment and the genotype ($p = 0.0026$, $F(1, 375) = 9.224$, $\omega^2 = 0.024$) was observed. The genotype itself was not rated significant in control, GADL, phalloidin as well as PP2 treatment conditions. Treatment with PP2 or phalloidin had no effect on the size of lysosomes (See Figure 47 D).

3.2.1.2. Microfluidic chambers

The amount of lysosomes per arbitrary neurite length was assessed in MFCs in respect to proximal and distal position. Mature neurons, which were generated by MSN differentiation protocol, showed a significant influence of the genotype ($p = 0.0391$, $F(1, 90) = 4.384$, $\omega^2 = 0.054$) but no influence of the position or any interaction. Aspect ratio of the observed lysosomes of mixed striatal cultures was influenced by the genotype ($p = 0.0096$, $F(1, 90) = 6.994$, $\omega^2 = 0.077$) and the position ($p = 0.0267$, $F(1, 90) = 5.075$, $\omega^2 = 0.058$). There was no interaction observed (See Figure 48 B).

The amount of lysosomes of mature neurons that were obtained from mDAN protocol exhibited no influence of the genotype but the influence of the position was considered significant ($p < 0.0001$, $F(1, 432) = 17.86$, $\omega^2 = 0.042$) (See Figure 48 C). Aspect ratio of lysosomes of mDAN cultures showed no influence of the genotype. The position, however, had a significant influence ($p < 0.0001$, $F(1, 432) = 23.96$, $\omega^2 = 0.054$) and there was a significant interaction observed ($p = 0.0439$, $F(1, 432) = 4.086$, $\omega^2 = 0.011$) (See Figure 48 D).

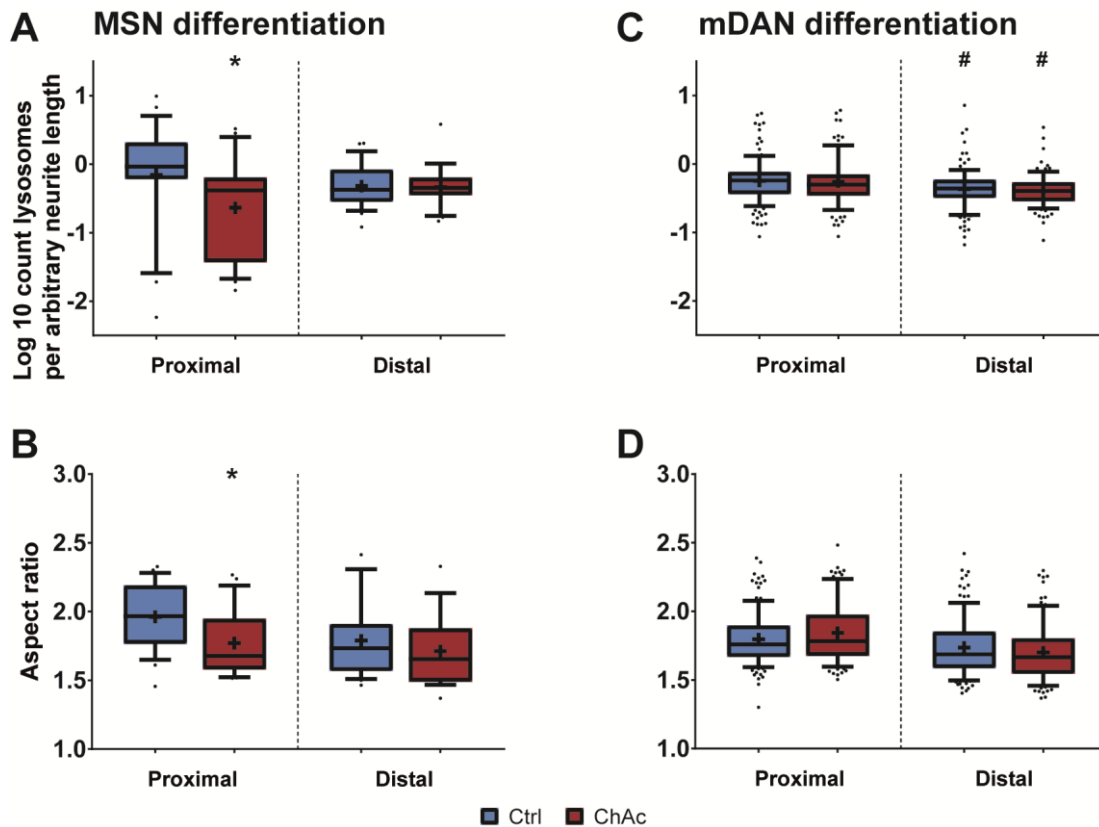


Figure 48: Morphological analysis of MFC cultures. A) MSN differentiated cultures showed a reduction in number of lysosomes per neurite length in ChAc lines at proximal region. While wild type lines experienced a reduction in lysosome count, ChAc lines exhibited a similar amount in distal as observed in proximal part. B) MSN differentiated cultures showed a significant reduction of the aspect ratio in proximal parts not present in distal parts. $N(A/B) \geq 6$. C) mDAN differentiated cultures showed no reduction in the count of lysosomes mitochondria per neurite length that was attributed to the genotype. There was a reduction observed in the distal parts of the neurite. D) Lysosomes of mDAN differentiated neurons had a reduced aspect ratio when proximal position was compared to distal. $n(C/D) \geq 18$. Boxes represent 25-75 percentiles, line represents median, whiskers represent 10-90%, + represents mean. * indicate significant differences within a treatment. # represents $p=0.05$, respectively.

In summary, when the phenotype was investigated in undirected 96-well under control conditions, there were less lysosomes observed in both differentiation protocols in ChAc lines. In addition, the size of ChAc patient's lysosomes was reduced in mixed striatal cultures. When the cell lines were cultivated and analyzed in MFC, there was general reduction in the amount of lysosomes and their aspect ratio observed when proximal and distal position was investigated. Phenotype related differences were observed in proximal parts of MSN and resulted in a reduced amount and reduced aspect ratio. Midbrain dopaminergic cultures showed no differences in MFC. When the cells were treated with GADL the size and the aspect ratio increased in all investigated cell lines, hence no

disease specific effect was observed. PP2 treatment had didn't affect mDAN cultures but increased the size of lysosomes in both wild type and ChAc lines (See Table 27).

Table 27: Summary of morphological features of lysosomes in ChAc

	MSN differentiation	mDAN differentiation
96well	no difference in the amount of lysosomes	no difference in the amount of lysosomes
	no difference in the aspect ratio of	Lysosomes of ChAc lines have an reduced aspect ratio under GADL treatment conditions
	no difference in the size of lysosomes	
	no response to treatments	Lysosomes of ChAc lines have an increased size under GADL treatment conditions
		PP2 had no influence on count, aspect ratio or size
MFC	ChAc lines had fewer lysosomes in proximal parts when compared to wild type	No differences between wild type and ChAc
	Distal parts had fewer lysosomes than proximal parts	Distal parts had fewer lysosomes than proximal parts
	ChAc lines had a reduced aspect ratio in proximal parts when compared to wild type	
	No difference of count or aspect ratio between wild type and ChAc in distal parts	

3.2.2. Trafficking

3.2.2.1. 96 well

The trafficking of lysosomes was characterized by assessing the moving objects and the motility of that fraction. The same regression analysis that was conducted on the mitochondria was used on the lysosomal fraction. Examples of fitted curves are shown in Figure 49. The obtained parameters of the regression are shown in the supplement.

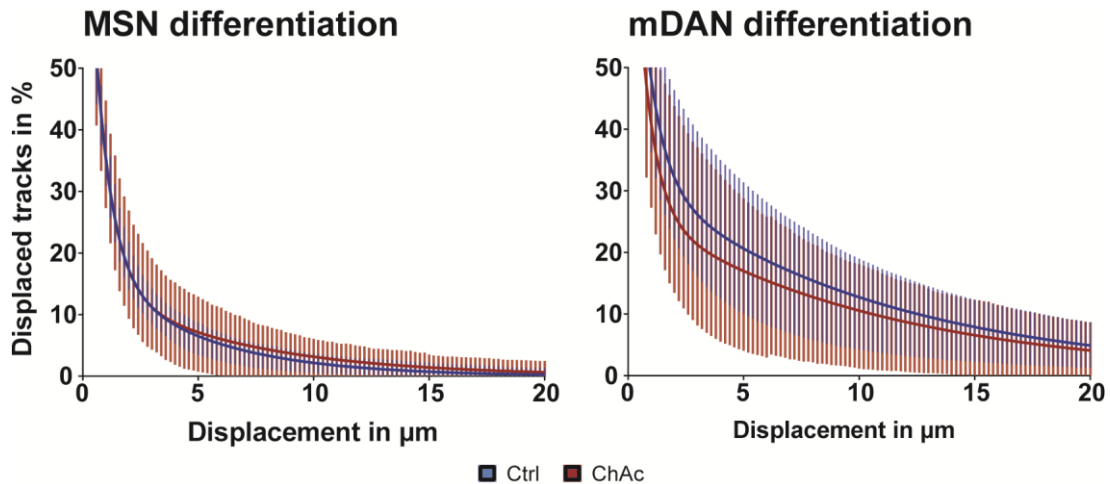


Figure 49: Examples of plots obtained from trafficking analysis of lysosomes. Stripes indicate the standard deviation of the amount of displaced tracks of the original data set. Lines indicate the fitted curves of the calculated two-phase decay model regression.

When the control condition of MSN differentiations was analyzed, the moving fraction was significantly increased by a very large amount ($p=0.048$, $t(9)=2.287$, $d=1.43$). The mean speed of this fraction increased as well and the effect rated very large ($p=0.0143$, $t(9)=3.027$, $d=1.89$). The next experiment conducted focused on GADL treatment. The amount of moving lysosomes was influenced by the genotype ($p=0.0086$, $F(1, 18)=8.678$, $\omega^2=0.326$) but not the treatment or the interaction between the treatment and the genotype. The motility was not influenced by the genotype or the treatment. The interaction, however, was considered significant ($p=0.0028$, $F(1, 18)=11.98$, $\omega^2=0.384$). Treatment with PP2 resulted in a significant influence of the genotype ($p=0.0252$, $F(1, 16)=6.096$, $\omega^2=0.294$) on the stationary fraction. But neither the treatment nor the interaction had an influence. The motility of the lysosomes upon PP2 intervention was not influenced by genotype, treatment or any interaction (See Figure 50 A & B).

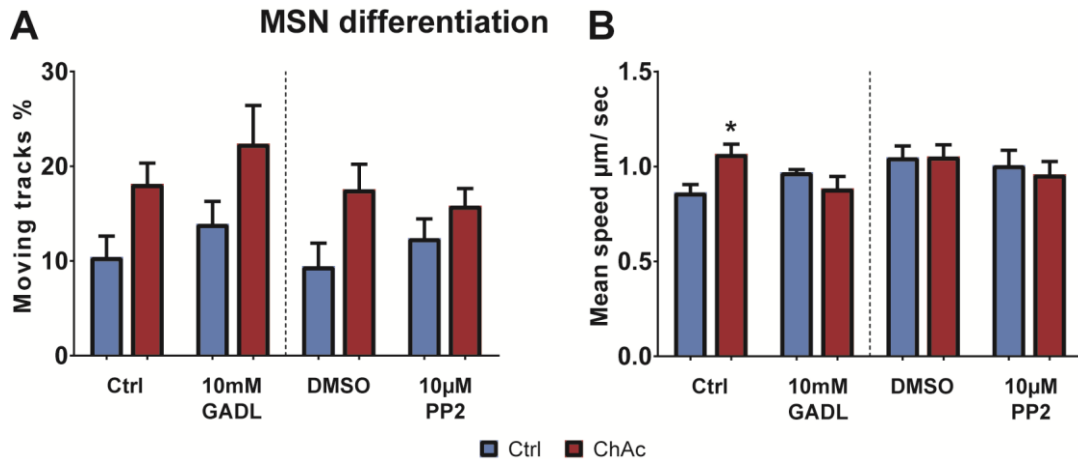


Figure 50: Trafficking analysis of lysosomes of MSN differentiated cultures. A) MSN differentiated cultures showed an increased movement of lysosomes that was present in ChAc lines. GADL treatment further increased that movement. B) There was a significant increase of the mean speed of moving lysosomes in ChAc lines under control conditions. GADL had a differential effect on the average speed. Bars represent mean + SEM. $n \geq 4$. * indicate significant differences within a treatment. * represent $p=0.05$

Initial investigation of the control condition of mature neurons that have been derived by mDAN differentiation protocol showed no significant difference in the fraction size of moving lysosomes. However, there was a huge effect on the mean speed observed ($p < 0.0001$, $t(20)=6.758$, $d=3.23$). When treated with GADL no significant influence of the genotype and no interaction between genotype and treatment was found, but the treatment itself had a significant influence ($p < 0.001$, $F(1, 81)=7659$, $\omega^2=0.093$) on the moving lysosomal fraction. The motility under GADL treatment conditions was not significantly influenced by the genotype but the treatment itself did influence the motility significantly ($p=0.0219$, $F(1, 81)=5.461$, $\omega^2=0.069$). An interaction between genotype and treatment was not observed. Treatment with phalloidin resulted in changes in the moving fraction that was significantly influenced by the genotype ($p=0.0024$, $F(1, 65)=9.945$, $\omega^2=0.131$) but not the treatment. The interaction between both was rated significant ($p=0.0435$, $F(1, 65)=4.239$, $\omega^2=0.063$). The motility of the observed lysosomes was influenced by the genotype ($p < 0.0001$, $F(1, 65)=28.86$, $\omega^2=0.283$) but not the treatment. The observed interaction between genotype and treatment was significant as well ($p=0.0034$, $F(1, 65)=9.245$, $\omega^2=0.097$). The moving fraction that was observed upon PP2 treatment was not significantly influenced by the genotype, treatment or any interaction. The motility of the trafficking lysosomes in PP2 treated conditions was not influenced by the genotype. The influence of the treatment was significant ($p < 0.0001$, $F(1, 59)=33.32$, $\omega^2=0.359$), but the interaction was not significant (See Figure 51 A & B).

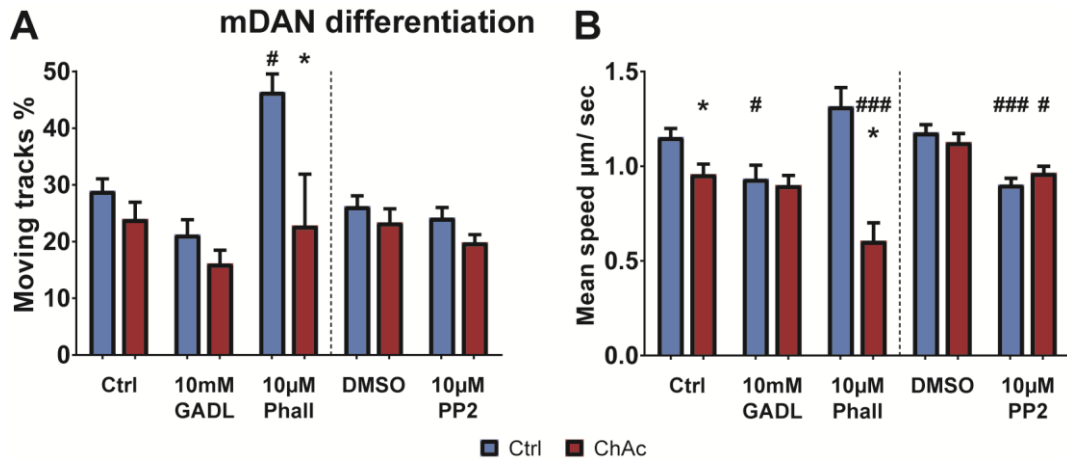


Figure 51: Trafficking analysis of lysosomes of mDAN differentiated cultures. A) mDAN differentiated cultures showed an decreased movement of lysosomes in ChAc lines. GADL treatment further decreased that movement. Phallacidin increased the movement of lysosomes in wild type lines but not ChAc lines. B) There was a significant decrease of the mean speed of moving lysosomes in ChAc lines under control conditions. GADL treatment only affected wild type lines and caused a drop of the means speed to ChAc levels. Phallacidin had a differential effect depending on the genotype. PP2 treatment similarly reduced the mean speed of moving lysosomes. Bars represent mean + SEM. $n \geq 5$. * indicate significant differences within a treatment. # indicate significant differences to control condition. */**/*; #/###/#### represent $p=0.05/0.01/0.001$, respectively.

The directedness of lysosome trafficking was investigated similar to the mitochondrial studies. Mature neurons derived from MSN differentiation protocol were analyzed under control condition and when treated with GADL. There was no influence of the genotype or the treatment on the directedness. Furthermore, no interaction was observed. When PP2 was added and compared to DMSO the directedness was influenced significantly by the genotype ($p=0.0016$, $F(1, 95)=10.61$, $\omega^2=0.109$) but not the treatment or any interaction (See Figure 52 A).

The directedness of trafficking of lysosomes of mDAN was analyzed as well. Without any treatment there was an small reduction of directly moving lysosomes observed ($p=0.0001$, $t(288.8)=3.86$, $d=0.42$). Treatment with GADL revealed an influence of the genotype ($p=0.0001$, $F(1, 435)=14.9$, $\omega^2=0.033$) as well as an influence of the treatment ($p<0.0001$, $F(1, 435)=28.59$, $\omega^2=0.062$). But there was no interaction. Phallacidin treatment showed that there was a significant influence of the genotype ($p<0.0001$, $F(1, 386)=29.04$, $\omega^2=0.070$) and of the treatment ($p=0.0093$, $F(1, 386)=6.835$, $\omega^2=0.018$). The interaction between phallacidin treatment and genotype was rated significant ($p=0.017$, $F(1, 386)=5.743$, $\omega^2=0.016$). Analysis of the DMSO/ PP2 treatments showed no influence of the genotype and no interaction between treatment and genotype. The treatment itself was rated significant ($p=0.0007$, $F(1, 271)=11.65$, $\omega^2=0.044$) (See Figure 52 B).

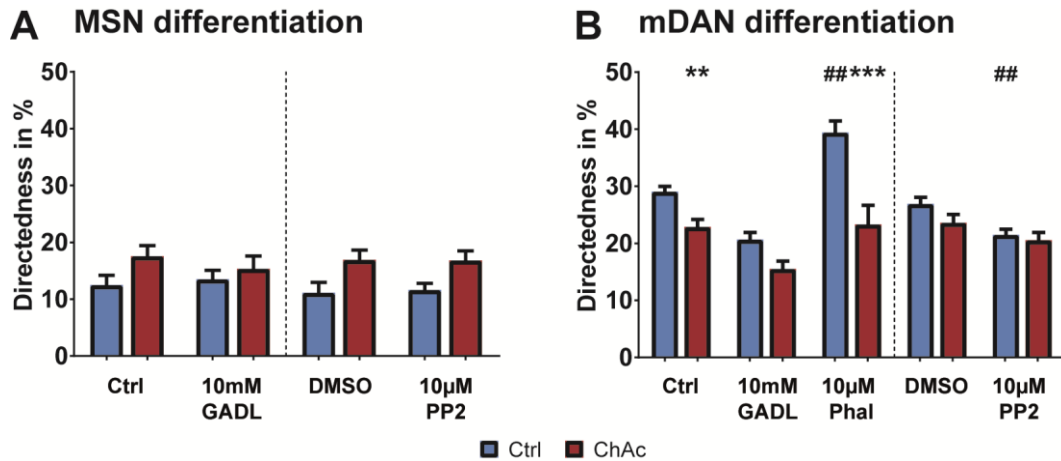


Figure 52: Analysis of direct movement in both differentiation protocols. A) MSN differentiation had no significant difference in the fraction of direct movement but there was a trend observed where ChAc lines exhibited an increased amount of direct movement. B) Fraction of direct movement was influenced by the genotype as well as the treatment in mDAN differentiation. Application of GADL decreased the directedness while phalloidin caused differential response in wild type and ChAc lines. Bars represent mean + SEM. $n \geq 4$. * indicate significant differences within a treatment. # indicate significant differences to control condition. */**/***; #/###/#### represent $p=0.05/0.01/0.001$, respectively.

The top decile of the fastest tracks was analyzed for lysosomes as well. Even though there was very large effect on the top speed in MSN differentiated mature neurons, resulting an increase of the velocity ($p=0.0377$, $t(9)=2.434$, $d=1.53$), no difference for the treatments with GADL or PP2 and no influence of the genotype were observed when the cells were treated. There was no interaction observed as well (See Figure 53 A).

In mDAN differentiated neurons there was a moderate effect observed that resulted in the reduction of the velocity of the fastest tracks ($p=0.0058$, $t(56)=2.871$, $d=0.76$). When treated with GADL the analysis revealed a significant influence of the genotype ($p=0.0179$, $F(1, 81)=5.841$, $\omega^2=0.074$), however, no treatment effect or interaction was observed. The addition of phalloidin revealed a significant influence of the genotype as well ($p<0.0001$, $F(1, 65)=30.39$, $\omega^2=0.295$) and, furthermore, an interaction that was considered significant ($p=0.0025$, $F(1, 65)=9.873$, $\omega^2=0.102$). The treatment itself was not considered significant. Upon investigation of PP2, there was an influence of the treatment observed ($p<0.0001$, $F(1, 59)=18.43$, $\omega^2=0.245$) but not of the genotype or any interaction (See Figure 53 B).

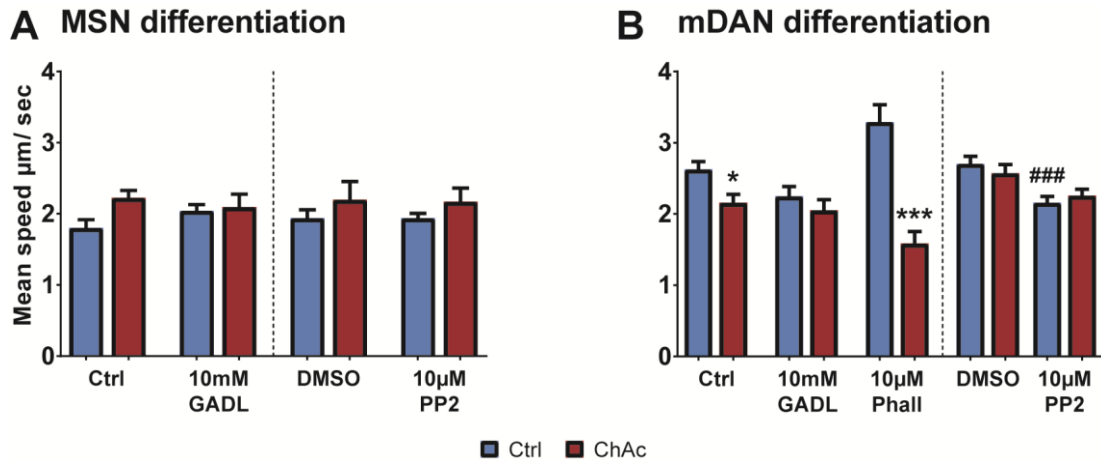


Figure 53: Speed of the top decile of the fastest lysosomes of both differentiation protocols. A) There was no difference observed in MSN differentiated neurons. B) mDAN differentiated neurons had no difference in the max speed that was accounted to influence of the genotype. Differential response to phalloidin treatment was observed. PP2 treatment decreased the directness as well. Bars represent mean + SEM. $n \geq 5$. * indicate significant differences within a treatment. # indicate significant differences to control condition. */**/**; #/###/### represent $p=0.05/0.01/0.001$, respectively.

3.2.2.2. Microfluidic chambers

Motility of lysosomes in MFCs was analyzed similar to mitochondria by first investigating the fraction of moving organelles and comparing the motility of this moving fraction. The amount of moving lysosomes of mixed striatal cultures was not influenced by the genotype, the position or any interaction. The motility was not influenced by any of these factors as well (See Figure 54 A & B).

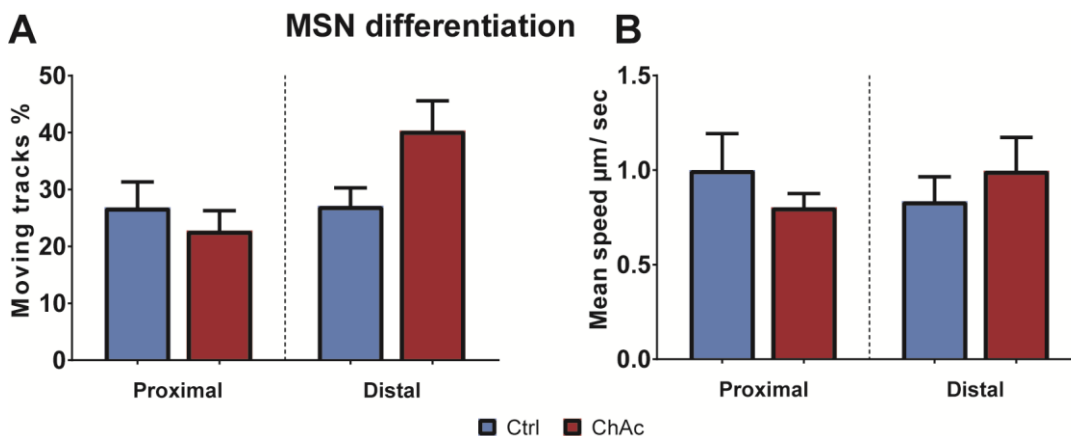


Figure 54: Trafficking analysis of lysosomes of MSN differentiated MFC cultures. A) No significant differences were observed although a trend on increased movement was noticed in distal position was. B) MSN differentiated cultures had no difference that was significantly influenced by position or genotype. Bars represent mean + SEM. $n \geq 6$.

The fraction of moving lysosomes of neurons derived from mDAN differentiation was not influenced by the genotype but by the position ($p < 0.0458$, $F(1, 85) = 4.11$, $\omega^2 = 0.057$). Furthermore there was no significant interaction observed. The motility of the moving fraction was influenced by the genotype ($p = 0.0093$, $F(1, 85) = 7.082$, $\omega^2 = 0.085$) but not the position or the interaction between the both (See Figure 55 A & B).

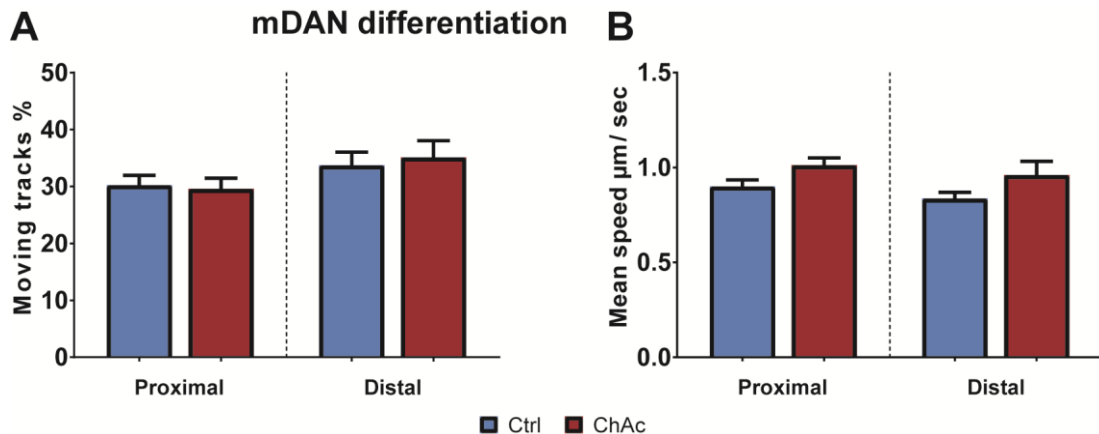


Figure 55: Trafficking analysis of lysosomes of mDAN differentiated MFC cultures. A) mDAN differentiated cultures showed no differences in regards to the genotype but a trend of increased amount of moving organelles was observed in a distal position in ChAc lines. B) Mean speed of lysosomes of mDAN differentiated cultures was increased for ChAc lines. Bars represent mean + SEM. $n \geq 18$. * indicate significant differences within a treatment.

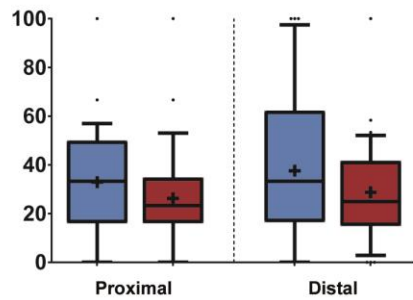
The antero- and retrograde transport of lysosomes in MFCs was assessed as well. The same requirement of a directness above 0.75 for each track was used. When mixed striatal cultures were investigated, no difference was observed in respect to genotype or proximal vs. distal position (See Figure 56 A). Anterograde or retrograde speed of lysosomes was not influenced by the genotype or the position. No interactions were observed as well (See Figure 56 B).

The fraction of anterograde transport in mature neurons obtained from mDAN differentiation protocol was not influenced by genotype but by the position within the neurite ($p = 0.011$, $F(1, 443) = 6.524$, $\omega^2 = 0.017$) (See Figure 56 D).

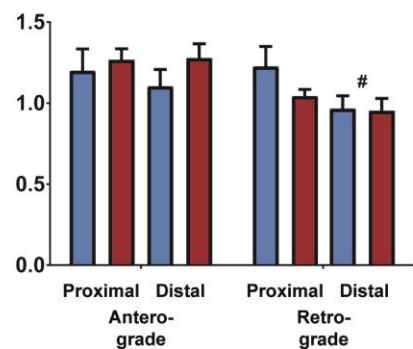
The speed of the anterograde fraction was not significantly influenced by the genotype or position (See Figure 56 E). The speed of the retrograde moving fraction, however, was influenced by the genotype ($p < 0.0001$, $F(1, 443) = 16.53$, $\omega^2 = 0.036$) as well as the position within the neurite ($p < 0.0001$, $F(1, 443) = 23.46$, $\omega^2 = 0.05$) (See Figure 56 E).

MSN differentiation

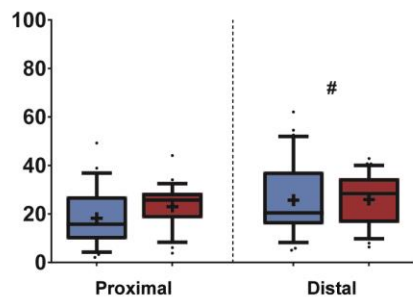
A Anterograde moving in %



B Mean speed in $\mu\text{m}/\text{sec}$

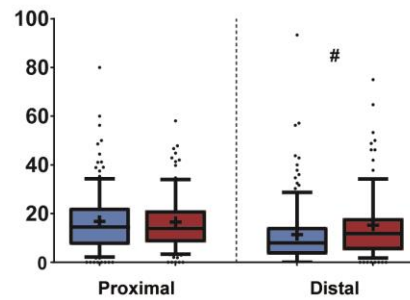


C Direct movement in %

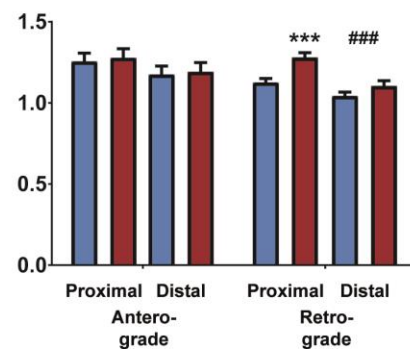


mDAN differentiation

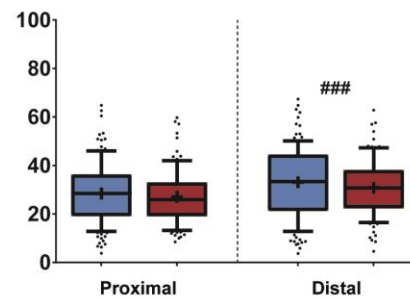
D Anterograde moving in %



E Mean speed in $\mu\text{m}/\text{sec}$



F Direct movement in %



■ Ctrl ■ ChAc

Figure 56: Detailed characterization of lysosomes trafficking in MFC. A) There is no difference in the anterograde fraction of moving lysosomes. B) Genotype and position had no influence on the mean speed of anterograde moving lysosomes. ChAc lines had a slightly, but not significantly, increased speed. For retrograde movement, there was no significant difference found as well. But a trend in the proximal position indicated decreased mean speed for ChAc lines. C) Increased direct movement was detected in distal positions of MSN differentiations. $n(\text{A-C}) \geq 6$. D) Difference in anterograde moving fraction detected between proximal and distal position in mDAN differentiations was observed. Genotype showed no influence. E) Mean speed of anterograde moving lysosomes was lower in distal parts. ChAc lines showed an increased mean speed in proximal positions that reduced to wild type level in distal parts. $n(\text{D-F}) \geq 18$. F) Direct movement of lysosomes was increased in distal parts. Bars represent mean + SEM. Boxes represent 25-75 percentiles, line represents median, whiskers represent 10-90%, + represents mean. * indicate significant differences within a treatment. # indicate significant differences to control condition. */**/**; #/###/#### represent $p=0.05/0.01/0.001$, respectively.

The directedness of lysosomal trafficking was investigated dependent on the axonal position. Mixed striatal cultures showed a significant influence of the position ($p=0.0254$, $F(1, 111)=5.134$, $\omega^2=0.051$) but no influence of the genotype and no interaction between the two (See Figure 56 C).

Directedness in mature neurons from the mDAN protocol was also not sensitive to influence of the genotype. The influence of the position, however, was significant ($p=0.0006$, $F(1, 443)=11.81$, $\omega^2=0.028$) (See Figure 56 F).

The analysis of the ten percent fastest tracks revealed no significant influence of the genotype, treatment or interaction in mixed striatal cultures (See Figure 57 A). Differentiated mDAN cultures that were subjected to the same conditions showed a significant influence of the genotype ($p=0.0152$, $F(1, 85)=6.138$, $\omega^2=0.077$) but no influence of the position and no interaction (See Figure 57 B).

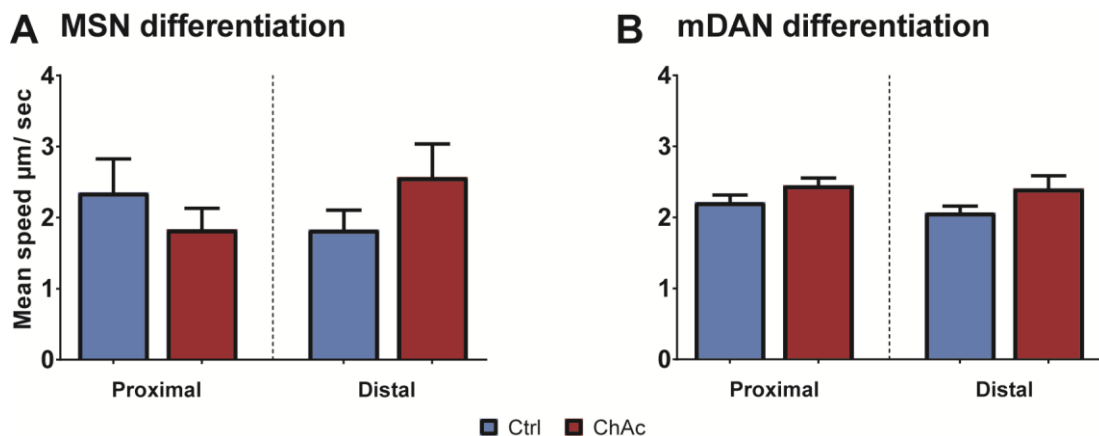


Figure 57: Mean speed of the top decile fastest lysosomes in MFC of both differentiation protocols. A) MSN differentiated neurons indicate no difference in the top speed. $n \geq 6$. B) mDAN differentiation revealed an increased average speed of fast moving lysosomes. $n \geq 18$. There was no influence of the position discovered. Bars represent mean + SEM.

In summary, when undirected 96-well cultures were investigated ChAc lines in mixed striatal cultures showed an increase in the moving fraction and an increase in the mean and top speed, while mDAN cultures harbored a reduced moving fraction and decreased in mean and top speed. The directedness as unaffected in MSN cultures but upon mDAN differentiation ChAc patients' lysosomes moved less direct than wild type ones. Investigation of MFC showed that, in general, distal parts had more moving lysosomes that also travelled more direct. The majority of these lysosomes moved in an retrograde fashion. Treatment with GADL increased the moving fraction of MSN cultures further and decreased it when applied to mDAN cultures. The mean speed of lysosomes was not affected in either differentiation protocol. The directedness was not influenced in mixed

striatal but in midbrain dopaminergic cultures. Application of PP2 had no effect on MSN differentiated neurons but lowered the mean and top speed of wild type and ChAc lines in mDAN cultures (See Table 28).

Table 28: Summary of analysis of dynamic parameters of lysosomes

96 well	MSN differentiation	mDAN differentiation
Movement	ChAc lines had more moving lysosomes	no difference between wild type and ChAc under GADL and PP2 treatment conditions
Mean Speed	ChAc lysosomes moved faster under control conditions	ChAc lines had slower lysosomes in control conditions
Directedness	ChAc lysosomes had increased directedness in DMSO/PP2 set	ChAc lysosomes moved less direct in control conditions
Max Speed	no difference between wild type and ChAc	ChAc lines had slower lysosomes in control conditions
MFC	MSN differentiation	mDAN differentiation
Movement	no difference between wild type and ChAc no difference between proximal and distal parts no difference between wild type and ChAc no difference between proximal and distal	no difference between wild type and ChAc distal parts had more moving lysosomes than proximal parts ChAc lysosomes were faster Anterograde and retrograde moving lysosomes in proximal parts are faster than the ones in distal regions
Mean Speed	Retrograde moving lysosomes in proximal parts are faster than the ones in distal regions Directedness is increased in distal position	Retrograde moving lysosomes in ChAc lines were moving faster than wild type ones in proximal parts Directedness is increased in distal position
Directedness	no difference between wild type and ChAc no difference between proximal and distal	ChAc lysosomes had a higher max speed no difference between proximal and distal

Treatment	MSN differentiation	mDAN differentiation
Movement	No significant influence of the treatment	GADL treatment reduced the moving fraction
Mean Speed	no response to any treatment	PP2 treatment reduced speed
Directedness	No significant influence of the treatment	PP2 treatment reduced directedness
Max Speed	no response to any treatment	PP2 treatment reduced max speed

4. Comparison with Huntington's disease

Neurons that are primarily affected by Huntington's disease are the MSNs of the basal ganglia. To elucidate whether the discovered ChAc phenotypes are specific, some experiments were conducted on a Huntington line. Since investigation was limited to one Huntington line and not all experiments were repeated, this section focuses on differences between ChAc and Huntington rather than an in depth analysis of Huntington's disease.

4.1. DNA damage

There was no difference between ChAc and Huntington lines during assessment of γ H2A.X. Treatment with etoposide was significant ($p < 0.0001$, $F(1, 663) = 140.3$, $\omega^2 = 0.175$). The area of the spot sizes was analyzed as well and showed a significant influence of the treatment ($p = 0.0015$, $F(1, 1842) = 10.17$, $\omega^2 = 0.006$) and a significant interaction ($p < 0.0001$, $F(1, 1842) = 15.34$, $\omega^2 = 0.009$) (See Figure 58 A & B).

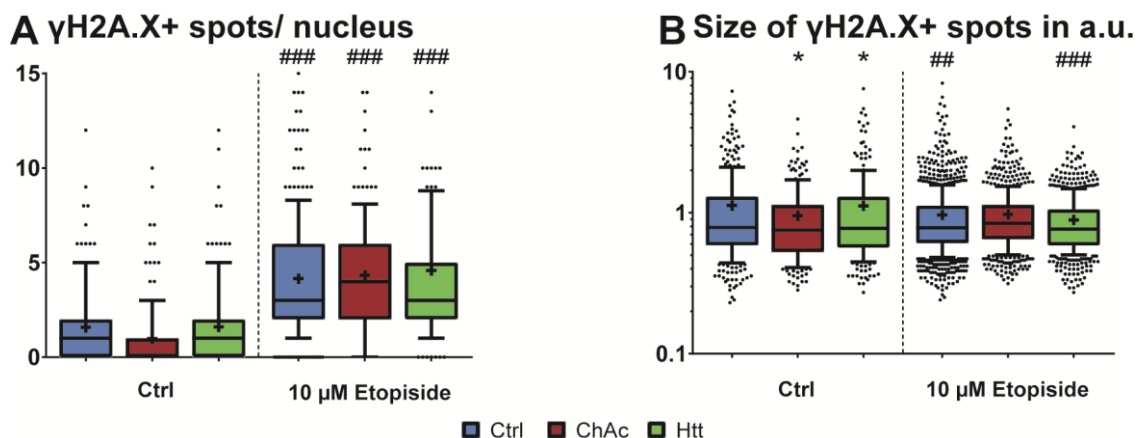


Figure 58: DNA damage in mature MSN of Htt lines. A) More DSB upon acute treatment for 1h with 10 μ M etoposide. B) Size of spots is unaffected by genotype and treatment. Boxes represent 25-75 percentiles, line represents median, whiskers represent 10-90%, + represents mean. n = at least 139 nucleoli from 3 independent experiments * indicate significant differences within a treatment. # indicate significant differences to control condition. *, ##/###/#### represent $p = 0.05/0.01/0.001$, respectively.

4.2. Characterization of metabolism

When the parameters of energy metabolism were investigated, the Huntington line behaved similar to ChAc lines. There was no difference observed in glycolytic increase, glycolytic reserve, non-respiratory acidification, coupling efficiency and spare respiratory capacity. The non-respiratory oxygen consumption, however, was significantly lower in Huntington ($p=0.0037$) and resembled the data obtained from wild type. A trend of increased spare respiratory capacity was observed. The result was, however, not rated significant (See Figure 59).

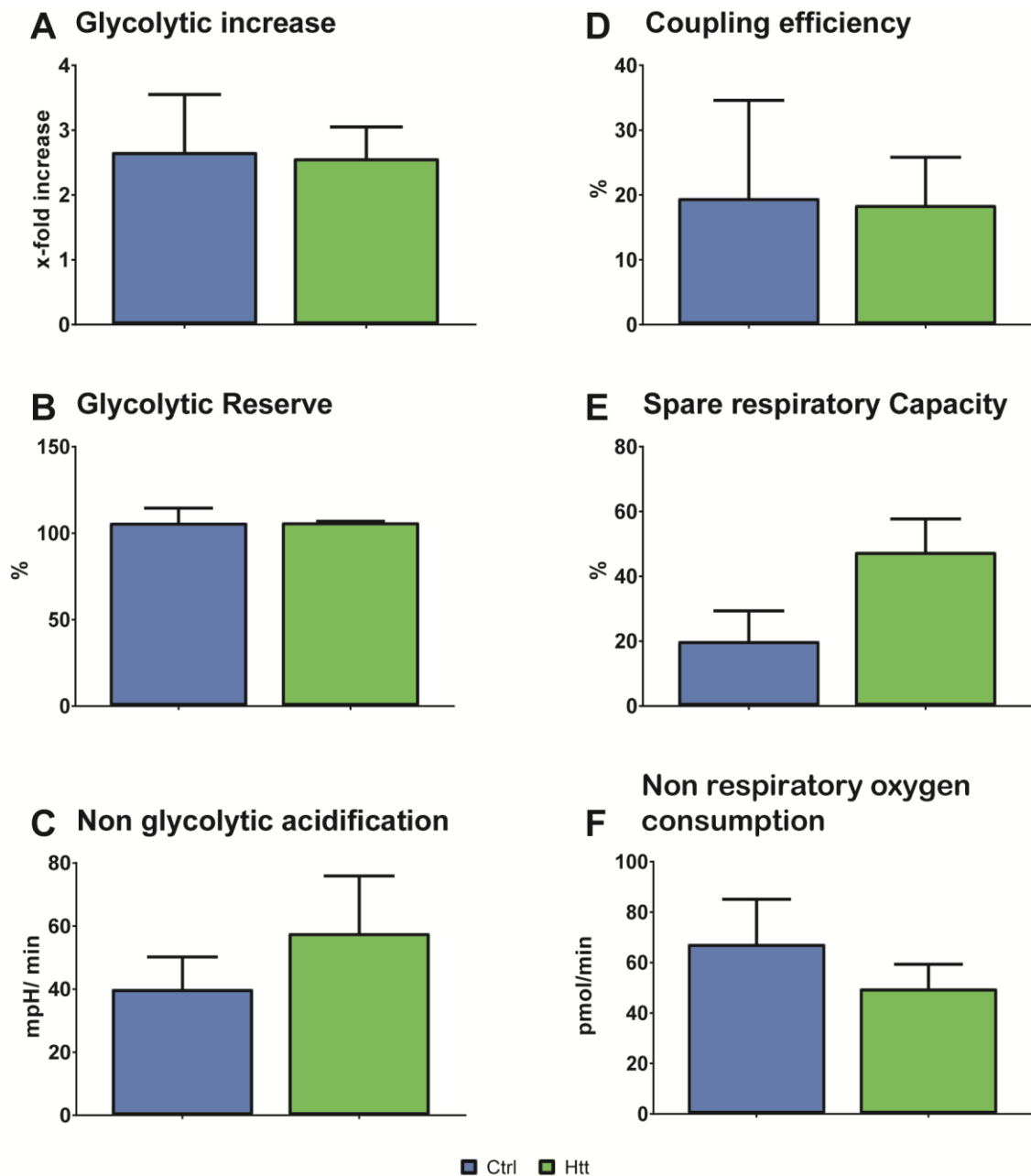


Figure 59: Metabolic characterization of mature MSN of Htt lines. A-F) No differences were observed during the characterization of glycolysis and oxidative phosphorylation. $n \geq 3$

4.3. Live cell imaging

Live cell imaging was performed, using the same workflow as was established previously.

4.3.1. Mitochondria

4.3.1.1. Morphological analysis

The morphology of Huntington patients' mitochondria was assessed in 96 well plates. When the count per arbitrary neurite length was calculated, there was a significant interaction between genotype and treatment with GADL ($p=0.0462$, $F(1, 45)=4.202$, $\omega^2=0.101$). The absence of any significant influence of the genotype showed that there was no difference between ChAc and Huntington. Mitochondrial count of the investigated Huntington line was in between the values of ChAc and wild type. Importantly, the reaction to the treatment was similar to that of the wild type. Treatment with PP2 showed no influence of genotype, treatment or interaction (See Figure 60 A).

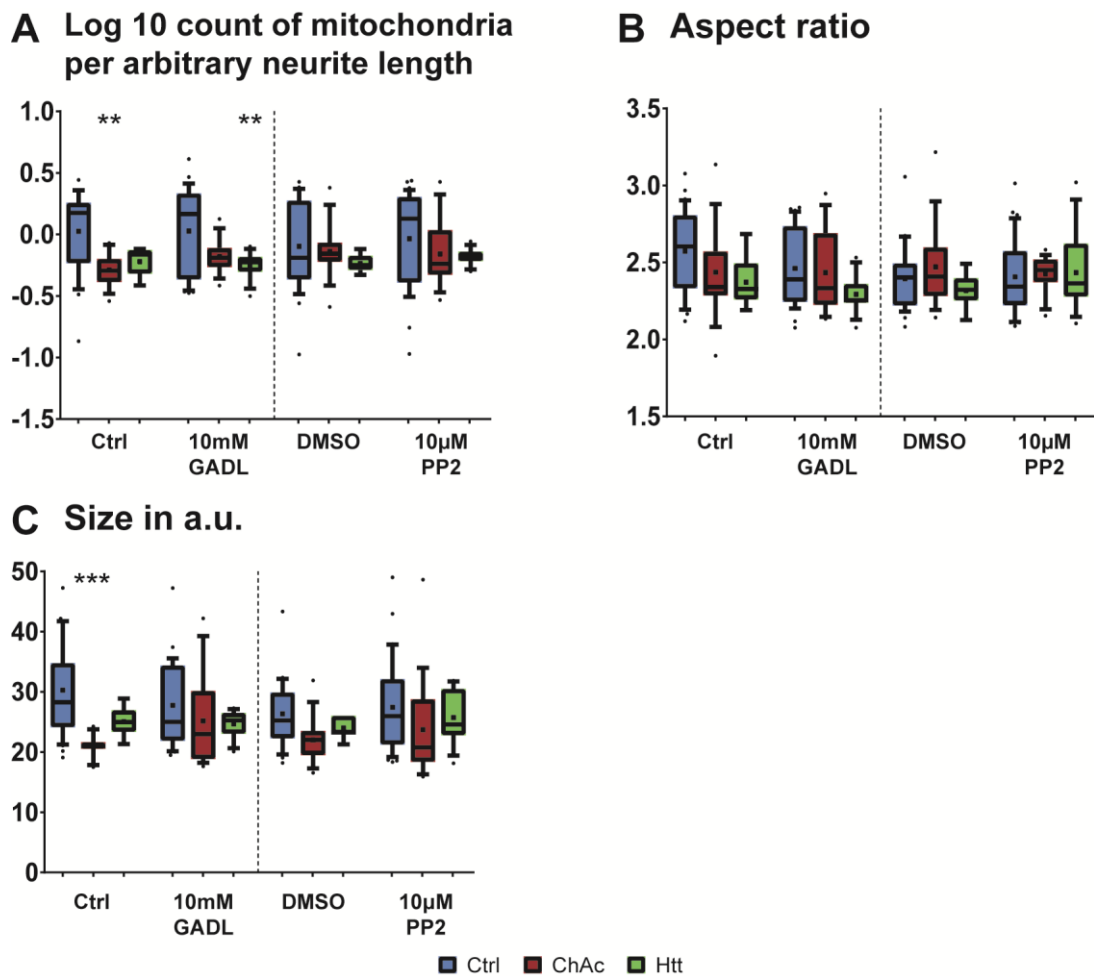


Figure 60: Morphological analysis of mitochondria of Htt lines in MSN differentiation. A) MSN differentiation showed that Htt lines had a reduced amount of mitochondria per arbitrary neurite length. B) The aspect ratio was reduced in Htt lines when compared to wild type. C) The size of

mitochondria was reduced in Htt lines. Boxes represent 25-75 percentiles, line represents median, whiskers represent 10-90%, + represents mean. n = at least 7 images from 3 independent experiments. * indicate significant differences within a treatment. **/***; represent p=0.01/0.001, respectively.

The aspect ratio of investigated mitochondria was not different between ChAc and Huntington under GADL and PP2 treatment conditions. There was, however, a trend observed that Huntington patients' mitochondria have a slightly decreased aspect ratio. When compared to wild type lines within the ctrl/GADL set, there was a significant phenotype observed ($p=0.0016$, $F(1, 83)=10.62$, $\omega^2=0.119$) (See Figure 60 B).

The size of mitochondria was not significantly influence by genotype, any treatment or any interaction. The obtained values were in between ChAc and wild type. Treatment effects were comparable to wild type (See Figure 60 C).

4.3.1.2. Trafficking

The trafficking of mitochondria was investigated using MitoTracker Deepred staining in 96 well plates. The amount of moving mitochondria was significantly reduced in Huntington during GADL treatment. All parameters of the two-way ANOVA were significant. The genotype ($p<0.0001$, $F(1, 10)=64.6$, $\omega^2=0.409$), the treatment ($p<0.0001$, $F(1, 10)=67.77$, $\omega^2=0.429$) as well as the interaction ($p=0.0026$, $F(1, 10)=15.9$, $\omega^2=0.101$) were rated significant. When DMSO and PP2 sets were analyzed, the significant influence of the genotype remained ($p<0.0001$, $F(1, 10)=55.9$, $\omega^2=0.821$) (See Figure 61 A).

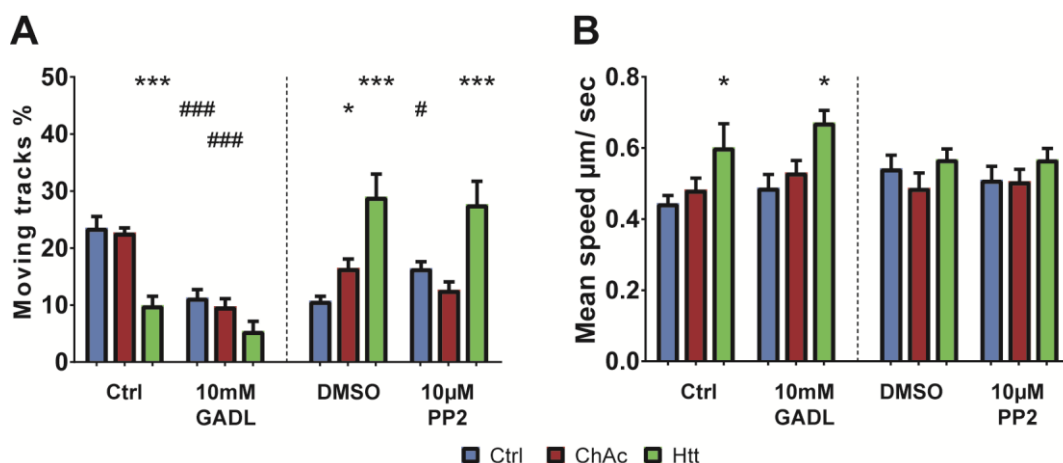


Figure 61: Trafficking analysis of mitochondria of Htt lines in MSN differentiated cultures. A) MSN differentiated cultures showed an decreased movement of mitochondria that was present in Htt lines. GADL treatment further decreased that movement. The moving fraction of Htt lines was increased under DMSO mock conditions. B) There was a significant increase of the mean speed of moving mitochondria in Htt lines under control conditions. Bars represent mean + SEM. n ≥ 3.* indicate significant differences within a treatment. **/*** represent p=0.05/0.01

Analysis of mitochondria motility under GADL treatment conditions showed a significant influence of the genotype ($p=0.0027$, $F(1, 10)=15.68$, $\omega^2=0.555$) when ChAc was compared to Huntington. When DMSO and PP2 sets were investigated, however, the influence of the genotype, the treatment and the interaction were not rated significant (See Figure 61 B).

The directedness of movement was reduced in Huntington compared to ChAc. This was observed under GADL and PP2 treatment conditions. During addition of GADL, the influence of genotype was significant ($p=0.0098$, $F(1, 51)=7.204$, $\omega^2=0.133$). When PP2 was used, this finding could be observed as well ($p=0.0327$, $F(1, 52)=4.814$, $\omega^2=0.094$) (See Figure 62 B).

The speed of the top decile of the fastest tracks was investigated as well. In GADL treatment conditions, there was no difference observed. Influence of the genotype, treatment and interaction were not significant. When PP2 treatment was applied, there was a significant influence of the genotype observed ($p=0.0341$, $F(1, 10)=6.012$, $\omega^2=0.409$) (See Figure 62 A).

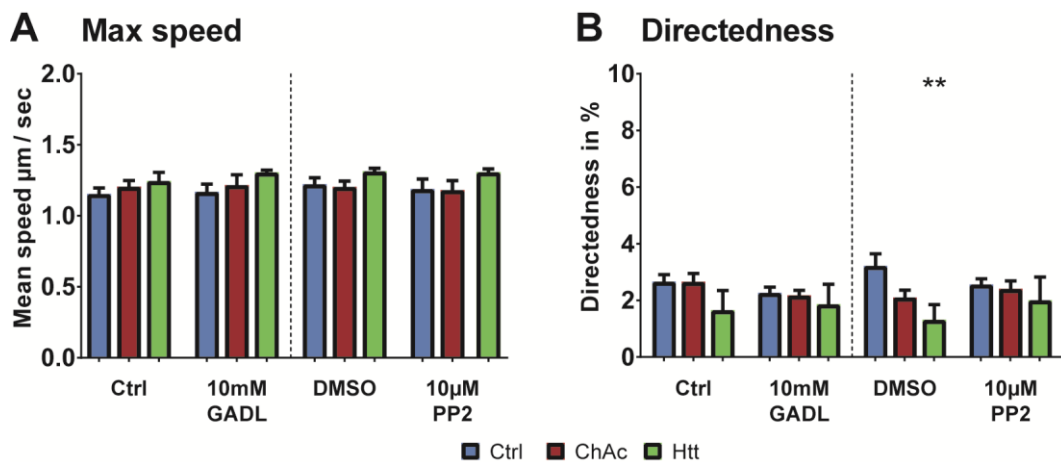


Figure 62: Analysis of top speed and direct movement of Htt lines. A) There was no difference observed in the fastest moving mitochondria of Htt lines. B) Direct movement was impaired for Htt lines. Bars represent mean + SEM. $n \geq 3$. * indicate significant differences within a treatment. ** represents $p=0.01$, respectively.

4.3.1.3. JC-1

Mitochondria potential was investigated under GADL and PP2 treatment conditions. When treated with GADL, there was no significant influence of the genotype, treatment or interaction. Huntington lines had an increased ratio of the red and green channel when compared to wild type, highly similar to ChAc. Treatment response was similar to wild type, but the influence of the treatment was not significant. When DMSO and PP2 sets were

investigated, there was a significant influence of the genotype observed ($p=0.0025$, $F(1, 85)=9.722$, $\omega^2=0.111$). The ratio of the Huntington line was in between the values of wild type and ChAc. The treatment response resembled wild type rather than ChAc. The treatment itself, however, failed to be considered significant even when wild type and Huntington lines were directly compared (See Figure 63).

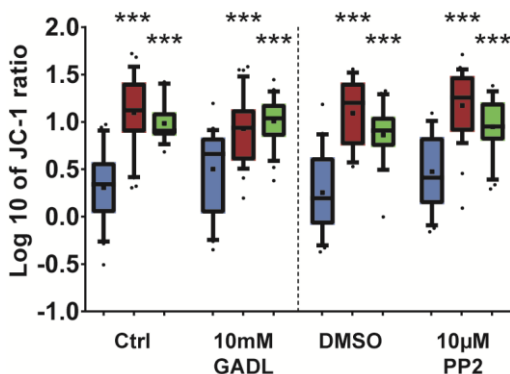


Figure 63: Analysis of membrane potential marker JC-1. Htt lines showed a significantly increased ratio of JC-1 in MSN differentiation conditions. GADL treatment increased the ratio in wildtype but not Htt lines. Boxes represent 25-75 percentiles, line represents median, whiskers represent 10-90%, + represents mean. $n =$ at least 18 images from 3 independent experiments. * indicate significant differences within a treatment. *** represent $p=0.001$, respectively.

4.3.2. Lysosomes

4.3.2.1. Morphological analysis

The morphology of Huntington patients' lysosomes was assessed in 96 well plates. When the count per arbitrary neurite length was calculated, there was no significant influence of genotype, any treatment or any interaction observed. The absence of any significant influence showed that there was no difference between ChAc and Huntington. Lysosomal count of the investigated Huntington line was in between the values of ChAc and wild type. Importantly, the reaction to the treatment was again similar to that of the wild type. Analysis of the aspect ratio of lysosomal compartments revealed no differences between ChAc and Huntington (See Figure 64 A & B).

Investigation of the size of LysoTracker-positive objects under GADL treatment conditions showed decrease in the Huntington line in comparison to ChAc. This was calculated by a significant influence of the genotype ($p=0.0068$, $F(1, 44)=8.073$, $\omega^2=0.164$). A similar behavior was observed in the DMSO and PP2 sets. The influence of the genotype was rated significant as well ($p=0.0016$, $F(1, 45)=11.26$, $\omega^2=0.205$) (See Figure 64 C).

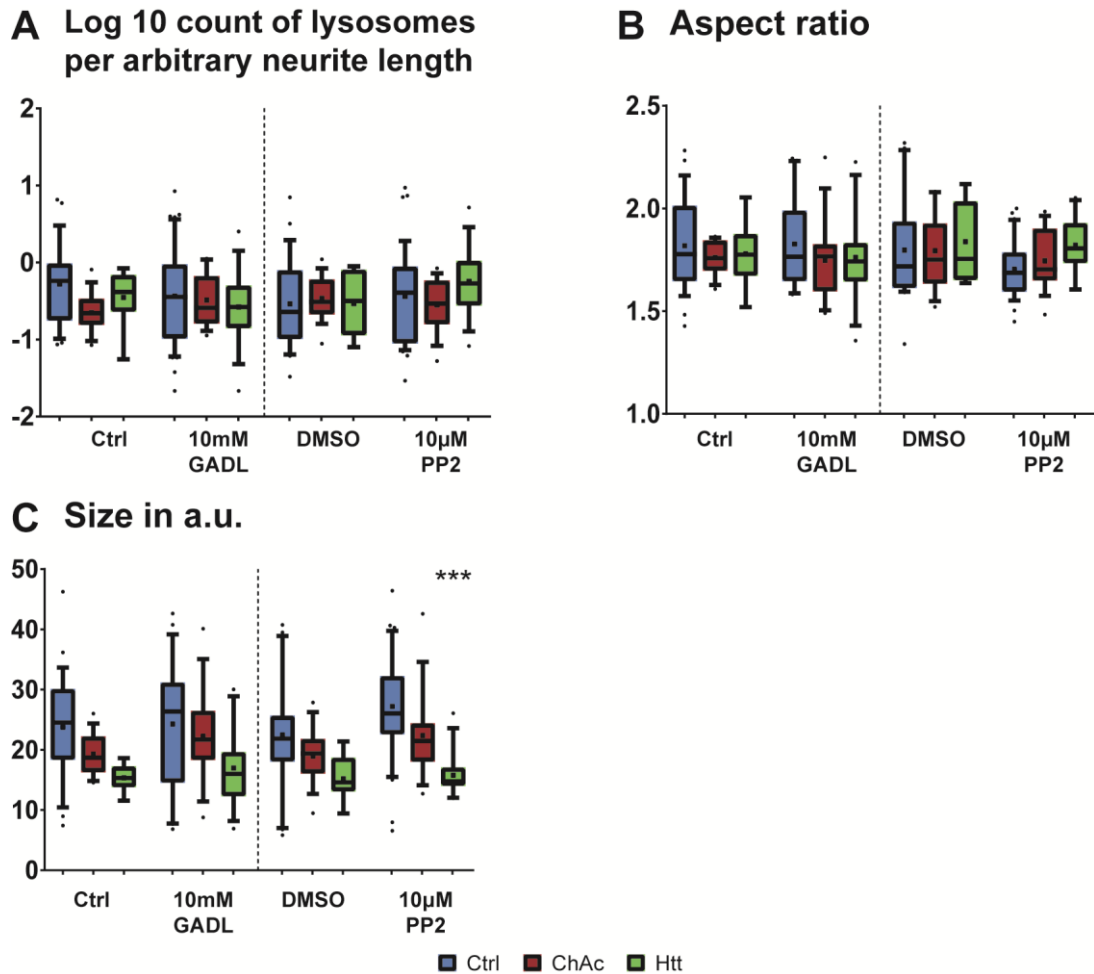


Figure 64: Morphological analysis of lysosomes of Htt lines in MSN differentiation. A) MSN differentiation showed no significant difference in the number of lysosomes per neurite length. B) The aspect ratio was not altered in MSN differentiated neurons under control conditions but in GADL and PP2 treatments. C) The size of the observed lysosomes is reduced in Htt lines. Boxes represent 25-75 percentiles, line represents median, whiskers represent 10-90%, + represents mean. $n \geq 3$. * indicate significant differences within a treatment. ***; represent $p=0.001$, respectively.

4.3.2.2. Trafficking

The trafficking of lysosomal compartments was investigated using 96 well plates. The amount of moving lysosomes was significantly reduced in Huntington when compared to ChAc. This was highlighted when the influence of the genotype was calculated under Ctrl/GADL conditions ($p=0.0075$, $F(1, 10)=11.14$, $\omega^2=0.465$). During DMSO and PP2 conditions, the influence of the genotype was significant as well ($p=0.0117$, $F(1, 10)=9.481$, $\omega^2=0.502$). There was no difference observed when Huntington was compared to wild type (See Figure 65 A).

When the motility of the lysosomes was investigated, there was no difference of between ChAc and Huntington, regardless of the treatment conditions. When compared to wild

type lines, GADL treatment revealed an increased motility of lysosomes in Huntington. The influence of the genotype was rated significant ($p=0.0063$, $F(1, 16)=9.887$, $\omega^2=0.304$). There was an interaction observed as well ($p=0.009$, $F(1, 16)=8.82$, $\omega^2=0.275$). This interaction is specific for the wild type vs. Huntington comparison and not the ChAc vs. Huntington analysis. The treatment response to GADL on lysosomal motility was the same in Huntington and ChAc and was considered significant ($p=0.0170$, $F(1, 10)=8.171$, $\omega^2=0.44$) (See Figure 65 B).

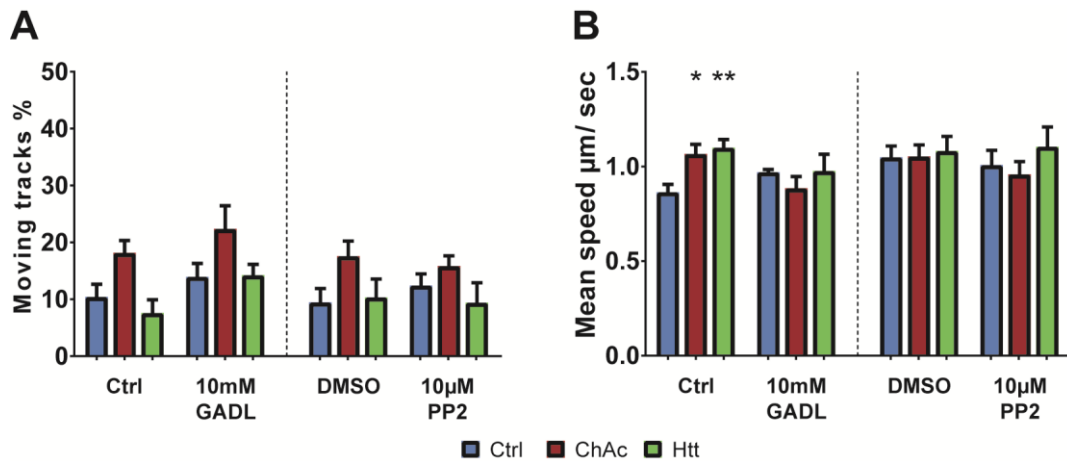


Figure 65: Trafficking analysis of lysosomes of Htt lines in MSN differentiated cultures. A) Htt lines have a similar moving fraction when compared to wild type. B) There was a significant increase of the mean speed of moving lysosomes in Htt lines under control conditions. GADL had a differential effect on the average speed. Bars represent mean + SEM. $n \geq 3$. * indicate significant differences within a treatment. **/*** represent $p=0.05/0.01$

The directedness of lysosomal trafficking was significantly reduced in Huntington lines. This was calculated for ctrl and GADL conditions with the influence of the genotype ($p<0.0001$, $F(1, 50)=21.58$, $\omega^2=0.307$) as well as under DMSO and PP2 conditions ($p<0.0001$, $F(1, 51)=38.57$, $\omega^2=0.437$). When compared to wild type lines, it was significantly reduced for GADL treatment conditions ($p=0.0142$, $F(1, 82)=6.281$, $\omega^2=0.081$) as well as when treated with PP2 ($p=0.0119$, $F(1, 84)=6.614$, $\omega^2=0.083$) (See Figure 66 B).

When the top speed of the fastest decile of moving objects was analyzed, there was no difference observed between ChAc and Huntington (See Figure 66 A).

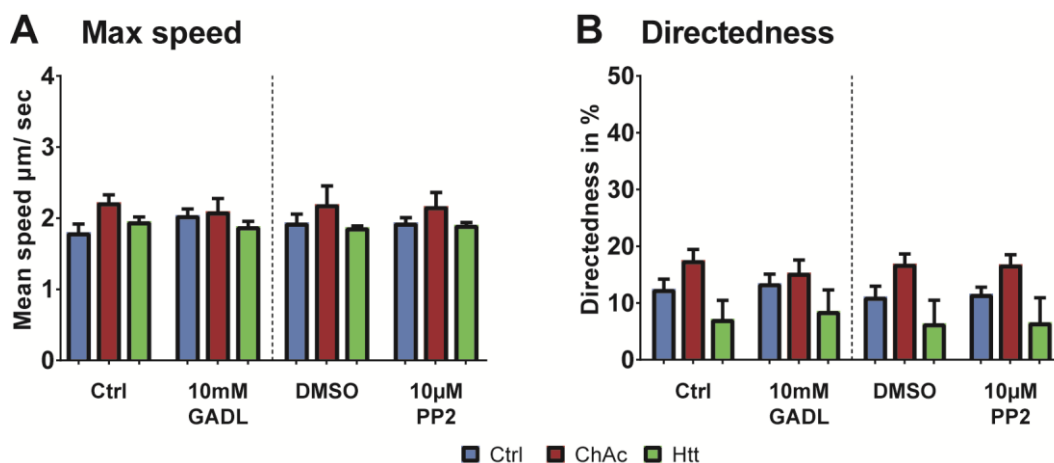


Figure 66: Analysis of top speed and direct movement of Htt lines. A) There was no difference observed in the fastest moving mitochondria of Htt lines. B) Direct movement was similar in Htt lines and wild type lines. Bars represent mean + SEM. $n \geq 3$.

To summarize the findings of the investigation regarding the behavior of Huntington lines, their results were mainly compared to ChAc lines. Huntington lines harbored a similar amount of DNA damage when treated with Etoposide, when compared to ChAc lines. The treatment resulted in an increase in DSB. The metabolic characterization, using Seahorse, showed that there are no differences between ChAc and Huntington. The non-respiratory oxygen consumption, however, was similar to wild type conditions, thus lower than in ChAc lines. When mitochondria were investigated in Huntington lines, their count was reduced, they were smaller in size and shorter compared to wild type lines, resembling the ChAc phenotype. The results of the treatments, however, resembled the wild type. Analysis of the dynamic parameters of the live cell imaging revealed, that fewer mitochondria move in Huntington, but these move faster when compared to ChAc or wildtype. The directedness was reduced and the max speed showed no difference when Huntington lines were compared to ChAc lines. The results of the treatments were similar to the ones obtained in wild types. Assessment of mitochondria potential with the JC-1 dye showed that the potential is, similar to ChAc lines, increased when compared to wild type. When lysosomes were investigated, the count and size was reduced compared to ChAc. The Aspect ratio remained unchanged. Treatment had the same effects on Huntington that it had on wild type and ChAc lines. The amount of moving lysosomes as was similar to wild type lines, while the mean speed was comparable to ChAc levels, thus larger than wild type. The directedness was reduced but the max speed similar to wild type lines. The treatment response of the dynamic parameters of lysosomes was similar to ChAc lines.

	ChAc vs. Huntington	
DNA damage	Etoposide treatment increased the amount of DSB	
	No difference between ChAc and Htt	
metabolic characterization	No difference in the glycolytic parameters	
	Non-respiratory oxygen consumption is reduced to wild type levels in Htt when compared to ChAc	
	Morphology	Trafficking
Live cell imaging mitochondria	Mitochondria count was similar to ChAc	Fewer mitochondria are moving in Htt
	Reduced aspect ratio was observed	Moving mitochondria are faster in Htt
	No difference in size of mitochondria	Directedness is reduced in Htt
	Treatment responses resemble wild type	Mitochondria potential was increased
		Treatment responses similar to wild type
	Morphology	Trafficking
Live cell imaging lysosomes	Lysosome count was similar to ChAc	Moving Htt lysosomes similar to wild type
	Aspect ratio was similar to ChAc	Speed is increased in Htt
	Size was smaller in Htt	Directedness reduced in Htt
		Treatment response similar to ChAc

Discussion

The reprogramming of somatic cells of ChAc patients into iPSCs using a polycistronic lenti viral vector system was successfully achieved for the first time (Warlich, et al., 2011). Even though this system offers high efficiency, reproducibility and is easy to handle, during the course of the work, an even more refined system using Sendai virus became available, which, due to its non-integrative approach of delivery of exogenous factors, would be the system of choice for further establishment of disease specific iPSC lines. In this work the guidelines of Maherali and Hoechedlinger for good scientific practice were followed (Maherali and Hoechedlinger, 2008). Only iPSC that showed a bona fide morphology, featuring densely packed small cells that were growing as a monolayer with a distinct border, AP positive, silenced for the exogenous transcription factors, were positive for pluripotency markers, capable of three germ layer formation and showed no aberrant karyotype were used for disease modeling. A notable exception is the clone ChAc 1.1, which was further used in experiments albeit the high residual expression of about 17%. It displayed bona fide iPSC morphology with activation of endogenous factors. Within the culture, there was a subpopulation of fast growing cancer like cells that most likely is responsible for the unsilenced transgene expressions. These patches were easily identified and scrapped off before every passaging and before the start of a new differentiation to prevent overgrowth. As a last step, it has to be shown that the disease defining mutations are still in place and have not been altered by the reprogramming process. Western blot was conducted to prove the absence CHOREIN protein (Dobson-Stone, et al., 2002). This procedure is also part of the clinical diagnosis of ChAc and, therefore, appropriate to determine the status of generated cell lines (Dobson-Stone, et al., 2004). Already established and published ChAc lines were used as either negative or positive controls. The Antibody used for the blot has been used in other studies as well and the observed pattern is similar to the one reported by other groups (Hayashi, et al., 2012). Each line investigated showed the proper expression of CHOREIN. Some of the generated lines were already shared with other labs and contributed to the field.

1. Characterization of ChAc lines

1.1. ChAc stem cell lines show no impaired differentiation potential

The differentiation protocols for mixed striatal cultures and dopaminergic neurons that have been used in this work were chosen to reflect two distinct populations that are affected by the disease. The MSN differentiation protocol was successfully established to

investigate the neuronal population, whose degeneration is causing the main choreiform symptoms of ChAc. mDAN differentiation protocol was used to investigate the degeneration of neurons that are related to Parkinsonism, which is present in roughly 50% of the patients (Velayos Baeza A, 2014). Starting from NPC stage the mDAN protocol is quicker and yields a more homogenous culture compared to MSN protocol (Reinhardt, et al., 2013). One of the questions of this thesis is to evaluate the mDAN protocol as a replacement for the MSN protocol and whether the results obtained from both are comparable.

Both protocols were able to generate mature neurons as shown by MAP2 staining. The semi-automated macros used for quantification of these pictures increased the throughput and allowed an unbiased background controlled detection of positive cells. Even though detection of false positive and false negative signals was a problem, the quantifications of wild type and ChAc cell were conducted with the same settings, hence, any error caused by the macro is systematic and only affects the absolute values but not relative quantification. Both differentiation protocols yielded similar efficiencies for wild type and ChAc lines. MSN derived neurons were only 45-80% positive for the markers DARPP32 and GABA. Remaining neurons were CHAT positive and most likely cholinergic interneurons. Therefore, these cultures were referred to as mixed striatal cultures. During midbrain dopaminergic differentiation, ChAc lines followed were not different from wild type ones. This result is reflecting the clinical disease phenotype, since ChAc has no known developmental implications. Only a minor fraction of neurons were identified as motor neurons in undirected 96-well cultures. However, when the mDAN differentiation was conducted in MFC, the yield of TH positive neurons dropped significantly. Addition of cues that are known to attract dopaminergic neurons, like Netrin-1, can be tested to improve the growth of in MFC. The trend of faster differentiation of ChAc lines, albeit not significant, was observed in both protocols. This might be an artifact of the *in vitro* cell culture or a line specific observation, since no isogenic controls were used. Both protocols showed a large remaining pool of SOX2-positive stem cells. Other protocols that are available to yield MSN and mDAN address this problem by exposing the remaining stem cells to supplements that either boost their differentiation, like TGF β 3 and ACTIVIN A, or inhibit their growth, like DAPT (Caiazzo, et al., 2011; Crawford and Roelink, 2007; Kawasaki, et al., 2000; Lee, et al., 2000; Perrier, et al., 2004). Even though DAPT itself has no direct toxic effect on neurons, it can be detrimental because the early maturation can facilitate detachment of the generated neurons (Kirkeby, et al., 2012).

The hierarchical clustering of the PCR data showed that there was a clustering of the iPSCs and the mature MSN cultures, showing that these populations are very distinct from each other. The small clusters that were found within the differentiated cells indicate that the biological variance between experiments might be bigger than the variance between wild type and ChAc lines, in regards to the investigated markers. The hierarchical clustering of mDAN differentiation gave two different results depending on the implementation of one of the previous mentioned genes discovered by CHIP analysis. When NNAT was not included, there was no clear clustering of the lines. Every line was fairly unique and there was no clear clustering. All wild type lines behaved more similar than the different ChAc lines. When the gene NNAT was included in the analysis, there was a clear separation of wild type and ChAc lines. Expression of NNAT was 10000 fold increased in ChAc when compared to controls. Wt 2.2 is a notable exception since it also had an increased expression and clustered within the ChAc lines, which shows that the grouping in this setting was solely achieved by the parameter of NNAT expression. The interpretation of this finding is very difficult. There is very little known about NNAT and its product NEURONATIN. It is known that this gene is paternal imprinted and responsible for brain development (Joseph, 2014). In the adult brain, NEURONATIN is expressed in parvalbumin-positive GABAergic interneurons (Sharma, et al., 2013). Recent research shows that NEURONATIN might be stress induced and a common feature in neurodegenerative diseases (Joseph, 2014; Shinde, et al., 2016). These data might recapitulate the finding of the observed trend of faster differentiation and suggest, that there is either a sublime developmental phenotype in mDAN cultures or that the mature cultures might be more stressed than their healthy wild type controls. Due to the epigenetic changes that cells undergo during reprogramming, it has been shown that imprinted genes could randomly be reactivated and subsequently silenced again in a randomized pattern, thus rendering the speculations about the effect of these genes in reprogrammed cell lines futile (Chang, et al., 2014; Hewitt and Garlick, 2013). The only differences between ChAc and wild type lines that were found in the differentiation capacity were minor and negligible and therefore don't impair the further experiments, highlighting the phenotype of the disease.

1.2. Neurons from MSN differentiation have an altered G/F actin ratio

Investigations of the cytoskeleton included the characterization of the G/F actin ratio, the G/F tubulin ratio and the amount of acetylated tubulin relative to total α tubulin. Mixed striatal cultures showed a phenotype in the G/F actin ratio similar to the one reported in the literature while there was none observed in mDAN cultures. (Foller, et al., 2012). This

can be attributed to the huge differences in the differentiation protocols. There is another possibility that actin cytoskeleton can be affected in dopaminergic cells beyond the simple ratio of globular and filamentous actin. Functional assay like growth cone dynamics, outgrowth assays or the proper internalization of receptors need to be done to further characterize the actin cytoskeleton. Tubulin filaments play a major role in organelle trafficking and cell homeostasis (Maeder, et al., 2014). Acetylation of tubulin, is important for enhancing the binding of KINESIN1 and therefore initiating trafficking (Chen, et al., 2010). This is important for proper guidance and distribution of travelling organelles. In neither mature MSN nor mDAN cultures was any difference in the G/F tubulin ratio or the acetylated tubulin ratio observed. These data suggest that the homeostasis of the tubulin related cytoskeleton remains intact in ChAc derived neurons in regards to overall G/F ratios and modifications.

1.3. Mature neurons from ChAc lines are susceptible to UPR, proteotoxicity and DNA damage

Because over the course of the differentiation there was no major difference in cell survival or morphological abnormalities observed, mature cultures were treated with substances to investigate whether ChAc lines are more susceptible to certain kind of stress. ChAc lines proved to be more vulnerable to the application of tunicamycin, an inducer of ER-related UPR, as well as L-canavanine, an inducer of proteotoxic stress, when compared to wild type lines. At a concentration of 1mM for L-canavanine and 10 μ M for tunicamycin, there was little to no effect to the neurons over the time course of six days, while 2mM and 5mM of L-canavanine and 50 μ M and 100 μ M of tunicamycin, respectively, showed a strong effect on cell survival. These low concentrations could be used for chronic stress conditions or to assess cross talk between different disease pathways that could affect other organelles or cell homeostasis. The data obtained by MSN protocol suggest different mechanisms for the substances when compared to mDAN differentiated cells. L-canavanine seems to induce cell death quicker in MSN, suggesting that cells can cope worse with misfolded protein or higher demand in protein biogenesis in comparison to mDAN, which seem to be able to resist the stress for a longer time but then decompensate very quickly once a certain threshold is reached. Tunicamycin seems to have similar effects on MSN and mDAN differentiated neurons. Both protocols exhibit reduced metabolic activity, but, while MSN protocols have similar rates of cell death, mDAN neurons seem to suffer from acute cell death. This is in accordance with the finding that that silencing of VPS13A in HeLa cells caused disruption of the autophagy pathway (Munoz-Braceras, et al., 2015). It is possible that fusion and fission of vesicles, which is

pivotal for proper protein recycling, is disturbed in ChAc lines. This is backed up by publications that showed that loss of VPS13 in yeast led to major impairments in the phosphoinositol pathway, which were also observed in humans, and an important player in vesicle fusion and fission (Park, et al., 2015; Park and Neiman, 2012). Taken together this data suggests a different penetrance of the susceptibility to UPR and protein misfolding depending on the cell type investigated. The exact differences of the involved pathways, however, remain elusive and cannot be clarified with experiments conducted within this work.

1.4. ChAc neurons are not susceptible to DNA damage

It has been shown that in most neurodegenerative diseases DNA damage plays a pivotal role (Madabhushi, et al., 2014). Whether this is causative to the disease, a result of the degeneration or if these cells have impaired DNA damage repair mechanisms remains elusive. Importantly, this was recently reported for Huntington's disease (Mollica, et al., 2016). γ H2A.X, a histone modification that is important for initiation of DSB repair was investigated to assess the susceptibility to DNA damage (Kinner, et al., 2008). Treatment with 10 μ M etoposide, a substance known to induce DSB, was used as a positive control as well as inducer of stress. Both differentiation protocols showed a weak susceptibility to DNA damage as determined by a very small effect size. The Huntington cell lines showed results similar to ChAc, having no intrinsic accumulations of DNA damage under control conditions, but increased DSB when treated with etoposide. Even though in mice, DNA damage was suggested to play a role in disease progression of Huntington, the experimental setup in this study yielded different results (Cardinale, et al., 2015). Since DNA damage can accumulate over time and even minute changes to gene expression profiles can have a huge impact on cell metabolism it is, however, possible that these vulnerabilities are important aspects of the ChAc phenotype. The aspect of recovery after DNA damage was not assessed with the experimental setup, but could highlight more differential results.

1.5. Energy dynamics in ChAc and Huntington lines feature a shift to glycolysis

Neurons are highly specialized cells with a tremendous energy demand needed for organelle transport along neurites, biosynthesis of proteins and propagation of action potentials (Berndt and Holzhammer, 2013). Many neurodegenerative diseases have been linked to deficits to meet this energy demands (Lezi and Swerdlow, 2012). The analysis of MSN differentiated cultures revealed that there was no difference in parameters characterizing the glycolysis. The OCR related measurements, however, revealed that the oxidative phosphorylation of the mitochondria was impaired and the non-respiratory

oxygen consumption increased. These data suggest that the cells rely more on glycolysis than on oxidative phosphorylation. This might be the case because of an elevated fraction of stem cells in the cell culture even after prolonged maturation, which are known to rely on glycolysis (Shyh-Chang, et al., 2013). The increase in non-respiratory oxygen consumption can be related to microsomal activities or cell surface oxygen consumption, which is a regulator of glycolysis (Rosenfeld, et al., 2002). Whether these processes are overly activated in ChAc patients remains elusive and has to be addressed by other means. The data obtained from the Huntington line recapitulated the findings in ChAc cells. There was no overall phenotype in glycolysis or oxidative phosphorylation. The major difference that was observed between ChAc and Huntington was the decrease in non-respiratory oxygen consumption. This parameter was similar to wild types in the Huntington line and can be an indication that this parameter might be a crucial hall mark of ChAc pathology. Analysis of mature dopaminergic cultures harbored no differences in the parameters of glycolysis as well. The coupling efficiency as well as the spare respiratory capacity, however, was increased in ChAc lines. These findings would suggest that the function of the respiratory chain is maintained. However, since patient cells don't seem to utilize it as much as wild type and given a normal function of the proton pumps together with a non-pathological coupling efficiency could hint to a complex V deficiency (Hroudova, et al., 2014). It is, however, not possible to clearly deduct this from the given results and further experiments that back up this hypothesis have to be conducted. Since the unraveled differences are presented as relative changes compared to wild type cell lines, only a selective vulnerability to cell death of the ChAc lines could explain this. Because no vulnerability was observed in other experiments without specific cell stressors, the obtained data indicates that the observed phenotype is disease relevant. There was an article published recently that focused on the interaction of VPS13 with the membrane of mitochondria-endosome junctions (Park, et al., 2016). The authors suggested that there might be a basal impairment of mitochondria in ChAc patients. Since disturbance of energy homeostasis seems to be downstream of different pathways in mDAN and MSN cultures, analyzing the ultrastructure of the mitochondria with electron microscopy, including their cristae, can be beneficial to exclude structural differences as a cause.

2. Live cell imaging of ChAc lines

2.1. Video analysis is reproducible and sensitive

Because the cultures obtained by the differentiation protocols are a mixture of various cell types, the underlying background noise from non-neuronal cells renders observation of minute changes impossible. Live cell imaging of labelled cell organelles can give

information about morphological aspects as well as functional readout, when their trafficking is analyzed. With the proper placement of the field of view, it is possible to keep the background signal of non-neuronal cells to a minimum. Furthermore, when MFC are used it is possible to distinguish between proximal and distal parts of a neuron as well as antero- and retrograde movement. The establishment of MFCs as a novel cell culture system for spatiotemporal analysis of neuronal cultures was achieved recently (Folch, et al., 1999; Reyes, et al., 2004). Due to the small dimensions of the channels only neurites can grow into the device and imaging readout is not influenced by non-neuronal cells or perinuclear organelles. The markers used in this study are MitoTracker DeepRed, Lyso Red and JC-1. Since none of these dyes requires excitation in UV or blue light, induction of phototoxicity and therefore detrimental effects on the illuminated cells are minimized (Douthwright and Sluder, 2016). Shape analysis was conducted using semi-automated macros and fitting algorithms. Trafficking analysis was based on the assumption of two distinct populations, which describe a stationary and a moving fraction, that were modeled on the data obtained from the well-established Fiji Plugin TrackMate. Conducting a regression analysis by using a two-phase decay model yields two e-functions that describe parameters of these populations, which can be used to assess the individual trafficking parameters of each video. This approach has the advantage of not relying on a possibly biased and arbitrary fixed threshold that is used in some publication (Atkin, et al., 2011; Brickley and Stephenson, 2011; Cai, et al., 2005). The fraction of moving organelles varies between different cell types and their culture conditions. Furthermore, different publications utilize different methods of quantifying the amount of moving objects. Therefore comparison of the results obtained in the herein presented experimental setup cannot directly be compared to other reported values. The spectrum of physiological movement ranges from 10% to 40% (Schwarz, 2013). The mean speed of motile mitochondria in this experimental setup was 0.4 to 0.6 $\mu\text{m}/\text{sec}$. Even though the reported values vary in between publications, the expected velocity ranges from 0.3 to 1.0 $\mu\text{m}/\text{sec}$ (MacAskill and Kittler, 2010). The fraction of moving lysosomes is considered to be roughly 50% (Cordonnier, et al., 2001; Stagi, et al., 2014). In this work 10-30% of the lysosomes were considered moving. The calculated mean speed of the lysosomes was about 0.6 to 1.2 $\mu\text{m}/\text{sec}$. It is reported that the average speed of lysosomes is about $0.67 \pm 0.79\mu\text{m}/\text{sec}$, showing that the data obtained by the algorithm is with a physiological range (Bandyopadhyay, et al., 2014).

The discrepancies between different publications as well as when compared to this work can be explained by the criteria considered defining a track as moving and the technique applied. Kymographs that are generated and evaluated by hand are most often used to

investigate organelle trafficking. Some publications consider an object as moving if its maximum velocity is above 0.1 μ m/sec (Lee, et al., 2011). Due to the small time interval in between pictures that was used in the setup of the present work, a speed of 0.1 μ m/sec would be obtained when an object displaces only 30nm in between two pictures. However, this displacement is below the resolution of the used imaging system and when this criterion was used to assess the size of the moving fraction of lysosomes a result of 99.177% \pm 1.654% for moving tracks was obtained. This is clearly overestimating the moving fraction and not representing the subjective impression of the videos and therefore cannot be applied to the imaging setup used in this study. The investigated time frame plays a crucial role for the quantification of moving fraction. A lot of organelles can pause during their movement by detaching from microtubules and remain stationary for a prolonged time (Ori-McKenney, et al., 2010). Since images are only taken over a course of 2min, there is a possibility that stationary tracks would have moved at a given time if the imaging period was extended. Considering these drawbacks of the system, a relative evaluation in regards to genotype, treatment or position is still possible since the error caused has a systematic nature and affects wild type as well as ChAc lines. The quality of the algorithm can easily be determined by interrogation of regression parameters like the regression coefficient.

2.2. ChAc lines have altered mitochondria shape and trafficking

The morphological features of ChAc patients' mitochondria were similar in mixed striatal as well as dopaminergic cultures. The count per neurite length was reduced in both protocols leading to an overall smaller population. These mitochondria had a smaller size as well. Furthermore, in mDAN cultures they exhibited a reduced aspect ratio, which was not significantly reduced in MSN differentiations. Even though the size was reduced in mDAN differentiated ChAc lines, this is most likely a resemblance of the shortening and not a reduction that goes beyond this morphological change. Shortening of mitochondria can be an indication for problems with control of fusion and fission events. These alterations suggest that ChAc cells might have an underlying impaired mitochondria homeostasis that results in reduced mitochondria biomass and can subsequently cause deficits in energy homeostasis. This theory can be backed up by the fact, that CHOREIN is involved in signaling of mitochondria and other organelle at specific junctions (Park, et al., 2016). Huntington lines behaved very similar to ChAc. The organelle count, was diminished in Huntington but not as much as in ChAc. While an observed decrease in size was stronger in ChAc, reduction of the aspect ratio was more pronounced in Huntington. One possible explanation of the observed phenotype is that striatal neurons from

Huntington lines exhibit excessive mitochondrial fission resulting in shortened mitochondria (Guedes-Dias, et al., 2015). When MFC were investigated they were similar to the results obtained in undirected 96wells. The count was reduced in proximal parts of MSN, but not in mDAN cultures. The aspect ratio was reduced in distal parts of mDAN cultures suggesting that for midbrain dopaminergic cultures the neurons observed in undirected 96wells are of distal nature. A possible explanation for this is the different neuronal subtype that grew through the MFC channels. In the case of mixed striatal cultures only cholinergic interneurons grew through the channels. This might be a certain characteristic of MSN, since these cells don't grow over large distances *in vivo* as well (Koos, et al., 2004). Other chemical cues might be sufficient however to drive their outgrowth. In midbrain dopaminergic cultures, only SMI32 positive motor neurons crossed the channels. This significant difference in neuronal subtype can also explain why there was no significant reduction in the count of mitochondria observed in mDAN cultures. This behavior can be explained by the lack of appropriate chemical cues for growth. Further addition of Netrin-1 into the terminal side could be tested to increase the fraction of TH-positive dopaminergic neurons that grow along the channels (Lin and Isacson, 2006). Since some dopaminergic neurons were found to grow through the channels and exhibited a healthy morphology, the low amount TH-positive cells is most likely attributed to the lack of neurotrophic factors they receive on the soma side. But once they grow through the channel, the supplied factors on the terminal side are sufficient for their survival.

The analysis of the dynamic movement of mitochondria revealed that there in mixed striatal cultures no difference in the moving fraction and their mean speed was observed. In midbrain dopaminergic cultures there were more mitochondria moving, however, their mean speed was reduced. It is possible that the reduction of the mean speed is causing problems in the cell's energy homeostasis and therefore more mitochondria are moving to reach hot spots of energy demand or return to the perinuclear area for recycling (Sheng, 2014). To address the fact that mitochondria don't move randomly but in a coordinated fashion, the directedness of wild type and ChAc lines was compared (Berndt and Holzhutter, 2013; Zajac, et al., 2013). In both protocols there was no difference observed in the directedness, suggesting that signaling and positioning of mitochondria under control conditions is not impaired in ChAc line derived MSN and mDAN. Interestingly the amount of direct movement was almost doubled in mDAN compared to MSN cultures. This data suggests that, due to the decreased moving fraction under control conditions in mDAN cultures, the remaining moving fraction had to traffic more coordinated. When the fastest 10% of moving mitochondria were analyzed, there were no differences found

between wild type and ChAc. When the Huntington line was investigated, there were fewer mitochondria moving in Huntington's patients differentiated mixed striatal cultures, and these mitochondria moved faster and less direct. There is evidence in the literature that mitochondrial transport in Huntington is impaired and causes more stops and a decrease in the distance of progressive movement (Weiss and Littleton, 2016). It is very likely that the reduction in moving fraction caused an increase of the average speed in the moving fraction, since the local energy demands in the axons pose a stronger chemical cue. The decreased directedness observed in the trafficking analysis is likely to reflect the increase in pauses. The measured velocities were still below the technical limitation of the tracking algorithm, which can theoretically detect up to 6µm/sec. Another important fraction is the slowest, non-stationary fraction. This slow but coherent transport of mitochondria along axons is very important (Miller and Sheetz, 2006). This fraction was, however, not investigated due to the short timeframe of only 2min for each video.

When trafficking was investigated in MFC, there was no difference observed in the moving fraction of wild type and ChAc lines in both protocols. The trend of an increased mean speed that was observed in proximal parts of MSN cultures was rated significant in mDAN differentiations. In mDAN cultures there was an increase in retrograde transport observed, which was absent in MSN differentiations. While there was no difference in the mean speed observed for anterograde transport, retrograde transport showed an increased mean speed in the proximal conditions. Since the directedness was not affected by anterograde/retrograde, proximal/distal or wild type/ChAc conditions in both protocols this increased mean speed is not an artifact from the absence of stop events. This elevated retrograde transport of mitochondria in MSN and mDAN cultures might be a hint for an increase in mitochondria damage since retrograde transport occurs when damaged mitochondria have to be recycled (Saxton and Hollenbeck, 2012).

While there seem to be no alterations in the distal parts of the cultures, proximal parts show a clear phenotype. This seems to recapitulate the findings of the morphological analysis in MFC, where the distal phenotype was established closer to the soma in ChAc lines when compared to wild type lines. Anterograde transport seems to be unaffected, indicating that newly generated perinuclear mitochondria are healthy but are either more susceptible to damaging in the distal part or that there is an underlying problem with proper recycling. Because mitochondrial trafficking is linked to dynein and kinesin function, another possible explanation is a selective disturbance of dynein motor protein which is responsible for retrograde transport. However, since obtained transport speeds at distal

position were similar in wild type and ChAc lines, there seems to be no generalized motor protein deficit in ChAc patients.

2.3. Treatments are not selective on ChAc lines mitochondria

Application of GADL had the biggest effect when mDAN cultures were treated. Even though the aspect ratio of mitochondria in mDAN cultures of ChAc lines was restored to normal levels, this increase was also observed in wild type lines. Therefore this treatment is unspecific. Since none of the assessed morphological parameters of mitochondria in mixed striatal cultures was influenced by GADL, it is likely that the pathogenesis is different in mDAN and MSN.

Furthermore, GADL treatment increased the amount of the moving fraction in mDAN cultures even further. Even though mean speed of wild type and ChAc mitochondria was not different anymore when the cells were treated with GADL, the speed of ChAc mitochondria was not increased to wild type levels, but wild type mitochondria moved slower. Therefore, GADL cannot be considered a cure for the ChAc phenotype, since it only affected the speed of wild type lines. The directedness of mitochondria movement in MSN cultures was not influenced by GALD, however, when mDAN cultures were treated, their levels dropped to values similar to MSN cultures.

In summary GADL treatment had different effects in MSN and mDAN cultures that were, however, stronger in mDAN differentiations. This can be seen in accordance with the differential results of mitochondria electron transport chain that was already observed in the seahorse experiment. To see whether treatment with GADL has a direct impact on electron transport chain, metabolic characterization of GADL treated neurons with a seahorse device needs to be conducted.

Treatment with PP2 and phalloidin showed almost no effect on the evaluated parameters of morphology and trafficking. This suggests that the phenotype described in this thesis is not related to a hyper activation of LYN or an disturbed G/F actin ratio but is acting in parallel and can be considered as a novel impairment of ChAc patients.

Importantly, treatment response of the Huntington line was akin to wild type and not ChAc lines. This strongly suggests a different pathological pathway of the disease progression that resulted in the same morphological observation.

2.4. Mitochondrial potential is altered in ChAc lines

Potential of mitochondria is an important aspect of proper function and was visualized by JC-1 staining. MSN and mDAN cultures yielded differential results. While ChAc lines in MSN differentiations showed an increase under control conditions, the ratio was reduced

in mDAN differentiations. Investigation of the ratio in Huntington lines showed an increased mitochondrial potential that was in between the values of wild type and ChAc, indicating a similar yet not as severe progression. When mDAN MFC cultures were investigated, there was no difference in the proximal position. In the distal position, however, there was a significant increase in JC-1 ratio in ChAc lines, while the wild type lines were similar to proximal side. This resembles the findings of undirected MSN cultures and could be caused by the absence of dopaminergic cells in the channels of MFC, or the MFC system itself which might pose a certain stress due to possible lack of nutrition and oxygen. After MSN differentiation, GADL treatment increased the potential in wild type but decreased it in ChAc lines, while in mDAN cultures the potential was further decreased in both genotypes. Huntington lines reacted to GADL similar to wild type rather than ChAc, suggesting a different underlying mechanism.

Even though there is a differential phenotype in MSN compared to mDAN cultures, which reflects the findings of the seahorse experiments and the GADL treatment on the trafficking, it is clear that VPS13A mutations in ChAc lines cause impairment to their mitochondria homeostasis. It has been reported that increased as well as decreased mitochondria potential may impair mitochondrial function (Gottlieb, et al., 2000). Some articles in the literature link an increased mitochondrium potential to putative neuronal degeneration (Green and Reed, 1998; Kroemer, et al., 1998). Hyperpolarization can be utilized by the cell to prevent apoptosis (Ward, et al., 2007). A recent published paper linked the function of VPS13 directly to mitochondria und suggests a direct interaction at the endosomal mitochondria interface (Park, et al., 2016).

2.5. ChAc lysosomes feature normal morphology but altered trafficking

The lysosomal system, which is important for protein homeostasis by participating in autophagy and the endosomal pathway, and was already shown to be impaired to some extent, when cells were treated with tunicamycin and L-canavanine, was visualized and analyzed using the readily commercial available probe LysoTracker. Both differentiation protocols had less lysosomal organelles and their aspect ratio was not altered. Furthermore, mixed striatal cultures showed that ChAc lines had smaller compartments. Since LysoTracker stains unselectively for acidic cell compartments, thus labelling lysosomes, hybrid lyso-endosomes, autolysosomes and mature autophagosomes, it is possible that the composition of these organelles is changed in ChAc. Of the aforementioned compartments lysosomes are the smallest and a decrease in overall size could be a sign of an accumulation of them. However, because the overall count is diminished as well, it is more likely that progression within the lysosomal pathway is

impaired. Findings of disturbance of autophagic flux in HeLa cells as well as disruption of organelle-to-organelle signaling in CHOREIN knock-out lines is supporting this theory (Munoz-Braceras, et al., 2015; Park, et al., 2016). Huntington lines had morphological features that were similar to ChAc. However, the size of the lysosomes was reduced. Since a possible shift in the composition of the lysosomal compartments cannot be excluded, different markers that allow the identification of different vesicles, like early or late endosomes have to be used to investigate these organelles independently. There is evidence in the literature that defective Huntingtin can cause a shift in the positioning of lysosomes that affects their function (Erie, et al., 2015). When MFCs were investigated the reduction of the amount of lysosomal organelle was confirmed in MSN but not mDAN cultures. The trend, that distal parts harbor fewer organelles was observed in MSN and was rated significant in mDAN differentiations. The aspect ratio was found to be smaller in distal parts than in proximal parts, which reflects the fact, that lysosomal compartments carry more cargo in proximal parts and already underwent several fusion events that potentially alter their shape. Compared to undirected cultures, the aspect ratios of lysosomes in MFC seem to be elevated in both differentiation protocols. Since it was shown that distal parts have a lower aspect ratio, and given the fact the only significant differences between wild type lines and ChAc were found in the proximal position, it seems that the data of undirected cultures resembles more the distal part. This finding is in accordance with the observation achieved with MitoTracker. The aspect ratio was lower ChAc line MSN differentiations when compared to wild type. This suggests that MSN cultures are heavier impaired in their lysosomal homeostasis, which could be a first link to the disease progression. Early clinical symptoms are also caused by cell death of MSN. While Parkinsonism, a symptom of the later ChAc stages, is cause by death of dopaminergic neurons.

Differences between MSN and mDAN cultures were also present in the analysis of lysosomal trafficking. While MSN differentiated ChAc lines had more moving lysosomes in and a significantly increased mean speed in control conditions, mDAN differentiated cultures highlighted no difference of the moving fraction between wild type and ChAc. The fraction of direct movement was smaller in MSN differentiations when compared to mDAN cultures. Furthermore, the trend observed in mixed striatal cultures that show an increase in ChAc lines was reversed in dopaminergic neurons, where there was a significant reduction. The fact that directness resembles the actual moving fraction indicates that almost all moving organelles move in a directed manner. Therefore, the organelles can be put in two groups, stationary lysosomes and direct moving lysosomes. Stopping events and change of direction, however, would result in a decrease in

directedness. This suggests that the movement is unidirectional, meaning once an organelle starts moving only a small fraction changes its direction or stops, because these events would cause a violation of the inclusion criteria for this analysis.

The maximum speed of lysosomes was significantly increased in ChAc lines of MSN, but decreased in ChAc lines of mDAN cultures. These substantial differences can be attributed to a different composition of the lysosomal system as well. Therefore it is important to further investigate with more precise markers to which extent specific organelles are affected. The amount of moving lysosomes of Huntington's patients was more similar to wild types. However, the speed of the lysosomes was increased, similar to ChAc lines. Since different lysosomal organelles travel with a different speed according to their cargo and position, it is very likely that the observed tracks represent a specific subset of lysosomal compartments that is increased in Huntington. The directedness of movement was strongly reduced and might be a phenotype that is specifically pronounced in Huntington, since these findings were unique to the investigated line. These findings suggest that the effect on the lysosomal pathway is very different between ChAc and Huntington. Some evidence was found in the literature where expression of mutant Huntingtin was sufficient to disrupt axonal transport of lysosomes. The authors hypothesized a potential inhibition of autophagosome/lysosome fusion, which would be in line with our data showing especially the fraction of small lysosomes affected (Wong and Holzbaur, 2014).

Moving fraction and mean speed lysosomes in MFCs of MSN cultures were not significantly different for wild type/ChAc and proximal/distal comparisons. In MFCs of mDAN cultures there were more moving lysosomes in the distal position. Furthermore, ChAc lysosomes were faster. In general, the percentage of moving tracks was higher in MFC than in undirected cultures. The mean speed was similar. The trend of increased movement in ChAc vs wild type was observed in distal parts of the MFC indicating again that the undirected cultures yielded results more akin to distal positions. The increase in mean speed observed in the ChAc lines and the absence of different movement in proximal and distal positions did not recapitulate the findings of undirected cultures. This might be due to the fact that mainly motor neurons were observed in MFC. Similar to the diametric results of the mitochondrial analysis, this data reflects the differences between ChAc phenotypes in motor neurons vs dopaminergic neurons.

In both protocols the majority of lysosomes move retrograde. This finding is well established in the literature (Lee, et al., 2011). In mDAN MFC cultures, a further reduction of anterograde transport was observed in distal positions. There was a strong trend observed in the speed of retrograde transport in MSN MFCs. In both protocols no

difference was observed for the velocity of anterograde movement. The speed of retrograde moving ChAc lysosomes in proximal parts was similar to the distal counterpart, while wild type lines exhibited an increased speed in the proximal region. In mDAN MFC the velocity of retrograde transport was increased for ChAc. Furthermore there the speed was reduced in distal parts. The amount of direct movement was similar to the overall moving fraction, suggesting that all movement is highly directed. Directedness was not different for ChAc lines but an increase in distal parts was observed in both protocols. This behavior was observed in 96 wells as well, indicating that undirected cultures are represented by the distal parts of MFCs.

The top speed of lysosomes in MFC cultures of ChAc lines did not yield any significant differences, similar to undirected wells. It is very likely that the effect on the speed of trafficking vesicles is occurring not only on a separate subpopulation but is an overall effect. The mechanism behind this increase remains elusive.

2.6. Lysosomes of MSN cultures respond poorly to treatments

When GADL was added to MSN cultures the morphological parameters of the lysosomal fraction did not change. In mDAN differentiations an increase in the size and aspect ratio was observed that was larger in ChAc lines. Furthermore, the treatment showed a trend to increase the moving fraction of lysosomes in MSN, but decreased it in mDAN cultures. Since all moving lysosomes move in a direct manner, the same effects were observed for directness. The mean speed and top speed were unaffected.

PP2 treatment caused differential results in the size of lysosomes. While it increased the size in MSN, it did not affect mDAN cultures. Aspect ratio and count remained unaffected by the treatment. When trafficking was investigated, a trend of decrease in the moving fraction of ChAc lysosomes in MSN cultures was observed, while wild type lines responded with an increase. This trend of decrease in ChAc lines was observed for mDAN differentiations as well. The directedness behaved similar and the decrease was rated significant in mDAN cultures of ChAc lines. The treatment response of the Huntington line was comparable to effects in ChAc lines.

Taken this data together, the differential behavior in regards to wild type/ChAc differences and response to chemical intervention, suggests that there is a substantial difference in the disease phenotype in the investigated neuronal subtypes. The fact that MSN cultures failed to significantly respond to any treatment, even though ChAc lines were impaired, suggests that the treatments do not interact directly with the lysosomal system. Hence, observed effects in mDAN cultures might be attributed to bystander effects. One of these

effects was recently highlighted by a group that showed that impairment of mitochondria results in lysosomal impairment by the production of ROS (Demers-Lamarche, et al., 2016). This interaction is very likely because previous experiments already showed an influence of the treatments with the mitochondrial system.

3. MSN and mDAN differentiation highlight different aspects of the disease

Conclusions that were drawn from the present work feature important aspects for disease modelling of Chorea acanthocytosis that can also extend to other diseases. For the first time detailed experiments that highlight specific susceptibility of ChAc patient derived neurons are presented and show opportunities for putative treatments. Showing the complexity of the disease phenotypes being present on a functional level in pivotal pathways including endo-lysosomal pathway, energy metabolism and organelle trafficking, further emphasizes the importance of CHOREIN protein on cell homeostasis. The differential results obtained from midbrain dopaminergic neurons and mixed striatal cultures suggest that the disease progression differs between different cell types. Therefore, upcoming treatment approaches have to be verified under different culture conditions as well. Taking all data into account, it is highly advised to not substitute one differentiation protocol with the other because the treatment responses and underlying mechanisms have to be considered on an individual level. Therefore, a combination of experimental setups with mDAN, MSN or other cultures has to be established. Furthermore there were significant differences found when ChAc was compared to Huntington, a disease that features similar clinical symptoms but is caused by an entirely different genotype. These differential results show clearly that the pathological progression follows a different pathway in both diseases and potential medications that will be developed for treatment of Huntington or ChAc cannot simply be applied to the other respective disease due to different underlying mechanisms. Even though morphological phenotypes observed for the mitochondria were very similar in both diseases, differences observed in the aspect ratio as well as the differences in the moving fraction and motility can be a downstream symptom of both diseases. Reduction in aspect ratio was observed in mitochondria of mDAN differentiated ChAc lines as well. Homeostasis of mitochondria by selective biogenesis and mitophagy is a complex problem in many if not all neurodegenerative diseases (Aufschnaiter, et al., 2016; Chen, et al., 2016; Giachin, et al., 2016; Hung and Calkins, 2016; Osborne, et al., 2016). With the experiments conducted in this work, it cannot be determined whether the disruptions are causative or symptomatic.

This work combined state of the art approaches using microfluidic cell culture systems with high temporal resolution live cell imaging, semi-automated image analysis and a data mining workflow that is robust and sensitive enough to detect minute changes in organelle morphology and trafficking patterns. The proposed protocols can be easily extended to cover an even broader range of trafficking readouts, once they are peer reviewed and published. They can be modified for complex screening approaches as well. Due to the nature of MFCs selecting purely for neurons and providing defined media composition as well as positional control over the readout, it is further advised to conduct upcoming experiments in this cell culture system rather than classical undirected well dishes. However, their influence on the cells due to local deprivation of oxygen and nutrition as well as the steric challenges of the narrow channels needs to be investigated in the future.

References

A. Storch ML. 2010. Experimentelle Therapiestrategien

Ansätze für eine neurorestaurative Behandlung des Morbus Parkinson.

Nervenheilkunde(6):6.

Aasen T, Raya A, Barrero MJ, Garreta E, Consiglio A, Gonzalez F, Vassena R, Bilic J, Pekarik V, Tiscornia G and others. 2008. Efficient and rapid generation of induced pluripotent stem cells from human keratinocytes. *Nat Biotechnol* 26(11):1276-84.

Agnello M, Morici G, Rinaldi AM. 2008. A method for measuring mitochondrial mass and activity. *Cytotechnology* 56(3):145-9.

Atkin TA, MacAskill AF, Brandon NJ, Kittler JT. 2011. Disrupted in Schizophrenia-1 regulates intracellular trafficking of mitochondria in neurons. *Mol Psychiatry* 16(2):122-4, 121.

Aufschnaiter A, Kohler V, Diessl J, Peselj C, Carmona-Gutierrez D, Keller W, Buttner S. 2016. Mitochondrial lipids in neurodegeneration. *Cell Tissue Res*.

Bandyopadhyay D, Cyphersmith A, Zapata JA, Kim YJ, Payne CK. 2014. Lysosome transport as a function of lysosome diameter. *PLoS One* 9(1):e86847.

Berndt N, Holzhutter HG. 2013. The high energy demand of neuronal cells caused by passive leak currents is not a waste of energy. *Cell Biochem Biophys* 67(2):527-35.

Brickley K, Stephenson FA. 2011. Trafficking kinesin protein (TRAK)-mediated transport of mitochondria in axons of hippocampal neurons. *J Biol Chem* 286(20):18079-92.

Burd JF, Usategui-Gomez M. 1973. A colorimetric assay for serum lactate dehydrogenase. *Clin Chim Acta* 46(3):223-7.

Bustin SA, Benes V, Garson JA, Hellemans J, Huggett J, Kubista M, Mueller R, Nolan T, Pfaffl MW, Shipley GL and others. 2009. The MIQE guidelines: minimum information for publication of quantitative real-time PCR experiments. *Clin Chem* 55(4):611-22.

Cai Q, Gerwin C, Sheng ZH. 2005. Syntabulin-mediated anterograde transport of mitochondria along neuronal processes. *J Cell Biol* 170(6):959-69.

Caiazzo M, Dell'Anno MT, Dvoretzkova E, Lazarevic D, Taverna S, Leo D, Sotnikova TD, Menegon A, Roncaglia P, Colciago G and others. 2011. Direct generation of functional dopaminergic neurons from mouse and human fibroblasts. *Nature* 476(7359):224-7.

Cardinale A, Paldino E, Giampa C, Bernardi G, Fusco FR. 2015. PARP-1 Inhibition Is Neuroprotective in the R6/2 Mouse Model of Huntington's Disease. *PLoS One* 10(8):e0134482.

Chan SW, Egan PA. 2005. Hepatitis C virus envelope proteins regulate CHOP via induction of the unfolded protein response. *FASEB J* 19(11):1510-2.

Chang G, Gao S, Hou X, Xu Z, Liu Y, Kang L, Tao Y, Liu W, Huang B, Kou X and others. 2014. High-throughput sequencing reveals the disruption of methylation of imprinted gene in induced pluripotent stem cells. *Cell Res* 24(3):293-306.

Chen H, Denton TT, Xu H, Calingasan N, Beal MF, Gibson GE. 2016. Reductions in the mitochondrial enzyme alpha-ketoglutarate dehydrogenase complex in neurodegenerative disease - beneficial or detrimental? *J Neurochem*.

Chen S, Owens GC, Makarenkova H, Edelman DB. 2010. HDAC6 regulates mitochondrial transport in hippocampal neurons. *PLoS One* 5(5):e10848.

Coppede F, Migliore L. 2015. DNA damage in neurodegenerative diseases. *Mutat Res* 776:84-97.

Cordonnier MN, Dauzonne D, Louvard D, Coudrier E. 2001. Actin filaments and myosin I alpha cooperate with microtubules for the movement of lysosomes. *Mol Biol Cell* 12(12):4013-29.

Crawford TQ, Roelink H. 2007. The notch response inhibitor DAPT enhances neuronal differentiation in embryonic stem cell-derived embryoid bodies independently of sonic hedgehog signaling. *Dev Dyn* 236(3):886-92.

Danek A. 2005. Neuroacanthocytosis Syndromes: What Links Red Blood Cells and Neurons? In: Danek A, editor. *Neuroacanthocytosis Syndromes*. Dordrecht: Springer Netherlands. p 1-14.

Danek A, Walker RH. 2005. Neuroacanthocytosis. *Curr Opin Neurol* 18(4):386-92.

Davie CA. 2008. A review of Parkinson's disease. *Br Med Bull* 86:109-27.

De Franceschi L, Tomelleri C, Matte A, Brunati AM, Bovee-Geurts PH, Bertoldi M, Lasonder E, Tibaldi E, Danek A, Walker RH and others. 2011. Erythrocyte membrane changes of chorea-acanthocytosis are the result of altered Lyn kinase activity. *Blood* 118(20):5652-63.

Demers-Lamarche J, Guillebaud G, Tlili M, Todkar K, Belanger N, Grondin M, Nguyen AP, Michel J, Germain M. 2016. Loss of Mitochondrial Function Impairs Lysosomes. *J Biol Chem* 291(19):10263-76.

Dobson-Stone C, Danek A, Rampoldi L, Hardie RJ, Chalmers RM, Wood NW, Bohlega S, Dotti MT, Federico A, Shizuka M and others. 2002. Mutational spectrum of the CHAC gene in patients with chorea-acanthocytosis. *Eur J Hum Genet* 10(11):773-81.

Dobson-Stone C, Velayos-Baeza A, Filippone LA, Westbury S, Storch A, Erdmann T, Wroe SJ, Leenders KL, Lang AE, Dotti MT and others. 2004. CHOREIN detection for the diagnosis of chorea-acanthocytosis. *Ann Neurol* 56(2):299-302.

Dobson-Stone C, Velayos-Baeza A, Jansen A, Andermann F, Dubeau F, Robert F, Summers A, Lang AE, Chouinard S, Danek A and others. 2005. Identification of a VPS13A founder mutation in French Canadian families with chorea-acanthocytosis. *Neurogenetics* 6(3):151-8.

Dogan I, Eickhoff SB, Schulz JB, Shah NJ, Laird AR, Fox PT, Reetz K. 2013. Consistent neurodegeneration and its association with clinical progression in Huntington's disease: a coordinate-based meta-analysis. *Neurodegener Dis* 12(1):23-35.

Douthwright S, Sluder G. 2016. Live cell imaging: Assessing the phototoxicity of 488 nm and 546 nm light and methods to alleviate it. *J Cell Physiol*.

Erie C, Sacino M, Houle L, Lu ML, Wei J. 2015. Altered lysosomal positioning affects lysosomal functions in a cellular model of Huntington's disease. *Eur J Neurosci* 42(3):1941-51.

Folch A, Ayon A, Hurtado O, Schmidt MA, Toner M. 1999. Molding of deep polydimethylsiloxane microstructures for microfluidics and biological applications. *J Biomech Eng* 121(1):28-34.

Foller M, Hermann A, Gu S, Alesutan I, Qadri SM, Borst O, Schmidt EM, Schiele F, vom Hagen JM, Saft C and others. 2012. CHOREIN-sensitive polymerization of cortical actin and suicidal cell death in chorea-acanthocytosis. *FASEB J* 26(4):1526-34.

Fusaki N, Ban H, Nishiyama A, Saeki K, Hasegawa M. 2009. Efficient induction of transgene-free human pluripotent stem cells using a vector based on Sendai virus, an

RNA virus that does not integrate into the host genome. *Proc Jpn Acad Ser B Phys Biol Sci* 85(8):348-62.

Giachin G, Bouverot R, Acajjaoui S, Pantalone S, Soler-Lopez M. 2016. Dynamics of Human Mitochondrial Complex I Assembly: Implications for Neurodegenerative Diseases. *Front Mol Biosci* 3:43.

Gottlieb E, Vander Heiden MG, Thompson CB. 2000. Bcl-x(L) prevents the initial decrease in mitochondrial membrane potential and subsequent reactive oxygen species production during tumor necrosis factor alpha-induced apoptosis. *Mol Cell Biol* 20(15):5680-9.

Green DR, Reed JC. 1998. Mitochondria and apoptosis. *Science* 281(5381):1309-12.

Guedes-Dias P, de Proenca J, Soares TR, Leitao-Rocha A, Pinho BR, Duchen MR, Oliveira JM. 2015. HDAC6 inhibition induces mitochondrial fusion, autophagic flux and reduces diffuse mutant huntingtin in striatal neurons. *Biochim Biophys Acta* 1852(11):2484-93.

Gurdon JB. 1962. The developmental capacity of nuclei taken from intestinal epithelium cells of feeding tadpoles. *J Embryol Exp Morphol* 10:622-40.

Han DW, Tapia N, Hermann A, Hemmer K, Hoing S, Arauzo-Bravo MJ, Zaehres H, Wu G, Frank S, Moritz S and others. 2012. Direct reprogramming of fibroblasts into neural stem cells by defined factors. *Cell Stem Cell* 10(4):465-72.

Hayashi T, Kishida M, Nishizawa Y, Iijima M, Koriyama C, Nakamura M, Sano A, Kishida S. 2012. Subcellular localization and putative role of VPS13A/CHOREIN in dopaminergic neuronal cells. *Biochem Biophys Res Commun* 419(3):511-6.

Hewitt KJ, Garlick JA. 2013. Cellular reprogramming to reset epigenetic signatures. *Mol Aspects Med* 34(4):841-8.

Howes SC, Alushin GM, Shida T, Nachury MV, Nogales E. 2014. Effects of tubulin acetylation and tubulin acetyltransferase binding on microtubule structure. *Mol Biol Cell* 25(2):257-66.

Hroudova J, Singh N, Fisar Z. 2014. Mitochondrial dysfunctions in neurodegenerative diseases: relevance to Alzheimer's disease. *Biomed Res Int* 2014:175062.

Hung KM, Calkins MJ. 2016. Mitochondrial homeostatic disruptions are sensitive indicators of stress in neurons with defective mitochondrial DNA transactions. *Mitochondrion*.

Joseph RM. 2014. Neuronatin gene: Imprinted and misfolded: Studies in Lafora disease, diabetes and cancer may implicate NNAT-aggregates as a common downstream participant in neuronal loss. *Genomics* 103(2-3):183-8.

Kawasaki H, Mizuseki K, Nishikawa S, Kaneko S, Kuwana Y, Nakanishi S, Nishikawa SI, Sasai Y. 2000. Induction of midbrain dopaminergic neurons from ES cells by stromal cell-derived inducing activity. *Neuron* 28(1):31-40.

Khoury MJ, Beaty TH, Cohen BH. 1993. *Fundamentals of genetic epidemiology*. New York: Oxford University Press.

Kim J, Chu J, Shen X, Wang J, Orkin SH. 2008. An extended transcriptional network for pluripotency of embryonic stem cells. *Cell* 132(6):1049-61.

Kinner A, Wu W, Staudt C, Iliakis G. 2008. Gamma-H2AX in recognition and signaling of DNA double-strand breaks in the context of chromatin. *Nucleic Acids Res* 36(17):5678-94.

Kirkeby A, Nelander J, Parmar M. 2012. Generating regionalized neuronal cells from pluripotency, a step-by-step protocol. *Front Cell Neurosci* 6:64.

Kolehmainen J, Black GC, Saarinen A, Chandler K, Clayton-Smith J, Traskelin AL, Perveen R, Kivitie-Kallio S, Norio R, Warburg M and others. 2003. Cohen syndrome is caused by mutations in a novel gene, COH1, encoding a transmembrane protein with a presumed role in vesicle-mediated sorting and intracellular protein transport. *Am J Hum Genet* 72(6):1359-69.

Koos T, Tepper JM, Wilson CJ. 2004. Comparison of IPSCs evoked by spiny and fast-spiking neurons in the neostriatum. *J Neurosci* 24(36):7916-22.

Kroemer G, Dallaporta B, Resche-Rigon M. 1998. The mitochondrial death/life regulator in apoptosis and necrosis. *Annu Rev Physiol* 60:619-42.

Lako M, Armstrong L, Stojkovic M. 2010. Induced pluripotent stem cells : it looks simple but can looks deceive? *Stem Cells* 28(5):845-50.

Landry JJ, Pyl PT, Rausch T, Zichner T, Tekkedil MM, Stutz AM, Jauch A, Aiyar RS, Pau G, Delhomme N and others. 2013. The genomic and transcriptomic landscape of a HeLa cell line. *G3 (Bethesda)* 3(8):1213-24.

Lee S, Sato Y, Nixon RA. 2011. Lysosomal proteolysis inhibition selectively disrupts axonal transport of degradative organelles and causes an Alzheimer's-like axonal dystrophy. *J Neurosci* 31(21):7817-30.

Lee SH, Lumelsky N, Studer L, Auerbach JM, McKay RD. 2000. Efficient generation of midbrain and hindbrain neurons from mouse embryonic stem cells. *Nat Biotechnol* 18(6):675-9.

Lesage S, Drouet V, Majounie E, Deramecourt V, Jacoupy M, Nicolas A, Cormier-Dequaire F, Hassoun SM, Pujol C, Ciura S and others. 2016. Loss of VPS13C Function in Autosomal-Recessive Parkinsonism Causes Mitochondrial Dysfunction and Increases PINK1/Parkin-Dependent Mitophagy. *Am J Hum Genet* 98(3):500-13.

Lezi E, Swerdlow RH. 2012. Mitochondria in neurodegeneration. *Adv Exp Med Biol* 942:269-86.

Lin L, Isacson O. 2006. Axonal growth regulation of fetal and embryonic stem cell-derived dopaminergic neurons by Netrin-1 and Slits. *Stem Cells* 24(11):2504-13.

Long BH, Musial ST, Brattain MG. 1985. Single- and double-strand DNA breakage and repair in human lung adenocarcinoma cells exposed to etoposide and teniposide. *Cancer Res* 45(7):3106-12.

Lupo F, Tibaldi E, Matte A, Sharma AK, Brunati AM, Alper SL, Zancanaro C, Benati D, Siciliano A, Bertoldi M and others. 2016. A new molecular link between defective autophagy and erythroid abnormalities in chorea-acanthocytosis. *Blood*.

MacAskill AF, Kittler JT. 2010. Control of mitochondrial transport and localization in neurons. *Trends Cell Biol* 20(2):102-12.

Madabhushi R, Pan L, Tsai LH. 2014. DNA damage and its links to neurodegeneration. *Neuron* 83(2):266-82.

Maeder CI, Shen K, Hoogenraad CC. 2014. Axon and dendritic trafficking. *Curr Opin Neurobiol* 27:165-70.

Maherali N, Hochedlinger K. 2008. Guidelines and techniques for the generation of induced pluripotent stem cells. *Cell Stem Cell* 3(6):595-605.

Masters JR. 2002. HeLa cells 50 years on: the good, the bad and the ugly. *Nat Rev Cancer* 2(4):315-9.

Maynard S, Fang EF, Scheibye-Knudsen M, Croteau DL, Bohr VA. 2015. DNA Damage, DNA Repair, Aging, and Neurodegeneration. *Cold Spring Harb Perspect Med* 5(10).

Miller KE, Sheetz MP. 2006. Direct evidence for coherent low velocity axonal transport of mitochondria. *J Cell Biol* 173(3):373-81.

Mollica PA, Reid JA, Ogle RC, Sachs PC, Bruno RD. 2016. DNA Methylation Leads to DNA Repair Gene Down-Regulation and Trinucleotide Repeat Expansion in Patient-Derived Huntington Disease Cells. *Am J Pathol* 186(7):1967-76.

Munoz-Braceras S, Calvo R, Escalante R. 2015. TipC and the chorea-acanthocytosis protein VPS13A regulate autophagy in Dictyostelium and human HeLa cells. *Autophagy* 11(6):918-27.

Mytilineou C, McNaught KS, Shashidharan P, Yabut J, Baptiste RJ, Parnandi A, Olanow CW. 2004. Inhibition of proteasome activity sensitizes dopamine neurons to protein alterations and oxidative stress. *J Neural Transm (Vienna)* 111(10-11):1237-51.

Nicholls DG, Bernson VS, Heaton GM. 1978. The identification of the component in the inner membrane of brown adipose tissue mitochondria responsible for regulating energy dissipation. *Experientia Suppl* 32:89-93.

Ori-McKenney KM, Xu J, Gross SP, Vallee RB. 2010. A cytoplasmic dynein tail mutation impairs motor processivity. *Nat Cell Biol* 12(12):1228-34.

Osborne B, Bentley NL, Montgomery MK, Turner N. 2016. The role of mitochondrial sirtuins in health and disease. *Free Radic Biol Med*.

Pankratz MT, Li XJ, Lavaute TM, Lyons EA, Chen X, Zhang SC. 2007. Directed neural differentiation of human embryonic stem cells via an obligated primitive anterior stage. *Stem Cells* 25(6):1511-20.

Papakonstanti EA, Stournaras C. 2007. Actin cytoskeleton architecture and signaling in osmosensing. *Methods Enzymol* 428:227-40.

Papapetrou EP, Tomishima MJ, Chambers SM, Mica Y, Reed E, Menon J, Tabar V, Mo Q, Studer L, Sadelain M. 2009. Stoichiometric and temporal requirements of Oct4, Sox2, Klf4, and c-Myc expression for efficient human iPSC induction and differentiation. *Proc Natl Acad Sci U S A* 106(31):12759-64.

Park JS, Halegoua S, Kishida S, Neiman AM. 2015. A conserved function in phosphatidylinositol metabolism for mammalian Vps13 family proteins. *PLoS One* 10(4):e0124836.

Park JS, Neiman AM. 2012. VPS13 regulates membrane morphogenesis during sporulation in *Saccharomyces cerevisiae*. *J Cell Sci* 125(Pt 12):3004-11.

Park JS, Thorsness MK, Policastro R, McGoldrick LL, Hollingsworth NM, Thorsness PE, Neiman AM. 2016. Yeast Vps13 promotes mitochondrial function and is localized at membrane contact sites. *Mol Biol Cell* 27(15):2435-49.

Perrier AL, Tabar V, Barberi T, Rubio ME, Bruses J, Topf N, Harrison NL, Studer L. 2004. Derivation of midbrain dopamine neurons from human embryonic stem cells. *Proc Natl Acad Sci U S A* 101(34):12543-8.

Qiu C, Ma Y, Wang J, Peng S, Huang Y. 2010. Lin28-mediated post-transcriptional regulation of Oct4 expression in human embryonic stem cells. *Nucleic Acids Res* 38(4):1240-8.

Rampoldi L, Danek A, Monaco AP. 2002. Clinical features and molecular bases of neuroacanthocytosis. *J Mol Med (Berl)* 80(8):475-91.

Reinhardt P, Glatza M, Hemmer K, Tsytsyura Y, Thiel CS, Hoing S, Moritz S, Parga JA, Wagner L, Bruder JM and others. 2013. Derivation and expansion using only small molecules of human neural progenitors for neurodegenerative disease modeling. *PLoS One* 8(3):e59252.

Reyes DR, Perruccio EM, Becerra SP, Locascio LE, Gaitan M. 2004. Micropatterning neuronal cells on polyelectrolyte multilayers. *Langmuir* 20(20):8805-11.

Ring KL, Tong LM, Balestra ME, Javier R, Andrews-Zwilling Y, Li G, Walker D, Zhang WR, Kreitzer AC, Huang Y. 2012. Direct reprogramming of mouse and human fibroblasts into multipotent neural stem cells with a single factor. *Cell Stem Cell* 11(1):100-9.

Rosenfeld E, Beauvoit B, Rigoulet M, Salmon JM. 2002. Non-respiratory oxygen consumption pathways in anaerobically-grown *Saccharomyces cerevisiae*: evidence and partial characterization. *Yeast* 19(15):1299-321.

Safiulina D, Kaasik A. 2013. Energetic and dynamic: how mitochondria meet neuronal energy demands. *PLoS Biol* 11(12):e1001755.

Sasaki N, Nakamura M, Kodama A, Urata Y, Shiokawa N, Hayashi T, Sano A. 2016. CHOREIN interacts with alpha-tubulin and histone deacetylase 6, and overexpression preserves cell viability during nutrient deprivation in human embryonic kidney 293 cells. *FASEB J* 30(11):3726-3732.

Saxton WM, Hollenbeck PJ. 2012. The axonal transport of mitochondria. *J Cell Sci* 125(Pt 9):2095-104.

Schneider SA, Lang AE, Moro E, Bader B, Danek A, Bhatia KP. 2010. Characteristic head drops and axial extension in advanced chorea-acanthocytosis. *Mov Disord* 25(10):1487-91.

Schwarz TL. 2013. Mitochondrial trafficking in neurons. *Cold Spring Harb Perspect Biol* 5(6).

Shapovalov AI. 1974. Pyramidal and Extra-Pyramidal Control on Mammalian Alpha Motoneurons. In: Gydikov AA, Tankov NT, Kosarov DS, editors. *Motor Control*. Boston, MA: Springer US. p 95-111.

Sharma J, Mukherjee D, Rao SN, Iyengar S, Shankar SK, Satishchandra P, Jana NR. 2013. Neuronatin-mediated aberrant calcium signaling and endoplasmic reticulum stress underlie neuropathology in Lafora disease. *J Biol Chem* 288(13):9482-90.

Sheng ZH. 2014. Mitochondrial trafficking and anchoring in neurons: New insight and implications. *J Cell Biol* 204(7):1087-98.

Shinde V, Pitale PM, Howse W, Gorbatyuk O, Gorbatyuk M. 2016. Neuronatin is a stress-responsive protein of rod photoreceptors. *Neuroscience* 328:1-8.

Shiokawa N, Nakamura M, Sameshima M, Deguchi A, Hayashi T, Sasaki N, Sano A. 2013. CHOREIN, the protein responsible for chorea-acanthocytosis, interacts with beta-adducin and beta-actin. *Biochem Biophys Res Commun* 441(1):96-101.

Shyh-Chang N, Daley GQ, Cantley LC. 2013. Stem cell metabolism in tissue development and aging. *Development* 140(12):2535-47.

Smiley ST, Reers M, Mottola-Hartshorn C, Lin M, Chen A, Smith TW, Steele GD, Jr., Chen LB. 1991. Intracellular heterogeneity in mitochondrial membrane potentials revealed by a J-aggregate-forming lipophilic cation JC-1. *Proc Natl Acad Sci U S A* 88(9):3671-5.

Stagi M, Klein ZA, Gould TJ, Bewersdorf J, Strittmatter SM. 2014. Lysosome size, motility and stress response regulated by fronto-temporal dementia modifier TMEM106B. *Mol Cell Neurosci* 61:226-40.

Storch A, Kornhass M, Schwarz J. 2005. Testing for acanthocytosis A prospective reader-blinded study in movement disorder patients. *J Neurol* 252(1):84-90.

Sudharshan N, Hanstock C, Hui B, Pyra T, Johnston W, Kalra S. 2011. Degeneration of the mid-cingulate cortex in amyotrophic lateral sclerosis detected in vivo with MR spectroscopy. *AJNR Am J Neuroradiol* 32(2):403-7.

Sveinbjornsdottir S. 2016. The clinical symptoms of Parkinson's disease. *J Neurochem*.

Takahashi K, Yamanaka S. 2006. Induction of pluripotent stem cells from mouse embryonic and adult fibroblast cultures by defined factors. *Cell* 126(4):663-76.

Toyoda Y, Erkut C, Pan-Montojo F, Boland S, Stewart MP, Muller DJ, Wurst W, Hyman AA, Kurzchalia TV. 2014. Products of the Parkinson's disease-related glyoxalase DJ-1, D-lactate and glycolate, support mitochondrial membrane potential and neuronal survival. *Biol Open* 3(8):777-84.

Ueno E, Oguchi K, Yanagisawa N. 1982. Morphological abnormalities of erythrocyte membrane in the hereditary neurological disease with chorea, areflexia and acanthocytosis. *J Neurol Sci* 56(1):89-97.

Velayos Baeza A D-SC, Rampoldi L, Bader B, Walker RH, Danek A, Monaco AP. 2014. Chorea-Acanthocytosis. In: Pagon RA AM, Ardinger HH, et al., editor. GeneReviews. University of Washington.

Walker FO. 2007. Huntington's disease. *Lancet* 369(9557):218-28.

Walker RH. 2015. Untangling the Thorns: Advances in the Neuroacanthocytosis Syndromes. *J Mov Disord* 8(2):41-54.

Walker RH, Jung HH, Danek A. 2011. Neuroacanthocytosis. *Handb Clin Neurol* 100:141-51.

Walker RH, Morgello S, Davidoff-Feldman B, Melnick A, Walsh MJ, Shashidharan P, Brin MF. 2002. Autosomal dominant chorea-acanthocytosis with polyglutamine-containing neuronal inclusions. *Neurology* 58(7):1031-7.

Ward MW, Huber HJ, Weisova P, Dussmann H, Nicholls DG, Prehn JH. 2007. Mitochondrial and plasma membrane potential of cultured cerebellar neurons during glutamate-induced necrosis, apoptosis, and tolerance. *J Neurosci* 27(31):8238-49.

Warlich E, Kuehle J, Cantz T, Brugman MH, Maetzig T, Galla M, Filipczyk AA, Halle S, Klump H, Scholer HR and others. 2011. Lentiviral vector design and imaging approaches to visualize the early stages of cellular reprogramming. *Mol Ther* 19(4):782-9.

Warren L, Manos PD, Ahfeldt T, Loh YH, Li H, Lau F, Ebina W, Mandal PK, Smith ZD, Meissner A and others. 2010. Highly efficient reprogramming to pluripotency and directed differentiation of human cells with synthetic modified mRNA. *Cell Stem Cell* 7(5):618-30.

Wei Z, Yang Y, Zhang P, Andrianakos R, Hasegawa K, Lyu J, Chen X, Bai G, Liu C, Pera M and others. 2009. Klf4 interacts directly with Oct4 and Sox2 to promote reprogramming. *Stem Cells* 27(12):2969-78.

Weiss KR, Littleton JT. 2016. Characterization of axonal transport defects in *Drosophila* Huntingtin mutants. *J Neurogenet*:1-10.

Wernig M, Meissner A, Cassady JP, Jaenisch R. 2008. c-Myc is dispensable for direct reprogramming of mouse fibroblasts. *Cell Stem Cell* 2(1):10-2.

Wong YC, Holzbaur EL. 2014. The regulation of autophagosome dynamics by huntingtin and HAP1 is disrupted by expression of mutant huntingtin, leading to defective cargo degradation. *J Neurosci* 34(4):1293-305.

Yu J, Vodyanik MA, Smuga-Otto K, Antosiewicz-Bourget J, Frane JL, Tian S, Nie J, Jonsdottir GA, Ruotti V, Stewart R and others. 2007. Induced pluripotent stem cell lines derived from human somatic cells. *Science* 318(5858):1917-20.

Zajac AL, Goldman YE, Holzbaur EL, Ostap EM. 2013. Local cytoskeletal and organelle interactions impact molecular-motor- driven early endosomal trafficking. *Curr Biol* 23(13):1173-80.

Zarei S, Carr K, Reiley L, Diaz K, Guerra O, Altamirano PF, Pagani W, Lodin D, Orozco G, China A. 2015. A comprehensive review of amyotrophic lateral sclerosis. *Surg Neurol Int* 6:171.

Zhou H, Wu S, Joo JY, Zhu S, Han DW, Lin T, Trauger S, Bien G, Yao S, Zhu Y and others. 2009. Generation of induced pluripotent stem cells using recombinant proteins. *Cell Stem Cell* 4(5):381-4.

List of figures

Figure 1: Acanthocytes are a common feature of the neuroacanthocytosis syndromes ...	11
Figure 2: Image of the brain of a patient suffering from Chorea-Acanthocytosis.....	12
Figure 3: Time line of publications associated with the term "disease modelling"	14
Figure 4: Schematic of application iPSC technology in translational research.....	17
Figure 5: MSN differentiation scheme	46
Figure 6: mDAN differentiation scheme	47
Figure 7: Scheme for the assessment of cell composition at time point of measurement .	49
Figure 8: Scheme of processing work of tracking analysis.	59
Figure 9: Successful infection.	61
Figure 10: Hierarchical clustering of iPSC after silencing/characterization PCR.....	64
Figure 11: Alkaline phosphatase stainingl.	65
Figure 12: Pluripotency staining	67
Figure 13: Three germ layer formation I.....	68
Figure 14: Three germ layer formation II.....	69
Figure 15: CHOREIN western blot of generated lines.	70
Figure 16: MSN protocol characterization I	72
Figure 17: Quantification of MSN differentiation capacity	72
Figure 18: MSN protocol characterization II	73
Figure 19: mDAN protocol characterization I.....	74
Figure 20: mDAN protocol characterization II.....	75
Figure 21: Quantification mDAN differentiation capacity	75
Figure 22: Hierarchical clustering of PCR data for the characterization of MSN differentiation.	77
Figure 23: Hierarchical clustering of the PCR data of mDAN differentiation.	79
Figure 24: Evaluation of western blots of cytoskeleton proteins and acetylated tubulin ratio of both differentiation protocols	80
Figure 25: Survival of mature MSN cultures	82
Figure 26: Survival of mature mDAN cultures	84
Figure 27: DNA damage in MSN differentiation.....	85
Figure 28: DNA damage in mDAN differentiation.	86
Figure 29: Metabolic characterization of mature neurons after MSN differentiation.....	88
Figure 30: Metabolic characterization of mature neurons after mDAN differentiation.	89
Figure 31: Morphological analysis of mitochondria of MSN differentiation.....	92
Figure 32: Morphological analysis of mitochondria of mDAN differentiation	94
Figure 33: Characterization of the channel-exits of MFC.....	95

Figure 34: Morphological analysis of MFC cultures.....	96
Figure 35: Examples of plots obtained from trafficking analysis of mitochondria.	98
Figure 36: Trafficking analysis of mitochondria of MSN differentiated cultures.	99
Figure 37: Trafficking analysis of mitochondria of mDAN differentiated cultures.	100
Figure 38: Analysis of direct movement in both differentiations protocols.....	101
Figure 39: Speed of the top decile of the fastest mitochondria of both differentiation protocols.....	102
Figure 40: Trafficking analysis of mitochondria of MSN differentiated MFC cultures	102
Figure 41: Trafficking analysis of mitochondria of mDAN differentiated MFC cultures. ...	103
Figure 42: Detailed characterization of mitochondria trafficking in MFC	104
Figure 43: Mean speed of the top decile fastest mitochondria in MFC of both differentiation protocols.....	105
Figure 44: Analysis of membrane potential marker JC-1.....	108
Figure 45: Analysis of membrane potential marker JC-1 in MFC with mDAN differentiated neurons.....	109
Figure 46: Morphological analysis of lysosomes of MSN differentiation	110
Figure 47: Morphological analysis of lysosomes of mDAN differentiation.....	111
Figure 48: Morphological analysis of MFC cultures.....	113
Figure 49: Examples of plots obtained from trafficking analysis of lysosomes.....	115
Figure 50: Trafficking analysis of lysosomes of MSN differentiated cultures	116
Figure 51: Trafficking analysis of lysosomes of mDAN differentiated cultures.....	117
Figure 52: Analysis of direct movement in both differentiation protocols.	118
Figure 53: Speed of the top decile of the fastest lysosomes of both differentiation protocols.....	119
Figure 54: Trafficking analysis of lysosomes of MSN differentiated MFC cultures.....	119
Figure 55: Trafficking analysis of lysosomes of mDAN differentiated MFC cultures	120
Figure 56: Detailed characterization of lysosomes trafficking in MFC.....	121
Figure 57: Mean speed of the top decile fastest lysosomes in MFC of both differentiation protocols.....	122
Figure 58: DNA damage in MSN differentiation of Htt lines.....	124
Figure 59: Metabolic characterization of mature neurons of Htt lines after MSN differentiation.....	125
Figure 60: Morphological analysis of mitochondria of Htt lines in MSN differentiation. ...	126
Figure 61: Trafficking analysis of mitochondria of Htt lines.....	127
Figure 62: Analysis of top speed and direct movement of Htt lines.	128
Figure 63: Analysis of membrane potential marker JC-1.....	129

Figure 64: Morphological analysis of lysosomes of Htt lines in MSN differentiation..... 130
Figure 65: Trafficking analysis of lysosomes of Htt lines in MSN differentiated cultures .131
Figure 66: Analysis of top speed and direct movement of Htt lines.132

List of tables

Table 1: Cell lines and organism used during this thesis	21
Table 2: Instruments	21
Table 3: Primary antibodies used for ICC.....	23
Table 4: Primary antibodies used for western blot.....	25
Table 5: Secondary antibodies.....	25
Table 6: Fluorescent reporters	26
Table 7: Software.....	27
Table 8: Chemicals	27
Table 9: Consumables	32
Table 10: Assays and kits	33
Table 11: Primers designed	34
Table 12: Media compositions	38
Table 13: Setup of PCR experiments.....	48
Table 14: Experimental setup of Seahorse XFe96 device	52
Table 15: Primary antibody combinations used for ICC grouped by their application	53
Table 16: Settings for SDS PAGE electrophoresis for different applications	57
Table 17: Settings for Western Blot development	57
Table 18: Tracker and concentrations used for live cell imaging	58
Table 19: Silencing of generated iPSC lines	62
Table 20: Genes investigated to characterize MSN differentiation	76
Table 21: Genes investigated to characterize mDAN differentiation.....	78
Table 22: Characterization of the applied differentiation protocols	79
Table 23: Summary of stressing experiments	86
Table 24: Summary of the results of the metabolic analysis.....	90
Table 25: Summary of morphological features of mitochondria in ChAc.....	97
Table 26: Summary of analysis of the dynamic parameters of mitochondria	106
Table 27: Summary of morphological features of lysosomes in ChAc.....	114
Table 28: Summary of analysis of dynamic parameters of lysosomes	123

Acknowledgments

I want express my sincere gratitude to Prof. Dr. med. Alexander Storch, who allowed me to start my thesis in his laboratory, supported me and provided help whenever I faced problems. I would like to thank Prof. Dr. med. Dr. rer. med. Andreas Hermann for the project and access to all resources that were needed to overcome each challenge. The support for my own ideas and critical discussions helped me to improve myself beyond the point that I would have been able to achieve on my own.

I want to thank the lab members for the help, support and reassurance that I received when needed. Special thanks to Katja Zoschke, Julia Japtok, Nicole Kreitner, Marcel Naumann, Patrick Neumann, Xenia Lojewski and Arun Pal.

Thanks to Sumitra Srimasorn, who kept me sane for the last few years. Without your help this whole work wouldn't have been possible. You were always the first one to go to when a crazy idea hit me. Thank you for being my catalyst and always believing in me beyond everything else. **ขอบคุณมาก**

The work was supported in part by the Advocacy for Neuroacanthocytosis patients and by the Federal Ministry of Education and Research (BMF FKZ: 01GM1303) under the frame of E-Rare-2, the ERA-Net for Research on Rare Diseases (EMINA2 consortium). We thank the patients and the probands for donating skin biopsies.

Thanks to Anne Richard for being there for me in a critical time when I needed you.

I want to thank especially my family and friends for always being there for me when I needed them. You always believed in me and faced me not with ignorance and rejection but with compassion and motivation.

I want to dedicate this work to people I care for, because they gave me the strength I needed and made me able to pursue my dreams.

Ich möchte mich bei meiner Familie und meinen Freunden bedanken, die immer für mich da waren wenn ich sie brauchte. Ihr habt immer an mich geglaubt und seid mir nicht mit Ignoranz und Ablehnung begegnet sondern habt mich mit Verständnis und Mitgefühl aufgebaut und motiviert.

Ich widme diese Arbeit allen Menschen die mir wichtig sind und mir die Stärke gegeben haben um meine Träume zu verwirklichen. Im Besonderen widme ich diese Arbeit meinen Großeltern, speziell meinem Großvater.

Appendix

Anlage 1

Hiermit versichere ich, dass ich die vorliegende Arbeit ohne zulässige Hilfe Dritter und ohne Benutzung anderer als der angegebenen Hilfsmittel angefertigt habe; die aus fremden Quellen direkt oder indirekt übernommenen Gedanken sind als solche kenntlich gemacht. Die Arbeit wurde bisher weder im Inland noch im Ausland in gleicher oder ähnlicher Form einer anderen Prüfungsbehörde vorgelegt.

Die Dissertation wurde von Prof. Dr. med. Dr. rer. medic. Andreas Hermann, Medizinische Fakultät der Technischen Universität Dresden, Klinik und Poliklinik für Neurologie, betreut und im Zeitraum vom Juli 2012 bis Oktober 2017 verfasst.

Meine Person betreffend erkläre ich hiermit, dass keine früheren erfolglosen Promotionsverfahren stattgefunden haben. Ich erkenne die Promotionsordnung der Fakultät für Mathematik und Naturwissenschaften der Technischen Universität Dresden vom 23. Februar 2011 an.

Dresden, 13. Oktober 2017

Hannes Glaß

Hiermit bestätige ich die Einhaltung der folgenden aktuellen gesetzlichen

Vorgaben im Rahmen meiner Dissertation

X das zustimmende Votum der Ethikkommission bei Klinischen Studien,
epidemiologischen Untersuchungen mit Personenbezug oder Sachverhalten, die das
Medizinproduktegesetz betreffen

Aktenzeichen der zuständigen Ethikkommission:

EK 45022009, EK 47032006

X die Einhaltung der Bestimmungen des Tierschutzgesetzes

Aktenzeichen der Genehmigungsbehörde zum Vorhaben/zur Mitwirkung:

AZ: 24-9168.24-1/2011-19

X die Einhaltung des Gentechnikgesetzes

Projektnummer:

AZ: 56.8811.71/170 (02.03.2005) and AZ: 55-8811.72/32-13

X die Einhaltung von Datenschutzbestimmungen der Medizinischen Fakultät und des
Universitätsklinikums Carl Gustav Carus.

Dresden, 13.10.2017

Unterschrift des Doktoranden